Volume 16, Issue 3, September 2026
pISSN 2158-0510 eISSN - 2158-0529

IJBM

International Journal of BIOMEDICINE

www.ijbm.org

IJBM

INTERNATIONAL JOURNAL OF BIOMEDICINE

International Journal of Biomedicine (print ISSN - 2158-0510 and online ISSN - 2158-0529) is published four times a year by International Medical Research and Development Corp. (IMRDC). International Journal of Biomedicine (IJBM) is an international, peer-reviewed, open access journal. IJBM publishes scientific articles related to basic, applied, and translational research in biology and medicine. The main purpose of IJBM is to promote new scientific ideas and biomedical technologies. The distribution of freely accessible, high-quality content is a central mission of IJBM, aimed at increasing research visibility and accelerating scientific discovery. IJBM articles are published under a Creative Commons Attribution–NonCommercial–NoDerivatives 4.0 International (CC BY-NC ND 4.0) license.

International Journal of Biomedicine endorses and behaves in accordance with the codes of conduct and international standards established by the Committee on Publication Ethics (COPE).

Manuscript Submission: Original works will be accepted with the understanding that they are contributed solely to the Journal, are not under review by another publication, and have not previously been published except in abstract form.

IJBM

INTERNATIONAL JOURNAL OF BIOMEDICINE

IJBM
INTERNATIONAL JOURNAL OF BIOMEDICINE
www.ijbm.org
Volume 16 Issue 3 September 2026

CONTENTS

REVIEW ARTICLES

The Application of Artificial Intelligence in Detecting Prostate Cancer with Medical Imaging: A Literature Review
Abdulrahman Tajaldeen 294

Deep Learning–Based Convolutional Neural Networks for Brain Tumor Detection on CT scans: A Systematic Review
Sara Ali, Meaad Elbashir, Almohannad Hamzi, Imad Akour, Anwar Sheikhain, Raed Al-Shahri, Turkey Refaee, Ali Abdelrazig, Awatif M. Omer.....306

Rheumatoid Arthritis: Independent and Synergistic Effects of Vitamin D Deficiency and Smoking
Abdulsalam A. Noorwali 314

Impact of Adrenal Gland Dysfunction on Dental Implant Therapy and Osseointegration: A Narrative Review
Bylbyl Reçica, Vjosa Hamiti Krasniqi, Jehona Ahmedi, Besir Salihu 320

Incidence and Prevention of White Spot Lesions Associated with Fixed Orthodontic Appliances: A Literature Review
Gazmend Jusufi 327

ORIGINAL ARTICLES

Endothelial Dysfunction, Microalbuminuria, and Cardiac Biomarkers as Predictors of Preeclampsia in Gestational Arterial Hypertension
Mokhinur A. Sadulloeva, Feruza A. Zakirova, Saida A. Ikramova 333

Cord Blood Levels of IL-8, MCP-1 and MIP-1α as Possible Predictors of Late Sepsis Development in Preterm Neonates
Jelena Vucic, Karin Vasic, Sandra Stankovic, Voja Pavlovic 339

Integrated Immunomorphological and Molecular Profiling Predicts Response to Neoadjuvant Therapy in Breast Cancer
S.V. Vtorushin, N.A. Tarabanovskaya, N.V. Krakhmal, S.S. Naumov, N.V. Litviakov.....346

Ultrasound Evaluation of Lower Limb Arteries in Non-Diabetic Controls and Diabetic Patients
Adel Alzahrani, Omar Alserihy, Asma Alkhaldi, Khadijah Alshuqyfii, Ahmed Monis, Yaser Khojah, Nawaf Alsaedi, Reem T. Alturki, Salahaden R Sultan..... 352

Radiation Dose Evaluation and Optimization for Digital Chest and Abdominal Radiography: Establishing Local Diagnostic Reference Levels in Taif City, Saudi Arabia
Fahad Riyadh Otaibi, Fahad Sultan ALWagdani, Ahmed Turki Al-Osaimi, Omar Abed Al-Salmi, Fahad Hussain Alwagdany, Hamid Osman, Mohamed Elsamani, Sahal Alotaibi, Osama Awad Alotaibi, Samih Kajoak.....357

CONTENTS

Risk Factors for Intestinal Anastomotic Leakage After Hemicolectomy: A Single-Center Retrospective Study
E. A. Toneev, D. D. Prokhorov, M. A. Iglina, S. R. Ziganshina, D. R. Pyatikop, D.V. Golovko, Z. Yu. Yunkina 364

Ginsenoside Rg3 Induces Apoptosis While Attenuates Collagen Metabolism in Human Vocal Cord Scar Fibroblasts In Vitro
Yan Qin, Kang Wang, Zhi-Mao Zhang, Ting Wu, Long Zhang, Jun Liu 372

Digital Platform for the Prediction of 3D Visual and 3D Ultrastructural Morphology of the Urinary Tract
Boris A. Berdichevskiy, Grigory V. Zubik.....378

Impact of Magnets Inserted into Overdentures on the Periodontal Indices
Snežana V. Brković, Srđan D. Poštić, Veljko D. Ilić, Branimir D. Stošić, Pavle D. Ilić 383

CASE REPORTS

Sacroiliitis in Systemic Lupus Erythematosus–Systemic Sclerosis Overlap Syndrome: A Therapeutic Challenge
Mousa A. Albalwi 388

When One Antibody Disappears, and Others Emerge: A Six-Year Evolution of Antiphospholipid Antibodies in a Pregnant Woman with Systemic Lupus Erythematosus
Ina Toska, Rexhep Shkurti, Ervin Rapushi, Anila Mitre 395

Demyelinating Sensorimotor Polyneuropathy in a Pediatric Patient with a Kif1B Variant: A Case Report
Armand Shehu, Anita Pilika, Aida Bushati, Kristi Aleksi, Xhentila Doka, Era Kurti, Era Shehu 398

Diagnostic Reappraisal after 12-Year Follow-up of Pediatric Myopathy with Heterozygous NEB Variants and Dystrophy-Like Progression
Afërdita Tako, Mirela Tabaku, Aida Bushati, Rovena Aliaj, Armand Shehu, Sindi Dizdari, Paskal Cullufi 401

Food noise, intrusive thoughts, and depression, improvement on tirzepatide: A case-report
Amirah Alhowiti 406

READER SERVICES

Instructions for Authors 410

International Journal of Biomedicine 16(3) (2026) 294-305
http://dx.doi.org/10.21103/Article16(3)_RA1

REVIEW ARTICLE

INTERNATIONAL JOURNAL OF BIOMEDICINE

The Application of Artificial Intelligence in Detecting Prostate Cancer with Medical Imaging: A Literature Review

Abdulrahman Tajaldeen[1*]

[1]*Department of Applied Radiologic Technology, College of Applied Medical Sciences, University of Jeddah, Jeddah, Saudi Arabia*

Abstract

Background: Prostate cancer (PCa) is the world's second most common cancer in men and a major cause of cancer death. Studies published from 2023 to 2026 have shown that the use of artificial intelligence (AI) can significantly enhance several imaging modalities for PCa detection, Gleason grading, and risk stratification, such as multiparametric magnetic resonance imaging (mpMRI), transrectal ultrasound (TRUS), micro-ultrasound, prostate-specific membrane antigen positron emission tomography/computed tomography (PSMA-PET/CT), and digital pathology using whole-slide image (WSI) analysis. Although the potential of mpMRI guided by the Prostate Imaging Reporting and Data System (PI-RADS) is significant, considerable inter-reader variability still results in missed diagnoses and unnecessary biopsies. These limitations are mitigated by the development of AI-based systems, including deep learning (DL), machine learning (ML), and radiomics, which are designed to address them.

Methods and Results: The Web of Science and PubMed databases were searched on 3 May 2026 using a three-domain Boolean strategy encompassing PCa-specific, AI-specific, and imaging/pathology-specific terminology. A total of 4,791 records from Web of Science and 2,910 from PubMed were retrieved; following deduplication (n = 4,054), year filtering (2023–2026), and quality screening, n = 2,348 records remained eligible. Only studies using AI in medical imaging or digital pathology in PCa detection, grading, or staging were included in a narrative synthesis.

AI applications were identified across four imaging modalities: mpMRI, ultrasound/micro-ultrasound, PSMA-PET/CT, and digital pathology. Studies consistently illustrate that AI makes meaningful contributions to the detection and characterization of prostate cancer, provides high accuracy, sensitivity, and specificity across all modalities, and that several validated systems approach or equal the performance of trained radiologists and uropathologists.

Landmark studies, including the PI-CAI trial and the PANDA challenge, provided Level 1b evidence for AI in MRI-based csPCa detection and Gleason grading, respectively.

Conclusion: Across all reviewed modalities, AI contributes to the clinically meaningful detection, characterization, and grading of PCa. Widespread clinical integration depends on clinical transparency requirements and regulatory pathways that align with prospective multi-center, outcome-driven trials and standardized AI evaluation frameworks**.** (**International Journal of Biomedicine. 2026;16(3):294-305.**)

Keywords: prostate cancer • artificial intelligence • convolutional neural network • deep learning • multiparametric MRI

For citation: Tajaldeen A. The Application of Artificial Intelligence in Detecting Prostate Cancer with Medical Imaging: A Literature Review. International Journal of Biomedicine. 2026;16(3):294-305. doi:10.21103/Article16(3)_RA1

Abbreviations

ADC, apparent diffusion coefficient; **AI**, artificial intelligence; **AUC**, area under the receiver operating characteristic curve; **bpMRI**, biparametric MRI; **CAD**, computer-aided detection/diagnosis; **CNN**, convolutional neural network; **csPCa**, clinically significant prostate cancer; **DL**, deep learning; **DWI**, diffusion-weighted imaging; **GAN,** generative adversarial network **ISUP**, International Society of Urological Pathology; **ML**, machine learning; **mpMRI**, multiparametric magnetic resonance imaging; **PCa**, prostate cancer; **PI-RADS**, Prostate Imaging Reporting and Data System; **PSA**, prostate-specific antigen; **PSMA-PET/CT**, prostate-specific membrane antigen positron emission tomography/computed tomography; **TRUS**, transrectal ultrasound; **WSI**, whole-slide image; **XAI**, explainable artificial intelligence.

Introduction

Prostate cancer (PCa) is the second most commonly diagnosed malignancy in men worldwide, with an estimated 1.4 million new cases reported every year, and is the fifth leading cancer-related mortality in men worldwide.[1] It can vary from a low-grade indolent form that can be managed through active surveillance to a high-grade aggressive form, which may be metastatic and require multimodal systemic treatment. In addition to early detection, an important challenge in PCa management is distinguishing clinically significant PCa (csPCa, defined as International Society of Urological Pathology (ISUP) grade group ≥2) from clinically indolent disease, while also preventing overdiagnosis and overtreatment, and underdiagnosis and undertreatment.

Multiparametric MRI (mpMRI), interpreted according to the Prostate Imaging Reporting and Data System (PI-RADS) version 2.1, [2] has become the pre-biopsy standard of care for PCa localization and lesion characterization. The PROMIS trial found that pre-biopsy mpMRI could help 27% of men avoid an unnecessary biopsy compared to standard transrectal ultrasound-guided biopsy alone [3], and PRECISION, a randomized trial, showed that MRI-targeted biopsy revealed significantly more clinically significant cancer and less insignificant cancer than standard biopsy.[4] However, with a large proportion of equivocal PI-RADS 3 lesions, representing 20-35% of clinical reads, a significant inter-reader variability remains and leads to missed diagnosis of csPCa and unnecessary biopsies. Historically, (2) TRUS-guided systematic biopsy has been known to miss anterior and apical lesions and isoechoic PCa foci and has a large inter-reader variability. Micro-ultrasound at 29 MHz has proven to be an affordable alternative to MRI. The PRI-MUS protocol has shown that 29 MHz micro-ultrasound can define prostate tissue into five risk groups, with clinically significant prostate cancer being meaningfully discriminated.[5] PSMA-PET/CT has transformed primary staging, biochemical recurrence (BCR), and restaging. At the same time, prostate biopsy and radical prostatectomy specimens have been digitized, allowing for whole slide image (WSI) analysis for AI-based Gleason grading.[2]

Artificial Intelligence (AI), including ML, DL, radiomics, and now, transformer-based architectures, has become a revolutionary computational paradigm across all prostate imaging modalities.[6] Medical imaging is powered by modern AI, which is built on deep learning, a technique that uses multiple layers of computation to learn multiple levels of data representation.[7] DL models, especially CNNs and their variants, can automatically segment the prostate gland, detect prostate lesions, classify them into PI-RADS categories, predict Gleason grades, stage prostate cancer, and evaluate treatment response using large datasets that capture complex hierarchical imaging features. Recent studies from 2023 to 2026 have shown that AI algorithms perform at or above the level of top-tier experts in multi-institutional, blinded validation settings.

The classical computer-aided detection (CAD) systems designed to help radiologists analyze prostate MRI scans showed inconsistent performance, were associated with higher false-positive rates, and offered little or no improvement in cancer detection. Most of these disadvantages have been addressed by learning discriminative representations directly from raw imaging data using self-supervised, semi-supervised, or supervised learning paradigms, without relying on human-engineered feature descriptors. The primary benefit of DL architecture is their ability to learn hierarchical representations directly from data, yielding performance higher than that of rule-based CAD approaches.[8] This gradual shift from handcrafted features to learned representations has been well documented in a comprehensive survey of deep learning in medical image analysis. It is being acknowledged as the key methodological change that propelled the gains in modern AI.[7]

This literature review will explore peer-reviewed publications from 2023 to 2026 across four modalities (mpMRI, TRUS/micro-ultrasound, PSMA-PET/CT, and digital pathology/WSI) that use AI for the diagnosis, characterization, grading, and risk stratification of prostate cancer. The review collates the existing evidence base, outlines gaps in the evidence, and outlines regions of uncertainty that need to be addressed before regular use in clinical practice. A recent study of the entire PCa pathway also found that, despite some limitations, AI technology has now achieved clinically relevant performance in screening, imaging, pathology, and biomarker assessment.[9]

Materials and Methods

Search Strategy

A literature search was performed on 3 May 2026 in Web of Science (WoS) Core Collection and MEDLINE/PubMed. A three-domain Boolean search structure was used. The first set included PCa-specific terms: “prostate cancer,” “prostatic neoplasms,” “prostate carcinoma,” “prostate adenocarcinoma,” “PCa,” “castration-resistant prostate cancer,” “CRPC,” “biochemical recurrence,” and “prostate-specific antigen. The second domain included terms related to AI: “artificial intelligence,” “machine learning,” “deep learning,” “neural networks,” “convolutional neural networks,” “CNN,” “transformer,” “attention mechanism,” “radiomics,” “computer-aided detection,” “computer-aided diagnosis,” “CAD,” “natural language processing,” “NLP,” “large language models,” and “foundation models. The third domain contained imaging and pathology terms: "MRI," "multiparametric MRI," "mpMRI," "ultrasound," "TRUS," "PET," "PSMA-PET," "medical imaging," "histopathology," "digital pathology," "whole slide images," "biopsy," "Gleason score," "ISUP grade," and "pathology."

Eligibility Screening

A total of 4,791 records were found in WoS and 2,910 records in PubMed (total 4,054 after deduplication) (Figure 1). An authorized year filter (2023–2026) returned 2,348 documents for eligibility screening. The following criteria were included for the studies: (i) used at least one AI technique for prostate cancer imaging or pathology; (ii) provided quantitative performance metrics; (iii) were published from January 2023 to 3 May 2026. Editorials, conference abstracts with incomplete data, and reports of all non-PCa malignancies were excluded. The final narrative synthesis included only

primary studies, systematic reviews, and meta-analyses found in PubMed or WoS with a verifiable digital object identifier (DOI).

Figure 1. *PRISMA flow of prostate cancer*

Data Extraction and Quality Assessment

The primary author extracted the data, which was then verified separately. For each abstracted study, the following data were collected: first author, year of publication, journal, imaging modality, AI technique, study design, sample size, reference standard, and key performance metrics (AUC, sensitivity, specificity, accuracy, and concordance coefficient). Diagnostic accuracy studies were appraised using the QUADAS-2 tool when applicable. AMSTAR-2 was used to appraise systematic reviews and meta-analyses. The Oxford Center for Evidence-Based Medicine (OCEBM) 2011 classification was used for the level of evidence.

Results

A total of fifteen primary studies, systematic reviews, and meta-analyses were included in the narrative synthesis for the four modalities (mpMRI, ultrasound/micro-ultrasound, PSMA-PET/CT, and digital pathology/WSI). The characteristics of all included studies are provided in Table 1, and the performance of the diagnostics, in terms of accuracy and specificity, is summarized in Table 2.

Multiparametric and Biparametric MRI

The largest, most rigorously validated body of evidence for PCa detection comes from combining mpMRI with AI, among all imaging modalities. In a retrospective study of 1,108 patients, Hamm et al. [10] created an interactive explainable AI (XAI) model for csPCa diagnosis at biparametric MRI (bpMRI) at Charité Universitätsmedizin Berlin. The model performed well on the internal and external test sets for csPCa detection, with AUCs of 0.89 and 0.87, respectively, and a sensitivity of 93% (95% CI: 87–98%). Most importantly, XAI-assisted reading led to greater confidence in assessing PI-RADS 3 lesions (4.1 vs. 3.4 on a five-point Likert scale; P=0.007) and shorter reading time (58 seconds; P=0.009) among non-expert readers. The visual and textual explanations were accurate in 80% (1,080 of 1,352) of cases, directly addressing the transparency barrier that has hindered clinical adoption of black-box AI systems.

Saha et al. [11] published the landmark Prostate Cancer AI Challenge (PI-CAI) study, which is the largest and best-designed study to date to validate AI in prostate MRI. The study included 10,207 MRI exams from hospitals in the Netherlands and Norway, of which 9,207 were used to train the AI models. Performance was assessed by either an ensemble of the best-performing AI systems or by one of 62 radiologists, in a paired, non-inferiority confirmatory design. For the detection of csPCa, the AI ensemble outperformed the average study radiologist (0.91 vs. 0.86). Importantly, the AI's performance was not shown to be non-inferior to radiologists' readings obtained in routine multidisciplinary clinical practice, which is the critical distinction between research and operational (clinical) benchmarks. The study confirmed that AI detection of csPCa on bpMRI is a clinically relevant ability and identified the additional research needed before AI can be used without human assistance.

Cai et al. [12] from the Mayo Clinic published a fully automated DL model trained on 5,735 mpMRI exams to predict patient-level csPCa without tumor location annotations. The model's performance was statistically comparable to that of highly trained abdominal radiologists on an internal test set of 400 examinations and an external, independent test set of 204 cases (ProstateX). The method is automated and does not require expert lesion segmentation—a process that typically poses the main obstacle to large-scale development of AI models due to the limited volume of expert-annotated training data.

Bosma et al. [13] proposed a report-guided semi-supervised learning (RG-SSL) algorithm that used diagnostic radiology reports to obtain pseudo-labels and expand the number of labels for training a model for csPCa detection on bpMRI. When trained with 100 manually annotated examinations, but tested on 300 examinations from an external center, RG-SSL attained the highest examination-level AUC (0.86 ± 0.01), outperforming fully supervised learning (0.78 ± 0.03) as well as existing semi-supervised approaches (0.81 ± 0.02). The work showed how to eliminate the expert-labeling time required for AI development.

Radiomics-based methods complement end-to-end DL models, especially for characterizing PI-RADS 3 lesions. Extracting quantitative imaging features, such as first-, second-, and higher-order statistics, using radiomics techniques can be done in a high-throughput manner, and these values can be used in conjunction with other patient information to build decision-support models, transforming images into "mineable data" not visible to the human eye.[14] The discriminatory power of multi-parametric radiomics integration is further improved: in the Radiomics-PCa literature, the AUCs reported for Gleason score prediction range from 0.50 to 0.92, with combined clinical and radiomic models outperforming imaging-only models.[15] Huynh et al. [16] summarized MRI-based radiomic models for PCa risk stratification, reporting AUCs ranging from 0.50 to 0.92 across

33 studies. The multi-parametric radiomics models based on T2-weighted imaging and DWI/ADC features consistently outperformed single-sequence models. Salimi et al. [17] included 24 studies, of which 14 were meta-analyzed, reporting pooled AUC, sensitivity, and specificity values of 0.75, 72%, and 78%, respectively, for MRI-based radiomics ML models predicting post-treatment biochemical recurrence (BCR). A thorough meta-analysis also demonstrated that MRI radiomics models for PCa risk stratification have pooled AUC values of 0.83–0.87 for Gleason grade prediction, when all multi-parametric features are combined. [18] The value of data integration was highlighted, as combined models with clinical data performed better at prognostication than models that included only radiomics data.

The systematic review by Molière et al. [19], which evaluated the diagnostic accuracy of DL models for the automatic detection, localization, and characterization of csPCa, showed consistently promising performance for csPCa detection, with some models attaining an AUC above 0.85 in internal validation. The major obstacles to clinical adoption were identified as a lack of external validation, heterogeneous reporting of results, and difficulty obtaining training data from a single center.

Ultrasound and Micro-Ultrasound

The use of AI in ultrasound plays a strategic role in the PCa diagnostic pathway, as it provides procedural guidance, reduces infrastructure costs, and is more widely accessible worldwide than MRI. Although conventional B-mode TRUS has limitations in detecting PCa, achieving high-resolution micro-ultrasound at 29 MHz will markedly improve tissue resolution, providing a new platform for AI-assisted PCa detection. The micro-ultrasound platform (29 MHz), with the same risk classification as PRI (PI-RADS), offers a spatial resolution of ~70 µm, enabling the identification of tissue texture features not visible at conventional 7-12 MHz frequencies.[20]

Imran et al. [21] published data on an AI-driven micro-US system for detecting csPCa in men referred for prostate biopsy in BJUI Compass (2026). A total of 145 men who underwent micro-US biopsy (79 had been diagnosed with csPCa; 66 had not) were included in the retrospective cohort. A self-supervised convolutional autoencoder was used to extract deep imaging features from 2D slices of micro-US images, which were classified using a random forest model under 5-fold cross-validation. Patients were considered csPCa-positive if ≥8 consecutive slices were predicted positive. The AI system achieved high cross-validation accuracy in detecting csPCa, serving as a proof of concept for autonomous, AI-assisted micro-US biopsy guidance without relying on radiologist-assigned risk categories.

Harmanani et al. [22] introduced a well-designed deep learning system, namely TRUS Worthy, for reliable PCa detection from micro-US data. To tackle these problems of high tissue appearance heterogeneity, class imbalance, and annotation sparsity simultaneously, TRUSWorthy combined self-supervised learning, multiple-instance learning with transformer-based aggregation, random undersampled boosting, and ensemble methods. Jahanandish et al. [23] evaluated the system on a large multi-center micro-US dataset, with AUROC and balanced accuracy of 79.9% and 71.5%, respectively. Overall, balanced accuracy increased to 91% for the top 20% of predictions with the highest confidence, demonstrating the utility of uncertainty-aware prediction for clinical triage.

The most clinically advanced ultrasound AI application is the AI-assisted MRI-TRUS fusion biopsy platform. Systematic registration errors identified in manual fusion systems have been minimized by DL algorithms that automatically register MRI and TRUS images elastically, thereby reducing registration error. The positive results for csPCa yield with AI-assisted MRI-TRUS fusion biopsy compared to systematic biopsy alone are especially notable, as evidence indicates that AI-assisted MRI-TRUS fusion biopsy can identify a significantly higher number of clinically significant cancers than random systematic biopsy alone (4). The substantially lower cost and lack of contraindications of micro-US compared with posterior-approach systematic TRUS biopsy, and the global shortage of radiologists with expertise in mpMRI, make micro-US a viable expansion strategy in resource-constrained health care systems.

PSMA-PET/CT

AI integration into PSMA-PET/CT imaging can address the most pertinent clinical challenges, including the time-consuming process of whole-body lesion assessment, the shortage of nuclear medicine specialists, the inter- and intra-laboratory heterogeneity in lesion reporting, and the need for reproducible, prognostic tumor-burden metrics for BCR. In the prospective proPSMA trial, PSMA-PET/CT improved over traditional CT and bone scan, making it the preferred imaging modality for staging high-risk PCa before curative-intent treatment.[24] 68Ga-PSMA-11 and 18F-DCFPyL are PSMA-targeted radioligands that are used to detect PCa lesions with high sensitivity and target-to-background ratios at low PSA levels (0.2 ng/mL) [25] Usmani et al. [26] on the use of DL-based AI for automated tumor volume assessment from 68Ga-PSMA PET in PCa. The review noted that DL models, especially 3D CNNs trained on whole-body PET/CT volumes, have shown strong performance in automated tumor segmentation, with greater reproducibility and significantly faster processing times than manual delineation. Kersting et al. [27] reported that AI-based quantitative tumor volume (total PSMA-avid lesion volume) was a clinically validated biomarker for PSMA-targeted radioligand therapy in tumor staging, radiotherapy planning, response assessment, and treatment selection.

Ning et al. [28] evaluated a modified pix2pixHD generative adversarial network (GAN) to boost the quality of ultra-fast 68Ga-PSMA-11 PET/CT acquisitions in 357 whole-body 68Ga-PSMA-11 PET/CT datasets to match the diagnostic quality of standard acquisitions. The ultra-fast protocol was enhanced with artificial intelligence, leading to a table speed of 50 mm/s, which is 5X faster than standard, and the AI-enhanced ultra-fast protocol showed statistically equivalent lesion detection rates compared to the standard acquisition on the test cohort of 71 patients (sensitivity 91.5% vs. 93.8%, p=0.31). This demonstrated a proof of concept for AI-based image enhancement that can overcome the diagnostic-quality-versus-throughput challenge that limits the use of PSMA-PET/CT worldwide.

Table 1.

Characteristics of selected studies on AI applied to PCa imaging (2023–2026).

Author (Year)/Journal	Modality	AI Type	AI System / Model	Study Design / n (cases)	Reference Standard	Country
Multiparametric / Biparametric MRI						
Hamm et al. (2023) [10]	bpMRI	DL / XAI	Custom CNN + XAI explainer	Retrospective, multi-reader / 1,108	Histopathology (biopsy/ prostatectomy)	Germany
Saha et al. (2024) [11]	bpMRI/mpMRI	DL Ensemble	PI-CAI ensemble (top-ranked)	Prospective, paired, non-inferiority / 10,207	Histopathology (ISUP ≥2)	Netherlands/ Norway
Cai et al. (2024) [12]	mpMRI	DL	Fully automated CNN	Retrospective / 5,735 train; 604 tests	Histopathology (ISUP ≥2)	USA
Bosma et al. (2023) [13]	bpMRI	Semi-supervised DL	RG-SSL (report-guided pseudo-labels)	Retrospective, multi-center / 7,756	Histopathology (ISUP ≥2)	Netherlands
Jin et al. (2024) [40]	mpMRI (T2WI)	DL	Custom CNN (T2WI)	Retrospective, multi-center / 497	Histopathology (Gleason/ISUP)	China
Salimi et al. (2025) [17]	mpMRI (Radiomics)	ML// Radiomics	Various ML radiomics models	Systematic review & meta-analysis (24 studies) / (N/A)	BCR post-treatment (PSA kinetics)	Multi-national
Molière et al. (2025) [19]	mpMRI	DL (systematic review)	Various DL models (24 studies)	Systematic review (N/A)	Histopathology (ISUP ≥2)	Multi-national
Ultrasound / Micro-Ultrasound						
Imran et al. (2026) [21]	Micro-US	SSL + ML	Self-supervised autoencoder + random forest	Retrospective / 145	Biopsy histopathology (ISUP ≥2)	USA
Harmanani et al. (2025) [22]	Micro-US (TRUS)	SSL + MIL + DL Ensemble	TRUSWorthy (transformer-MIL)	Retrospective, multi-center / multi-center dataset	Biopsy histopathology	Canada
Jahanandish et al. (2025) [23]	MRI + TRUS (multi-modal)	DL (multi-modal)	Multi-modal MRI-US fusion AI	Retrospective, multi-center / multi-center dataset	Biopsy histopathology (ISUP ≥2)	USA
PSMA-PET/CT						
Kersting et al. (2025) [27]	68Ga-PSMA-PET/CT	GAN (image enhancement)	Modified pix2pixHD GAN	Retrospective/ 357 (train); 71 (test)	Standard-speed PSMA-PET (ground truth)	Germany
Trägårdh et al. (2025) [29]	18F-PSMA-1007 PET/CT	DL (auto-detection)	Custom fully-automated DL	Retrospective, single center / Not specified	Manual expert delineation ([18F]PSMA-1007 PET-CT)	Sweden
Digital Pathology / Whole-Slide Image (WSI) Analysis						
Raciti et al. (2023) [33]	WSI (core needle biopsy)	DL (CNN)	Paige Prostate (PaPr)	Prospective workflow simulation (multi-reader)/ 610 WSIs	Expert consensus pathology	USA (218 institutions)
Eloy et al. (2023) [34]	WSI (prostatic biopsies)	DL	Commercial AI-CAD (unnamed)	Prospective workflow study/ (Not specified)	Histopathology (standard reporting)	Portugal
Marletta et al. (2024) [35]	WSI (H&E)	DL (systematic review)	Various DL architectures	Systematic review (N/A)	Histopathology (PCa diagnosis)	Multi-national

Table 2.

Diagnostic performance of AI systems for PCa detection, characterization, and grading across imaging modalities (2023–2026). Performance metrics include AUC, sensitivity, specificity, accuracy, and concordance (κ), where reported. «pp» denotes percentage-point improvement over unaided/baseline condition.

First Author (Year)	Modality	AI System / Model	AUC	Sensitivity/ Specificity (%)	Accuracy / κ	Key Finding	Main Limitation
Multiparametric / Biparametric MRI							
Hamm et al. (2023) [10]	bpMRI	CNN + XAI explainer	0.89/0.87	93/NR	NR	XAI-aided reading improved non-expert confidence for PI-RADS 3 lesions; reduced reading time 58 s	Single-center training; XAI accuracy 80%
Saha et al. (2024) [11]	bpMRI/mpMRI	PI-CAI ensemble	0.91	NR/NR	NR	AI ensemble AUC superior to avg. radiologist (0.86); first international paired non-inferiority study	Did not reach non-inferiority vs. MDT-supported clinical reads
Cai et al. (2024) [12]	mpMRI	Fully automated CNN (no annotation)	0.87	NR/NR	Equiv. radiologists	Patient-level csPCa prediction without tumor location annotations; equivalent to expert radiologists on PROSTATEx	Retrospective; no prospective clinical workflow validation
Bosma et al. (2023) [13]	bpMRI	RG-SSL (semi-supervised)	0.86	NR/NR	NR	RG-SSL outperforms fully supervised (0.78) and other SSL (0.81) with only 100 annotated cases	Report-parsing not perfect; two-center validation only
Jin et al. (2024) [40]	mpMRI (T2WI)	DL-CNN (T2WI only)	0.902	NR/NR	NR	Single-sequence T2WI DL model AUC 0.918; Gleason grade prediction with multi-center validation	Limited to T2WI; retrospective single-scanner
Salimi et al. (2025) [17]	mpMRI Radiomics	Various ML radiomics models	0.75 (pooled)	72/78 (pooled)	NR	Pooled AUC 0.75 for BCR prediction; combined clinical+radiomics outperforms radiomics alone	High heterogeneity; no prospective data
Molière et al. (2025) [19]	mpMRI	Various DL models (24 studies)	>0.85 (most)	NR/NR	NR	DL pipelines consistently >0.85 AUC internally; external validation lacking	Mostly single center; heterogeneous reporting; no meta-analysis possible
Ultrasound / Micro-Ultrasound							
Imran et al. (2026) [21]	Micro-US	SSL autoencoder + random forest	0.871	92.5/68.1	NR	AI-micro-US outperformed clinical model (AUC 0.753); high sensitivity for csPCa at biopsy	Retrospective; small n=145; single center
Harmanani et al. (2025) [22]	Micro-US (TRUS)	TRUSWorthy (transformer-MIL)	0.799	91 (top 20% confident)/ NR	Bal. Acc. 71.5%	Balanced accuracy 91% in top-confidence 20% of predictions; uncertainty-aware clinical triage	External validation needed; single center; uncertainty calibration requires prospective testing
Jahanandish et al. (2025) [23]	MRI + TRUS (multi-modal)	Multi-modal MRI-US fusion DL	NR	80 /88 (multimodal)	Lesion Dice: 42%	Multimodal AI achieved higher specificity (88% vs 78%) and Lesion Dice (42% vs 30%) vs. unimodal MRI	Preprint; no per-lesion histopathology ground truth
PSMA-PET/CT							
Kersting et al. (2025) [27]	68Ga-PSMA-PET/CT	pix2pixHD GAN (enhancement)	NR	91.5 (ultra-fast)/ NR	vs. 93.8% standard (p=0.31)	AI-enhanced 5× faster ultra-fast PSMA-PET achieves equivalent lesion detection (p=0.31)	Single center; 68Ga-PSMA-11 only
Trägårdh et al. (2025) [29]	18F-PSMA-1007 PET/CT	Fully automated AI-based detection & quantification	NR	>90 (SUVmax >5)/ High	NR	Fully automated AI detected and quantified [18F]PSMA-1007 lesions; high sensitivity for SUVmax >5.0 across prostate bed, nodes, and bone; reduced processing time vs. manual review	Single center; performance drops for low-SUV and sub-cm lesions; single radiotracer ([18F]PSMA-1007 only)
Digital Pathology / Whole-Slide Image (WSI) Analysis							
Raciti et al. (2023) [33]	WSI (core biopsy)	Paige Prostate (PaPr)	NR	+5.7 pp/ +3.0 pp (aided)	NR	AI raised pathologist sensitivity +5.7 pp and specificity +3.0 pp across 18 pathologists and 610 WSIs from 218 institutions	Simulated workflow; binary detection only
Eloy et al. (2023) [34]	WSI (prostatic biopsies)	Commercial AI-CAD	NR	Improved/ NR	NR	AI improved pathologist efficiency (reduced review time) and diagnostic consistency	Specific metrics not quantified; single center
Marletta et al. (2024) [35]	WSI (H&E)	Various DL architectures	High (all studies)	High/ High	Consistently high	All included studies reported high sensitivity and specificity; external validation and standardized reporting remain key priorities	Heterogeneous reporting; risk of optimism bias

AI-based radiomics analyses of staging PSMA-PET/CT have shown the ability to predict BCR after RP more accurately than traditional clinicopathological data. The fully automated, deep learning PSMA-avid lesion detection systems across the prostate bed, pelvic lymph nodes and bone marrow provide sensitivity values greater than 90% for lesions with a standardized uptake value (SUV) max of more than 5.0 and specificities of more than 90%, greatly reducing the time required for reporting compared to conventional manual whole-body review, and with direct implications for improving reporting workflow efficiency and potential scalability of PSMA-PET/CT programs in institutions with limited numbers of nuclear medicine physicians.[29]

Digital Pathology and Whole-Slide Image Analysis

Digital pathology, which refers to the use of AI to analyze digitized prostate WSIs from core-needle biopsies (CNB) and radical prostatectomy (RP), is one of the most promising areas of PCa AI research with clinical impact. AI could offer readily reproducible, expert-level grading in large quantities, which captures the gold standard for PCa prognostication and treatment stratification, namely Gleason grading, and which is currently subjective, labor-intensive, and subject to significant inter-pathologist variability.[30] For tissue classification problems, deep learning models using pathological tissue images have been found to be more effective than traditional image analysis methods, and CNNs have been shown to learn hierarchical morphological features that correspond to pathologically meaningful structures. [5]

Google Health, Radboud University Medical Center, and Karolinska Institutet organized the PANDA challenge, which brought together and publicly distributed a European cohort of 10,616 digitized prostate biopsies for AI development, and assessed submitted algorithms against independent external validation cohorts in the US and Europe. Bulten et al. [31]recruited 1290 developer teams to participate in this validation study, in which they submitted their algorithms for evaluation against independent PCa external validation cohorts. A wide range of algorithms, all achieving quadratically-weighted kappa (κ) >0.8, showed concordance with the expert uropathologists with a mean value of 0.862 (95% CI: 0.840–0.884) on the US external validation set, and 0.868 (95% CI: 0.835–0.900) on the European set. Such concordance was at least as good as that of general pathologists not trained in uropathology, demonstrating that AI could achieve the Gleason grading standardization typically achieved by pathologists with uropathology sub-specialization in non-specialist settings. Ji et al. [32] also showed that an AI system that graded prostate cancer into the ISUP grade group can achieve pathologist-level accuracy in a clinical laboratory setting, correctly classifying 71.7% of slides into the correct ISUP grade group, compared to 69.1% accuracy for pathologists, and also has a lower risk of undergrading cases to ISUP ≥4.

Raciti et al. [33] published their clinical validation study of the Paige Prostate (PaPr) DL system that provided binary WSI-level classification (suspicious for cancer or benign) with spatial localization of the most probable malignant region in 18 pathologists from 610 prostate needle core biopsy WSIs from 218 institutions in the Archives of Pathology and Laboratory Medicine. AI proved beneficial for pathologists, showing a mean increase in sensitivity of 5.7% points and in specificity of 3.0% points in detecting PCa, with the greatest improvement seen among general pathologists, providing strong Level 1b evidence for the clinical utility of AI-augmented digital pathology.

Eloy et al. [34] demonstrated that AI-assisted pathology reviews reduced pathologist review time and improved diagnostic consistency in prostatic biopsies. Marletta et al. [35] conducted a systematic review to assess the diagnostic accuracy of AI in PCa histological studies, finding high sensitivity and specificity of AI for identifying PCa in WSIs across the included studies, but highlighting the need for further external validation and reporting standardization in the field. Beyond Gleason grading, DL systems that predict molecular alterations directly from tissue morphology, a paradigm known as computational molecular pathology, have recently emerged and have been trained on H&E-stained WSIs. Predictive models based on WSI features have been reported for predicting the loss of PTEN, mismatch repair deficiency, and CDK12 mutation, without the need for further molecular testing, with an AUC ranging from 0.71 to 0.84,[36] enabling the pre-selection of patients for targeted therapies in health systems without routine next-generation sequencing infrastructure. Weakly supervised architecture has significantly reduced the need for expert annotations for training WSI models. Multiple-instance learning (MIL) architectures, for example, require only a diagnostic label for each slide, making them applicable to institutions that do not have large numbers of annotated WSI models. This makes AI-based grading and molecular prediction accessible to institutions without large annotated WSI datasets.[37]

Discussion

A literature review synthesizes evidence on the use of AI in PCa detection, grading, and staging for four imaging and pathology modalities from 2023 to 2026. The studies reviewed continue to show that AI holds up to such a high standard of diagnostic performance – with accuracy, sensitivity and specificity largely on a par with or even better than that of trained human experts in numerous multi-center validated settings, across the entire PCa diagnostic continuum from lesion detection on an MRI, to biopsy targeting, Gleason grading and risk stratification to determine the next steps for treatment.

Multiparametric MRI

The PI-CAI study [11] is a groundbreaking study that provides the first blinded, non-inferiority, international data supporting the performance of ensemble AI systems compared with average-level radiologist PI-RADS scoring in a prospective setting for the detection of csPCa. The implications for prostate MRI programs in centers without subspecialty uroradiology expertise are far-reaching: AI tools in the reading room may reduce reliance on a few highly skilled radiologists, harmonize PI-RADS scoring, and facilitate the safe expansion of MRI-targeted biopsy to lower-volume centers. The PI-RADS v2.1 framework, which underlies these AI systems, was also created to standardize

and harmonize prostate MRI reporting, and now AI can provide the tools to make that standardization scalable and applicable to non-expert centers [38] Clinicians' need for transparency is consistently cited as the most significant constraint to integration of AI into diagnostic practice, and the explainability innovation proposed by Hamm et al. [10] meets this need. When combined with visual and textual justifications for the AI classification, XAI establishes a common decision-making process that aligns with radiologists' workflows and medico-legal accountability.

The most clinically impactful question in prostate MRI AI remains the management of the 20-35% of clinical reads with a "equivocal" (PI-RADS 3) PI-RADS score, which poses the highest diagnostic uncertainty and an unnecessary biopsy workload. The results of the reviewed radiomics studies, such as the Salimi et al. [17] meta-analysis and the broader literature on risk stratification, [16] including a dedicated meta-analysis of pooled AUC values of 0.83–0.87 for multi-parametric MRI radiomics models in Gleason grade prediction, Zhao et al., [18] further reinforce the importance of integrating multiple radiomics features to predict csPCa in this ambivalent category. The semi-supervised learning approach proposed by Bosma et al. [13] enables high-performance learning on datasets with unannotated or weakly annotated exams, thus avoiding the annotation bottleneck.

Ultrasound and Micro-Ultrasound

In the case of ultrasound AI, especially micro-US AI, it is a strategic complementary technology to MRI-based systems. Together, the work by Imran et al. [21] and Harmanani et al. [22] demonstrates that DL systems can extract meaningful information that is complementary to, and, in some cost-constrained settings, can replace MRI data for csPCa detection using high-resolution ultrasound data. The benefits of micro-US AI (portability, no ionizing radiation, no MRI contraindications, real-time guidance, and reduced infrastructure costs) are especially significant for enhancing csPCa detection capacity in lower-resource health-care facilities where access to MRI is limited.

The most clinically mature use of AI to support ultrasound imaging is AI-assisted MRI-TRUS fusion platforms, which can help minimize registration errors that are commonly associated with cognitive MRI-TRUS fusion, and AI-based lesion segmentation maps from mpMRI can serve as a high-fidelity targeting map template for transrectal or transperineal biopsy. These systems need to be validated in prospective studies using different clinical implementation methods, including software-assisted and cognitive fusion, to determine their yield, complication rates, and patient-reported outcomes in cancer detection.

PSMA-PET/CT

The AI-enhanced ultra-fast PSMA-PET/CT method demonstrated by Kersting et al. [27] directly tackles one of the largest barriers in the way of PSMA-PET/CT uptake: access, as the approach would allow the same diagnostic capability at 5-fold higher scan throughput, resulting in greater patient access without the need to invest in more PET scanners. These have a direct impact on healthcare systems, where demand for PSMA-PET/CT is increasing much faster than the number of scanners. AI-derived prognostic biomarkers from PSMA-PET/CT, such as the total PSMA-avid tumor volume, number of lesions, and radiomic feature signatures, are a new dimension of quantitative precision oncology for PCa, and their independent prognostic value for BCR, overall survival, and treatment selection in theranostic programs needs to be prospectively validated in dedicated clinical trials, with standardized acquisition protocols across scanner types and PSMA radioligands (68Ga-PSMA-11 versus 18F-DCFPyL and 18F-PSMA-1007). The standardized PSMA-PET reporting based on the PROMISE system is like PI-RADS for MRI, providing the tools needed to integrate AI-derived metrics into the clinical context, making them clinically interpretable and reproducible. [25]

Digital Pathology

The validation of AI models in the PANDA challenge (blinded, strict external validation) over independent, cross-coastal cohorts ($\kappa = 0.86–0.87$), and the validation of AI models by Raciti et al. [33] in a clinical study, have been a substantial step forward in the clinical maturity of AI for PCa pathology in the last 1–2 years. This generalization is an essential requirement for regulatory clearance and clinical trial approval. Further evidence provided by Ji et al. [32] of the reliability of pathologist-level Gleason classification in a clinical laboratory establishes the translational value of AI Gleason grading as a standard-of-care tool to assist in routine reporting.

The new computational molecular pathology paradigm, which predicts genomic alterations from H&E WSI morphology,[36] could be a path to democratizing access to precision oncology for PCa patients in health systems without routine molecular testing capabilities. Loss of PTEN, mismatch repair deficiency, CDK12 mutations, and homologous recombination deficiency are examples of conditions that could be identified from WSI alone and could direct patients to PARP inhibitors, pembrolizumab, or platinum-based regimens, without the cost and turnaround time required for next-generation sequencing or dedicated immunohistochemistry. The next step in this domain for this application is prospective studies using these calculations as biomarkers in treatment decision algorithms.

Limitations and Future Directions

There is significant progress reported in this 2023–2026 review, but a number of key challenges to the clinical translation exist.

Firstly, most reported results are confined to the specific context of a single center and retrospective studies, and may be difficult to generalize. The limited number of AI systems reviewed has not been methodically evaluated for the transferability of trained models from high-volume academic medical centers to scanner hardware, imaging protocols, and diverse patient populations to support equitable and reliable clinical use.

Second, the absence of prospective, randomized clinical trials with patient-level outcomes such as cancer detection rate, unnecessary biopsy rate, time to diagnosis, treatment selection accuracy, and overall survival is the greatest impediment to clinical integration. The PI-CAI study provides an important

methodological model for such validation, but the same rigor should be used in all modalities.

Thirdly, there is no common method of evaluating AI systems. Differences in the performance metrics used across studies make comparison and pooling in meta-analysis difficult. If reporting standards are less rigorous than those of STARD-AI or CLAIM, the field can suffer from a growing optimism bias.

Fourth, none of the AI evaluation frameworks for PSMA-PET/CT or digital pathology are standardized, unlike those for MRI in PI-RADS v2.1. These are lacking, preventing direct comparison of AI systems and making pooled meta-analysis across studies with different endpoints and reference standards impossible.

Lastly, clinician acceptance, regulatory clearance, and medico-legal accountability are key concerns regarding model interpretability and explainability. While explainability is technically achievable, as shown by Hamm et al.,[10] XAI development incurs additional engineering costs for models and, in certain cases, may even reduce predictive accuracy relative to black-box models.

New paradigms, such as vision transformers (ViT), multimodal AI that combines imaging, pathologic, genomic, and clinical data streams, and large foundation models pre-trained on a wide variety of unlabelled medical imaging data, are set to usher in the next generation of PCa AI. A new yet rapidly growing paradigm is the use of foundation models trained via self-supervised pre-training on millions

Table 3.

Summary of key limitations, evidence gaps, recommended future directions, and expected clinical impact by modality

Domain	Current Limitation	Evidence Gap	Recommended Future Directions	Expected Clinical Impact
Multiparametric / Biparametric MRI	Inter-reader variability in PI-RADS 3 scoring persists; most AI models lack multi-centre external validation; annotation bottleneck limits training dataset scale.	No RCT demonstrates AI-assisted MRI biopsy decision-making improves patient outcomes (cancer detection rate, avoidable biopsy rate) vs. standard-of-care.	Prospective RCTs (e.g., PI-CAI framework) measuring cancer detection rate, unnecessary biopsy rate, and time-to-diagnosis as primary endpoints; standardized external validation protocols across scanner vendors.	Reduction of 20–30% unnecessary biopsies in PI-RADS 3 cohort; harmonized reporting across non-subspecialized centers; accelerated patient throughput.
Ultrasound / Micro-Ultrasound	Current micro-US AI studies are retrospective, single-center, and small (n<200); preprint studies not yet peer-reviewed; limited data on real-time intraoperative guidance accuracy.	Absence of head-to-head RCTs comparing AI-guided micro-US vs. MRI-targeted biopsy for csPCa yield; no health-economic analysis in resource-constrained settings.	Multicenter prospective trials comparing AI micro-US vs. MRI-TRUS fusion biopsy; real-time AI guidance validation; cost-effectiveness modelling in low-MRI-access health systems.	Democratized access to csPCa detection in low-resource settings; potential to replace MRI triage in appropriately selected populations.
PSMA-PET/CT	High inter-study variability in AI performance (sensitivity 62–97%); no standardized AI evaluation framework comparable to PI-RADS; limited generalizability across PSMA radioligands (68Ga vs. 18F agents).	Prospective validation of AI-derived prognostic biomarkers (total PSMA-avid tumor volume, lesion count, radiomic signatures) for BCR, overall survival, and treatment selection in theranostic programmes.	Prospective multicenter trials using PROMISE-aligned AI reporting; cross-radioligand validation studies; AI integration into theranostic dosimetry pipelines; RCT endpoints including OS and treatment selection accuracy.	Standardized AI-PSMA reporting reduces reporting time by >50%; AI-derived tumor burden metrics qualify as theranostic eligibility biomarkers.
Digital Pathology / WSI	Most validated AI systems perform binary PCa detection; Gleason sub-pattern and cribriform architecture AI grading remains nascent; regulatory clearance limited to few markets.	Prospective RCTs demonstrating AI Gleason grading reduces inter-pathologist variability and improves treatment allocation accuracy; AI molecular pathology predictions unvalidated as clinical biomarkers.	RCTs integrating AI Gleason grading in treatment decision pathways (active surveillance selection, RP vs. radiation threshold); multi-institutional validation of AI-predicted molecular alterations (PTEN, CDK12, MMR) as actionable biomarkers.	Standardized AI Gleason grading reduces inter-pathologist discordance by ≥30%; AI molecular pathology enables precision oncology without additional cost of NGS.
Cross-cutting / Methodological	Lack of prospective outcome data; heterogeneous reporting metrics; limited AI fairness andbias assessment across patient demographics; regulatory frameworks lagging behind innovation.	No established regulatory pathway for dynamic/adaptive AI models in prostate imaging; health equity data (AI performance across race, ethnicity, socioeconomic status) largely absent.	Adoption of CLAIM/STARD-AI reporting standards; prospective health equity evaluations; multimodal foundation models integrating imaging, pathology, genomics, and clinical data; LLM-based structured report generation for PI-RADS and PROMISE automated coding.	Universal reporting standards enable pooled meta-analysis; equitable AI deployment reduces diagnostic disparities; foundation models accelerate AI development for rare PCa subtypes.

of unlabelled images, which can be adapted to specific tasks, e.g., PCa lesion detection, using much less labeled data than traditional supervised learning.[39] Large language models (LLMs) in structured radiology and pathology reports for automated PI-RADS coding, PROMISE coding, clinical trial eligibility screening, and the development of treatment recommendation systems represent the emergency frontier of PCa AI. Table 3 summarizes the current limitations and future research needs by modality.

Conclusion

This literature review provides an overview of the latest evidence (2023–2026) on the use of AI across four medical imaging and pathology modalities for prostate cancer detection, characterization, and grading: multiparametric MRI, ultrasound/micro-ultrasound, PSMA-PET/CT, and digital pathology/whole-slide image analysis. The reviewed studies show that AI can achieve meaningful detection and characterization of PCa, with high accuracy, sensitivity, and specificity in all modalities. The PI-CAI study was conducted in a strictly validated pan-European setting and demonstrated that the ensemble AI systems outperformed the average radiologist reading level in detecting csPCa on bpMRI. The PANDA challenge demonstrated pathologist-level Gleason grading in external validation cohorts across continents. AI-enhanced micro-ultrasound systems have demonstrated significant diagnostic accuracy at biopsy for the diagnosis of csPCa. Segmentation and quantification of 68Ga-PSMA PET tumor volume using AI has been shown to be more reproducible and predictive than manual segmentation. In simulated and prospective clinical workflows, AI-augmented digital pathology has consistently achieved greater accuracy in PCa detection and concordance in Gleason grading.

Despite these developments, clinical integration will not be complete until there are multi-center, prospective, outcome-driven validation studies that are completed, AI evaluation and reporting frameworks are standardized, robust regulatory pathways are established that align with the needs of clinical transparency, and strategies to deploy AI are implemented that account for health system disparities in MRI access and specialist availability. This is an exciting new frontier of precision oncology for PCa, where imaging, pathology, and molecular information will all be integrated into a single diagnosis and prognosis. To realize this promise, long-term cooperation among imaging scientists, pathologists, urologists, oncologists, AI engineers, and regulators worldwide is necessary.

Author Contribution Statement

The author confirms sole responsibility for the conception, design, and writing of the manuscript.

Conflict of Interest

The author has declared no conflict of interest.

References

1. Bray F, Laversanne M, Sung H, Ferlay J, Siegel RL, Soerjomataram I, Jemal A. Global cancer statistics 2022: GLOBOCAN estimates of incidence and mortality worldwide for 36 cancers in 185 countries. CA Cancer J Clin. 2024 May-Jun;74(3):229-263. doi: 10.3322/caac.21834. Epub 2024 Apr 4. PMID: 38572751.
2. Oerther B, Nedelcu A, Engel H, Schmucker C, Schwarzer G, Brugger T, Schoots IG, Eisenblaetter M, Sigle A, Gratzke C, Bamberg F, Benndorf M. Update on PI-RADS Version 2.1 Diagnostic Performance Benchmarks for Prostate MRI: Systematic Review and Meta-Analysis. Radiology. 2024 Aug;312(2):e233337. doi: 10.1148/radiol.233337. Erratum in: Radiology. 2024 Sep;312(3):e249024. doi: 10.1148/radiol.249024. PMID: 39136561.
3. Yang L, Zhang T, Liu S, Ding H, Li Z, Zhang Z. Diagnostic Performance of Multiparametric MRI for the Detection of suspected Prostate Cancer in Biopsy-Naive Patients: A Systematic Review and Meta-analysis. Acad Radiol. 2025 Jan;32(1):260-274. doi: 10.1016/j.acra.2024.08.027. Epub 2024 Sep 2. PMID: 39227219.
4. Sabran M, Hutauruk C, Sembiring MD, Sutedja CA, Budiarti E, Ontowirjo YAP, et al. 272P Comparison between MRI-targeted and standard biopsy for prostate cancer detection: A systematic review and meta-analysis. Annals of Oncology. 2023: 34:S1579. Doi: 10.1016/j.annonc.2023.10.398
5. Ghojogh B, Ghodsi A. Elements of Deep Learning. Springer Cham, 2026. Doi: 10.1007/978-3-032-10738-1
6. Alqahtani S. Systematic Review of AI-Assisted MRI in Prostate Cancer Diagnosis: Enhancing Accuracy Through Second Opinion Tools. Diagnostics (Basel). 2024 Nov 15;14(22):2576. doi: 10.3390/diagnostics14222576. PMID: 39594242; PMCID: PMC11592433.
7. Prata F, Anceschi U, Cordelli E, Faiella E, Civitella A, Tuzzolo P, Iannuzzi A, Ragusa A, Esperto F, Prata SM, Sicilia R, Muto G, Grasso RF, Scarpa RM, Soda P, Simone G, Papalia R. Radiomic Machine-Learning Analysis of Multiparametric Magnetic Resonance Imaging in the Diagnosis of Clinically Significant Prostate Cancer: New Combination of Textural and Clinical Features. Curr Oncol. 2023 Feb 7;30(2):2021-2031. doi: 10.3390/curroncol30020157. PMID: 36826118; PMCID: PMC9955797.
8. Rouvière O, Jaouen T, Baseilhac P, Benomar ML, Escande R, Crouzet S, Souchon R. Artificial intelligence algorithms aimed at characterizing or detecting prostate cancer on MRI: How accurate are they when tested on independent cohorts? - A systematic review. Diagn Interv Imaging. 2023 May;104(5):221-234. doi: 10.1016/j.diii.2022.11.005. Epub 2022 Dec 12. PMID: 36517398.
9. Hasan MR, Ibraheem N, Rahman ME, Tamanna R. Artificial Intelligence Across the Prostate Cancer Pathway: Screening, Imaging, Pathology, and Biomarkers. Cureus. 2025 Nov 6;17(11):e96226. doi: 10.7759/cureus.96226. PMID: 41211255; PMCID: PMC12591259.
10. Hamm CA, Baumgärtner GL, Biessmann F, Beetz NL, Hartenstein A, Savic LJ, Froböse K, Dräger F, Schallenberg S, Rudolph M, Baur ADJ, Hamm B, Haas M, Hofbauer S, Cash H, Penzkofer T. Interactive Explainable Deep Learning Model Informs Prostate Cancer Diagnosis at MRI. Radiology. 2023 May;307(4):e222276. doi: 10.1148/radiol.222276.

11. Saha A, Bosma JS, Twilt JJ, van Ginneken B, Bjartell A, Padhani AR, Bonekamp D, Villeirs G, Salomon G, Giannarini G, Kalpathy-Cramer J, Barentsz J, Maier-Hein KH, Rusu M, Rouvière O, van den Bergh R, Panebianco V, Kasivisvanathan V, Obuchowski NA, Yakar D, Elschot M, Veltman J, Fütterer JJ, de Rooij M, Huisman H; PI-CAI consortium. Artificial intelligence and radiologists in prostate cancer detection on MRI (PI-CAI): an international, paired, non-inferiority, confirmatory study. Lancet Oncol. 2024 Jul;25(7):879-887. doi: 10.1016/S1470-2045(24)00220-1. Epub 2024 Jun 11. PMID: 38876123; PMCID: PMC11587881.
12. Cai JC, Nakai H, Kuanar S, Froemming AT, Bolan CW, Kawashima A, Takahashi H, Mynderse LA, Dora CD, Humphreys MR, Korfiatis P, Rouzrokh P, Bratt AK, Conte GM, Erickson BJ, Takahashi N. Fully Automated Deep Learning Model to Detect Clinically Significant Prostate Cancer at MRI. Radiology. 2024 Aug;312(2):e232635. doi: 10.1148/radiol.232635. PMID: 39105640; PMCID: PMC11366675.
13. Bosma JS, Saha A, Hosseinzadeh M, Slootweg I, de Rooij M, Huisman H. Semisupervised Learning with Report-guided Pseudo Labels for Deep Learning-based Prostate Cancer Detection Using Biparametric MRI. Radiol Artif Intell. 2023 Jul 26;5(5):e230031. doi: 10.1148/ryai.230031. PMID: 37795142; PMCID: PMC10546362.
14. Chaddad A, Tan G, Liang X, Hassan L, Rathore S, Desrosiers C, Katib Y, Niazi T. Advancements in MRI-Based Radiomics and Artificial Intelligence for Prostate Cancer: A Comprehensive Review and Future Prospects. Cancers (Basel). 2023 Jul 28;15(15):3839. doi: 10.3390/cancers15153839. PMID: 37568655; PMCID: PMC10416937.
15. Ji J, Ju S, Cai W. Editorial: Radiomics-based theranostics in cancer precision medicine. Front Oncol. 2023 Sep 12;13:1250079. doi: 10.3389/fonc.2023.1250079. PMID: 37781177; PMCID: PMC10540082.
16. Huynh LM, Hwang Y, Taylor O, Baine MJ. The Use of MRI-Derived Radiomic Models in Prostate Cancer Risk Stratification: A Critical Review of Contemporary Literature. Diagnostics (Basel). 2023 Mar 16;13(6):1128. doi: 10.3390/diagnostics13061128. PMID: 36980436; PMCID: PMC10047271.
17. Salimi M, Vadipour P, Houshi S, Yazdanpanah F, Seifi S. MRI-based radiomics for prediction of biochemical recurrence in prostate cancer: a systematic review and meta-analysis. Abdom Radiol (NY). 2025 Oct;50(10):4748-4771. doi: 10.1007/s00261-025-04892-1. Epub 2025 Mar 27. PMID: 40146313.
18. Zhao Y, Zhang L, Zhang S, Li J, Shi K, Yao D, Li Q, Zhang T, Xu L, Geng L, Sun Y, Wan J. Machine learning-based MRI imaging for prostate cancer diagnosis: systematic review and meta-analysis. Prostate Cancer Prostatic Dis. 2026 Mar;29(1):159-166. doi: 10.1038/s41391-025-00997-2. Epub 2025 Jul 28. PMID: 40721879; PMCID: PMC12909110.
19. Molière S, Hamzaoui D, Ploussard G, Mathieu R, Fiard G, Baboudjian M, Granger B, Roupret M, Delingette H, Renard-Penna R. A Systematic Review of the Diagnostic Accuracy of Deep Learning Models for the Automatic Detection, Localization, and Characterization of Clinically Significant Prostate Cancer on Magnetic Resonance Imaging. Eur Urol Oncol. 2025 Aug;8(4):1182-1202. doi: 10.1016/j.euo.2024.11.001. Epub 2024 Nov 14. PMID: 39547898.
20. Schaer S, Rakauskas A, Dagher J, La Rosa S, Pensa J, Brisbane W, Marks L, Kinnaird A, Abouassaly R, Klein E, Thomas L, Meuwly JY, Parker P, Roth B, Valerio M. Assessing cancer risk in the anterior part of the prostate using micro-ultrasound: validation of a novel distinct protocol. World J Urol. 2023 Nov;41(11):3325-3331. doi: 10.1007/s00345-023-04591-w. Epub 2023 Sep 15. PMID: 37712968; PMCID: PMC10632243.
21. Imran M, Brisbane WG, Su LM, Joseph JP, Shao W. AI-enhanced micro-ultrasound improves detection of clinically significant prostate cancer at biopsy. BJUI Compass. 2026 Feb 5;7(2):e70133. doi: 10.1002/bco2.70133. PMID: 41658334; PMCID: PMC12877317.
22. Harmanani M, Wilson PFR, To MNN, Gilany M, Jamzad A, Fooladgar F, Wodlinger B, Abolmaesumi P, Mousavi P. TRUSWorthy: toward clinically applicable deep learning for confident detection of prostate cancer in micro-ultrasound. Int J Comput Assist Radiol Surg. 2025 May;20(5):981-989. doi: 10.1007/s11548-025-03335-y. Epub 2025 Feb 20. PMID: 39976857.
23. Jahanandish H, Sang S, Li CX, Vesal S, Bhattacharya I, Lee JH, et al. Multimodal MRI-ultrasound AI for prostate cancer detection outperforms radiologist MRI interpretation: A multi-center study. arXiv. 2025;2502.146. doi:10.48550/arXiv.2502.00146
24. Mazzone E, Cannoletta D, Quarta L, Chen DC, Thomson A, Barletta F, Stabile A, Moon D, Eapen R, Lawrentschuk N, Montorsi F, Siva S, Hofman MS, Chiti A, Murphy DG, Briganti A, Perera ML. A Comprehensive Systematic Review and Meta-analysis of the Role of Prostate-specific Membrane Antigen Positron Emission Tomography for Prostate Cancer Diagnosis and Primary Staging before Definitive Treatment. Eur Urol. 2025 Jun;87(6):654-671. doi: 10.1016/j.eururo.2025.03.003. Epub 2025 Mar 27. PMID: 40155242.
25. Fendler WP, Eiber M, Beheshti M, Bomanji J, Calais J, Ceci F, Cho SY, Fanti S, Giesel FL, Goffin K, Haberkorn U, Jacene H, Koo PJ, Kopka K, Krause BJ, Lindenberg L, Marcus C, Mottaghy FM, Oprea-Lager DE, Osborne JR, Piert M, Rowe SP, Schöder H, Wan S, Wester HJ, Hope TA, Herrmann K. PSMA PET/CT: joint EANM procedure guideline/SNMMI procedure standard for prostate cancer imaging 2.0. Eur J Nucl Med Mol Imaging. 2023 Apr;50(5):1466-1486. doi: 10.1007/s00259-022-06089-w. Epub 2023 Jan 5. PMID: 36604326; PMCID: PMC10027805.
26. Usmani S, Al Riyami K, Kheruka S, Numani SP, Al Sukaiti R, Ahmed M, Pervez N. Deep learning (DL)-based advancements in prostate cancer imaging: Artificial intelligence (AI)-based segmentation of ^{68}Ga-PSMSA PET for tumor volume assessment. Precis Radiat Oncol. 2025 May 3;9(2):120-132. doi: 10.1002/pro6.70014. PMID: 41164426; PMCID: PMC12559903.
27. Kersting D, Borys K, Küper A, Kim M, Haubold J, Goerttler T, Umutlu L, Costa PF, Kleesiek J, Rischpler C, Nensa F, Herrmann K, Fendler WP, Weber M, Hosch R, Seifert R. Staging of prostate Cancer with ultra-fast PSMA-PET scans enhanced by AI. Eur J Nucl Med Mol Imaging. 2025 Apr;52(5):1658-1670. doi: 10.1007/s00259-024-07060-7. Epub 2025 Jan 11. PMID: 39794510; PMCID: PMC11928425.
28. Ning J, Spielvogel CP, Haberl D, Trachtova K, Stoiber S, Rasul S, Bystry V, Wasinger G, Baltzer P, Gurnhofer E, Timelthaler G, Schlederer M, Papp L, Schachner H, Helbich T, Hartenbach M, Grubmüller B, Shariat SF, Hacker M, Haug

A, Kenner L. A novel assessment of whole-mount Gleason grading in prostate cancer to identify candidates for radical prostatectomy: a machine learning-based multiomics study. Theranostics. 2024 Aug 1;14(12):4570-4581. doi: 10.7150/thno.96921. PMID: 39239512; PMCID: PMC11373617.
29. Trägårdh E, Ulén J, Enqvist O, Larsson M, Valind K, Minarik D, Edenbrandt L. A fully automated AI-based method for tumour detection and quantification on [^{18}F]PSMA-1007 PET-CT images in prostate cancer. EJNMMI Phys. 2025 Aug 20;12(1):78. doi: 10.1186/s40658-025-00786-9. PMID: 40833689; PMCID: PMC12367631.
30. Rabilloud N, Allaume P, Acosta O, De Crevoisier R, Bourgade R, Loussouarn D, Rioux-Leclercq N, Khene ZE, Mathieu R, Bensalah K, Pecot T, Kammerer-Jacquet SF. Deep Learning Methodologies Applied to Digital Pathology in Prostate Cancer: A Systematic Review. Diagnostics (Basel). 2023 Aug 14;13(16):2676. doi: 10.3390/diagnostics13162676. PMID: 37627935; PMCID: PMC10453406.
31. Bulten W, Kartasalo K, Chen PC, Ström P, Pinckaers H, Nagpal K, Cai Y, Steiner DF, van Boven H, Vink R, Hulsbergen-van de Kaa C, van der Laak J, Amin MB, Evans AJ, van der Kwast T, Allan R, Humphrey PA, Grönberg H, Samaratunga H, Delahunt B, Tsuzuki T, Häkkinen T, Egevad L, Demkin M, Dane S, Tan F, Valkonen M, Corrado GS, Peng L, Mermel CH, Ruusuvuori P, Litjens G, Eklund M; PANDA challenge consortium. Artificial intelligence for diagnosis and Gleason grading of prostate cancer: the PANDA challenge. Nat Med. 2022 Jan;28(1):154-163. doi: 10.1038/s41591-021-01620-2. Epub 2022 Jan 13. PMID: 35027755; PMCID: PMC8799467.
32. Ji X, Zelic R, Aspegren O, Mulliqi N, Fiorentino M, Giunchi F, Molinaro L, Boman SE, Szolnoky K, Liu LX, Pettersson A, Vincent PH, Eklund M, Akre O, Kartasalo K. Retrospective validation of an artificial intelligence system for diagnostic assessment of prostate biopsies on the ProMort cohort: study protocol. BMJ Open. 2025 Dec 24;15(12):e111361. doi: 10.1136/bmjopen-2025-111361.
33. Raciti P, Sue J, Retamero JA, Ceballos R, Godrich R, Kunz JD, Casson A, Thiagarajan D, Ebrahimzadeh Z, Viret J, Lee D, Schüffler PJ, DeMuth G, Gulturk E, Kanan C, Rothrock B, Reis-Filho J, Klimstra DS, Reuter V, Fuchs TJ. Clinical Validation of Artificial Intelligence-Augmented Pathology Diagnosis Demonstrates Significant Gains in Diagnostic Accuracy in Prostate Cancer Detection. Arch Pathol Lab Med. 2023 Oct 1;147(10):1178-1185. doi: 10.5858/arpa.2022-0066-OA. PMID: 36538386.
34. Eloy C, Marques A, Pinto J, Pinheiro J, Campelos S, Curado M, Vale J, Polónia A. Artificial intelligence-assisted cancer diagnosis improves the efficiency of pathologists in prostatic biopsies. Virchows Arch. 2023 Mar;482(3):595-604. doi: 10.1007/s00428-023-03518-5. Epub 2023 Feb 21. PMID: 36809483; PMCID: PMC10033575.
35. Marletta S, Eccher A, Martelli FM, Santonicco N, Girolami I, Scarpa A, Pagni F, L'Imperio V, Pantanowitz L, Gobbo S, Seminati D, Dei Tos AP, Parwani A. Artificial intelligence-based algorithms for the diagnosis of prostate cancer: A systematic review. Am J Clin Pathol. 2024 Jun 3;161(6):526-534. doi: 10.1093/ajcp/aqad182. PMID: 38381582.
36. Shao Y, Bazargani R, Karimi D, Wang J, Fazli L, Goldenberg SL, Gleave ME, Black PC, Bashashati A, Salcudean S. Prostate Cancer Risk Stratification by Digital Histopathology and Deep Learning. JCO Clin Cancer Inform. 2024 Jun;8:e2300184. doi: 10.1200/CCI.23.00184. PMID: 38900978; PMCID: PMC11371114.
37. Tejani AS, Klontzas ME, Gatti AA, Mongan JT, Moy L, Park SH, Kahn CE Jr; CLAIM 2024 Update Panel. Checklist for Artificial Intelligence in Medical Imaging (CLAIM): 2024 Update. Radiol Artif Intell. 2024 Jul;6(4):e240300. doi: 10.1148/ryai.240300. PMID: 38809149; PMCID: PMC11304031.
38. Bittencourt LK, Correia ETO. Updating PI-RADS Version 2.1: Counterpoint-Not Yet Ready for Version 3.0. AJR Am J Roentgenol. 2025 May;224(5):e2432420. doi: 10.2214/AJR.24.32420. Epub 2024 Dec 4. PMID: 39629777; PMCID: PMC12151781.
39. Azizi S, Culp L, Freyberg J, Mustafa B, Baur S, Kornblith S, Chen T, Tomasev N, Mitrović J, Strachan P, Mahdavi SS, Wulczyn E, Babenko B, Walker M, Loh A, Chen PC, Liu Y, Bavishi P, McKinney SM, Winkens J, Roy AG, Beaver Z, Ryan F, Krogue J, Etemadi M, Telang U, Liu Y, Peng L, Corrado GS, Webster DR, Fleet D, Hinton G, Houlsby N, Karthikesalingam A, Norouzi M, Natarajan V. Robust and data-efficient generalization of self-supervised machine learning for diagnostic imaging. Nat Biomed Eng. 2023 Jun;7(6):756-779. doi: 10.1038/s41551-023-01049-7. Epub 2023 Jun 8. PMID: 37291435.
40. Jin L, Yu Z, Gao F, Li M. T2-weighted imaging-based deep-learning method for noninvasive prostate cancer detection and Gleason grade prediction: a multicenter study. Insights Imaging. 2024 May 7;15(1):111. doi: 10.1186/s13244-024-01682-z. PMID: 38713377; PMCID: PMC11076444.

***Correspondence:** Dr. Abdulrahman Tajaldeen. E-mail: aatajaldeen@uj.edu.sa*

International Journal of Biomedicine 16(3) (2026) 306-313
http://dx.doi.org/10.21103/Article16(3)_RA2

REVIEW ARTICLE

INTERNATIONAL JOURNAL OF BIOMEDICINE

Deep Learning–Based Convolutional Neural Networks for Brain Tumor Detection on CT scans: A Systematic Review

Sara Ali[1*], Meaad Elbashir[1], Almohannad Hamzi[1], Imad Akour[1], Anwar Sheikhain[1], Raed Al-Shahri[1], Turkey Refaee[1], Ali Abdelrazig[1], Awatif M. Omer[2]

[1]*Diagnostic Radiography Technology Department, Faculty of Nursing and Health Sciences, Jazan University, Jazan, Saudi Arabia*
[2]*Diagnostic Radiography Technology Department, College of Applied Medical Sciences, Taibah University, Madinah, Saudi Arabia*

Abstract

This systematic review evaluates the efficacy and diagnostic performance of deep learning algorithms for detecting brain tumors from computed tomography (CT) data. To assess the diagnostic performance of convolutional neural network (CNN)-based models, a descriptive analysis of metrics such as accuracy, specificity, and precision was conducted. Results from nine recent studies demonstrated high diagnostic performance for deep learning methods. Most models achieved accuracy, precision, and specificity exceeding 95% in the differential diagnosis of neoplastic versus non-neoplastic lesions on imaging. These findings highlight the potential of CNNs to facilitate the early diagnosis of brain tumors, particularly in emergency settings where CT serves as the first-line imaging modality.

The analyzed studies employed a wide range of CNN architectures—from pre-trained models to custom-designed networks—yielding consistent and reliable results. However, several limitations were identified, including small sample sizes, reliance on retrospective data, insufficient external validation, and variations in approaches to interpreting results. Despite these limitations, the consistency of findings across independent studies confirms the reliability and practical potential of CNN-based methods for brain tumor detection in CT imaging. Future research should focus on prospective study designs, larger multicenter datasets, standardized reporting, and enhanced model interpretability to ensure safe and effective integration into clinical practice. (**International Journal of Biomedicine. 2026;16(3):306-313.**)

Keywords: deep learning • convolutional neural network • brain tumour • computed tomography

For citation: Ali S, Elbashir M, Hamzi A, Akour I, Sheikhain A, Al-Shahri R, Refaee T, Abdelrazig A, Omer AM. Deep Learning–Based Convolutional Neural Networks for Brain Tumor Detection on CT scans: A Systematic Review. International Journal of Biomedicine. 2026;16(3):306-313. doi:10.21103/Article16(3)_RA2

Abbreviations

AI, artificial intelligence; **CT**, computed tomography; **CNN**, convolutional neural network; **CAD**, computer-aided detection; **MRI**, magnetic resonance imaging; **ROC**, receiver operating characteristic

Introduction

Brain tumors represent a major global health challenge due to high morbidity and mortality rates.[1] A lack of timely diagnosis and treatment for these neoplasms can lead to severe neurological impairment and death. Consequently, diagnostic accuracy and timeliness play a pivotal role in determining patient prognosis and survival. Recent studies indicate that only about 35.6% of adult patients diagnosed with a malignant central nervous system tumor survive beyond the five-year mark.[2] Such statistics underscore the urgent need to develop methods for early and reliable diagnosis.

Clinical evidence consistently demonstrates that early detection and timely intervention significantly improve patient outcomes. For instance, in cases of glioblastoma multiforme—one of the most aggressive primary brain tumors—diagnosis within two weeks of symptom onset is associated with significantly higher survival rates compared to

cases involving delayed diagnosis.[3] However, early diagnosis is challenging because brain tumors often present with nonspecific neurological symptoms common to a wide range of other conditions.

The diagnostic process is further complicated by the need to differentiate suspected brain tumors from numerous other conditions. Imaging findings and clinical presentations can mimic metastatic lesions, inflammatory processes, vascular anomalies, or other non-neoplastic neurological disorders.[4] Conversely, some brain neoplasms may lack the classic signs of a space-occupying lesion, making it difficult to distinguish them from benign processes during both imaging and histopathological examination.[5] These challenges highlight the need for reliable diagnostic tools to support clinical decision-making.

Medical imaging techniques play a pivotal role in the diagnosis and management of patients with brain tumors. Advances in computed tomography (CT) and magnetic resonance imaging (MRI), alongside the development of specialized imaging modalities, have significantly enhanced the ability to detect and characterize pathological lesions.[6] CT remains a first-line imaging modality in many clinical scenarios—particularly in emergency medicine—due to its rapid image acquisition, widespread availability, and cost-effectiveness. Despite these advantages, CT has several known limitations. Compared to MRI, CT offers lower soft-tissue contrast, and artifacts caused by the "beam hardening" effect as radiation passes through the skull can obscure subtle pathological changes. Furthermore, the use of ionizing radiation and limited spatial resolution reduces the method's diagnostic sensitivity, especially when detecting small or isodense lesions. Such limitations can lead to missed pathologies and significant inter-observer variability among radiologists, particularly under high workloads. To address these issues, the potential of computer-aided detection (CAD) systems as an assistive tool for reviewing imaging results is being investigated. Early CAD methods relied heavily on manually extracted image features, such as intensity distribution, texture descriptors, and morphological characteristics. However, these methods often lacked robustness and generalizability, limiting their diagnostic efficacy and potential for clinical implementation.[7]

In recent years, artificial intelligence, particularly deep learning, has emerged as a powerful tool, fundamentally transforming approaches to medical image analysis. Deep convolutional neural networks (CNNs) can automatically learn to extract complex hierarchical features directly from raw imaging data, eliminating the need for manual feature engineering. Consequently, CNN-based models have demonstrated state-of-the-art performance across a wide range of radiological tasks, including the detection, classification, and segmentation of pathological lesions. In the field of neuroimaging, several studies have demonstrated the high diagnostic accuracy of CNN models for analyzing CT data; some achieved accuracy rates of approximately 96%, with similarly high sensitivity and specificity.[6] These findings suggest that deep learning methods can complement radiologists' expertise, reduce diagnostic variability, and enhance clinical efficiency.[8] Furthermore, recent efforts have focused on developing lightweight, computationally efficient CNN architectures that enable real-time analysis and deployment in clinical settings with limited computing resources, further underscoring the potential of AI for CT image interpretation.

Despite these promising results, the existing body of evidence on deep learning for brain tumor detection in CT images remains fragmented. Existing reviews in neuro-oncology primarily focus on MRI analysis methods, whereas systematic summaries of data specifically concerning computed tomography are relatively scarce.[9] Moreover, individual studies vary significantly in terms of the CNN architectures employed, training strategies, dataset composition, and evaluation metrics. Such methodological heterogeneity complicates direct comparisons of results and limits the ability to draw clinically relevant, actionable conclusions about the efficacy and reliability of deep learning models for CT data analysis.[10]

Concurrently, promising approaches such as secure federated deep learning, implemented on high-performance computing (HPC) infrastructure, are attracting increasing attention. These are considered scalable solutions that ensure privacy during collaborative analysis of medical images. Federated learning enables multiple medical institutions to jointly train deep learning models without exchanging raw patient data, thereby addressing critical issues related to data protection and regulatory compliance. When combined with secure aggregation methods and HPC resources, federated approaches have demonstrated high efficacy and strong generalization capabilities in classifying brain tumors using MRI data from heterogeneous sources.[11] These advances underscore the growing importance of computational efficiency, data diversity, and privacy preservation in modern medical imaging research. Although most federated learning applications have been investigated in the context of brain tumor analysis using MRI data, these approaches are becoming increasingly relevant for CT as well—particularly in emergency care settings and multicenter studies, where data-sharing restrictions, variations in scanner characteristics, and the need for rapid system deployment pose significant challenges.

The accurate classification of brain tumors is a critical task in medical imaging, directly influencing diagnosis, treatment planning, and patient survival. Early detection not only improves clinical outcomes but also facilitates the development of more effective and targeted therapeutic strategies.[12] More broadly, machine learning methods—a key field of artificial intelligence that employs probabilistic approaches and optimization algorithms to extract meaningful patterns from vast, complex datasets—drive progress across various stages of patient management in neuro-oncology, including diagnosis, prognosis, and the monitoring of treatment efficacy.[13,14]

In this context, a comprehensive and targeted analysis of existing scientific data is essential. This systematic review aimed to evaluate the performance of deep learning algorithms in detecting brain tumors using computed tomography (CT)

data. By systematically synthesizing performance metrics such as accuracy, specificity, and precision, the study assessed the diagnostic value, reliability, and limitations of CNN- based models. Furthermore, the review sought to identify common methodological approaches, persistent challenges, and research gaps that may affect model reproducibility and generalizability, and to assess their potential for implementation in clinical practice across various medical institutions.

Methodology

Information Sources and Search Strategy

A comprehensive systematic search was conducted across electronic databases, including PubMed, Scopus, and Google Scholar, to identify relevant studies. The search employed combinations of keywords and MeSH terms, such as "deep learning," "convolutional neural network," "brain tumor," and "CT imaging," along with Boolean operators to ensure a comprehensive selection. The search was limited to English-language, peer-reviewed articles published between 2017 and 2024.

All retrieved records were uploaded to the Rayyan QCRI platform, a web-based tool designed to facilitate the study selection phase of a systematic review. Duplicates were removed automatically, then manually verified. This review was conducted and reported in accordance with the PRISMA-DTA guidelines for diagnostic test accuracy studies.

Study Selection Process

Two researchers independently assessed the titles and abstracts against the established inclusion criteria. Full-text articles were obtained for all potentially eligible studies and were also independently evaluated by the same researchers. Disagreements were resolved through discussion; if consensus was not reached, a third researcher was brought in. The study selection process and reasons for exclusion at each stage are presented in the PRISMA flow diagram (Figure 1).

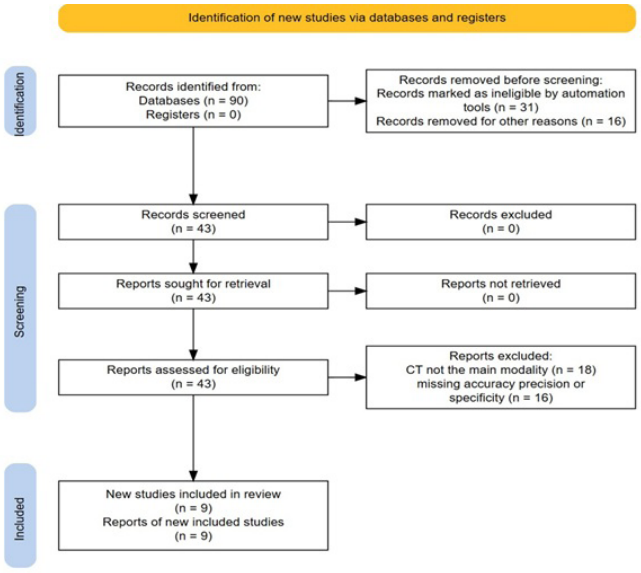

Figure 1. *Study selection.*

The review included peer-reviewed original research articles involving human subjects that employed deep learning CNNs to detect or classify brain tumors using CT imaging data and reported quantitative metrics of diagnostic performance (accuracy, sensitivity, specificity, or precision). Only full-text journal articles in English were considered.

Studies based exclusively on MRI or other imaging modalities (other than CT) were excluded, as were review articles, editorials, conference abstracts, case reports, animal studies, and studies using phantoms. Additionally, studies lacking sufficient methodological detail or key quantitative performance metrics (e.g., unclear descriptions of the CNN methodology or insufficient data on diagnostic accuracy) were excluded. All inclusion and exclusion criteria were defined a priori and applied consistently throughout the selection process.

Rationale for Quantitative Synthesis Approach

Due to the significant heterogeneity in CNN architectures, dataset characteristics, validation strategies, and reporting methods for results—as well as the incomplete reporting of variability measures and confidence intervals in primary studies—conducting a formal meta-analysis to estimate pooled effect sizes was not feasible. Consequently, the synthesis of results was conducted using a structured, descriptive, and comparative quantitative approach, in accordance with the PRISMA-DTA guidelines for diagnostic test accuracy reviews, which do not allow statistical pooling of data.

This systematic review was not registered with PROSPERO.

The PRISMA flow diagram illustrates the study screening and inclusion process: identification of records, removal of duplicates, screening of records by title and abstract, assessment of full-text versions against eligibility criteria, and the final list of included studies.

All titles and abstracts of identified records were screened for inclusion in the review. Two researchers independently evaluated each record based on predefined selection criteria. Following the removal of duplicates, titles and abstracts of all remaining records were screened, and full-text articles were retrieved for potentially eligible studies. Subsequently, the full texts were evaluated in detail against inclusion and exclusion criteria. The number of studies included and excluded at each stage is shown in Figure 1, prepared in accordance with standard PRISMA methodology.

This systematic review was conducted and reported in accordance with the PRISMA-DTA guidelines for diagnostic test accuracy studies.

Data Extraction

Data extraction was performed independently by two researchers using a standardized and pilot-tested data extraction form. Extracted information included study identifiers (authors, publication year, country), study design characteristics (sample size and study population), details on CNN models (architecture and training data), and performance metrics such as accuracy, specificity, precision, and the area under the ROC curve (AUC). Where available, data on validation strategies (e.g., internal or external) and dataset

characteristics were also collected, as these are essential for interpreting model performance and subsequently assessing the risk of bias.

All extracted data were organized in Microsoft Excel tables to facilitate comparison and synthesis. Disagreements between researchers were resolved through discussion and consensus. To ensure transparency and reproducibility, the complete data extraction table and supplementary materials are available from the corresponding author upon reasonable request.

Risk of Bias Assessment

Figure 2 presents a summary of the risk-of-bias assessment for all studies included in the review. The bar chart illustrates the proportion of studies with low, high, or unclear risk of bias across each methodological domain. Overall, most studies showed a low risk of bias, particularly in the domains of outcome measurement and model performance assessment, indicating consistently high methodological quality. However, some studies exhibited an unclear or elevated risk of bias in domains related to patient selection and the handling of confounding factors, reflecting variations in study design and data reporting practices. The assessment was conducted in accordance with established guidelines for systematic reviews of diagnostic accuracy studies.

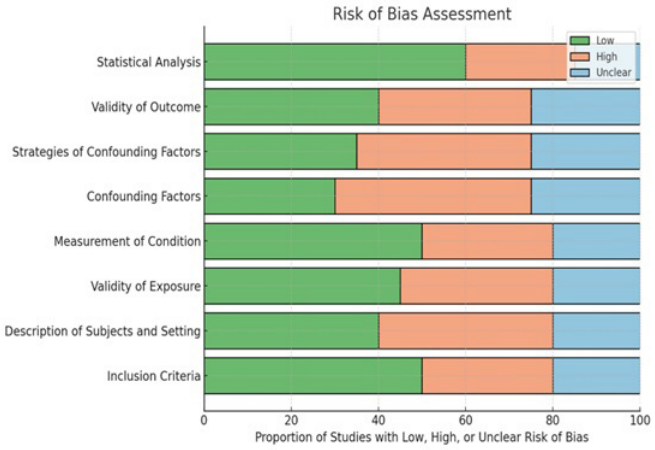

Figure 2. *Risk of bias assessment.*

The risk of bias for each included study was assessed across specific domains using the QUADAS-2 tool, which is widely recommended for systematic reviews of diagnostic accuracy studies. Four key domains were evaluated: patient selection, the index test (CNN-based CT model), the reference standard, and flow and timing. The risk of bias in each domain was classified as low, high, or unclear based on predefined criteria, including the clarity of the inclusion criteria, the adequacy of the dataset and population descriptions, the validity of outcome labeling, the correctness of the analytical methods, and the consideration of potential confounding factors.

Figure 2 presents the distribution of studies across risk categories for each domain. The color-coded visualization reflects the overall consistency of methodological quality across the included CNN-based CT studies. As shown in Figure 2, a low risk of bias predominated across most domains, particularly regarding outcome assessment and model quality evaluation, thereby increasing confidence in the reported diagnostic performance. Moderate concerns arose primarily from potential confounding factors, including variations in dataset size, class imbalance, and differences in validation strategies. These methodological aspects were taken into account when interpreting the findings, enabling a balanced and cautious assessment of the evidence base while avoiding overestimating numerical performance metrics.

To assess the robustness of the findings, a sensitivity analysis was conducted to evaluate the impact of excluding studies with a high risk of bias based on one or more critical criteria. Excluding such studies did not substantially alter the overall pattern of diagnostic performance observed in the remaining studies, indicating that the main conclusions were not driven by studies with higher methodological risk.

Risk of bias assessments were conducted using the QUADAS-2 framework, with results summarized and visualized using standard spreadsheet software. Findings from the risk of bias evaluation were considered in the descriptive synthesis of results, particularly when comparing studies with differing methodological characteristics. Domains demonstrating higher or unclear risk of bias, especially those related to data selection and confounding control, were recognized as potential sources of variability across studies. ChatGPT by OpenAI was used to enhance figure presentation. The authors independently verified all scientific information and approved the final version of the manuscript.

The methodological quality of each included study was independently assessed by two experts using established risk of bias criteria adapted for diagnostic accuracy research. Aspects such as patient selection, image acquisition and interpretation, outcome measurement, and data transparency were evaluated. The risk of bias in each category was classified as low, high, or unclear in accordance with published guidelines; disagreements were resolved through discussion. An overall assessment of study quality was conducted using a cautious approach, placing greater weight on aspects most critical to diagnostic validity.

Results

Table 1 presents pre-trained CNN architectures, including ResNet-50, EfficientNet-B0, MobileNet-V1, VGG-16, and GoogLeNet. Accuracy metrics ranged from approximately 94% to 99%, with the highest values observed in studies utilizing EfficientNet-B0, ensemble models (combinations of multiple architectures), and 3D CNNs with data fusion. Custom-designed CNN architectures also demonstrated high diagnostic accuracy, particularly when employing optimization strategies or modules based on expert knowledge. Sensitivity values were inconsistently reported across the included studies, and information on sample size and validation type was frequently unavailable or limited to internal validation only. Overall, the results indicate high diagnostic performance across various CNN-based approaches, alongside diverse model designs and data representation methods (Figures 3-5).

Table 1.

Characteristics of selected studies.

Study (First Author, Year)	CNN Architecture	Specificity, %	Accuracy, %	Precision, %
Woźniak et al., 2023 [17]	Custom 8-layer CNN + CLM support	96.00	95.00	95.00
Anjum et al., 2022 [20]	ResNet-50 (transfer learning)	96.00	94.00	96.00
ARI et al., 2018 [31]	EfficientNet-B0 (transfer learning)	97.12	97.18	96.80
Moe et al., 2019 [30]	MobileNet-V1 (transfer learning)	97.00	97.00	97.00
Mahmud et al., 2023 [19]	Custom CNN (hyperparameter tuned)	97.00	93.30	90.00
Negm et al., 2023 [18]	VGG-16 + ResNet (ensemble)	98.74	98.45	97.93
Mehrotra et al., 2020 [25]	GoogLeNet (transfer learning)	99.29	99.04	99.30
Rao et al., 2019 [24]	Custom CNN + knowledge module	94 .00	93	88.00
Almadhoun et al., 2022 [32]	3D CNN + data fusion	99.00	99.88	99.00

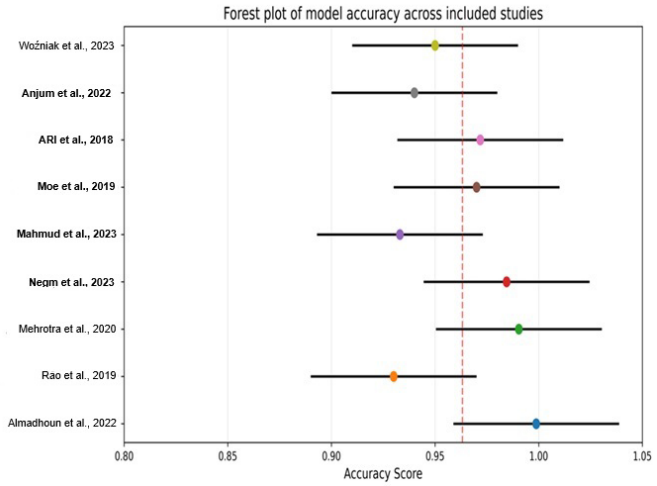

Figure 3. *Forest plot showing individual study accuracy estimates for CNN-based brain tumor detection using CT imaging. Each square represents the accuracy reported by an individual study, with horizontal lines indicating the corresponding confidence intervals where available. Variability in accuracy reflects differences in CNN architectures, dataset characteristics, and validation strategies.*

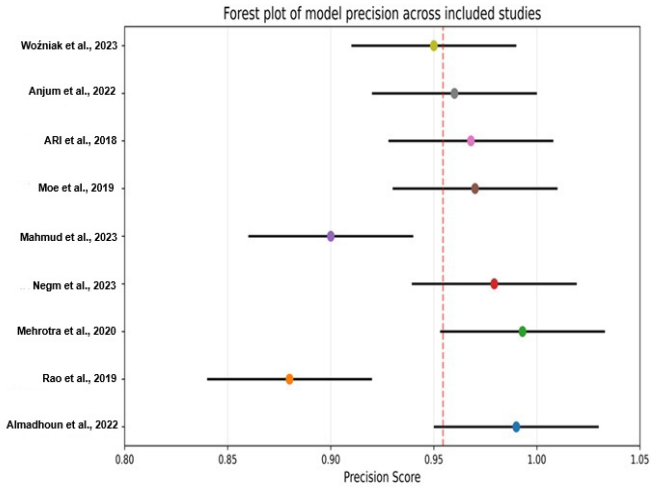

Figure 4. *Forest plot illustrating model precision (positive predictive value, %) across the included studies. Precision values varied between studies, reflecting differences in CNN architectures, training strategies, and dataset characteristics, including the use of transfer learning, ensemble models, and custom-designed networks. The figure is presented to facilitate visual comparison of precision performance across individual studies.*

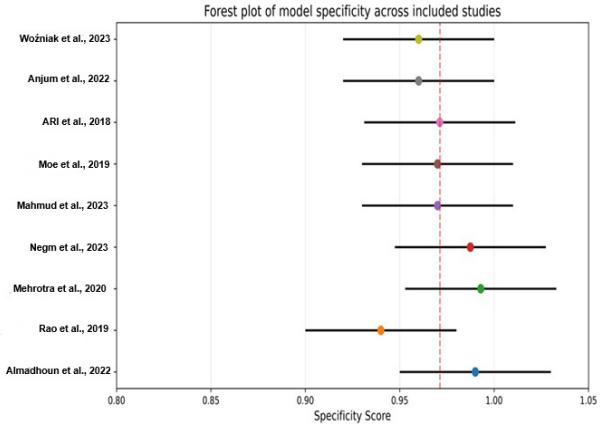

Figure 5. *Forest plot illustrating specificity values (%) reported across the included studies. Specificity varied between studies, reflecting differences in CNN architectures, training strategies, and dataset characteristics, including the use of transfer learning, ensemble approaches, and custom-designed networks. The figure is presented to support visual comparison of specificity performance across individual studies.*

Discussion

This systematic review demonstrates that deep learning methods, specifically CNN-based models, consistently achieve high diagnostic performance for detecting brain tumors on CT scans. Across the nine studies included in the review, the CNN architecture demonstrated high accuracy, specificity, and precision, underscoring its robust ability to distinguish between cases with and without tumors. These findings reinforce the growing role of artificial intelligence in extracting clinically significant information from standard CT scans, which remain widely available and are frequently utilized in emergencies and acute care settings.[15]

Clinical Significance of AI in CT Image Analysis

A key strength of this review is its exclusive focus on CT-based tumor detection. This addresses a gap in the scientific literature on AI applications in neuroimaging, where the primary focus has historically been on MRI-based methods. Although MRI-related studies predominated during the initial selection phase, limiting the sample to CT-based research enabled an assessment specific to this imaging modality, thereby eliminating confounding factors. Given that CT is often the first-line imaging modality in emergency departments—owing to its rapid image acquisition, accessibility, and suitability for patients in critical or unstable condition—AI-assisted CT interpretation could facilitate earlier tumor detection when MRI is unavailable, delayed, or contraindicated.[16] AI-based CT analysis should not be viewed as a replacement for MRI; rather, it serves as a complementary tool that streamlines patient triage and supports timely clinical decision-making in time-critical situations.

Consistency of Performance Metrics across Various CNN Architectures

Despite differences in model architectures and training strategies, all the studies included in the review yielded favorable diagnostic results, underscoring the reliability of CNN-based methods for detecting brain tumors in CT scans. Models employing transfer learning based on established architectures—such as ResNet-50, EfficientNet-B0, MobileNet-V1, and GoogLeNet—consistently demonstrated high performance. This confirms the effectiveness of pre-trained neural networks in medical imaging, particularly when training datasets are limited.[17,18]

More advanced approaches, including ensemble models that combine different architectures (e.g., VGG-16 and ResNet), achieved further improvements in specificity and accuracy. This supports the hypothesis that integrating diverse feature representation methods enhances the system's ability to distinguish between pathological and normal states.[19] Furthermore, studies using 3D CNNs combined with data fusion techniques reported the highest accuracy, highlighting the importance of volumetric information and spatial context for brain tumor detection in CT data. Custom-designed CNN architecture also yielded competitive results when optimized through hyperparameter tuning or curriculum learning, although the slightly lower accuracy observed in some studies may reflect dataset imbalance, limited sample size, or increased model complexity.[20,21]

Generalizability, Scanner Variability, and Reliability

Consistently high specificity and accuracy across studies indicate that CNN-based systems can reduce false-positive rates. This is crucial for clinical implementation, as it helps avoid unnecessary follow-up examinations and patient anxiety. However, model performance was influenced by CT image acquisition protocols and specific scanner characteristics. Optimal results were often observed when training and testing data originated from similar distributions or were acquired using similar equipment.[21,22] This dependency highlights the issue of "domain shift" in applying AI to radiology and underscores the need for multi-center datasets—acquired with equipment from various manufacturers—to ensure robust generalizability of results across diverse clinical settings.

Risk of Bias, Validation Practices, and Interpretation of Performance Metrics

The studies were predominantly retrospective in nature and varied in sample size and patient selection criteria. Typical limitations included the narrow scope of the groups studied and insufficient descriptions of confounding factors,[23,24] which could lead to inflated efficacy estimates when test datasets were highly similar to training datasets. Furthermore, not all studies reported sensitivity data (with greater emphasis often placed on accuracy, specificity, and precision), limiting the ability to comprehensively evaluate model performance, particularly with respect to false-negative results. Consistent with broader trends in the AI radiology literature, studies incorporating external validation generally showed a slight decline in performance metrics relative to internal validation results, reflecting the impact of data heterogeneity and domain shift.[18,25] Only a small fraction of the studies evaluated models on independent external datasets; these datasets often lacked geographic and demographic diversity and provided insufficient descriptions of population characteristics. Furthermore, none of the included studies conducted formal temporal validation across different time periods, limiting the ability to assess model stability over time. Although a heightened risk of bias in certain methodological aspects reduced confidence in the accuracy of quantitative metrics, no study was deemed methodologically flawed to the extent that its conclusions were called into question. Overall, the available evidence supports the efficacy of CNN-based approaches for detecting brain tumors in CT scans; however, it highlights the need for cautious interpretation of near-perfect performance metrics and for adopting more rigorous validation strategies in future research.[26,23]

Practical Significance and Future Directions

No clear evidence of publication bias was found, although the limited number of studies reporting low performance or negative results may reflect either publication bias or the inherently high efficacy of CNN-based methods in this field.[27,28] Despite the relatively small number of eligible studies, due to the specific focus on CT imaging, the consistency of findings across independent studies reinforces confidence in the conclusions.[29,30] Emerging research indicates that advanced post-processing techniques and optimized image representations can further suppress false positives and enhance object detection performance.[19] Future research

should prioritize prospective designs, standardized reporting systems, and rigorous external and temporal validation across diverse clinical settings. Addressing these issues is crucial for confirming the reliability of CT-based tumor detection systems that utilize CNNs and for ensuring their responsible implementation in clinical practice.

Conclusion

This systematic review indicates that deep learning models, specifically CNN-based architectures, demonstrate consistently high diagnostic performance in detecting brain tumors on CT images. In the studies analyzed, CNN-based methods exhibited high accuracy, specificity, and precision, comparable to expert assessment results reported in previous literature. This highlights their potential as an assistive tool in diagnostic radiology, particularly in emergency care and resource-constrained settings.

By focusing specifically on CT images, this review addresses a significant gap in the existing literature and demonstrates that CNNs can effectively extract informative features despite inherent CT limitations, including reduced soft-tissue contrast and inter-observer variability in interpretation. However, many studies relied on retrospective datasets with limited diversity and lacked robust external or temporal validation, raising questions about the generalizability of the findings.

Overall, deep learning with CNNs is a promising and evolving approach for improving brain tumor detection in CT data. Despite encouraging results, widespread clinical implementation requires larger multicenter studies, prospective validation, and performance assessment in real-world clinical settings. This review can serve as a foundation for future research aimed at the safe, effective, and evidence-based integration of artificial intelligence tools into neuro-oncology practice involving CT imaging.

Data Availability Statement

All data associated with this study will be available based on the reasonable request to corresponding author.

AI Statement

The authors acknowledge ChatGPT-4 for assistance with proofreading and language editing during the writing process. After using this tool, the authors reviewed and edited the content. The authors take full responsibility for the final version of the manuscript.

Author Contributions

Sara Ali: Conceptualization, validation, formal analysis, investigation, data curation, writing—original draft, writing—review and editing, visualization, supervision, project administration.
Meaad Elbashir: Investigation, data curation, writing—original draft, and writing—review and editing.
Almohannad Hamzi: Investigation, data curation
Imad Akour: Investigation, data curation
Anwar Sheikhain: Investigation, data curation
Raed Al-Shahri: Investigation, data curation
Turkey Refaee: Validation, writing—review and editing, supervision.
Ali Abdelrazig: Investigation, data curation, visualization, and writing—original draft
Awatif M. Omer: Investigation, and writing—original draft.
All authors have approved the final article.

Acknowledgment

The authors would like to express their appreciation to all individuals who contributed to the preparation of this manuscript. Their support and valuable insights helped improve the quality of this work.

Conflict of Interest

The authors have declared no conflict of interest.

Funding Resource

Not applicable.

References

1. Kumar A, Pandey SK, Varshney N, Singh KU, Singh T, Shah MA. Distinctive approach in brain tumor detection and feature extraction using biologically inspired DWT method and SVM. Sci Rep. 2023 Dec 20;13(1):22735. doi: 10.1038/s41598-023-50073-9. PMID: 38123666; PMCID: PMC10733354.
2. Dorfner FJ, Patel JB, Kalpathy-Cramer J, Gerstner ER, Bridge CP. A review of deep learning for brain tumor analysis in MRI. NPJ Precis Oncol. 2025 Jan 3;9(1):2. doi: 10.1038/s41698-024-00789-2. PMID: 39753730; PMCID: PMC11698745.
3. Kawauchi D, Ohno M, Miyakita Y, Takahashi M, Yanagisawa S, Omura T, Yoshida A, Kubo Y, Igaki H, Ichimura K, Narita Y. Early Diagnosis and Surgical Intervention Within 3 Weeks From Symptom Onset Are Associated With Prolonged Survival of Patients With Glioblastoma. Neurosurgery. 2022 Nov 1;91(5):741-748. doi: 10.1227/neu.0000000000002096. Epub 2022 Aug 15. Erratum in: Neurosurgery. 2023 Feb 01;92(2):e44. doi: 10.1227/neu.0000000000002281. PMID: 35951724; PMCID: PMC9531976.
4. Mesfin FB, Karsonovich T, Al-Dhahir MA. Gliomas. 2024 Aug 12. In: StatPearls [Internet]. Treasure Island (FL): StatPearls Publishing; 2026 Jan–. PMID: 28722904.
5. Behin A, Hoang-Xuan K, Carpentier AF, Delattre JY. Primary brain tumours in adults. Lancet. 2003 Jan 25;361(9354):323-31. doi: 10.1016/S0140-6736(03)12328-8. PMID: 12559880.
6. Bruzzone MG, D'Incerti L, Farina LL, Cuccarini V, Finocchiaro G. CT and MRI of brain tumors. Q J Nucl Med Mol Imaging. 2012 Apr;56(2):112-37. PMID: 22617235.
7. Aberle D, El-Saden S, Abbona P, Gomez A, Motamedi K, Ragavendra N et al. A primer on imaging anatomy and

physiology. In Medical imaging informatics. Boston, MA: Springer US, 2009:15-90.
8. Mienye ID, Swart TG, Obaido G, Jordan M, Ilono P. Deep Convolutional Neural Networks in Medical Image Analysis: A Review. Information. 2025; 16(3):195. doi: 10.3390/info16030195
9. Khalighi S, Reddy K, Midya A, Pandav KB, Madabhushi A, Abedalthagafi M. Artificial intelligence in neuro-oncology: advances and challenges in brain tumor diagnosis, prognosis, and precision treatment. NPJ Precis Oncol. 2024 Mar 29;8(1):80. doi: 10.1038/s41698-024-00575-0. PMID: 38553633; PMCID: PMC10980741.
10. Zhou SK, Greenspan H, Davatzikos C, Duncan JS, van Ginneken B, Madabhushi A, Prince JL, Rueckert D, Summers RM. A review of deep learning in medical imaging: Imaging traits, technology trends, case studies with progress highlights, and future promises. Proc IEEE Inst Electr Electron Eng. 2021 May;109(5):820-838. doi: 10.1109/JPROC.2021.3054390.
11. Appasami G, Savarimuthu N. Cross-dataset performance evaluation and secure federated learning with weighted model aggregation for MRI brain tumor image classification. J Supercomput. 2025;81:1555.
12. Appasami G, Savarimuthu N. Federated learning for secure medical MRI brain tumor image classification. Eur Phys J Spec Top. 2025;*234:*4813–4827. doi:10.1140/epjs/s11734-025-01516-z
13. Appasami G, Savarimuthu N. A novel lightweight CNN design for MRI brain tumor image classification with performance-driven optimization. Discov Computing. 2025;28:206. doi:10.1007/s10791-025-09603-4
14. Al-Rahbi A, Al-Habsi T, Al-Suli A, et al. Artificial intelligence use in diagnosis, grading, and segmentation of neuro-oncology: a narrative review. Egypt J Neurol Psychiatry Neurosurg.2025;61:54. doi:10.1186/s41983-025-00980-7
15. Patil V, Madgi M, Kiran A. Early prediction of Alzheimer's disease using convolutional neural network: a review. Egypt J Neurol Psychiatry Neurosurg. 2022;58:130. doi.org/10.1186/s41983-022-00571-w
16. Illimoottil M, Ginat D. Recent Advances in Deep Learning and Medical Imaging for Head and Neck Cancer Treatment: MRI, CT, and PET Scans. Cancers (Basel). 2023 Jun 21;15(13):3267. doi: 10.3390/cancers15133267. PMID: 37444376; PMCID: PMC10339989.
17. Woźniak M, Siłka J, Wieczorek M. Deep neural network correlation learning mechanism for CT brain tumor detection. Neural Comput & Applic.2023;**35:**14611–14626 (2023). doiDoi:10.1007/s00521-021-05841
18. Negm N, Aldehim G, Nafie FM, Marzouk R, Assiri M, Alsaid MI, et al. Intracranial haemorrhage diagnosis using willow catkin optimization with voting ensemble deep learning on CT brain imaging. IEEE Access. 2023;11:75474-75483. doi:10.1109/ACCESS.2023.3297281
19. Mahmud MI, Mamun M, Abdelgawad A. A Deep Analysis of Brain Tumor Detection from MR Images Using Deep Learning Networks. Algorithms. 2023; 16(4):176. doi:10.3390/a16040176
20. Anjum S, Hussain L, Ali M, Alkinani MH, Aziz W, Gheller S, et al. Detecting brain tumors using deep learning convolutional neural network with transfer learning approach. International Journal of Imaging Systems and Technology. 2022;32(1), 307-323. doi:10.1002/ima.22641 12
21. Chang K, Balachandar N, Lam C, Yi D, Brown J, Beers A, Rosen B, Rubin DL, Kalpathy-Cramer J. Distributed deep learning networks among institutions for medical imaging. J Am Med Inform Assoc. 2018 Aug 1;25(8):945-954. doi: 10.1093/jamia/ocy017. PMID: 29617797; PMCID: PMC6077811.
22. Hossain T, Shishir FS, Ashraf M, Nasim MA, Muhammad Shah F. Brain Tumor Detection Using Convolutional Neural Network. 2019 1st International Conference on Advances in Science, Engineering and Robotics Technology (ICASERT*)*, 2019:1-6.
23. Ramspek CL, Jager KJ, Dekker FW, Zoccali C, van Diepen M. External validation of prognostic models: what, why, how, when and where? Clin Kidney J. 2020 Nov 24;14(1):49-58. doi: 10.1093/ckj/sfaa188. PMID: 33564405; PMCID: PMC7857818.
24. Rao SKV, Lingappa B. Image Analysis for MRI Based Brain Tumour Detection Using Hybrid Segmentation and Deep Learning Classification Technique. International Journal of Intelligent Engineering & Systems. 2019;12(5). doi: 10.22266/ijies2019.1031.06
25. Mehrotra R, Ansari MA, Agrawal R, Anand RS. A transfer learning approach for AI-based classification of brain tumors. Machine Learning with Applications.2020;2:100003. doi:10.1016/j.mlwa.2020.100003
26. Anderson AW, Marinovich ML, Houssami N, Lowry KP, Elmore JG, Buist DSM, Hofvind S, Lee CI. Independent External Validation of Artificial Intelligence Algorithms for Automated Interpretation of Screening Mammography: A Systematic Review. J Am Coll Radiol. 2022 Feb;19(2 Pt A):259-273. doi: 10.1016/j.jacr.2021.11.008.
27. Kaifi R. A Review of Recent Advances in Brain Tumor Diagnosis Based on AI-Based Classification. Diagnostics (Basel). 2023 Sep 20;13(18):3007. doi: 10.3390/diagnostics13183007. PMID: 37761373; PMCID: PMC10527911.
28. Mäenpää SM, Korja M. Diagnostic test accuracy of externally validated convolutional neural network (CNN) artificial intelligence (AI) models for emergency head CT scans - A systematic review. Int J Med Inform. 2024 Sep;189:105523.
29. Takao H, Amemiya S, Kato S, Yamashita H, Sakamoto N, Abe O. Deep-learning single-shot detector for automatic detection of brain metastases with the combined use of contrast-enhanced and non-enhanced computed tomography images. Eur J Radiol. 2021 Nov;144:110015. doi: 10.1016/j.ejrad.2021.110015. Epub 2021 Nov 1. PMID: 34742108.
30. Moe YM, Groendahl AR, Mulstad M, Tomic O, Indahl U, Dale E, et al. Deep learning for automatic tumour segmentation in PET/CT images of patients with head and neck cancers. arXiv preprint arXiv:1908.00841. doi:10.48550/arXiv.1908.00841
31. ARI A, HANBAY D. Deep learning based brain tumor classification and detection system. Turk J Elec Eng & Comp Sci (2018) 26: 2275 – 2286. doi:10.3906/elk-1801-8
32. Almadhoun HR, Abu-Naser SS. Detection of Brain Tumor Using Deep Learning. Int J Acad Eng Res (IJAER). 2022;6(3):29–47.

Corresponding author:
Dr. Sarra Hassan Khalifa Ali. E-mail: sarraali@jazanu.edu.sa

International Journal of Biomedicine 16(3) (2026) 314-319
http://dx.doi.org/10.21103/Article16(3)_RA3

REVIEW ARTICLE

INTERNATIONAL JOURNAL OF BIOMEDICINE

Rheumatoid Arthritis: Independent and Synergistic Effects of Vitamin D Deficiency and Smoking

Abdulsalam A. Noorwali

Department of Internal Medicine, Faculty of Medicine, Umm Al-Qura University, Makkah 21955, Saudi Arabia

Abstract

Rheumatoid arthritis (RA) is a long-term autoimmune disease in which the immune system mistakenly attacks the joint linings. The exact cause of RA is still not evident. However, a combination of environmental and genetic factors is considered to contribute to RA. Smoking is an established environmental condition/ risk that exacerbates the disease activity and severity, including faster joint damage, increased lung and other systemic complications, and decreased efficacy of medication used by RA patients. There are a number of factors that synergistically affect the health of smokers, RA patients, or smoking RA patients. Vitamin D (VitD) is one of the main factors involved in smoking and RA. Regarding synergistic influences and interactions, assessing inflammatory biomarker levels (e.g., high-sensitivity C-reactive protein [hs-CRP]) indicates that the inflammatory influence of VitD deficiency is significantly amplified and stronger in smokers than in non-smokers. Furthermore, smoking, a known environmental factor in interaction with the genetic factors, causes a synergistic risk of severe RA. Although both smoking and VitD are established risk factors for RA, the intricate details about how they influence independently are not clearly known. (International Journal of Biomedicine. 2026;16(3):314-319.)

Keywords: rheumatoid arthritis • smoking • vitamin D

For citation: Noorwali AA. Rheumatoid Arthritis: Independent and Synergistic Effects of Vitamin D Deficiency and Smoking. International Journal of Biomedicine. 2026;16(3):314-319. doi:10.21103/Article16(3)_RA3

Abbreviations

Anti-CCP, anti-cyclic citrullinated peptide; **CRP**, C-reactive protein; **CVDs**, cardiovascular diseases; **DAS28**, disease Activity Score 28; **DMARDs**, disease-modifying antirheumatic drugs; **ESR**, erythrocyte sedimentation rate; **hs-CRP**, high-sensitivity C-reactive protein; **MS**, multiple sclerosis; **25(OH)D**, 25-hydroxyvitamin D or vitamin D; **PMP-RA**, postmenopausal rheumatoid arthritis patients; **PTH**, parathyroid hormone; **RA**, rheumatoid arthritis; **RF**, rheumatoid factor; **Th1**, T lymphocyte helper 1; **Th7**, T lymphocyte helper 7; **VitD**, vitamin D; **VDR**, vitamin D receptor.

Introduction

Rheumatoid arthritis (RA) is a long-term autoimmune disease in which the immune system mistakenly attacks the joint linings.[1] Joints are primarily affected, presenting with swelling, stiffness, pain, and bone erosion. The wrist and hands are most commonly involved. Stiffness and pain often worsen after rest. Joints of both hands or both knees are affected symmetrically, and discomfort can spread to the lungs, heart, eyes, skin, blood, and nerves, leading to a range of complications.[2-4] The patients with RA may have a fever. Symptoms may take weeks to months to appear gradually.[1,5] The exact cause of RA is still not evident. However, a combination of environmental and genetic factors is considered to contribute to RA.[6] A comprehensive account of the cellular and molecular mechanisms, as well as effective therapies, for RA has been reviewed.[7]

Smoking is an established environmental condition/ risk that exacerbates the disease activity and severity, including faster joint damage, increased lung and other systemic complications, and decreased efficacy of medication used by RA patients8. Smoking can trigger the immune system in individuals with specific genes, leading to the production of antibodies such as anti-CCP (anti-cyclic citrullinated peptide) and RF (rheumatoid factor).[8,9]

There are a number of factors that synergistically affect

***Corresponding author:** Abdulsalam A. Noorwali, MD. Department of Internal Medicine, Faculty of Medicine, Umm Al-Qura University, Makkah 21955, Saudi Arabia. E-mail: aanoorwali@uqu.edu.sa*

the health of smokers, RA patients, or smoking RA patients. However, Vitamin D (VitD) or serum 25-hydroxyvitamin D [25(OH)D] is one of the main factors involved in smoking, RA, or smoking RA.[10] VitD levels in active smokers are significantly lower compared to those of non-smoking individuals.[11] The cumulative effect of VitD deficiency and smoking on systemic inflammation is more severe in smoking RA patients than in non-smoking RA patients, which makes it more difficult to manage.[12] Similarly, VitD and smoking synergistically influence disease activity, severity, and exacerbation of symptoms in RA patients.[13-16] To have insight into the independent effect of smoking on RA, the effect of VitD on smoking, and VitD on RA, as well as the cumulative or synergistic effect of smoking and VitD on RA, the present review was planned to be carried out.

Vitamin D in Healthy Individuals and Smokers

For general health, 600-800 international units (IUs) daily dosages of VitD are recommended generally, whereas deficiency conditions require 1000-2000 IUs daily, and severe deficiency conditions require 50,000 IUs weekly dosages. Deficiency levels <20 ng/mL (<50 nmol/L) indicate poor bone health (severe deficiency < 10 ng/mL may cause osteomalacia in adults and rickets in children). Sufficient levels>30 ng/mL (>75 nmol/L) are required for bone/ overall health. The insufficient levels of 20–30 ng/mL (52-72 nmol/L) or the sub-optimal levels require the administration/ supplementation of VitD to sufficient levels (> 30 ng/mL). VitD levels of above 150 ng/mL (375 nmol/L) cause toxicity and hypercalcemia. [17-19]

Main factors influencing the serum VitD levels are the extent of exposure to sun, age (older people have higher risk of VitD deficiency), skin pigmentation (less VitD production by darker skin via sun exposure), and malabsorption disorders.[20,21] Table-1 shows the VitD levels, status and cinical implications, explaining the outcomes in the statuses of sufficient or desirable, optimal, insufficient, and deficient levels and toxicity.

It is usually overlooked, but smoking is one of the main causes of the VitD deficiency.[11] Low VitD levels and VitD deficiency have been noted to increase impairment of the body's defense/immune system, especially lung damage.[4,22] Success in smoking cessation/quitting was obtained more in patients with high VitD levels.[23] It was found that there is a direct association of a decrease in VitD level with the number of cigarettes smoked as well as the duration of smoking habit.[24]

Deficient levels of VitD, causing increased levels of oxidative stress due to smoking, can increase the pulmonary conditions and the risks of having cancer, and its higher and beneficial levels are immunomodulatory and anti-inflammatory.[4] In smokers with sufficient VitD levels, lung function decreases more slowly over time than in those with insufficient VitD levels.[22]

VitD deficiency in second-hand or passive smoking occurs independently in adults and young children.[25,26] Both active and passive smokers may have a high risk of VitD deficiency, which can disrupt the VitD metabolism since exposure to smoking interferes with the process of VitD synthesis in the body.[11,26,27]

Smoking can alter the gene expression and VitD receptor (VDR) genes. It downregulates VitD receptors in the lungs, leading to a decline in circulating VitD.[28,29] VitD is necessary for calcium uptake. VitD-parathyroid hormone (PTH) axis and calcium absorption in the intestine are disrupted, leading to bone-related complications, e.g., osteoporosis, and bone loss due to cigarette smoking. Such effects occur due to the

Table 1.

Vitamin D levels, status, and clinical implications

Status	VitD serum levels	Risks/clinical implications/outcomes
Sufficient/ Desirable	≥ 30 ng/mL (≥75 nmol/L)	Reduction in the fall/fractures, sufficient for normal bone health and immune functions. Minimizes parathyroid hormone (PTH), increases calcium absorption and neuromuscular performance/activities.
Optimal	30-50 ng/mL (75-125 nmol/L)	Although 30 ng/mL is sufficient, 30-60 ng/mL is considered safe for general health. The levels of higher than 40 ng/mL improve immunity and reduce the risk of cardiovascular diseases (CVDs), multiple sclerosis (MS), and certain types of cancers.
Insufficient	21-29 ng/mL (50-75 nmol/L)	Insufficient or suboptimal levels associated with decreased calcium absorption may lead to lower bone density and secondary hyperparathyroidism.
Deficient	< 20 ng/mL (< 50 nmol/L)	Severe deficiency could be the risk for osteomalacia and rickets, respectively, in adults and children. Risks of falls/fractures, bone loss, weakness of proximal muscles, and chronic pain occur.
Toxicity	>100 ng/mL (>250 nmol/L)	Hypercalcemia, kidney damage, and related disorders occur.

Table 2.

Influence of smoking on VitD levels

Findings	Descriptions	Study Sources
Dose dependance	Vitamin D correlates inversely with the number of cigarettes smoked/ day	11,24
Decreased VitD levels	Smokers present lower VitD levels than non-smokers.	11
Increased risk of VitD deficiency	Daily smoking is associated with high vitamin D deficiency.	11,24
Cessation/ quitting smoking	High vitD levels are associated with high success rates for cessation/ quitting smoking.	23
Mechanisms	Smoking influences calcium levels, increases bone loss, and change gene expression	11,30

combined effect of nicotine and low levels of VitD.[30]

Smoking influences the sensitive association between VitD and parathyroid hormone and increases the bone mineral density, leading to the risk of osteoporosis.[30]

Thousands of toxic components of smoke can influence the endocrine system.[11,26] Liver and kidneys are involved in converting VitD to the usable active form. Smoking toxins change the expression of required enzymes and break the VitD before it can be used in the body.[11,26,27] Furthermore, cigarette smoking exacerbates chronic rhinosinusitis.[31]

Table 2 presents the influence of smoking on VitD levels, including dose dependence, decreased VitD levels, increased risk of VitD deficiency, cessation/ quitting of smoking, and the mechanisms whereby smoking influences VitD levels.

Vitamin D in Rheumatoid Arthritis

Vitamin D, or serum 25-hydroxyvitamin D [25(OH) D] (VitD), is considered a useful biomarker for assessing disease activity in patients with RA.[32,33] Appropriate doses of VitD improve Disease Activity Score 28 (DAS28), C-reactive protein (CRP) levels, and visual analog scale (VAS) for subjectively rating pain or global health, from "no pain" to "worst pain," in RA.[34,35] VitD has been shown to be significantly lower in RA compared to healthy controls.[36] Adequate levels of VitD are important for maintaining adequate bone density in RA patients with elevated chronic inflammation and osteoporosis.[37]

Strong bones are built if the required level of VitD is present to absorb calcium. Patients with RA experience altered bone turnover and mineralization. Hence, the patients with RA are supplemented with the necessary VitD to prevent bone loss and weakness.[38]

Important representative information of VitD levels in patients with RA is presented in Table 3. Lower serum vitamin D (VitD) levels are commonly observed in patients with RA, though a large proportion of patients show VitD deficiency due to increased disease activity and elevated inflammation/ pain.[39,40]

VitD deficiency in 22.3% RA patients (<20 ng/mL) and insufficiency in 42.7 % (20-29 ng/mL) was investigated in Saudi patients.[41] Another study revealed that RA with high disease activity showed the lowest VitD levels (18.25±8.3 nmol/L), moderate activity (VitD: 35.13±15.2 nmol/L), and low disease activity (VitD: 38.05±7.3 nmol/L).[42] Rossini et al.[43] found VitD deficiency in 29% (42/145) postmenopausal RA (PMP-RA) patients. A meta-analysis study presented lower levels of VitD (mean difference: 16.52 nmol/L) in RA.[44] Table 3 describes the VitD levels in patients with rheumatoid arthritis.

Several other authors have suggested their views and research output on the impact of VitD in patients with RA.[10,45-48] The safe upper intake limit for correcting VitD deficiency is generally 1000-4000 IU per day, and higher doses (e.g., 50,000 IU weekly) are used to monitor RA, whereas the recommended dosage is 1000-2000 IU of VitD, though this depends on specific cases.[46,48] VitD Supplementation with disease-modifying antirheumatic drugs (DMARDs) reduces erythrocyte sedimentation rate and other inflammatory biomarkers. The prevalence of VitD deficiency in RA patients ranges from 30% to 63%.[45]

VitD decreases the proliferation activity of inflammation-related Th1 (T lymphocyte helper 1) and Th7 (T lymphocyte helper 7) cells and increases the regulatory T cells to manage autoimmune joint damage.[46] As concerns disease activity, decreased vitamin D levels are inversely associated with higher DAS28 (Disease Activity Score 28) and, hence, lower levels of VitD are correlated with more joint swelling and worse symptoms.[10]

Some of the important findings includes, a) the role of VitD in RA correlating inversely to the level or scores

Table 3.

Vitamin D levels in patients with rheumatoid arthritis

Study	Subjects	Important findings
39	RA & healthy controls	VitD deficiency in 84% of RA patients compared with 34% of control subjects.
41	Saudi RA patients	VitD deficiency in 22.3% of RA (<20 ng/mL) and insufficiency in 42.7% (20-29 ng/mL).
42	RA & healthy controls	RA with high disease activity showed the lowest VitD levels (18.25±8.3 nmol/L), VitD levels in RA with moderate (35.13±15.2 nmol/L) and low (38.05±7.3 nmol/L) disease activity.
43	PMP-RA	VitD deficiency in 29% (42/145) of RA patients.
44	Meta-analysis	Lower levels of VitD (mean difference: 16.52 nmol/L) in RA

PMP-RA: postmenopausal patients with rheumatoid arthritis

Table 4.

Independent and synergistic effects of VitD and smoking in patients with rheumatoid arthritis.

Factors	Independent and synergistic effects in RA	Clinical consequences
VitD deficiency	High prevalence of RA	High disease activity, low functional capability, heightened level of pain
Smoking	Higher risk factor	Lower efficacy of medication, heightened level of susceptibility, and worsening of the symptoms of RA.
VitD supplementation	Efficacious	Decrease in disease activity and pain, especially in the starting phase of RA.
VitD deficiency+smoking	Synergistic effects	Decreasing trend for VitD and rising trend in inflammation.

of disease activity and to some of the known inflammatory biomarkers e.g., C-reactive protein (CRP) and erythrocyte sedimentation rate (ESR),[49] b): the prevalence studies showing deficiency of VitD (less than 30 ng/ml) in 84% of the RA patients whereas 34 % in control subjects,[39] though the mean VitD levels documented in RA are usually lower (21.05±10.02 and 18.09± 8.99 ng/ml),[39] c): the supplementation of 50,000 IU of VitD3 was found affective for decreasing fatigue, pain and the disease activity in patients with RA,[49] and d): the immunomodulatory effect of VitD for differentiation of T-cells and production of cytokines manifests the beneficial effect of VitD for autoimmune disorders.[36]

VitD acts as an immunomodulator, helping reduce systemic inflammation, joint stiffness, and the severity of RA symptoms.[48] Furthermore, VitD is involved in promoting the differentiation process for regulatory T-cells, which does not allow the immune system to attack the joints mistakenly.[50]

The Birmingham early inflammatory cohort did not find a clear correlation between VitD and RA diagnosis/ progression, and no significant decrease in pain or fatigue was observed.[10] Another study[34] documented a strong negative association between high levels of hypovitaminosis and RA disease activity in their clinical trial and found that VitD supplements significantly improved DAS28 scores.

Vitamin D, Smoking, and Rheumatoid Arthritis

The impact and availability of VitD are changed significantly by smoking in RA patients, and deficiency of VitD in such conditions leads to inflammatory risks and disease severity.[51,52] Remission becomes quite low when, besides low VitD, the RA patient is a smoker.[10] It is known that smoking and RA both disturb bone metabolism, e.g., a high risk of osteoporosis. Smoking itself disrupts the VitD regulation and parathyroid actions, and more severe dysregulations occur in patients with RA.[52] The synergistic effect of VitD and smoking occurs. The association between VitD and high CRP (C-reactive protein) levels is significantly stronger in smoking RA patients.[12]

As presented in Table 4, there are independent effects of VitD as well as smoking in patients with RA. However, interlinked and synergistic effects of VitD and smoking lead to worsening of the disease activity/ outcomes as smoking is an important environmental factor that triggers the RA disease activity, and the deficiency of VitD causes increased disease activity/ severity, amplified inflammation, and bone fractures, disruption of bone metabolism, and decreased calcium absorption.[10,13,39,46, 51, 53]

Conclusion

Quitting smoking is a lifestyle intervention that is highly helpful, especially for someone with RA. It leads to improved bodily functions, reduced active symptoms, and greater treatment efficacy.[8] It is necessary to consult healthcare personnel for people who smoke to have their VitD level checked. The relevant consultant can determine the supplementation dose, taking into account respiratory risks and associated conditions.[22,23,26] It is essential to achieve the required level of VitD in patients with rheumatoid arthritis. The rheumatologist routinely recommends the VitD test. If VitD deficiency is confirmed, sunlight exposure, important dietary sources (e.g., fish [salmon, tuna, etc.], fortified foods, egg yolks), and supplementation with VitD are recommended.[33]

Correcting the VitD deficiency to >30 ng/mL helps decrease the DAS28 (Disease Activity Score) and improve the health of RA patients.[41] The condition of the patients with RA is assessed by the DAS28 clinical index, which measures the activity of RA by checking 28 important joints for their tenderness as well as swelling.[54]

Regarding synergistic influences and interactions, assessing inflammatory biomarker levels (e.g., high-sensitivity C-reactive protein [hs-CRP]) indicates that the inflammatory influence of VitD deficiency is significantly amplified and stronger in smokers than in non-smokers. Furthermore, smoking is a known environmental factor in interaction with genetic factors, causing a synergistic risk of severe RA. Although both smoking and VitD are established risk factors for RA, the intricate details about how they influence independently require further studies.

Sources of Funding

This research received no external funding.

Disclosure and Conflicts of Interest

The author declares that he has no conflicts of interest.

Disclaimer

The views expressed in the submitted article are those of the author and not those of the institution.

Author Contribution Statement

The author confirms sole responsibility for the conception, design, and writing of the manuscript.

References

1. Majithia V, Geraci SA. Rheumatoid arthritis: diagnosis and management. Am J Med. 2007 Nov;120(11):936-9. doi: 10.1016/j.amjmed.2007.04.005. PMID: 17976416.
2. Turesson C, O'Fallon WM, Crowson CS, Gabriel SE, Matteson EL. Extra-articular disease manifestations in rheumatoid arthritis: incidence trends and risk factors over 46 years. Ann Rheum Dis. 2003 Aug;62(8):722-7. doi: 10.1136/ard.62.8.722. PMID: 12860726; PMCID: PMC1754626.
3. Cutolo M, Kitas GD, van Riel PL. Burden of disease in treated rheumatoid arthritis patients: going beyond the joint. Semin Arthritis Rheum. 2014 Feb;43(4):479-88. doi: 10.1016/j.semarthrit.2013.08.004. Epub 2013 Sep 27. PMID: 24080116.
4. Zeng H, Yuan Z, Wu RT, Huang Z. Research progress on complications of rheumatoid arthritis. Front Immunol. 2025 May 27;16:1561926. doi: 10.3389/fimmu.2025.1561926. PMID:

40496851; PMCID: PMC12149157.
5. Jahid M, Khan KU, Rehan-Ul-Haq, Ahmed RS. Overview of Rheumatoid Arthritis and Scientific Understanding of the Disease. Mediterr J Rheumatol. 2023 Aug 1;34(3):284-291. doi: 10.31138/mjr.20230801.oo. PMID: 37941854; PMCID: PMC10628871.
6. Masoumi M, Solaymani M, Abbasifard M, Houshmandfar S, Iravani P, Saeedi-Boroujeni A, Karami J. The genetic puzzle of rheumatoid arthritis: Causes, progression, and treatment. Biochem Biophys Rep. 2025 Jul 21;43:102148. doi: 10.1016/j.bbrep.2025.102148. PMID: 40734997; PMCID: PMC12305329.
7. Han P, Liu X, He J, Han L, Li J. Overview of mechanisms and novel therapies on rheumatoid arthritis from a cellular perspective. Front Immunol. 2024 Sep 23;15:1461756. doi: 10.3389/fimmu.2024.1461756. PMID: 39376556; PMCID: PMC11456432.
8. Masuko K. Cigarette Smoking: A Modifiable Environmental Factor in the Pathogenesis of Rheumatoid Arthritis. JMA J. 2025 Oct 15;8(4):1077-1086. doi: 10.31662/jmaj.2025-0029. Epub 2025 Oct 3. PMID: 41220506; PMCID: PMC12598268.
9. Baka Z, Buzás E, Nagy G. Rheumatoid arthritis and smoking: putting the pieces together. Arthritis Res Ther. 2009;11(4):238. doi: 10.1186/ar2751. Epub 2009 Aug 3. PMID: 19678909; PMCID: PMC2745780.
10. Harrison SR, Jutley G, Li D, Sahbudin I, Filer A, Hewison M, Raza K. Vitamin D and early rheumatoid arthritis. BMC Rheumatol. 2020 Jul 27;4:38. doi: 10.1186/s41927-020-00134-7. PMID: 32728658; PMCID: PMC7384217.
11. Yang L, Zhao H, Liu K, Wang Y, Liu Q, Sun T, Chen S, Ren L. Smoking behavior and circulating vitamin D levels in adults: A meta-analysis. Food Sci Nutr. 2021 Aug 5;9(10):5820-5832. doi: 10.1002/fsn3.2488. PMID: 34646549; PMCID: PMC8497833.
12. Lee H, Kim KN, Lim YH, Hong YC. Interaction of Vitamin D and Smoking on Inflammatory Markers in the Urban Elderly. J Prev Med Public Health. 2015 Sep;48(5):249-56. doi: 10.3961/jpmph.15.042. Epub 2015 Sep 17. PMID: 26429291; PMCID: PMC4592026.
13. Kostoglou-Athanassiou I, Athanassiou P, Lyraki A, Raftakis I, Antoniadis C. Vitamin D and rheumatoid arthritis. Ther Adv Endocrinol Metab. 2012 Dec;3(6):181-7. doi: 10.1177/2042018812471070. PMID: 23323190; PMCID: PMC3539179.
14. Chang K, Yang SM, Kim SH, Han KH, Park SJ, Shin JI. Smoking and rheumatoid arthritis. Int J Mol Sci. 2014 Dec 3;15(12):22279-95. doi: 10.3390/ijms151222279. PMID: 25479074; PMCID: PMC4284707.
15. Noorwali AA. Comorbidities in smoking and nonsmoking male Saudi patients with rheumatoid arthritis. Int J Biol Biotech. 2023;20 (23): 195-99.
16. Noorwali AA. Serum vitamin-D inversely associates with the duration of disease in male patients with rheumatoid arthritis. Int J Biol Biotech. 2023;20 (2): 201-06.
17. Kennel KA, Drake MT, Hurley DL. Vitamin D deficiency in adults: when to test and how to treat. Mayo Clin Proc. 2010 Aug;85(8):752-7; quiz 757-8. doi: 10.4065/mcp.2010.0138. PMID: 20675513; PMCID: PMC2912737.
18. Holick MF, Binkley NC, Bischoff-Ferrari HA, Gordon CM, Hanley DA, Heaney RP, Murad MH, Weaver CM; Endocrine Society. Evaluation, treatment, and prevention of vitamin D deficiency: an Endocrine Society clinical practice guideline. J Clin Endocrinol Metab. 2011 Jul;96(7):1911-30. doi: 10.1210/jc.2011-0385. Epub 2011 Jun 6. Erratum in: J Clin Endocrinol Metab. 2011 Dec;96(12):3908. Erratum in: J Clin Endocrinol Metab. 2024 Sep 16;109(10):e1991. doi: 10.1210/clinem/dgae373. PMID: 21646368.
19. Kaur J, Khare S, Givler A. Vitamin D Deficiency. 2025 Feb 15. In: StatPearls [Internet]. Treasure Island (FL): StatPearls Publishing; 2026 Jan–. PMID: 30335299.
20. Bordelon P, Ghetu MV, Langan RC. Recognition and management of vitamin D deficiency. Am Fam Physician. 2009 Oct 15;80(8):841-6. Erratum in: Am Fam Physician. 2009 Dec 15;80(12):1357. PMID: 19835345.
21. Boucher BJ. The problems of vitamin d insufficiency in older people. Aging Dis. 2012 Aug;3(4):313-29. Epub 2012 Jun 6. PMID: 23185713; PMCID: PMC3501367.
22. Lange NE, Sparrow D, Vokonas P, Litonjua AA. Vitamin D deficiency, smoking, and lung function in the Normative Aging Study. Am J Respir Crit Care Med. 2012 Oct 1;186(7):616-21. doi: 10.1164/rccm.201110-1868OC. Epub 2012 Jul 19. PMID: 22822023; PMCID: PMC3480523.
23. Koçak MB, Kavuncuoğlu D. The relationship between smoking cessation and vitamin D. Ir J Med Sci. 2026 Apr;195(2):1165-1172. doi: 10.1007/s11845-026-04290-6. Epub 2026 Feb 28. PMID: 41762403; PMCID: PMC13190799.
24. Jiang CQ, Chan YH, Xu L, Jin YL, Zhu T, Zhang WS, Cheng KK, Lam TH. Smoking and serum vitamin D in older Chinese people: cross-sectional analysis based on the Guangzhou Biobank Cohort Study. BMJ Open. 2016 Jun 23;6(6):e010946. doi: 10.1136/bmjopen-2015-010946. PMID: 27338881; PMCID: PMC4932269.
25. Nwosu BU, Kum-Nji P. Tobacco smoke exposure is an independent predictor of vitamin D deficiency in US children. PLoS One. 2018 Oct 8;13(10):e0205342. doi: 10.1371/journal.pone.0205342. PMID: 30296288; PMCID: PMC6175516.
26. Yang L, Sato M, Saito-Abe M, Miyaji Y, Sato C, Nishizato M, Kumasaka N, Mezawa H, Yamamoto-Hanada K, Ohya Y. Smoking Exposure Is Associated with Serum Vitamin D Deficiency in Children: Evidence from the Japan Environment and Children's Study. Nutrients. 2022 Jul 29;14(15):3121. doi: 10.3390/nu14153121. PMID: 35956297; PMCID: PMC9370804.
27. Yuan L, Ni J. The association between tobacco smoke exposure and vitamin D levels among US general population, 2001-2014: temporal variation and inequalities in population susceptibility. Environ Sci Pollut Res Int. 2022 May;29(22):32773-32787. doi: 10.1007/s11356-021-17905-5. Epub 2022 Jan 12. PMID: 35020139; PMCID: PMC8752386.
28. Okrit F, Chantranuwatana P, Werawatganon D, Chayanupatkul M, Sanguanrungsirikul S. Changes of vitamin D receptors (VDR) and MAPK activation in cytoplasmic and nuclear fractions following exposure to cigarette smoke with or without filter in rats. Heliyon. 2021 Jan 30;7(1):e05927. doi: 10.1016/j.heliyon.2021.e05927. PMID: 33553726; PMCID: PMC7851787.
29. Voltan G, Cannito M, Ferrarese M, Ceccato F, Camozzi V. Vitamin D: An Overview of Gene Regulation, Ranging from Metabolism to Genomic Effects. Genes (Basel). 2023 Aug 25;14(9):1691. doi: 10.3390/genes14091691. PMID: 37761831; PMCID: PMC10531002.
30. Al-Bashaireh AM, Haddad LG, Weaver M, Chengguo X, Kelly DL, Yoon S. The Effect of Tobacco Smoking on Bone Mass: An Overview of Pathophysiologic Mechanisms. J Osteoporos. 2018 Dec 2;2018:1206235. doi: 10.1155/2018/1206235. PMID: 30631414; PMCID: PMC6304634.
31. Mulligan JK, Nagel W, O'Connell BP, Wentzel J, Atkinson

C, Schlosser RJ. Cigarette smoke exposure is associated with vitamin D3 deficiencies in patients with chronic rhinosinusitis. J Allergy Clin Immunol. 2014 Aug;134(2):342-9. doi: 10.1016/j.jaci.2014.01.039. Epub 2014 Mar 31. PMID: 24698317.
32. Azzeh FS, Kensara OA. Vitamin D Is a Good Marker for Disease Activity of Rheumatoid Arthritis Disease. Dis Markers. 2015;2015:260725. doi: 10.1155/2015/260725. Epub 2015 May 10. PMID: 26063950; PMCID: PMC4441987.
33. Lee YH, Bae SC. Vitamin D level in rheumatoid arthritis and its correlation with the disease activity: a meta-analysis. Clin Exp Rheumatol. 2016 Sep-Oct;34(5):827-833. Epub 2016 Apr 6. PMID: 27049238.
34. Guan Y, Hao Y, Guan Y, Bu H, Wang H. The Effect of Vitamin D Supplementation on Rheumatoid Arthritis Patients: A Systematic Review and Meta-Analysis. Front Med (Lausanne). 2020 Oct 30;7:596007. doi: 10.3389/fmed.2020.596007. PMID: 33195358; PMCID: PMC7661491.
35. Khatirnamani Z, Hajian-Tilaki K, Heidari B, Sohrabi A. The Effect of Vitamin D Supplementation on Clinical and Laboratory Biomarkers in Patients with Rheumatoid Arthritis: A Systematic Review and Meta-Analysis of Randomised Controlled Trials. Mediterr J Rheumatol. 2025 Sep 30;36(3):428-439. doi: 10.31138/mjr.090725.lar. PMID: 41122185; PMCID: PMC12536741.
36. Vidal M, Lane NE. Vitamin D and Its Role in Rheumatic Diseases. Metabolites. 2025 Apr 9;15(4):259. doi: 10.3390/metabo15040259. PMID: 40278388; PMCID: PMC12029499.
37. Kwon OC, Oh JS, Park MC, Kim YG. Effect of Vitamin D Supplementation on Bone Mineral Density in Rheumatoid Arthritis Patients With Osteoporosis. Front Med (Lausanne). 2020 Aug 21;7:443. doi: 10.3389/fmed.2020.00443. PMID: 32974365; PMCID: PMC7473387.
38. Bellan M, Sainaghi PP, Pirisi M. Role of Vitamin D in Rheumatoid Arthritis. Adv Exp Med Biol. 2017;996:155-168. doi: 10.1007/978-3-319-56017-5_13. PMID: 29124698.
39. Meena N, Singh Chawla SP, Garg R, Batta A, Kaur S. Assessment of Vitamin D in Rheumatoid Arthritis and Its Correlation with Disease Activity. J Nat Sci Biol Med. 2018 Jan-Jun;9(1):54-58. doi: 10.4103/jnsbm.JNSBM_128_17. PMID: 29456394; PMCID: PMC5812075.
40. Mukherjee D, Lahiry S, Thakur S, Chakraborty DS. Effect of 1,25 dihydroxy vitamin D3 supplementation on pain relief in early rheumatoid arthritis. J Family Med Prim Care. 2019 Feb;8(2):517-522. doi: 10.4103/jfmpc.jfmpc_446_18. PMID: 30984665; PMCID: PMC6436291.
41. Alharbi S, Alharbi R, Alhabib E, Ghunaim R, Alreefi MM. Vitamin D Deficiency in Saudi Patients With Rheumatoid Arthritis. Cureus. 2023 Feb 9;15(2):e34815. doi: 10.7759/cureus.34815. PMID: 36793500; PMCID: PMC9924707.
42. Attar SM. Vitamin D deficiency in rheumatoid arthritis. Prevalence and association with disease activity in Western Saudi Arabia. Saudi Med J. 2012 May;33(5):520-5. PMID: 22588813.
43. Rossini M, Maddali Bongi S, La Montagna G, Minisola G, Malavolta N, Bernini L, Cacace E, Sinigaglia L, Di Munno O, Adami S. Vitamin D deficiency in rheumatoid arthritis: prevalence, determinants and associations with disease activity and disability. Arthritis Res Ther. 2010;12(6):R216. doi: 10.1186/ar3195. Epub 2010 Nov 29. PMID: 21114806; PMCID: PMC3046526.
44. Lin J, Liu J, Davies ML, Chen W. Serum Vitamin D Level and Rheumatoid Arthritis Disease Activity: Review and Meta-Analysis. PLoS One. 2016 Jan 11;11(1):e0146351. doi: 10.1371/journal.pone.0146351. PMID: 26751969; PMCID: PMC4709104.
45. Aslam MM, John P, Bhatti A, Jahangir S, Kamboh MI. Vitamin D as a Principal Factor in Mediating Rheumatoid Arthritis-Derived Immune Response. Biomed Res Int. 2019 May 7;2019:3494937. doi: 10.1155/2019/3494937. PMID: 31205940; PMCID: PMC6530219.
46. Charoenngam N. Vitamin D and Rheumatic Diseases: A Review of Clinical Evidence. Int J Mol Sci. 2021 Oct 1;22(19):10659. doi: 10.3390/ijms221910659. PMID: 34639000; PMCID: PMC8508879.
47. Clasen JL, Cole R, Aune D, Sellon E, Heath AK. Vitamin D status and risk of rheumatoid arthritis: systematic review and meta-analysis. BMC Rheumatol. 2023 Mar 15;7(1):3. doi: 10.1186/s41927-023-00325-y. PMID: 36918989; PMCID: PMC10015722.
48. Rexhepi M, Krasniqi B, Hoti K, Daci A, Rexhepi-Kelmendi B, Krasniqi S. Impact of vitamin D supplementation on disease activity and pain management in rheumatoid arthritis: a randomized double-blinded controlled study. BMC Rheumatol. 2025 Jul 11;9(1):87. doi: 10.1186/s41927-025-00543-6. PMID: 40646666; PMCID: PMC12247244.
49. Elfituri S. The effects of vitamin D supplementation on disease activity and fatigue in Libyan rheumatoid arthritis patients. Reumatologia. 2024;62(2):109-114. doi: 10.5114/reum/187391. Epub 2024 May 10. PMID: 38799782; PMCID: PMC11114129.
50. Ranjbar M, Rahimlou M, Fallah M, Djafarian K, Mohammadi H. Effects of vitamin D supplementation in patients with rheumatoid arthritis: A systematic review and meta-analysis. Heliyon. 2025 Feb 4;11(3):e42463. doi: 10.1016/j.heliyon.2025.e42463. PMID: 39995929; PMCID: PMC11849653.
51. Sukharani N, Dev K, Rahul F, Bai P, Ali A, Avinash F, Kammawal Y, Kumar N, Rizwan A. Association Between Rheumatoid Arthritis and Serum Vitamin D Levels. Cureus. 2021 Sep 24;13(9):e18255. doi: 10.7759/cureus.18255. PMID: 34712532; PMCID: PMC8542394.
52. Hussain MS, Islam T, Islam MS, Danishuddin, Haque MA. Clinical insights into the role of smoking, diabetes, and rheumatoid arthritis in osteoporotic fractures. Arch Osteoporos. 2025 Jul 11;20(1):87. doi: 10.1007/s11657-025-01575-8. PMID: 40643730.
53. Hajjaj-Hassouni N, Mawani N, Allali F, Rkain H, Hassouni K, Hmamouchi I, Dougados M. Evaluation of Vitamin D Status in Rheumatoid Arthritis and Its Association with Disease Activity across 15 Countries: "The COMORA Study". Int J Rheumatol. 2017;2017:5491676. doi: 10.1155/2017/5491676. Epub 2017 Jun 1. PMID: 28656048; PMCID: PMC5471553.
54. Batista AAP, Lazzarin T, Pereira FWL, Baccaro A, Rocha OM, Narimatsu KL, Souza JT, Modesto PN, Zanati Bazan SG, Tanni SE, Okoshi MP, Polegato BF, Paiva SAR, Zornoff L, Minicucci MF, Azevedo PS. Serum Vitamin D Levels, Disease Activity Score-28 for Rheumatoid Arthritis with C-Reactive Protein (DAS28-CRP), and Cardiac Remodeling Determined by Ventricular Dimensions and Left Atrium Diameter in Patients with Rheumatoid Arthritis: A Prospective Observational Study. Med Sci Monit. 2023 Jan 7;29:e938989. doi: 10.12659/MSM.938989. PMID: 36609557; PMCID: PMC9832721.

International Journal of Biomedicine 16(3) (2026) 320-326
http://dx.doi.org/10.21103/Article16(3)_RA4

REVIEW ARTICLE

INTERNATIONAL JOURNAL OF BIOMEDICINE

Impact of Adrenal Gland Dysfunction on Dental Implant Therapy and Osseointegration: A Narrative Review

Bylbyl Reçica[1,2], Vjosa Hamiti Krasniqi[3,1*], Jehona Ahmedi[1], Besir Salihu[1]

[1]*Department of Oral Surgery, Clinical University Dentistry Center of Kosova, Prishtina, Kosovo*
[2]*Alma Mater Europaea, Campus College "Rezonanca", Prishtina, Kosovo*
[3]*UBT – Higher Education Institution, Prishtina, Kosovo*

Abstract

Background: Dental implant therapy is widely used for oral rehabilitation, with success largely dependent on bone metabolism and effective osseointegration. Systemic conditions, particularly endocrine disorders such as adrenal gland dysfunction, may influence these biological processes. However, the impact of adrenal disorders on dental implant outcomes remains insufficiently explored in current clinical guidelines.

Methods: A narrative review was conducted. An electronic search was performed in PubMed/MEDLINE, Scopus, and Web of Science databases for studies published through December 2024. Relevant studies addressing adrenal gland dysfunction, corticosteroid therapy, bone metabolism, and dental implant therapy were included. A total of 24 publications were selected based on their clinical relevance and contribution to evidence-based recommendations.

Results: Current evidence suggests that adrenal gland dysfunction should not be considered an absolute contraindication for dental implant therapy. Patients with well-controlled adrenal insufficiency may achieve favorable outcomes with appropriate medical management and perioperative corticosteroid supplementation protocols. In contrast, uncontrolled hypercortisolism and prolonged corticosteroid therapy may negatively affect bone metabolism, impair wound healing, and increase the risk of peri-implant complications. Risk stratification protocols enable clinicians to optimize outcomes through individualized treatment planning.

Conclusion: Adrenal gland dysfunction represents a relative risk factor rather than a contraindication to dental implant therapy. Careful patient evaluation, interdisciplinary collaboration with endocrinologists, and individualized treatment planning incorporating stress-reduction protocols and appropriate corticosteroid supplementation are essential to optimize clinical outcomes and ensure long-term implant success. Future prospective studies with standardized protocols are needed to establish comprehensive evidence-based guidelines for perioperative management and long-term implant outcomes in patients with adrenal dysfunction.(International Journal of Biomedicine. 2026;16(3):320-326.)

Keywords: adrenal insufficiency • hypercortisolism • Cushing syndrome • corticosteroid therapy • dental implants • bone metabolism

For citation: Reçica B, Krasniqi VH, Ahmedi J, Salihu B. Impact of Adrenal Gland Dysfunction on Dental Implant Therapy and Osseointegration: A Narrative Review. International Journal of Biomedicine. 2026;16(3):320-326. doi:10.21103/Article16(3)_RA4

Introduction

Dental implants have become an established treatment option for the rehabilitation of edentulous and partially edentulous patients, demonstrating high survival rates and predictable long-term outcomes in healthy individuals. [1,2] The success of implant therapy depends largely on osseointegration, a complex biological process involving direct structural and functional contact between living bone and the implant surface.[3]

Increasing attention has been directed toward the influence of systemic conditions on implant success. Systemic diseases affecting bone metabolism, immune response, and tissue healing may influence both the osseointegration process and the long-term stability of peri-implant tissues. [4,5] Endocrine disorders are particularly relevant because hormonal regulation plays an essential role in bone remodeling and inflammatory responses.[6]

Among endocrine disorders, adrenal gland dysfunction is clinically relevant, yet remains an underrepresented area of research in implant dentistry. The adrenal glands regulate several physiological processes through the secretion of glucocorticoids, mineralocorticoids, and adrenal androgens. Cortisol, the principal glucocorticoid, plays a central role in

stress response, immune regulation, and bone metabolism.[7] Alterations in cortisol levels may therefore influence bone turnover and wound-healing processes essential for successful implant integration. Despite these implications, adrenal disorders are rarely addressed explicitly in implant guidelines.[8,9] This narrative review aims to synthesize current evidence regarding adrenal gland dysfunction and its clinical implications for dental implant therapy, with particular emphasis on osseointegration, perioperative management, corticosteroid supplementation protocols, and clinical outcomes.

Materials and Methods

This study was conducted as a narrative review. Due to the limited number of studies specifically addressing adrenal dysfunction and dental implants, a narrative review methodology was selected to allow integration of evidence from implant dentistry, endocrinology, oral surgery, and bone metabolism literature.

An electronic search was performed in PubMed/MEDLINE, Scopus, and Web of Science databases for studies published through December 2024.

The search strategy included combinations of the following keywords: adrenal insufficiency, Addison's disease, Cushing syndrome, hypercortisolism, corticosteroid therapy, glucocorticoids, dental implants, osseointegration, bone metabolism, perioperative management, and oral surgery. Boolean operators (AND, OR) were used to combine the search terms and refine the results.

Articles published in English that discussed adrenal dysfunction, corticosteroid therapy, bone metabolism, and implant therapy were considered eligible. Narrative reviews, systematic reviews, clinical studies, and clinical practice guidelines were included. Animal and in vitro studies lacking direct clinical relevance were excluded.

Titles and abstracts of the retrieved articles were screened to identify relevant studies. Due to the limited number of publications specifically addressing dental implants in patients with adrenal disorders, additional relevant literature from related fields, particularly oral surgery, endocrinology, and bone physiology, was also considered.

A total of 24 publications met the inclusion criteria and were included in the final analysis. These studies were selected for their direct relevance to dental implant therapy and adrenal gland dysfunction, as well as their contributions to understanding the physiological mechanisms that influence bone metabolism, immune response, and surgical outcomes. Priority was given to studies that provided clinically applicable data and comprehensive reviews that addressed both endocrine and implant-related aspects.

Physiology of Adrenal Glands and Bone Metabolism

Glucocorticoids play a fundamental role in bone remodeling and bone tissue homeostasis by regulating the activity of osteoblasts and osteoclasts. Physiological levels of cortisol are essential for maintaining the balance between bone formation and bone resorption. However, chronic exposure to elevated levels of glucocorticoids inhibits the differentiation and activity of osteoblasts, increases osteocyte apoptosis, and stimulates osteoclast-mediated bone resorption.[11,12] Consequently, these alterations may lead to a reduction in bone mineral density and impairment of bone microarchitecture. These changes are of particular clinical significance, as bone quality and remodeling capacity represent key determinants for the successful osseointegration of dental implants.

At the molecular level, glucocorticoids inhibit collagen synthesis and interfere with signaling pathways involved in the regulation of osteogenesis. In addition, they modify the balance between the receptor activator of nuclear factor-κB ligand (RANKL) and osteoprotegerin (OPG), promoting osteoclast differentiation and activity and consequently enhancing bone resorption.[12] These mechanisms are of considerable relevance in implant dentistry, as successful osseointegration depends on early bone formation and the establishment of stable contact between the implant surface and the surrounding bone tissue.

In contrast to hypercortisolism, adrenal insufficiency primarily affects the body's physiological response to stress and does not directly cause pronounced bone catabolism. Reduced cortisol production may compromise the body's ability to respond adequately to surgical stress and may affect hemodynamic stability during invasive procedures, including oral and implant surgery.[10] However, with appropriate perioperative management and corticosteroid supplementation, these risks can be effectively mitigated.

Table 1.

Effects of cortisol on bone metabolism and dental implants.

Parameter	Physiological cortisol	Low cortisol (Adrenal Insufficiency)	High cortisol (Hypercortisolism)
Bone formation (Osteoblasts)	Normal	Slightly reduced	Significantly inhibited
Bone resorption (Osteoclasts)	Equilibrium	Normal	Markedly increased
Collagen synthesis	Normal	Slightly reduced	Significantly inhibited
Wound healing	Normal	May be delayed	Compromised
Bone quality	Good	Acceptable	Compromised
Stress response	Normal	Compromised	Impaired
Risk for osseointegration	Minimal	Low (with management)	Moderate to high

Adrenal Insufficiency and Dental Implant Surgery

Adrenal insufficiency may be classified as primary (Addison's disease) or secondary, most commonly resulting from prolonged corticosteroid therapy. In patients undergoing dental implant surgery, the main concern is not impaired osseointegration but rather the possibility of an inadequate physiological response to surgical stress.[13] Cortisol plays an essential role in maintaining metabolic stability, vascular tone, and an adequate stress response during surgical procedures.

Current evidence suggests that adrenal insufficiency should not be considered an absolute contraindication to dental implant placement. Patients with well-controlled disease may achieve favorable clinical outcomes when appropriate perioperative management strategies are implemented.[14] Therefore, careful medical evaluation, including assessment of the patient's endocrine status and current corticosteroid therapy, is essential before performing implant surgery.

Nevertheless, the risk of adrenal crisis during oral surgical procedures, although relatively rare, represents a potentially life-threatening complication. Adrenal crisis may manifest with hypotension, fatigue, nausea, and electrolyte imbalance, requiring immediate medical intervention.[15] For this reason, careful preoperative assessment and close clinical monitoring are recommended in patients with known adrenal insufficiency.

Perioperative Corticosteroid Supplementation

Dental implant placement is generally considered to induce mild to moderate surgical stress. The need for perioperative corticosteroid supplementation should be individualized based on patient factors, including disease control, medication regimen, and surgical complexity. For well-controlled adrenal insufficiency undergoing minor procedures such as single implant placement, current guidelines from endocrine societies suggest that standard replacement therapy may be adequate without additional "stress-dose" supplementation.[20,21]

However, for more extensive surgical procedures or in patients with inadequate disease control, perioperative corticosteroid supplementation is recommended. The standard approach involves administering 25 mg hydrocortisone intravenously (IV) at the time of surgical incision, with consideration for continued supplementation based on surgical duration and complexity.[8,10,15] This dosing protocol is supported by clinical practice guidelines from endocrine organizations and has demonstrated safety and efficacy in preventing perioperative adrenal crisis.[22]

Coordination with the patient's treating endocrinologist is essential to optimize the perioperative management plan and ensure seamless transition to standard replacement therapy in the postoperative period. With appropriate medical management and careful surgical planning, dental implant therapy can be performed safely in most patients with adrenal insufficiency.

Hypercortisolism and Cushing Syndrome

Hypercortisolism, whether endogenous or iatrogenic, has well-documented negative effects on bone metabolism and immune function. Chronic exposure to elevated cortisol levels is a major cause of secondary osteoporosis, characterized by reduced bone formation and increased bone resorption.[16] The severity of bone loss correlates with the duration and magnitude of cortisol excess, and recovery of bone density may be prolonged even after successful treatment of the underlying hypercortisolism.[23]

In implant dentistry, compromised bone quality may negatively influence primary implant stability and delay the osseointegration process. In addition, impaired soft-tissue healing and increased susceptibility to infection may elevate the risk of peri-implant complications, including peri-implantitis and implant loss.[17,23] Furthermore, patients with Cushing syndrome often present with multiple comorbidities, including hypertension, impaired glucose tolerance, and immunosuppression, that further compromise surgical outcomes and healing capacity.

Although direct clinical studies linking Cushing syndrome to implant failure remain limited, available evidence suggests that uncontrolled hypercortisolism should be considered a significant relative risk factor when planning implant therapy. Ideally, implant therapy should be deferred until the hypercortisolism is adequately controlled through medical or surgical intervention, with restoration of cortisol levels to physiological ranges.

Chronic Corticosteroid Therapy

Long-term systemic corticosteroid therapy represents another important factor that may influence implant outcomes. Prolonged glucocorticoid exposure negatively affects bone density, immune function, and wound healing while also suppressing the hypothalamic–pituitary–adrenal (HPA) axis.[12,17] Cumulative dose and duration of therapy are important determinants of bone loss and other metabolic complications.[23]

Despite these potential concerns, several studies suggest that implant therapy may still be successful in patients receiving corticosteroid treatment when systemic disease is well controlled and appropriate surgical precautions are taken.[18,23] Therefore, chronic corticosteroid therapy should generally be regarded as a relative risk factor rather than an absolute contraindication. However, patients on doses exceeding 10 mg daily prednisone equivalent warrant particular attention and more conservative surgical approaches.

Clinical Implications and Risk Stratification

A comprehensive medical evaluation is essential before implant placement in patients with adrenal dysfunction. Clinicians should obtain a detailed history of adrenal disease, current medications, corticosteroid dosage and duration, previous adrenal crises, and associated comorbidities. Laboratory assessment of baseline cortisol levels and ACTH concentrations may be useful for documenting disease control.

Interdisciplinary collaboration with endocrinologists is recommended, particularly when the patient's endocrine status or perioperative management is uncertain. Written communication with the treating endocrinologist regarding surgical timing, anesthetic approach, and perioperative

corticosteroid management is essential to ensure safe clinical outcomes.

Practical Considerations for Optimizing Clinical Outcomes

Stress-reduction protocol: The use of profound local anesthesia, short and atraumatic surgical procedures, and, when indicated, oral sedation may help minimize surgical stress and reduce the physiological demand for endogenous cortisol production.

Corticosteroid supplementation: As outlined in Section 4, the need for perioperative corticosteroid supplementation should be assessed on an individual basis in consultation with the patient's endocrinologist. For well-controlled patients undergoing minor procedures, standard replacement therapy may be adequate; however, more extensive procedures typically require supplementation with 25 mg hydrocortisone IV at induction.[8,10,15]

Surgical approach: Minimally invasive techniques, careful tissue handling, and atraumatic surgical execution are recommended to reduce trauma, inflammation, and healing time. When feasible, flapless techniques or limited-flap approaches may be advantageous in patients with compromised healing capacity.

Healing protocols: Delayed loading and extended osseointegration periods (6-8 months) may be beneficial in patients with compromised bone metabolism or significant cortisol excess. Progressive loading protocols should be considered in high-risk patients to allow adequate bone remodeling before full functional loading.

Infection prevention: Patients with adrenal dysfunction, particularly those with hypercortisolism or long-term corticosteroid use, are at increased risk of infection. Enhanced oral hygiene protocols, antimicrobial rinses, and consideration of prophylactic antibiotics may be warranted.[23] Long-term antimicrobial mouth rinses containing chlorhexidine or povidone-iodine may reduce early peri-implant complications.

In addition, clinicians should consider that patients with adrenal dysfunction, particularly those with hypercortisolism or long-term corticosteroid use, may present with associated comorbidities such as hypertension, impaired glucose

Table 2.

Risk stratification and management protocols for dental implants in patients with adrenal dysfunction

Risk category	Type of Dysfunction	Disease control	Surgical guidelines	Corticosteroid supplementation	Additional considerations
Low risk	Adrenal insufficiency	Well-controlled	Standard local anesthesia; Short procedure; Single implant	25 mg hydrocortisone IV at induction (8,10,15)	Coordination with endocrinologist; Standard post-op care
Moderate risk	Mild hypercortisolism or chronic low-dose corticosteroid therapy	Controlled	Minimally invasive technique; Extended healing period; Consider flapless approach	Depending on the endocrinologist's decision, additional supplementation may be required.	Enhanced infection prevention; Delayed loading (6-8 months)
High risk	Uncontrolled hypercortisolism or high-dose corticosteroid therapy (>10 mg prednisone equivalent daily)	Poorly controlled	Postpone elective procedure; Endocrinologist consultation; Consider systemic disease treatment first	Postpone procedure until disease control is achieved.	Defer implant therapy; Optimize systemic control; Reassess in 3-6 months

Table 3.

Summary of the impact of adrenal disorders on dental implant requirements and outcomes.

Component	Adrenal insufficiency	Hypercortisolism	Chronic corticosteroid therapy
Bone quality	Good (with adequate cortisol replacement)	Compromised (secondary osteoporosis)	Compromised (dose-dependent)
Wound healing	May be delayed (requires optimization)	Significantly compromised	Compromised (dose-dependent)
Immune response	Slightly reduced	Markedly compromised	Reduced (dose-dependent)
Implant stability (primary)	Good	Moderate to high risk	Moderate risk
Implant stability (long-term)	Good	High risk without disease control	Moderate to high risk
Management compatibility	Good (with perioperative supplementation)	Requires careful planning and disease control	Requires close monitoring and coordination
Risk of peri-implantitis	Low	Moderate to high	Moderate
Recommended loading protocol	Standard (3-6 months)	Delayed (6-8 months)	Delayed (6-8 months)

tolerance, osteoporosis, and delayed soft-tissue healing. These factors may further influence postoperative recovery and should be taken into account during comprehensive treatment planning.

Table 2 and Table 3 provide a comprehensive summary of how each category of adrenal disorder impacts critical parameters of dental implant therapy, including bone quality, wound healing, immune response, and implant stability. This comparative analysis is particularly useful for differentiated treatment planning and prognostication in distinct patient populations with adrenal dysfunction.

Limitations of Current Evidence

Direct clinical studies evaluating dental implant outcomes specifically in patients with adrenal gland disorders are scarce. Much of the available evidence is drawn from the broader literature on systemic diseases, oral surgery, bone metabolism, and endocrinology, necessitating careful extrapolation to the context of implant dentistry.

Several specific limitations merit discussion:

Limited prospective data: Most available evidence on implant outcomes in patients with adrenal disorders comes from small case reports, case series, or observational studies. Large-scale prospective clinical trials specifically evaluating implant success rates in patients with documented adrenal dysfunction are lacking.

Heterogeneity of patient populations: Variability in disease severity, medication regimens, dosages, duration of disease, and presence of comorbidities significantly complicates the interpretation and generalization of available findings. Patients with adrenal insufficiency on replacement therapy may have substantially different outcomes compared to those with uncontrolled hypercortisolism or those on high-dose corticosteroid therapy for systemic disease.

Lack of standardized protocols: Perioperative corticosteroid supplementation protocols vary widely across institutions and clinicians. No universally accepted, standardized protocols for dental implant surgery exist, making it difficult to compare outcomes across studies and to establish evidence-based recommendations.

Confounding variables: Many patients with chronic corticosteroid therapy have underlying systemic conditions (such as autoimmune diseases or malignancies) that independently affect bone metabolism, immune function, and healing capacity, making it difficult to isolate the effects of corticosteroids alone on implant outcomes.

Limited long-term follow-up data: Most available studies report short-term implant survival (1-3 years). Long-term follow-up data (5-10 years) specifically examining peri-implant bone loss, soft-tissue health, and functional outcomes in patients with adrenal dysfunction are sparse.

Outcome measurement heterogeneity: Studies use varying definitions and assessment methods for implant success, making meta-analysis and direct comparison problematic. Standardized outcome measures, including implant survival, marginal bone loss, peri-implant soft-tissue health, and patient-reported outcomes, are needed.

These limitations underscore the need for well-designed prospective studies with standardized protocols and comprehensive outcome reporting to establish robust evidence-based guidelines for implant dentistry in patients with adrenal disorders.

Future Research Directions

Future research should prioritize the following:

Prospective clinical trials: Multicenter prospective studies evaluating implant survival, osseointegration kinetics, marginal bone loss, and peri-implant tissue health in patients with documented adrenal insufficiency, hypercortisolism, and chronic corticosteroid therapy should be conducted with adequate follow-up periods (minimum 5 years).

Standardized perioperative protocols: Research should establish and validate standardized corticosteroid supplementation protocols specific to dental implant surgery in patients with adrenal dysfunction, including dose recommendations based on surgical complexity and disease control status.

Biomarker studies: Investigation of bone metabolism biomarkers (P1NP, CTX, RANKL/OPG ratios) in patients with adrenal dysfunction may help predict osseointegration potential and guide individualized treatment strategies.

Surgical technique evaluation: Comparative studies examining outcomes with different surgical approaches (conventional flap versus flapless, immediate versus delayed loading) in patients with adrenal dysfunction would inform evidence-based surgical decision-making.

Comorbidity assessment: Prospective evaluation of how comorbidities frequently associated with adrenal disorders (hypertension, diabetes, osteoporosis) modify implant outcomes would improve patient risk stratification.

Long-term peri-implant health: Longitudinal studies specifically examining rates of peri-implantitis, marginal bone loss, and soft-tissue complications in patients with adrenal disorders would establish long-term prognosis and guide maintenance protocols.

Patient-centered outcomes: Research incorporating patient-reported outcomes, quality of life measures, and functional assessments would provide a comprehensive understanding of implant therapy success beyond traditional survival metrics.

Conclusions

Adrenal gland dysfunction should be considered a relative risk factor rather than an absolute contraindication to dental implant therapy. Well-controlled adrenal insufficiency does not appear to significantly compromise osseointegration when appropriate perioperative corticosteroid supplementation (25 mg hydrocortisone IV) and medical management are implemented. Conversely, uncontrolled hypercortisolism and high-dose chronic corticosteroid therapy may negatively affect bone quality, healing capacity, and immune function, thereby increasing the risk of implant failure and peri-implant complications.

Successful implant outcomes depend on:

- Comprehensive preoperative medical assessment and documentation of endocrine disease control
- Interdisciplinary collaboration with endocrinologists to optimize perioperative management
- Individualized surgical planning incorporating risk stratification
- Implementation of stress-reduction protocols and appropriate corticosteroid supplementation
- Modified surgical techniques and healing protocols tailored to the patient's physiological status
- Enhanced infection prevention strategies in immunocompromised patients
- Consideration of extended osseointegration periods and delayed loading in high-risk patients

Furthermore, systemic conditions frequently associated with hypercortisolism—such as hypertension, impaired glucose metabolism, and osteoporosis—may also compromise soft-tissue healing, increase susceptibility to infection, and adversely affect long-term peri-implant health. Comprehensive patient management addressing these comorbidities is essential for optimizing implant prognosis.

Future prospective studies with standardized protocols, standardized outcome measures, and adequate long-term follow-up are essential to establish comprehensive evidence-based guidelines for perioperative management and long-term implant outcomes in patients with adrenal dysfunction. Until higher-quality evidence becomes available, clinicians should apply individualized risk assessment and interdisciplinary management strategies to optimize implant success in patients with adrenal dysfunction.

AI Statement

AI-assisted tools were used solely for language editing and manuscript formatting, based on scientific material provided by the authors.

Author Contributions

Bylbyl Reçica: Conceptualization, validation, formal analysis, investigation, data curation, writing—original draft, writing—review and editing, visualization, supervision, project administration.
Vjosa Hamiti Krasniqi: Investigation, data curation, writing—original draft, and writing—review and editing.
Jehona Ahmedi: Investigation, data curation.
Besir Salihu: Investigation, data curation.
All authors have approved the final article.

Competing interests

The authors declare no conflict of interest

Funding

This research received no external funding

References

1. Mombelli A, Cionca N. Systemic diseases affecting osseointegration therapy. Clin Oral Implants Res. 2006 Oct;17 Suppl 2:97-103. doi: 10.1111/j.1600-0501.2006.01354.x. Erratum in: Clin Oral Implants Res. 2006 Dec;17(6):746. PMID: 16968386.
2. Albrektsson T, Johansson C. Osteoinduction, osteoconduction and osseointegration. Eur Spine J. 2001 Oct;10 Suppl 2(Suppl 2):S96-101. doi: 10.1007/s005860100282. PMID: 11716023; PMCID: PMC3611551.
3. Brånemark PI. Osseointegration and its experimental background. J Prosthet Dent. 1983 Sep;50(3):399-410. doi: 10.1016/s0022-3913(83)80101-2. PMID: 6352924.
4. D'Ambrosio F, Amato A, Chiacchio A, Sisalli L, Giordano F. Do Systemic Diseases and Medications Influence Dental Implant Osseointegration and Dental Implant Health? An Umbrella Review. Dent J (Basel). 2023 Jun 5;11(6):146. doi: 10.3390/dj11060146. PMID: 37366669; PMCID: PMC10296829.
5. Sakka S, Baroudi K, Nassani MZ. Factors associated with early and late failure of dental implants. J Investig Clin Dent. 2012 Nov;3(4):258-61. doi: 10.1111/j.2041-1626.2012.00162.x. Epub 2012 Aug 27. PMID: 22927130.
6. Torrejon-Moya A, Izquierdo-Gómez K, Pérez-Sayáns M, Jané-Salas E, Marí Roig A, López-López J. Patients with Thyroid Disorder, a Contraindication for Dental Implants? A Systematic Review. J Clin Med. 2022 Apr 25;11(9):2399. doi: 10.3390/jcm11092399. PMID: 35566524; PMCID: PMC9102443.
7. Guyton AC, Hall JE. Textbook of Medical Physiology. 14th ed. Philadelphia: Elsevier; 2021.
8. Chan MH. Update on Management of the Oral and Maxillofacial Surgery Patient on Corticosteroids. Oral Maxillofac Surg Clin North Am. 2022 Feb;34(1):115-126. doi: 10.1016/j.coms.2021.08.011. Epub 2021 Oct 25. PMID: 34711466.
9. Carmona D, Ouanounou A. Adrenal Insufficiency and Its Implications on Dental Treatment. Compend Contin Educ Dent. 2021 Sep;42(8):422-428; quiz 429. PMID: 34449238.
10. Bornstein SR, Allolio B, Arlt W, Barthel A, Don-Wauchope A, Hahner S, et al. Diagnosis and treatment of primary adrenal insufficiency: Endocrine Society Clinical Practice Guideline. Lancet Diabetes Endocrinol. 2016 Mar;4(3):216-26.
11. Compston J. Glucocorticoid-induced osteoporosis. Lancet. 2018 Jun 9;391(10137):2345-2357.
12. Canalis E. Mechanisms of glucocorticoid action in bone. Endocrine. 2015;49:13-19.
13. Miller CS, Little JW, Falace DA. Supplemental corticosteroids for dental patients with adrenal insufficiency: reconsideration of the problem. J Am Dent Assoc. 2001 Nov;132(11):1570-9; quiz 1596-7. doi: 10.14219/jada.archive.2001.0092. PMID: 11806072.
14. Khalaf MW, Khader R, Cobetto G, Yepes JF, Karounos DG, Miller CS. Risk of adrenal crisis in dental patients: results of a systematic search of the literature. J Am Dent Assoc. 2013 Feb;144(2):152-60. doi: 10.14219/jada.archive.2013.0094. PMID: 23372131.
15. Salem M, Tainsh RE Jr, Bromberg J, Loriaux DL, Chernow B. Perioperative glucocorticoid coverage. A reassessment 42 years after emergence of a problem. Ann Surg. 1994 Apr;219(4):416-25. doi: 10.1097/00000658-199404000-

00013. PMID: 8161268; PMCID: PMC1243159.
16. Hahner S, Loeffler M, Fassnacht M, Weismann D, Koschker AC, Quinkler M, Decker O, Arlt W, Allolio B. Impaired subjective health status in 256 patients with adrenal insufficiency on standard therapy based on cross-sectional analysis. J Clin Endocrinol Metab. 2007 Oct;92(10):3912-22. doi: 10.1210/jc.2007-0685. Epub 2007 Aug 7. PMID: 17684047.
17. Arlt W, Baldeweg SE, Pearce SHS, Simpson HL. Endocrine management of severe illness in intensive care units: an Endocrine Society Clinical Practice Guideline. J Clin Endocrinol Metab. 2022 Feb 1;107(2):494-520.
18. Osella G, Terzolo M, Borretta G, Magro G, Conti M, Angeli A. Bone mineral density and bone metabolism in Cushing syndrome. J Clin Endocrinol Metab. 1994 Aug;79(2):487-493.
19. Newell-Price J, Bertagna X, Grossman AB, Nieman LK. Cushing's syndrome. Lancet. 2006 May 13;367(9522):1605-17. doi: 10.1016/S0140-6736(06)68699-6. PMID: 16698415.
20. van Staa TP, Leufkens HG, Abenhaim L, Zhang B, Cooper C. Oral corticosteroids and fracture risk: relationship to daily and cumulative doses. Rheumatology (Oxford). 2000 Dec;39(12):1383-9. doi: 10.1093/rheumatology/39.12.1383. PMID: 11136882.
21. Compston JE. Corticosteroid-induced bone loss. Endocr Rev. 2017;38:347-372.
22. Thygeson B. Systemic factors affecting wound healing in the oral cavity. J Oral Maxillofac Surg. 2020;78(2):217-228.
23. Moy PK, Medina D, Shetty V, Aghaloo TL. Dental implant failure rates and associated risk factors. Int J Oral Maxillofac Implants. 2005 Jul-Aug;20(4):569-77. PMID: 16161741.

***Corresponding author:** *Vjosa Hamiti Krasniqi. E-mail: vjosa.hamiti@gmail.com*

International Journal of Biomedicine 16(3) (2026) 327-332
http://dx.doi.org/10.21103/Article16(3)_RA5

REVIEW ARTICLE

INTERNATIONAL JOURNAL OF BIOMEDICINE

Incidence and Prevention of White Spot Lesions Associated with Fixed Orthodontic Appliances: A Literature Review

Gazmend Jusufi[1*]

[1]*Department of Orthodontics, International Balkan University, Skopje,North Macedonia*

Abstract

Background: White spot lesions (WSLs) are a common adverse effect of fixed orthodontic treatment, resulting from enamel demineralization associated with plaque accumulation around orthodontic appliances. Their prevention remains a clinical challenge in orthodontic practice. The present review aimed to evaluate the available evidence regarding the effectiveness of preventive strategies for reducing the risk of white spot lesion development in patients undergoing fixed orthodontic treatment.
Materials and Methods: A literature search was performed in Medline/PubMed and the Cochrane Library for English-language clinical studies published up to 2010. Controlled in vivo human studies reporting the incidence and/or prevalence of WSLs in patients undergoing fixed orthodontic treatment were included. Studies with a minimum treatment duration of 12 months were considered. Data regarding incidence, prevalence, risk factors, and preventive measures were extracted and analyzed descriptively.
Results: Ten studies involving 1,241 patients were included. The overall incidence of WSLs was 45.8%, while the prevalence was 68.4%. Reported risk factors included poor oral hygiene, younger age at treatment initiation, male sex, and longer treatment duration. Protective factors included adequate salivary flow and the use of fluoride-based preventive measures, which were associated with reduced lesion development.
Conclusion: WSLs are a frequent complication of fixed orthodontic treatment. Their development is multifactorial, with identifiable patient- and treatment-related risk factors. Preventive strategies, particularly fluoride-based interventions and improved oral hygiene measures, should be integrated into routine orthodontic care to reduce the risk of enamel demineralization.(**International Journal of Biomedicine. 2026;16(3):327-332.**)

Keywords: white spot lesions • orthodontic treatment • enamel demineralization • caries • fluoride • fixed appliances

For citation: Jusufi G. Incidence and Prevention of White Spot Lesions Associated with Fixed Orthodontic Appliances: A Literature Review. International Journal of Biomedicine. 2026;16(3):327-332. doi:10.21103/Article16(3)_RA5

Introduction

The demand for orthodontic treatment has increased considerably over recent decades, particularly in developed countries, owing to growing awareness of oral health and dental aesthetics.[1] Orthodontic treatment is indicated for the correction of dental malocclusions and craniofacial skeletal discrepancies resulting from genetic, familial, and environmental factors through the use of fixed or removable appliances.[2]

Despite the significant functional and aesthetic benefits achieved through orthodontic therapy, treatment with fixed appliances is frequently associated with adverse effects, among which white spot lesions (WSLs) are one of the most common complications. WSLs are early manifestations of enamel demineralization that appear clinically as opaque, chalky-white areas on the tooth surface. Their reported prevalence varies widely in the literature, ranging from 33.8% to 97%, depending on the diagnostic criteria, assessment methods, and units of analysis employed, as well as the inclusion or exclusion of pre-existing enamel lesions.[3-7]

Enamel demineralization may initially be reversible through natural remineralization processes mediated by saliva and its mineral components. Salivary proteins can partially restore mineral content and reduce the visual appearance of early lesions.[8] However, in patients undergoing orthodontic treatment, persistent plaque accumulation around orthodontic appliances often promotes the progression of these lesions, resulting in irreversible enamel damage and an increased risk of caries development.[9]

***Corresponding author**: Asst. Prof. Gazmend Jusufi. E-mail: gazmend.jusufi@ibu.edu.mk*

Dental caries is a multifactorial disease influenced by biological, behavioral, environmental, and socioeconomic factors. Established risk factors include frequent consumption of fermentable carbohydrates, inadequate oral hygiene, insufficient fluoride exposure, and irregular dental attendance. Demographic variables such as age, sex, educational level, income, and ethnicity may further influence susceptibility to caries.[10] Consequently, maintaining adequate oral hygiene practices and regular exposure to fluoride remain fundamental components of caries prevention.

The association between dietary sugar intake and dental caries has been extensively documented.[11,12] Frequent consumption of sugar-containing beverages, including soft drinks, fruit juices, and sports drinks, as well as confectionery products, contributes significantly to the risk of enamel demineralization. Dietary assessment and individualized nutritional counseling may therefore play an important role in reducing exposure to fermentable carbohydrates and limiting caries risk.[13] Although dietary habits are not routinely evaluated in orthodontic practice because of time and resource constraints, such assessments may contribute significantly to the prevention of WSL development.

Fixed orthodontic appliances create conditions that favor biofilm accumulation and enamel demineralization. Orthodontic brackets, bands, ligatures, and archwires introduce additional retentive sites that complicate oral hygiene procedures and facilitate plaque retention.[14] Furthermore, the surface characteristics of orthodontic materials influence bacterial colonization. Materials with greater surface roughness and higher surface free energy promote bacterial adhesion and biofilm formation, while bracket design and size also affect plaque accumulation. Consequently, simpler and smaller bracket designs have been suggested to reduce bacterial retention and minimize the risk of enamel demineralization.[15]

White spot lesions may develop on any tooth surface where microbial biofilm is allowed to accumulate over time. Numerous patient-related factors, including medical and dental history, medication use, dietary habits, salivary composition, fluoride exposure, and genetic predisposition, influence their development.[16] According to the American Dental Association Caries Classification System (ADA CCS), WSLs are classified as incipient non-cavitated carious lesions resulting from bacterial plaque activity.[17]

Host susceptibility plays a fundamental role in the pathogenesis of WSLs. Systemic factors, including salivary flow rate, buffering capacity, and enamel resistance to acid dissolution, contribute significantly to lesion development. Local factors such as dental malposition and the presence of fixed orthodontic appliances further increase the risk of demineralization by promoting plaque retention and impairing effective oral hygiene.[18]

Although fixed orthodontic appliances remain the most effective method for correcting many malocclusions, their use is associated with increased plaque accumulation and elevated levels of cariogenic microorganisms.[19] These changes in the oral environment contribute to enamel demineralization and the subsequent development of WSLs and dental caries. Nevertheless, evidence regarding the relationship between orthodontic treatment and caries development remains inconsistent, with some studies reporting conflicting findings.[20,21]

A variety of preventive strategies have been proposed to minimize the occurrence of WSLs during orthodontic treatment. These include topical fluoride applications, fluoride-releasing bonding materials, sodium fluoride mouth rinses, chlorhexidine products, and reinforcement of oral hygiene practices.[22-24] Adequate oral hygiene remains one of the most effective measures for preventing enamel demineralization and caries development during treatment.[24] In addition, the increasing use of fixed bonded retainers following both aligner-based and conventional orthodontic therapy may prolong plaque retention and potentially increase the risk of WSL formation after active treatment has been completed.[25]

Clinically, enamel demineralization initially presents as white, opaque lesions that may resemble dental fluorosis. However, unlike fluorosis, these lesions are associated with active mineral loss and an increased susceptibility to caries progression due to enamel porosity and enhanced plaque retention.[26,27] Demineralization involves the dissolution of mineral ions from hydroxyapatite crystals within enamel and other mineralized tissues, whereas remineralization refers to the restoration of these minerals. Although substantial mineral loss may occur without compromising enamel integrity, affected teeth often exhibit increased sensitivity to thermal, mechanical, and chemical stimuli.[28,29]

The characteristic appearance of WSLs is attributable to alterations in the refractive index (RI) of enamel. Sound enamel possesses an RI of approximately 1.66, whereas demineralized enamel exhibits lower values that vary according to lesion hydration. The presence of air within porous lesions increases light scattering, causing dehydrated WSLs to appear as opaque, milky-white areas that are more readily detectable during clinical examination.[30,31]

Several studies have investigated the prevalence and severity of WSLs among orthodontic patients. Mizrahi[32] reported significant increases in both lesion prevalence and severity following fixed appliance treatment, with male patients exhibiting greater lesion severity than females. Similarly, Gorelick et al.[33] observed a significantly higher frequency of WSLs in teeth fitted with fixed appliances compared with untreated controls, particularly in the maxillary lateral incisors. The absence of lesions on the lingual surfaces of mandibular incisors retained with bonded retainers suggested a protective effect of salivary flow.[34] Furthermore, Geiger et al.[7] demonstrated a significant association between poor compliance with preventive home-care measures and the development of WSLs.

White spot lesions are also recognized as important indicators of caries risk. Along with frank cavitation, proximal lesions, and recent restorations or extractions resulting from active disease, WSLs are considered strong clinical predictors of future caries activity.[35] Despite the availability of preventive measures, their routine implementation in orthodontic practice remains limited. Derks et al.[36] reported that although most orthodontists provide oral hygiene instructions, preventive agents such as fluoride varnishes, high-fluoride toothpaste, and chlorhexidine products are prescribed less frequently.

Fluoride remains a cornerstone of preventive dentistry because of its ability to enhance enamel remineralization and inhibit demineralization. By replacing hydroxyl ions within hydroxyapatite crystals, fluoride promotes the formation of fluorapatite, which exhibits greater resistance to acid dissolution and caries progression.[38] In contrast, patients presenting with enamel defects such as molar-incisor hypomineralization, amelogenesis imperfecta, or fluorosis may require special consideration before orthodontic treatment because of compromised enamel integrity and an increased risk of plaque accumulation and demineralization.[37]

Therefore, the present review aimed to evaluate the available evidence regarding the effectiveness of preventive strategies for reducing the risk of white spot lesion development in patients undergoing fixed orthodontic treatment.

Materials and Methods

Search Strategy

A literature search was conducted to identify studies investigating the incidence, prevalence, risk factors, and prevention of white spot lesions (WSLs) associated with fixed orthodontic treatment. Electronic searches were performed in the Medline/PubMed and Cochrane Library databases for studies published in English up to 2010.

The search strategy included combinations of the following keywords and Medical Subject Headings (MeSH) terms: orthodontics, fixed appliances, white spot lesions, demineralization, decalcification, and caries. Reference lists of relevant articles were also manually screened to identify additional eligible studies.

Eligibility Criteria

Studies were included in the review if they met the following criteria:

1.Human clinical studies involving patients undergoing fixed orthodontic treatment

2.Controlled in vivo study design

3.Assessment of the incidence and/or prevalence of white spot lesions

4.Outcomes reported at the patient level rather than at the tooth or surface level

5.Minimum orthodontic treatment duration of 12 months

6.Full-text articles available in English

Studies were excluded if they:

1.Included patients treated exclusively with removable appliances

2.Reported outcomes only at the tooth or surface level without patient-based data

3.Were case reports, narrative reviews, conference abstracts, letters, or in vitro studies

4.Did not provide sufficient information regarding WSL incidence or prevalence

Study Selection

Titles and abstracts identified through the electronic search were screened for relevance. Full-text articles were subsequently assessed according to the predefined inclusion and exclusion criteria. Studies meeting all eligibility criteria were included in the final analysis.

Data Extraction

The following information was extracted from each included study:

- Author and year of publication
- Study design
- Sample size
- Patient demographics
- Duration of orthodontic treatment
- Incidence and prevalence of white spot lesions
- Reported risk factors associated with WSL development
- Preventive measures evaluated during treatment

Outcome Measures

The primary outcomes of interest were the incidence and prevalence of white spot lesions in patients undergoing fixed orthodontic treatment. Secondary outcomes included the identification of risk factors associated with WSL development and the effectiveness of preventive strategies aimed at reducing enamel demineralization during treatment.

Results

Study Characteristics

A total of 10 studies fulfilled the eligibility criteria and were included in the review. These studies evaluated patients undergoing treatment with fixed orthodontic appliances and reported data regarding the incidence and/or prevalence of white spot lesions.

Incidence of White Spot Lesions

Across the included studies, 1,241 patients were assessed for the development of new white spot lesions during orthodontic treatment. A total of 635 patients developed at least one new lesion, corresponding to an overall incidence of 51.1%. These findings indicate that approximately one out of every two patients undergoing fixed orthodontic treatment experienced enamel demineralization during treatment.

Prevalence of White Spot Lesions

Data regarding WSL prevalence were available for 923 patients. Among these individuals, 640 presented with one or more white spot lesions, resulting in an overall prevalence of 69.3%. This finding demonstrates that WSLs are highly prevalent among orthodontic patients and represent a significant clinical challenge.

Summary of Findings

The results of the included studies consistently demonstrated that fixed orthodontic appliances are associated with a substantial risk of enamel demineralization. The high incidence and prevalence of WSLs observed across the reviewed literature emphasize the need for effective preventive strategies, including rigorous oral hygiene measures, fluoride therapy, dietary counseling, and regular professional monitoring throughout orthodontic treatment.

Discussion

The findings of the present review indicate that white spot lesions (WSLs) are a common adverse effect of fixed orthodontic treatment. The development of these lesions is multifactorial and influenced by patient-related, treatment-related, and

environmental factors. Understanding these risk factors is essential for implementing effective preventive strategies and reducing enamel demineralization during orthodontic therapy.

Gender

Several studies have suggested that gender may influence the incidence and severity of WSLs. Most authors reported a higher prevalence of lesions among male patients. Khalaf observed that males were nearly three times more likely to develop WSLs than females, while Boersma et al. reported a greater proportion of demineralized buccal surfaces in male patients. Similar findings were described by Julien et al., Tufekci et al., Lucchese and Gherlone, and Enaia et al., who also noted increased lesion severity among males.[39-44] These differences may be attributed to variations in oral hygiene practices, dietary habits, and compliance with preventive recommendations. However, the association between gender and WSL development remains controversial, as Gorelick et al. reported a higher incidence among female patients.[33] Consequently, although gender may contribute to lesion susceptibility, it should not be considered an independent predictor of WSL development.

Age

Patient age appears to play a significant role in the occurrence of WSLs. Adolescents have consistently been reported to be at greater risk than adults, potentially due to less effective oral hygiene practices and lower compliance with preventive measures. Khalaf found that adolescent patients were approximately twice as likely to develop WSLs as adults.[39] Similarly, Richter et al. reported a negative association between age and lesion development, demonstrating that the number of newly formed lesions decreased with increasing age.[45] These findings suggest that younger patients may require more intensive preventive interventions and closer monitoring throughout treatment.

Salivary Flow

Saliva plays a crucial protective role in maintaining enamel integrity through its buffering capacity, remineralizing potential, and mechanical cleansing action. Evidence supporting this protective effect was provided by Gorelick et al., who observed no WSLs on the lingual surfaces of mandibular incisors retained with a canine-to-canine bonded retainer.[33] The authors attributed this finding to the continuous exposure of these surfaces to salivary flow. Therefore, variations in salivary exposure may partly explain the distribution and severity of WSLs observed during orthodontic treatment.

Duration of Treatment

Treatment duration is consistently identified as one of the most important risk factors for WSL development. The prolonged presence of fixed orthodontic appliances promotes plaque accumulation and increases the likelihood of enamel demineralization. Khalaf reported a 3.65-fold increase in the risk of WSL formation among patients treated for more than 36 months compared with those treated for less than 24 months.[39] Likewise, Tufekci et al. and Lucchese and Gherlone demonstrated that lesions may develop within the first six months of treatment, with prevalence increasing as treatment progresses.[42,43] Richter et al. further confirmed a positive relationship between treatment duration and lesion development, reporting a substantial increase in the number of affected surfaces with longer treatment periods.[45] These findings emphasize the importance of minimizing treatment duration whenever clinically feasible.

Fluoride Use During Orthodontic Treatment

The preventive effect of fluoride on enamel demineralization has been well documented. Regular use of fluoride-containing products has been associated with significant reductions in both the incidence and prevalence of WSLs. Khalaf reported a significant reduction in lesion development among patients who routinely used fluoride mouth rinses during treatment.[39] Similarly, Geiger et al. observed a 30% reduction in prevalence and a 25% reduction in incidence among orthodontic patients using fluoride mouthwash.[7] These findings support the routine incorporation of fluoride-based preventive measures into orthodontic treatment protocols, particularly for patients at elevated risk of caries development.

Distribution of White Spot Lesions

The distribution of WSLs is not uniform throughout the dentition. Most studies reported a higher prevalence of lesions in the maxillary arch, particularly affecting the lateral incisors and canines.[7,33,39,41,46] These teeth are characterized by relatively small areas between the bracket and gingival margin, creating favorable conditions for plaque retention and hindering effective oral hygiene. In contrast, Mizrahi identified the first molars as the most frequently affected teeth[32], suggesting that lesion distribution may vary according to patient characteristics, oral hygiene practices, and appliance design.

The predominance of lesions in the maxillary arch may also be related to reduced salivary exposure compared with mandibular teeth. Furthermore, differences in brushing efficiency across various tooth surfaces may contribute to the observed distribution patterns.

Surface Distribution

Concerning lesion location, the gingival margin was consistently identified as the area most susceptible to WSL development. Khalaf reported that while lesions occurred throughout the maxillary dentition, they were predominantly localized to the gingival margins of mandibular teeth.[39] This finding is clinically relevant, as plaque accumulation is typically greatest in the region immediately adjacent to orthodontic brackets and gingival tissues. Consequently, preventive efforts should focus on improving plaque control in these high-risk areas.

Clinical Implications and Preventive Strategies

The management of WSLs should prioritize prevention, as established lesions can be difficult to reverse completely and may compromise the aesthetic outcomes of orthodontic treatment. Effective prevention requires a multifactorial approach that includes patient education, reinforcement of oral hygiene practices, dietary counseling, regular professional prophylaxis, and the use of preventive agents.

The combined use of fluoride and chemical plaque-control measures is particularly effective in reducing enamel demineralization. Geiger et al. demonstrated the benefits of fluoride mouth rinses during orthodontic treatment[7], while Ogaard et al. reported a 48% reduction in lesion depth following the application of fluoride varnish.[47] Various fluoride delivery systems, including toothpastes, mouth rinses, gels, varnishes, fluoride-releasing bonding materials, and fluoride-containing

elastomeric modules, have been proposed as effective adjuncts to conventional preventive measures.

Given the high prevalence of WSLs reported in the literature, orthodontists should identify high-risk patients before treatment initiation and implement individualized preventive protocols throughout treatment. Particular attention should be directed toward younger patients, individuals with poor oral hygiene, and those expected to undergo prolonged orthodontic therapy.

Conclusion

White spot lesions (WSLs) represent a common complication associated with fixed orthodontic treatment, with reported incidence and prevalence rates of 45.8% and 68.4%, respectively. These findings underscore the clinical relevance of enamel demineralization during orthodontic therapy and highlight the need for effective preventive strategies.

Multiple factors influence the development of WSLs. Increased risk has been associated with poor oral hygiene, younger age at treatment initiation, male sex, and prolonged treatment duration. Conversely, adequate salivary flow and the use of fluoride-based preventive measures appear to reduce the likelihood of lesion development.

Given the high prevalence of WSLs, careful patient risk assessment should be performed before and during orthodontic treatment. Particular attention should be given to individuals presenting with early signs of enamel demineralization, with preventive protocols tailored accordingly. Continuous monitoring and reinforcement of oral hygiene measures are essential to minimize adverse outcomes.

Overall, the evidence indicates that the risk of WSL development during fixed orthodontic treatment should not be underestimated, and greater emphasis should be placed on prevention, patient education, and individualized risk management strategies.

References

1. Grippaudo MM, Quinzi V, Manai A, Paolantonio EG, Valente F, La Torre G, Marzo G. Orthodontic treatment need and timing: Assessment of evolutive malocclusion conditions and associated risk factors. Eur J Paediatr Dent. 2020 Sep;21(3):203-208. doi: 10.23804/ejpd.2020.21.03.09.

2. Contaldo M, Lucchese A, Lajolo C, Rupe C, Di Stasio D, Romano A, et al. The Oral Microbiota Changes in Orthodontic Patients and Effects on Oral Health: An Overview. J Clin Med. 2021 Feb 16;10(4):780. doi: 10.3390/jcm10040780.

3. Agrawal A, Shigli A. Comparison of six different methods of cleaning and preparing occlusal fissure surface before placement of pit and fissure sealant: an in vitro study. J Indian Soc Pedod Prev Dent. 2012 Jan-Mar;30(1):51-5. doi: 10.4103/0970-4388.95582. PMID: 22565518.

4. Srivastava K, Tikku T, Khanna R, Sachan K. Risk factors and management of white spot lesions in orthodontics. J Orthod Sci. 2013 Apr;2(2):43-9. doi: 10.4103/2278-0203.115081.

5. Sundararaj D, Venkatachalapathy S, Tandon A, Pereira A. Critical evaluation of incidence and prevalence of white spot lesions during fixed orthodontic appliance treatment: A meta-analysis. J Int Soc Prev Community Dent. 2015 Nov-Dec;5(6):433-9. doi: 10.4103/2231-0762.167719.

6. Boersma JG, van der Veen MH, Lagerweij MD, Bokhout B, Prahl-Andersen B. Caries prevalence measured with QLF after treatment with fixed orthodontic appliances: influencing factors. Caries Res. 2005 Jan-Feb;39(1):41-7. doi: 10.1159/000081655.

7. Geiger AM, Gorelick L, Gwinnett AJ, Griswold PG. The effect of a fluoride program on white spot formation during orthodontic treatment. Am J Orthod Dentofacial Orthop. 1988 Jan;93(1):29-37. doi: 10.1016/0889-5406(88)90190-4.

8. Farooq I, Bugshan A. The role of salivary contents and modern technologies in the remineralization of dental enamel: a narrative review. F1000Res. 2020 Mar 9;9:171. doi: 10.12688/f1000research.22499.3.

9. Abou Neel EA, Aljabo A, Strange A, Ibrahim S, Coathup M, Young AM, Bozec L, Mudera V. Demineralization-remineralization dynamics in teeth and bone. Int J Nanomedicine. 2016 Sep 19;11:4743-4763. doi: 10.2147/IJN.S107624.

10. Favero R, Fabiane M, Zuccon A, Conte D, Ludovichetti FS. Maintaining Hygiene in Orthodontic Miniscrews: Patient Management and Protocols-A Literature Review. Dent J (Basel). 2024 Jul 19;12(7):227. doi: 10.3390/dj12070227.

11. Moynihan P, Petersen PE. Diet, nutrition and the prevention of dental diseases. Public Health Nutr. 2004 Feb;7(1A):201-26. doi: 10.1079/phn2003589.

12. Duggal MS, van Loveren C. Dental considerations for dietary counselling. Int Dent J. 2001;51(6 Suppl 1):408-12. doi: 10.1111/j.1875-595x.2001.tb00588.x. PMID: 11794563.

13. Marshall TA. Chairside diet assessment of caries risk. J Am Dent Assoc. 2009 Jun;140(6):670-4. doi: 10.14219/jada.archive.2009.0252.

14. An JS, Lim BS, Ahn SJ. Managing oral biofilms to avoid enamel demineralization during fixed orthodontic treatment. Korean J Orthod. 2023 Nov 25;53(6):345-357. doi: 10.4041/kjod23.184.

15. Benson PE, Parkin N, Millett DT, Dyer FE, Vine S, Shah A. Fluorides for the prevention of white spots on teeth during fixed brace treatment. Cochrane Database Syst Rev. 2004;(3):CD003809. doi: 10.1002/14651858.CD003809.pub2. Update in: Cochrane Database Syst Rev. 2013 Dec 12;(12):CD003809. doi: 10.1002/14651858.CD003809.pub3.

16. Mount, G.J. · Hume, W.R. Preservation and restoration of tooth structure Knowledge Books and Software, Queensland, Australia, 2005 61-82

17. Young DA, Nový BB, Zeller GG, Hale R, Hart TC, Truelove EL; American Dental Association Council on Scientific Affairs; American Dental Association Council on Scientific Affairs. The American Dental Association Caries Classification System for clinical practice: a report of the American Dental Association Council on Scientific Affairs. J Am Dent Assoc. 2015 Feb;146(2):79-86. doi: 10.1016/j.adaj.2014.11.018. Erratum in: J Am Dent Assoc. 2015 Jun ;146(6):364-5. PMID: 25637205.

18. Adina S, Dipalma G, Bordea IR, Lucaciu O, Feurdean C, Inchingolo AD, Septimiu R, Malcangi G, Cantore S, Martin D, Inchingolo F. Orthopedic joint stability influences growth and maxillary development: clinical aspects. J Biol Regul Homeost Agents. 2020 May-Jun;34(3):747-756. doi: 10.23812/20-204-E-52.

19. Miura KK, Ito IY, Enoki C, Elias AM, Matsumoto

MA. Anticariogenic effect of fluoride-releasing elastomers in orthodontic patients. Braz Oral Res. 2007 Jul-Sep;21(3):228-33. doi: 10.1590/s1806-83242007000300007.
20. Chen W, Zhou Y. Caries outcomes after orthodontic treatment with fixed appliances: a longitudinal prospective study. Int J Clin Exp Med. 2015 Feb 15;8(2):2815-22.
21. Kanthathas K, Willmot DR, Benson PE. Differentiation of developmental and post-orthodontic white lesions using image analysis. Eur J Orthod. 2005 Apr;27(2):167-72. doi: 10.1093/ejo/cjh084.
22. Ortendahl T, Thilander B, Svanberg M. Mutans streptococci and incipient caries adjacent to glass ionomer cement or resin-based composite in orthodontics. Am J Orthod Dentofacial Orthop. 1997 Sep;112(3):271-4. doi: 10.1016/S0889-5406(97)70255-5.
23. Jurela A, Repic D, Pejda S, Juric H, Vidakovic R, Matic I, Bosnjak A. The effect of two different bracket types on the salivary levels of S mutans and S sobrinus in the early phase of orthodontic treatment. Angle Orthod. 2013 Jan;83(1):140-5. doi: 10.2319/030612-187.1.
24. Fukae M, Yamamoto R, Karakida T, Shimoda S, Tanabe T. Micelle structure of amelogenin in porcine secretory enamel. J Dent Res. 2007 Aug;86(8):758-63. doi: 10.1177/154405910708600814.
25. Lanteri V, Farronato G, Lanteri C, Caravita R, Cossellu G. The efficacy of orthodontic treatments for anterior crowding with Invisalign compared with fixed appliances using the Peer Assessment Rating Index. Quintessence Int. 2018;49(7):581-587. doi: 10.3290/j.qi.a40511.
26. Robinson C, Connell S, Kirkham J, Brookes SJ, Shore RC, Smith AM. The effect of fluoride on the developing tooth. Caries Res. 2004 May-Jun;38(3):268-76. doi: 10.1159/000077766.
27. Stavrianos, C.; Papadopoul, C.; Vasiliadis, L.; Dagkalis, P.; Stavrianou, I.; Petalotis, N. Enamel Structure and Forensic Use. *Res. J. Biol. Sci.* 2010, *5*, 650–655.
28. Nanci, A. *Ten Cate's Oral Histology: Development, Structure, and Function*; Mosby: Maryland Heights, MO, USA, 2008; pp. 22–31.
29. Hart PS, Hart TC. Disorders of human dentin. Cells Tissues Organs. 2007;186(1):70-7. doi: 10.1159/000102682.
30. Puleio F, Fiorillo L, Gorassini F, Iandolo A, Meto A, D'Amico C, et al. Systematic Review on White Spot Lesions Treatments. Eur J Dent. 2022 Feb;16(1):41-48. doi: 10.1055/s-0041-1731931.
31. Shimada Y, Sato T, Inoue G, Nakagawa H, Tabata T, Zhou Y, et al. Evaluation of Incipient Enamel Caries at Smooth Tooth Surfaces Using SS-OCT. Materials (Basel). 2022 Aug 28;15(17):5947. doi: 10.3390/ma15175947.
32. Mizrahi E. Enamel demineralization following orthodontic treatment. Am J Orthod. 1982 Jul;82(1):62-7. doi: 10.1016/0002-9416(82)90548-6. PMID: 6984291.
33. Gorelick L, Geiger AM, Gwinnett AJ. Incidence of white spot formation after bonding and banding. Am J Orthod. 1982 Feb;81(2):93-8. doi: 10.1016/0002-9416(82)90032-x.
34. Ogaard B, Rølla G, Arends J, ten Cate JM. Orthodontic appliances and enamel demineralization. Part 2. Prevention and treatment of lesions. Am J Orthod Dentofacial Orthop. 1988 Aug;94(2):123-8. doi: 10.1016/0889-5406(88)90360-5.
35. Featherstone JD. The caries balance: the basis for caries management by risk assessment. Oral Health Prev Dent. 2004;2 Suppl 1:259-64. PMID: 15646583.
36. Derks A, Kuijpers-Jagtman AM, Frencken JE, Van't Hof MA, Katsaros C. Caries preventive measures used in orthodontic practices: an evidence-based decision? Am J Orthod Dentofacial Orthop. 2007 Aug;132(2):165-70. doi: 10.1016/j.ajodo.2005.10.028. PMID: 17693365.
37. Moher D, Liberati A, Tetzlaff J, Altman DG; PRISMA Group. Preferred reporting items for systematic reviews and meta-analyses: the PRISMA Statement. Open Med. 2009;3(3):e123-30. Epub 2009 Jul 21. PMID: 21603045; PMCID: PMC3090117.
38. Buzalaf MAR, Pessan JP, Honório HM, Ten Cate JM. Mechanisms of action of fluoride for caries control. Monogr Oral Sci. 2011;22:97-114. doi: 10.1159/000325151. Epub 2011 Jun 23. PMID: 21701194.
39. Khalaf K. Factors Affecting the Formation, Severity and Location of White Spot Lesions during Orthodontic Treatment with Fixed Appliances. J Oral Maxillofac Res. 2014 Apr 1;5(1):e4. doi: 10.5037/jomr.2014.5104. PMID: 24800054; PMCID: PMC4007370.
40. Boersma JG, van der Veen MH, Lagerweij MD, Bokhout B, Prahl-Andersen B. Caries prevalence measured with QLF after treatment with fixed orthodontic appliances: influencing factors. Caries Res. 2005 Jan-Feb;39(1):41-7. doi: 10.1159/000081655. PMID: 15591733.
41. Julien KC, Buschang PH, Campbell PM. Prevalence of white spot lesion formation during orthodontic treatment. Angle Orthod. 2013 Jul;83(4):641-7. doi: 10.2319/071712-584.1. Epub 2013 Jan 4. PMID: 23289733; PMCID: PMC8754044.
42. Tufekci E, Dixon JS, Gunsolley JC, Lindauer SJ. Prevalence of white spot lesions during orthodontic treatment with fixed appliances. Angle Orthod. 2011 Mar;81(2):206-10. doi: 10.2319/051710-262.1. PMID: 21208070; PMCID: PMC8925248.
43. Lucchese A, Gherlone E. Prevalence of white-spot lesions before and during orthodontic treatment with fixed appliances. Eur J Orthod. 2013 Oct;35(5):664-8. doi: 10.1093/ejo/cjs070. Epub 2012 Oct 8. PMID: 23045306.
44. Enaia M, Bock N, Ruf S. White-spot lesions during multibracket appliance treatment: A challenge for clinical excellence. Am J Orthod Dentofacial Orthop. 2011 Jul;140(1):e17-24. doi: 10.1016/j.ajodo.2010.12.016. PMID: 21724067.
45. Richter AE, Arruda AO, Peters MC, Sohn W. Incidence of caries lesions among patients treated with comprehensive orthodontics. Am J Orthod Dentofacial Orthop. 2011 May;139(5):657-64. doi: 10.1016/j.ajodo.2009.06.037.
46. Sagarika N, Suchindran S, Loganathan S, Gopikrishna V. Prevalence of white spot lesion in a section of Indian population undergoing fixed orthodontic treatment: An in vivo assessment using the visual International Caries Detection and Assessment System II criteria. J Conserv Dent. 2012 Apr;15(2):104-8. doi: 10.4103/0972-0707.94572. PMID: 22557804; PMCID: PMC3339000.
47. Ogaard B, Duschner H, Ruben J, Arends J. Microradiography and confocal laser scanning microscopy applied to enamel lesions formed in vivo with and without fluoride varnish treatment. Eur J Oral Sci. 1996 Aug;104(4 (Pt 1)):378-83. doi: 10.1111/j.1600-0722.1996.tb00095.x. PMID: 8930586.

International Journal of Biomedicine 16(3) (2026) 333-338
http://dx.doi.org/10.21103/Article16(3)_OA1

ORIGINAL ARTICLE

INTERNATIONAL JOURNAL OF BIOMEDICINE

Endothelial Dysfunction, Microalbuminuria, and Cardiac Biomarkers as Predictors of Preeclampsia in Gestational Arterial Hypertension

Mokhinur A. Sadulloeva[1*], Feruza. A. Zakirova[1], Saida A. Ikramova[2]

[1]*Republican Specialized Scientific and Practical Medical Center of Cardiology, Tashkent, Uzbekistan*
[2]*Tashkent State Medical University, Tashkent, Uzbekistan*

Abstract

Background: Gestational arterial hypertension (GAH) affects 6–10% of pregnancies and may progress to preeclampsia (PE) in up to 46% of cases. Early identification of patients at risk for this transformation remains a critical clinical challenge. This study aimed to identify independent clinical, laboratory, and hemodynamic predictors of PE development in women with GAH.
Methods and Results: This study enrolled 160 pregnant women after 20 weeks of gestation: 54 healthy controls and 106 with GAH. Among GAH patients, 46 (43.4%) subsequently developed PE. All participants underwent assessment of flow-mediated dilation (FMD), microalbuminuria (MAU), NT-proBNP, echocardiography, and 24-hour ambulatory blood pressure monitoring (ABPM) at the initial visit. Multivariate logistic regression identified five independent predictors: FMD <10% (aOR=7.15; 95% CI 1.84–27.78; P=0.005), BMI ≥30 kg/m² (aOR=4.52; 95% CI 1.36–15.03; P=0.014), MAU >30 mg/day (aOR=4.28; 95% CI 1.08–16.97; P=0.038), non-dipper profile (aOR=3.95; 95% CI 1.05–14.86; P=0.042), and NT-proBNP >125 pg/mL (aOR=3.67; 95% CI 1.01–13.35; P=0.049). ROC analysis demonstrated the highest discriminative ability for FMD (AUC=0.849) and MAU (AUC=0.821).
Conclusion: FMD, MAU, NT-proBNP, BMI, and non-dipper profile are independent predictors of PE in GAH patients. Integration of these biomarkers may enable early risk stratification and timely intervention.(**International Journal of Biomedicine. 2026;16(3):333-338.**)

Keywords: flow-mediated dilation • NT-proBNP • non-dipper • body mass index

For citation: Sadulloeva MA, Zakirova FA, Ikramova SA. Endothelial Dysfunction, Microalbuminuria, and Cardiac Biomarkers as Predictors of Preeclampsia in Gestational Arterial Hypertension. International Journal of Biomedicine. 2026;16(3):333-338. doi:10.21103/Article16(3)_OA1

Abbreviations

ABPM, ambulatory blood pressure monitoring; **AUC**, area under the curve; **BMI**, body mass index; **CI**, confidence interval; **DI SBP**, dipping index of systolic blood pressure; **FMD**, flow-mediated dilation; **GAH**, gestational arterial hypertension; **HDL-C**, high-density lipoprotein cholesterol; **LDL-C**, low-density lipoprotein cholesterol; **MAU**, microalbuminuria; **MS**, morning surge; **NT-proBNP**, N-terminal pro-brain natriuretic peptide; **OR**, odds ratio; **aOR**, adjusted odds ratio; **PE**, preeclampsia; **ROC**, receiver operating characteristic; **SBP**, systolic blood pressure; **TI SBP**, time index of systolic blood pressure; **TG**, triglycerides.

Introduction

Hypertensive disorders of pregnancy (HDP) remain a leading cause of maternal morbidity and mortality, accounting for approximately 14% of all maternal deaths worldwide.[1] According to global estimates by Abalos et al., the incidence of PE ranges from 2% to 8% of pregnancies, with substantially higher rates in low- and middle-income countries.[2] The Lancet Series on Preeclampsia (2021) emphasized that PE is a leading cause of iatrogenic preterm delivery and is associated with significant maternal and perinatal morbidity.[3]

Gestational arterial hypertension (GAH), defined as new-onset hypertension after 20 weeks of gestation without proteinuria, affects 6–10% of pregnancies.[4] Prospective

studies have demonstrated that 15–46% of women with GAH subsequently develop PE, with the highest risk in those presenting before 34 weeks.[5] Reliably predicting which GAH patients will progress to PE remains one of the most important unresolved challenges in obstetric medicine.[6]

The pathophysiology of PE is understood through the two-stage model: defective spiral artery remodeling and placental ischemia (Stage 1) trigger the release of anti-angiogenic factors—primarily soluble fms-like tyrosine kinase-1 (sFlt-1) and soluble endoglin—into the maternal circulation, causing systemic endothelial dysfunction and multi-organ damage (Stage 2).[7,17] Flow-mediated dilation (FMD) of the brachial artery is a validated non-invasive marker of endothelial function.[8] A meta-analysis by Weissgerber et al. (2016), encompassing 37 studies, demonstrated that FMD is significantly impaired before (SMD=−0.84), during (SMD=−1.41), and after (SMD=−0.90) preeclamptic pregnancies, establishing that endothelial dysfunction precedes, accompanies, and outlasts PE.[9]

Microalbuminuria (MAU), reflecting glomerular endothelial injury, predicts PE before overt proteinuria develops.[10] A 2025 systematic review and meta-analysis confirmed the association of albuminuria with increased risk of PE and its predictive value.[11] N-terminal pro-brain natriuretic peptide (NT-proBNP) has emerged as a cardiovascular stress marker in pregnancy: a 2025 meta-analysis of 31 studies (n=3,915) showed NT-proBNP levels are significantly elevated in PE, with a mean difference of 206.19 pg/mL (P≤0.001).[12] A multicenter longitudinal study demonstrated that adding NT-proBNP to the sFlt-1/PlGF ratio significantly improved short-term prediction of PE requiring delivery within one week.[13]

Ambulatory blood pressure monitoring (ABPM) has demonstrated superiority over office measurements in predicting adverse pregnancy outcomes.[14] The non-dipper pattern (nocturnal SBP reduction <10%) increases PE risk (OR=2.8; 95% CI 1.4–5.6).[15] Obesity (BMI ≥30 kg/m²) doubles PE risk according to a meta-analysis of 25 million pregnancies (pooled OR=2.8; 95% CI 2.6–3.1).[6,16]

Despite growing evidence on individual predictors, studies evaluating the combined predictive value of FMD, MAU, NT-proBNP, and ABPM parameters in women with GAH remain scarce, particularly in Central Asian populations. This study aimed to identify independent predictors of PE in GAH patients, evaluate their discriminative ability, and explore inter-relationships through correlation analysis.

Material and Methods

This study was conducted at the Republican Specialized Scientific and Practical Medical Center of Cardiology (Tashkent, Uzbekistan) between 2022 and 2025. A total of 160 pregnant women were enrolled after 20 weeks of gestation: 54 healthy controls and 106 with GAH diagnosed according to the International Society for the Study of Hypertension in Pregnancy (ISSHP) criteria(4)–systolic blood pressure ≥140 mmHg and/or diastolic blood pressure ≥90 mmHg first occurring after 20 weeks in a previously normotensive woman, without proteinuria or PE features at enrollment. During follow-up, 46 of 106 GAH patients (43.4%) developed PE. Exclusion criteria were chronic hypertension, secondary hypertension, pre-gestational diabetes mellitus, chronic kidney disease, autoimmune disorders, multiple pregnancy, and congenital fetal anomalies.

At the initial visit, all participants underwent clinical evaluation including anthropometric measurements (BMI) and office blood pressure measurement per ESC/ESH 2018 guidelines.[18] Laboratory investigations included serum creatinine, uric acid, fasting glucose, lipid profile (total cholesterol, triglycerides, HDL-C, LDL-C, atherogenic index), NT-proBNP (electrochemiluminescence immunoassay), and 24-hour microalbuminuria (enzymatic analysis). Standard echocardiography was performed using a Philips Affiniti 30 system. Brachial artery FMD was assessed per international guidelines(8) using a 7.5 MHz linear transducer; FMD <10% was considered indicative of endothelial dysfunction. Twenty-four-hour ABPM was performed using the Cardiospy recorder (LABTech LTD, Hungary) with measurements every 15 minutes (day) and 30 minutes (night). Parameters included dipping index of SBP (DI SBP), time index of SBP load (TI SBP), and morning surge (MS); non-dipper was defined as DI SBP <10%.

Statistical analysis was performed using R (version 4.3.0). Continuous variables were expressed as mean±SD or median [IQR]. Between-group comparisons used Student's t-test, Mann-Whitney U test, chi-square, or Fisher's exact test as appropriate. Univariate logistic regression was performed to screen potential predictors; variables with P<0.20 were subsequently entered into a multivariate logistic regression model to identify independent predictors. ROC analysis determined optimal cut-off values (Youden index). Spearman correlation analysis evaluated inter-variable relationships. P<0.05 was considered significant.

Results

Baseline clinical and laboratory characteristics are presented in Table 1. Women with GAH had significantly higher BMI (28.83±4.87 vs. 25.40±3.72 kg/m², P<0.001), office SBP (148.51±11.12 vs. 112.61±8.26 mmHg, P<0.001), and lower FMD (8.10±3.09% vs. 13.50±2.73%, P<0.001) compared to controls. The non-dipper prevalence was 59.4% vs. 9.3% (P<0.001).

The comparison of GAH subgroups at Visit 1 is shown in Table 2. Women who subsequently developed PE were older (31.65±6.31 vs. 28.02±4.71 years, P<0.001), had higher BMI (31.99 [28.33; 33.30] vs. 26.82 [25.10; 29.97] kg/m², P<0.001), elevated MAU (74.71 [56.96; 83.92] vs. 26.20 [13.25; 68.46] mg/day, P<0.001), higher NT-proBNP (174.53 [117.65; 209.53] vs. 105.09 [76.68; 165.89] pg/mL, P<0.001), and lower FMD (7.20 [6.47; 7.56] vs. 7.70 [7.09; 8.30]%, P<0.001). ABPM showed lower DI SBP (6.97 [6.37; 7.42] vs. 7.65 [6.73; 8.42]%, P=0.002) and higher TI SBP (44.56±13.25 vs. 34.82±8.48%, P<0.001) in the PE subgroup.

Univariate logistic regression and ROC analysis results are presented in Table 3. In univariate analysis, 11 potential predictors were evaluated, of which 9 demonstrated statistical significance (P<0.05). ROC analysis showed the highest AUC for FMD (0.849; cut-off ≤7.70%; sensitivity 82.6%; specificity

75.0%) and MAU (0.821; cut-off ≥55.60 mg/day; sensitivity 69.6%; specificity 98.3%). Multivariate logistic regression (Figure 1) identified five independent predictors: FMD <10% (aOR=7.15; 95% CI 1.84–27.78; P=0.005), BMI ≥30 kg/m² (aOR=4.52; 95% CI 1.36–15.03; P=0.014), MAU >30 mg/day (aOR=4.28; 95% CI 1.08–16.97; P=0.038), non-dipper profile (aOR=3.95; 95% CI 1.05–14.86; P=0.042), and NT-proBNP >125 pg/mL (aOR=3.67; 95% CI 1.01–13.35; P=0.049).

Table 1.

Clinical characteristics of the study participants.

Variable	Healthy (n=54)	GAH (n=106)	P
Age, years	28.87±5.25	29.64±5.61	0.514
Gestational age, weeks	24.54±3.80	23.93±3.34	0.338
BMI, kg/m²	25.40±3.80	28.83±5.21	<0.001
Office SBP, mmHg	101.22±10.53	147.41±11.22	<0.001
Office DBP, mmHg	64.20±6.12	86.21±10.04	<0.001
Office MBP, mmHg	76.53±7.16	106.51±10.02	<0.001
MAU, mg/day	12.01±5.11	46.73±38.96	<0.001
NT-proBNP, pg/mL	55.03±25.32	137.12±83.97	<0.001
Creatinine, μmol/L	44.20±10.20	64.75±15.36	<0.001
Fasting glucose, mmol/L	4.27±0.43	4.75±0.71	<0.001
Uric acid, mg/dL	4.70±0.45	5.43±1.03	<0.001
Triglycerides, mg/dL	175.00±45.78	259.76±67.99	<0.001
HDL-C, mg/dL	65.00±10.70	54.96±10.27	<0.001
Atherogenic index	2.77±0.88	3.57±0.96	<0.001
DI SBP, %	11.80±4.20	4.90±3.02	<0.001
TI SBP, %	7.91±6.58	37.81±11.28	<0.001
Morning surge, mmHg	18.20±17.80	42.64±7.85	<0.001
FMD, %	13.50±2.73	8.10±3.09	<0.001

Data presented as mean±SD. P-values from Mann-Whitney U test. BMI, body mass index; SBP, systolic blood pressure; DBP, diastolic blood pressure; MBP, mean blood pressure; MAU, microalbuminuria; DI SBP, dipping index of SBP; TI SBP, time index of SBP; FMD, flow-mediated dilation.

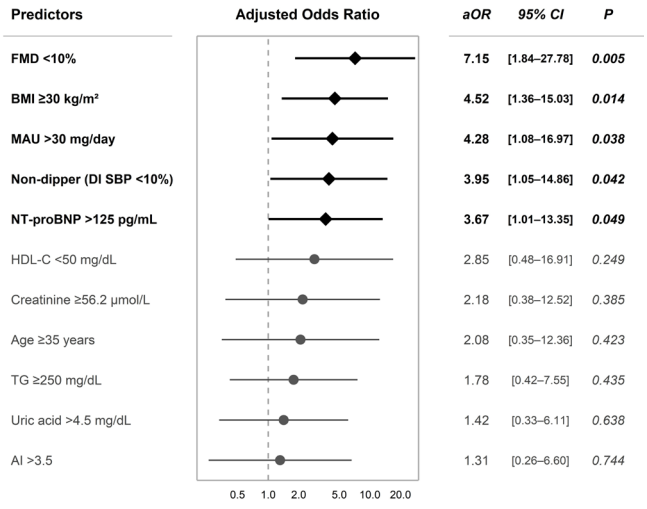

Figure 1. *Forest plot of adjusted odds ratios (aOR) from multivariate logistic regression analysis for predictors of preeclampsia in pregnant women with gestational hypertension (n=106). Diamond markers with bold labels indicate statistically significant independent predictors (P<0.05); circle markers indicate non-significant predictors. Horizontal lines represent 95% confidence intervals. The dashed vertical line denotes aOR=1.0.*

Table 2.

Baseline comparison of GAH and PE subgroups at Visit 1.

Variable	GAH (n=60)	PE (n=46)	P-value
Age, years	28.03±4.62	31.46±6.38	0.005
Gestational age, weeks	24.12±3.28	23.43±3.06	0.141
BMI, kg/m²	26.98±3.45	31.65±3.65	<0.001
Office SBP, mmHg	143.35±9.38	151.74±10.84	<0.001
Office DBP, mmHg	85.98±9.28	92.83±10.13	<0.001
Office MBP, mmHg	103.00±8.39	111.10±10.20	<0.001
MAU, mg/day	20.05±36.77	57.70±24.88	<0.001
NT-proBNP, pg/mL	103.25±82.22	176.88±79.41	<0.001
Creatinine, μmol/L	55.16±8.79	64.86±13.92	<0.001
Fasting glucose, mmol/L	4.74±0.60	5.13±0.78	0.009
Uric acid, mg/dL	5.25±0.82	5.70±1.21	0.069
Triglycerides, mg/dL	239.44±71.95	279.27±58.51	0.004
HDL-C, mg/dL	57.39±8.45	51.15±14.70	0.011
Atherogenic index	3.31±0.72	3.77±1.01	0.014
DI SBP, %	4.70±2.45	5.68±4.81	0.581
TI SBP, %	34.83±8.48	44.55±13.25	<0.001
Morning surge, mmHg	41.48±7.47	44.16±8.16	0.089
FMD, %	9.69±2.46	6.02±2.56	<0.001

Data presented as mean±SD. P-values from Mann-Whitney U test. GAH, gestational arterial hypertension; PE, preeclampsia. Other abbreviations as in Table 1.

Table 3.

Univariate logistic regression analysis and ROC characteristics for potential predictors of preeclampsia.

Predictor	OR (95% CI)	P	AUC	Cut-off (Se; Sp)
FMD <10%	**8.42 (3.12–22.73)**	**<0.001**	0.849	≤7.70% (82.6; 75.0)
BMI ≥30 kg/m²	**5.86 (2.38–14.43)**	**<0.001**	0.748	≥29.2 (71.7; 70.0)
MAU >30 mg/day	**4.30 (1.92–9.63)**	**<0.001**	0.821	≥55.6 (69.6; 98.3)
Non-dipper (DI SBP <10%)	**5.32 (2.17–13.04)**	**<0.001**	0.742	≤7.50% (73.9; 68.3)
NT-proBNP >125 pg/mL	**3.89 (1.68–9.01)**	**0.002**	0.780	≥154.6 (69.6; 85.0)
HDL-C <50 mg/dL	4.30 (1.63–11.34)	0.003	—	—
Creatinine ≥56.2 μmol/L	3.52 (1.52–8.15)	0.003	0.638	≥56.2 (63.0; 41.7)
Age ≥35 years	2.73 (1.10–6.78)	0.031	—	—
TG ≥250 mg/dL	2.48 (1.10–5.59)	0.029	—	—
Uric acid >4.5 mg/dL	1.74 (0.73–4.14)	0.211	—	—
AI >3.5	1.74 (0.79–3.83)	0.170	—	—

Bold indicates predictors that were significant in univariate analysis (P<0.05) and subsequently identified as independent predictors in multivariate analysis (Figure 1). OR, odds ratio; CI, confidence interval; AUC, area under the ROC curve; Se, sensitivity (%); Sp, specificity (%). Cut-off values determined by Youden index.

ROC analysis (Figure 2) demonstrated the highest discriminative ability for FMD (AUC=0.849; cut-off ≤7.70%; sensitivity 82.6%; specificity 75.0%), followed by MAU (AUC=0.821; cut-off ≥55.60 mg/day; sensitivity 69.6%; specificity 98.3%), NT-proBNP (AUC=0.780; cut-off ≥154.6 pg/mL; sensitivity 69.6%; specificity 85.0%), BMI (AUC=0.748; cut-off ≥29.2 kg/m²; sensitivity 71.7%; specificity 70.0%), and DI SBP (AUC=0.742; cut-off ≤7.50%; sensitivity 73.9%; specificity 68.3%).

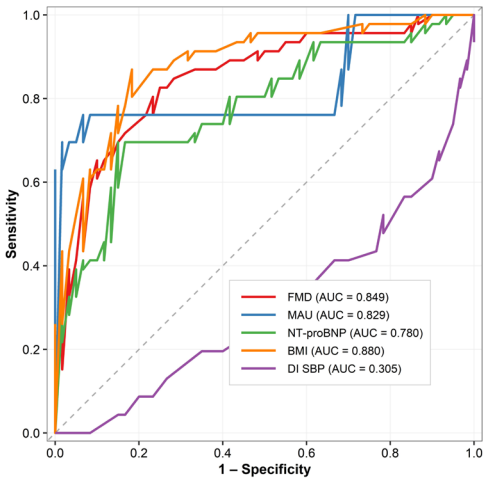

Figure 2. *Receiver operating characteristic (ROC) curves for continuous predictors of preeclampsia (n=106). Each curve represents the discriminative ability of a predictor, with the area under the curve (AUC) shown in the legend. The dashed diagonal line represents AUC=0.50.*

Table 4.

Significant Spearman correlation coefficients in women with gestational arterial hypertension (n=106).

Variable pair	Spearman r	Pathophysiological axis
FMD — NT-proBNP	−0.40***	Endothelial–cardiac
FMD — MAU	−0.33***	Endothelial–renal
MAU — Creatinine	+0.37***	Renal
MAU — TI SBP	+0.37***	Renal–hemodynamic
MAU — NT-proBNP	+0.35***	Renal–cardiac
DI SBP — TI SBP	−0.42***	Hemodynamic
IMT — HDL-C	−0.30**	Metabolic–lipid
IMT — Glucose	+0.30**	Metabolic
IMT — Creatinine	+0.29**	Metabolic–renal
HDL-C — TI SBP	−0.29**	Lipid–hemodynamic
MAU — BMI	+0.28**	Renal–metabolic
FMD — BMI	−0.27**	Endothelial–metabolic
Creatinine — HDL-C	−0.26**	Renal–lipid
FMD — HDL-C	+0.25**	Endothelial–lipid
NT-proBNP — HDL-C	−0.25**	Cardiac–lipid
NT-proBNP — BMI	+0.23*	Cardiac–metabolic
FMD — DI SBP	+0.22*	Endothelial–hemodynamic

**P<0.05; **P<0.01; ***P<0.001.*
FMD, flow-mediated dilation; MAU, microalbuminuria; BMI, body mass index; DI SBP, dipping index of systolic blood pressure; TI SBP, time index of systolic blood pressure; HDL-C, high-density lipoprotein cholesterol.

Spearman correlation analysis (Table 4) revealed distinct patterns in the GAH cohort (n=106). FMD demonstrated significant inverse correlations with NT-proBNP (r=−0.40, P<0.001), MAU (r=−0.33, P<0.001), and BMI (r=−0.27, P=0.005), and a positive correlation with HDL-C (r=+0.25, P=0.009). MAU was positively correlated with creatinine (r=+0.37, P<0.001), TI SBP (r=+0.37, P<0.001), NT-proBNP (r=+0.35, P<0.001), and BMI (r=+0.28, P=0.004). A strong inverse correlation was observed between DI SBP and TI SBP (r=−0.42, P<0.001). The endothelial-renal-cardiac triad (FMD–MAU–NT-proBNP) and the FMD–BMI relationship are illustrated in Figure 3A–D.

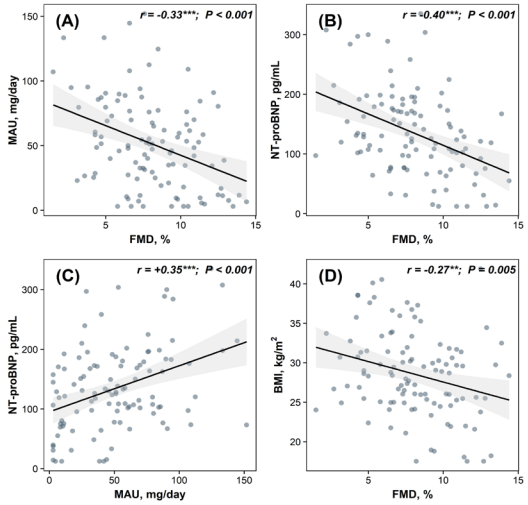

Figure 3. *Scatter plots of significant Spearman correlations in women with gestational arterial hypertension (n=106). (A) FMD versus MAU (r=−0.33, P<0.001). (B) FMD versus NT-proBNP (r=−0.40, P<0.001). (C) MAU versus NT-proBNP (r=+0.35, P<0.001). (D) FMD versus BMI (r=−0.27, P=0.005). Solid lines represent linear regression with 95% confidence intervals. **P<0.01; ***P<0.001.*

Discussion

This study identified five independent predictors of PE in women with GAH, with FMD demonstrating both the strongest predictive value (aOR=7.15) and the highest discriminative ability (AUC=0.849). These findings position endothelial function assessment as the cornerstone of PE risk stratification in GAH patients.

The primacy of FMD aligns with the two-stage model of PE, in which systemic endothelial dysfunction is the central pathogenic mechanism.[7] Our findings are supported by Weissgerber et al. (2016), who demonstrated significantly impaired FMD before PE onset (SMD=−0.84) across 37 studies,[9] and by Doganay et al. (2022), who confirmed impaired FMD in PE through a systematic review and meta-analysis.[19] The AUC of 0.849 in our study exceeds the 0.80 threshold considered excellent for diagnostic tests.

MAU emerged as the second-strongest predictor (aOR=4.28) with a remarkably high specificity of 98.3% at the optimal cut-off (55.60 mg/day), suggesting that elevated MAU in GAH is highly specific for subsequent PE. This

extends earlier observations[10] to a Central Asian population and is consistent with a 2025 systematic review confirming the predictive value of albuminuria for PE.[11] NT-proBNP as an independent predictor (aOR=3.67, AUC=0.780) is supported by the 2025 meta-analysis of 31 studies (n=3,915) confirming significantly elevated NT-proBNP in PE (mean difference 206.19 pg/mL, P≤0.001).[12] Our optimal cut-off (154.6 pg/mL) is consistent with the findings of Sabria et al. (2018), who demonstrated that NT-proBNP combined with the sFlt-1/PlGF ratio significantly improved prediction of PE requiring delivery within one week.[13] The non-dipper profile (aOR=3.95) underscores circadian blood pressure dysregulation in PE pathogenesis, consistent with Salazar et al. (2022), who reported an OR of 2.8 for nocturnal hypertension and PE risk.[15] In our study, non-dipper prevalence was 80.4% in the PE subgroup versus 43.3% in GAH (P<0.001). Obesity as a predictor (aOR=4.52) is consistent with the meta-analysis by Bartsch et al. (2016) of 25 million pregnancies (pooled OR=2.8).[16]

Importantly, correlation analysis in the total GAH cohort demonstrated an activated endothelial-renal-cardiac axis, with FMD occupying a central hub position (MAU: r=−0.33; NT-proBNP: r=−0.40). The inverse FMD–BMI correlation (r=−0.27, P=0.005) confirms that higher BMI is associated with greater endothelial impairment in GAH patients, consistent with evidence that obesity exacerbates endothelial dysfunction through chronic inflammation, oxidative stress, and reduced nitric oxide bioavailability.[20] MAU showed strong associations with creatinine (r=+0.37) and TI SBP (r=+0.37), linking renal injury to pressure overload. The inverse correlation between DI SBP and TI SBP (r=−0.42) confirms the hemodynamic significance of the non-dipper profile. Several univariate predictors (HDL-C, creatinine, atherogenic index) lost significance in multivariate analysis due to collinearity–creatinine in particular demonstrated low specificity (41.7%) and the lowest AUC (0.638), reflecting substantial renal functional reserve.

This study has limitations, including a relatively small sample size (n=106 GAH patients), a single-center design, and the absence of angiogenic biomarkers (sFlt-1/PlGF ratio). Recent predictive models combining NT-proBNP with angiogenic markers have demonstrated improved accuracy for PE prediction,[22,23] and PlGF-based testing has been validated in large multicenter trials.[25] However, FMD and MAU demonstrated comparable discriminative ability (AUC=0.849 and 0.821). The glomerular endotheliosis underlying MAU elevation in PE is well characterized,[21] and PE is associated with increased long-term cardiovascular risk,[24] reinforcing the importance of early identification. Future multicenter studies with larger cohorts incorporating angiogenic markers are warranted.

In conclusion, the present study demonstrates that endothelial dysfunction assessed by brachial artery FMD is the strongest independent predictor of PE in women with GAH (aOR=7.15; AUC=0.849), followed by BMI ≥30 kg/m² (aOR=4.52), MAU >30 mg/day (aOR=4.28), non-dipper blood pressure profile (aOR=3.95), and NT-proBNP >125 pg/mL (aOR=3.67). These five predictors represent distinct pathophysiological domains–endothelial function, metabolic risk, renal injury, circadian hemodynamics, and cardiac stress–providing a comprehensive multi-marker assessment of PE risk.

Integrating FMD, MAU, and NT-proBNP with ABPM-derived parameters into routine antenatal surveillance of GAH patients may substantially improve early risk stratification. This multimodal approach enables clinicians to identify those at highest risk before the clinical onset of PE, facilitating timely initiation of evidence-based preventive strategies including low-dose aspirin therapy, intensified surveillance protocols, and appropriate delivery planning. Further validation of this predictive panel in multicenter studies with diverse populations is warranted to confirm its clinical utility and cost-effectiveness.

Ethical Considerations

The study protocol was approved by the Ethics Committee of the Republican Specialized Scientific and Practical Medical Center of Cardiology. All participants provided written informed consent. The study was conducted in accordance with the Declaration of Helsinki.

Competing Interests

The authors declare that they have no competing interests.

Sources of Funding

This research received no external funding.

References

1. Say L, Chou D, Gemmill A, Tunçalp Ö, Moller AB, Daniels J, Gülmezoglu AM, Temmerman M, Alkema L. Global causes of maternal death: a WHO systematic analysis. Lancet Glob Health. 2014 Jun;2(6):e323-33. doi: 10.1016/S2214-109X(14)70227-X. Epub 2014 May 5. PMID: 25103301.

2. Abalos E, Cuesta C, Grosso AL, Chou D, Say L. Global and regional estimates of preeclampsia and eclampsia: a systematic review. Eur J Obstet Gynecol Reprod Biol. 2013 Sep;170(1):1-7. doi: 10.1016/j.ejogrb.2013.05.005. Epub 2013 Jun 7. PMID: 23746796.

3. Chappell LC, Cluver CA, Kingdom J, Tong S. Pre-eclampsia. Lancet. 2021 Jul 24;398(10297):341-354. doi: 10.1016/S0140-6736(20)32335-7. Epub 2021 May 27. PMID: 34051884.

4. Brown MA, Magee LA, Kenny LC, Karumanchi SA, McCarthy FP, Saito S, Hall DR, Warren CE, Adoyi G, Ishaku S; International Society for the Study of Hypertension in Pregnancy (ISSHP). Hypertensive Disorders of Pregnancy: ISSHP Classification, Diagnosis, and Management Recommendations for International Practice. Hypertension. 2018 Jul;72(1):24-43. doi: 10.1161/HYPERTENSIONAHA.117.10803. PMID: 29899139.

5. Barton JR, O'brien JM, Bergauer NK, Jacques DL, Sibai BM. Mild gestational hypertension remote from term:

progression and outcome. Am J Obstet Gynecol. 2001 Apr;184(5):979-83. doi: 10.1067/mob.2001.112905.
6. Poon LC, Shennan A, Hyett JA, Kapur A, Hadar E, Divakar H, et al. The International Federation of Gynecology and Obstetrics (FIGO) initiative on pre-eclampsia: A pragmatic guide for first-trimester screening and prevention. Int J Gynaecol Obstet. 2019 May;145 Suppl 1(Suppl 1):1-33. doi: 10.1002/ijgo.12802. Erratum in: Int J Gynaecol Obstet. 2019 Sep;146(3):390-391. doi: 10.1002/ijgo.12892. PMID: 31111484; PMCID: PMC6944283.
7. Redman CW, Sargent IL. Latest advances in understanding preeclampsia. Science. 2005 Jun 10;308(5728):1592-4. doi: 10.1126/science.1111726. PMID: 15947178.
8. Corretti MC, Anderson TJ, Benjamin EJ, Celermajer D, Charbonneau F, Creager MA, Deanfield J, Drexler H, Gerhard-Herman M, Herrington D, Vallance P, Vita J, Vogel R; International Brachial Artery Reactivity Task Force. Guidelines for the ultrasound assessment of endothelial-dependent flow-mediated vasodilation of the brachial artery: a report of the International Brachial Artery Reactivity Task Force. J Am Coll Cardiol. 2002 Jan 16;39(2):257-65. doi: 10.1016/s0735-1097(01)01746-6. Erratum in: J Am Coll Cardiol 2002 Mar 20;39(6):1082. PMID: 11788217.
9. Weissgerber TL, Milic NM, Milin-Lazovic JS, Garovic VD. Impaired Flow-Mediated Dilation Before, During, and After Preeclampsia: A Systematic Review and Meta-Analysis. Hypertension. 2016 Feb;67(2):415-23. doi: 10.1161/HYPERTENSIONAHA.115.06554. Epub 2015 Dec 28. PMID: 26711737; PMCID: PMC4713258.
10. Baweja S, Kent A, Masterson R, Roberts S, McMahon LP. Prediction of pre-eclampsia in early pregnancy by estimating the spot urinary albumin: creatinine ratio using high-performance liquid chromatography. BJOG. 2011 Aug;118(9):1126-32. doi: 10.1111/j.1471-0528.2011.02960.x.
11. Rashidian P, Parsaei M, Hantoushzadeh S, Salmanian B. Investigating the association of albuminuria with the incidence of preeclampsia and its predictive capabilities: a systematic review and meta-analysis. BMC Pregnancy Childbirth. 2025 Mar 20;25(1):322. doi: 10.1186/s12884-025-07444-z.
12. Suciu VE, Leucuța DC, Măluțan AM, Iuhas C, Oancea M, Bucuri CE, Roman MP, Ormindean C, Mihu D, Ciortea R. NT-proBNP and BNP as Biomarkers for Preeclampsia: A Systematic Review and Meta-Analysis. Int J Mol Sci. 2025 Jun 28;26(13):6272. doi: 10.3390/ijms26136272.
13. Sabriá E, Lequerica-Fernández P, Lafuente-Ganuza P, Eguia-Ángeles E, Escudero AI, Martínez-Morillo E, Barceló C, Álvarez FV. Addition of N-terminal pro-B natriuretic peptide to soluble fms-like tyrosine kinase-1/placental growth factor ratio >38 improves prediction of pre-eclampsia requiring delivery within 1 week: a longitudinal cohort study. Ultrasound Obstet Gynecol. 2018 Jun;51(6):758-767. doi: 10.1002/uog.19040. PMID: 29498431.
14. Stuurman KE, Mulder EJ, de Heus R, Visser GH, Grobbee DE, Franx A. Ambulatory blood pressure monitoring in pregnancy: a systematic review. Obstet Gynecol Surv. 2020;75(4):247-62. doi:10.1097/OGX.0000000000000770.
15. Salazar MR, Espeche WG, Leiva Sisnieguez CE, Minetto J, Balbín E, Soria A, Yoma O, Prudente M, Torres S, Grassi F, Santillan C, Carbajal HA. Nocturnal hypertension and risk of developing early-onset preeclampsia in high-risk pregnancies. Hypertens Res. 2021 Dec;44(12):1633-1640. doi: 10.1038/s41440-021-00740-z. Epub 2021 Sep 3. PMID: 34480133.
16. Bartsch E, Medcalf KE, Park AL, Ray JG; High Risk of Pre-eclampsia Identification Group. Clinical risk factors for pre-eclampsia determined in early pregnancy: systematic review and meta-analysis of large cohort studies. BMJ. 2016 Apr 19;353:i1753. doi: 10.1136/bmj.i1753.
17. Maynard SE, Min JY, Merchan J, Lim KH, Li J, Mondal S, Libermann TA, Morgan JP, Sellke FW, Stillman IE, Epstein FH, Sukhatme VP, Karumanchi SA. Excess placental soluble fms-like tyrosine kinase 1 (sFlt1) may contribute to endothelial dysfunction, hypertension, and proteinuria in preeclampsia. J Clin Invest. 2003 Mar;111(5):649-58. doi: 10.1172/JCI17189.
18. Williams B, Mancia G, Spiering W, Agabiti Rosei E, Azizi M, Burnier M, et al.; ESC Scientific Document Group. 2018 ESC/ESH Guidelines for the management of arterial hypertension. Eur Heart J. 2018 Sep 1;39(33):3021-3104. doi: 10.1093/eurheartj/ehy339. Erratum in: Eur Heart J. 2019 Feb 1;40(5):475. doi: 10.1093/eurheartj/ehy686. PMID: 30165516.
19. Doganay S, Doganay GD. Impaired flow-mediated dilation in preeclampsia: a systematic review and meta-analysis. J Matern Fetal Neonatal Med. 2022;35(25):9782-9. doi:10.1080/14767058.2022.2052824.
20. Redman CW, Staff AC. Preeclampsia, biomarkers, syncytiotrophoblast stress, and placental capacity. Am J Obstet Gynecol. 2015 Oct;213(4 Suppl):S9.e1, S9-11. doi: 10.1016/j.ajog.2015.08.003. PMID: 26428507.
21. Stillman IE, Karumanchi SA. The glomerular injury of preeclampsia. J Am Soc Nephrol. 2007 Aug;18(8):2281-4. doi: 10.1681/ASN.2007020255.
22. Lafuente-Ganuza P, Lequerica-Fernandez P, Carretero F, Escudero AI, Martinez-Morillo E, Sabria E, Herraiz I, Galindo A, Lopez A, Martinez-Triguero ML, Alvarez FV. A more accurate prediction to rule in and rule out pre-eclampsia using the sFlt-1/PlGF ratio and NT-proBNP as biomarkers. Clin Chem Lab Med. 2020 Feb 25;58(3):399-407. doi: 10.1515/cclm-2019-0939. PMID: 31734648.
23. Garrido-Giménez C, Cruz-Lemini M, Álvarez FV, Nan MN, Carretero F, Fernández-Oliva A, Mora J, Sánchez-García O, García-Osuna Á, Alijotas-Reig J, Llurba E, On Behalf Of The EuroPE Working Group. Predictive Model for Preeclampsia Combining sFlt-1, PlGF, NT-proBNP, and Uric Acid as Biomarkers. J Clin Med. 2023 Jan 5;12(2):431. doi: 10.3390/jcm12020431.
24. Wu P, Haththotuwa R, Kwok CS, Babu A, Kotronias RA, Rushton C, Zaman A, Fryer AA, Kadam U, Chew-Graham CA, Mamas MA. Preeclampsia and Future Cardiovascular Health: A Systematic Review and Meta-Analysis. Circ Cardiovasc Qual Outcomes. 2017 Feb;10(2):e003497. doi: 10.1161/CIRCOUTCOMES.116.003497.
25. Duhig KE, Myers J, Seed PT, Sparkes J, Lowe J, Hunter RM, Shennan AH, Chappell LC; PARROT trial group. Placental growth factor testing to assess women with suspected pre-eclampsia: a multicentre, pragmatic, stepped-wedge cluster-randomised controlled trial. Lancet. 2019 May 4;393(10183):1807-1818. doi: 10.1016/S0140-6736(18)33212-4.

***Corresponding author:** Mokhinur A. Sadulloeva, MD. E-mail: sadullaeva.mokh@gmail.com*

International Journal of Biomedicine 16(3) (2026) 339-345
http://dx.doi.org/10.21103/Article16(3)_OA2

ORIGINAL ARTICLE

INTERNATIONAL JOURNAL OF BIOMEDICINE

Cord Blood Levels of IL-8, MCP-1 and MIP-1α as Possible Predictors of Late Sepsis Development in Preterm Neonates

Jelena Vucic[1], Karin Vasic[2], Sandra Stankovic[3], Voja Pavlovic[4*]

[1]*Department of Neonatology, Children`s Hospital, Clinical Center Nis, 18000 Nis, Serbia*
[2]*Department of Cardiology, Children`s Hospital, Clinical Center Nis, 18000 Nis, Serbia*
[3]*Department of Endocrinology, Children`s Hospital, Clinical Center Nis, 18000 Nis, Serbia*
[4]*Department of Physiology, Medical Faculty in Nis, 18000 Nis, Serbia*

Abstract

Background: The immature immune system of preterm neonates is a key factor in increased vulnerability to infections and sepsis. Although neonatal sepsis requires diagnostic tests, evaluating some chemokines may help predict sepsis and support early diagnosis, improving clinical outcomes.

Methods and Results: In the current study, which involved 80 participants, we analyzed the role of interleukin 8 (IL-8), monocyte chemotactic protein 1 (MCP-1), and macrophage inflammatory protein 1α (MIP-1α) in cord and venous blood plasma with C-reactive protein (CRP) and procalcitonin (PCT) for sepsis prediction and development in premature neonates. Levels of IL-8 (in cord and venous blood plasma), together with MCP-1 and MIP-1α levels in cord blood, were markedly elevated (P<0.001) in sepsis groups (early and late onset sepsis), together with venous blood PCT levels (P<0.001), compared to premature neonates without sepsis. On the other hand, CRP levels showed no significant change in the evaluated groups compared to the control group (without sepsis development).

Conclusion: These findings suggest that levels of IL-8, MCP-1, and MIP-1α in cord blood, rather than venous blood levels, together with venous blood PCT values, may have a predictive role for late sepsis development in premature neonates. Additional studies are required to evaluate the role of complex multiple mediators in predicting neonatal sepsis and to avoid unnecessary antibiotic treatment with improved clinical outcomes. (**International Journal of Biomedicine. 2026;16(3):339-345.**)

Keywords: premature neonates • late sepsis • IL-8 • MCP-1 • MIP-1α

For citation: Vucic J, Vasic K, Stankovic S, Pavlovic V. Cord Blood Levels of IL-8, MCP-1 and MIP-1α as Possible Predictors of Late Sepsis Development in Preterm Neonates. International Journal of Biomedicine. 2026;16(3):339-345. doi:10.21103/Article16(3)_OA2

Introduction

Neonatal sepsis is a clinical syndrome manifested by nonspecific clinical signs and symptoms in response to pathogens[1] and still represents a major cause of morbidity and mortality in neonatal medicine.[2] This highly inflammatory disease may ultimately result in septic shock and multiple organ dysfunction as a result of enhanced activation of the inflammatory response.[3] However, the most detrimental effect is observed in preterm neonates, especially in those infants born <37 weeks of gestational age (GA).[4] Early onset sepsis (EOS) is associated with vertical acquisition of pathogens from mother to neonate and occurs in the first 72h of life, while late onset sepsis (LOS) is usually a horizontally acquired infection (hospital-acquired infection or community-acquired infection), which develops after 72h of life.[5] Even though the precise mechanisms of neonatal response to infection are not fully understood, the vulnerability of preterm neonates to infection mainly involves the status of the immune system.[6] The immune system of preterm neonates is not fully developed, including decreased numbers of certain cell frequencies and their functionality.[7] It is well known that sepsis initiation leads to an inflammatory reaction, which is useful and protective at a moderate level, but it is usually accompanied by an incompatible anti-inflammatory response.[8] Exaggerated production of pro-inflammatory mediators in sepsis may promote tissue damage and organ dysfunction,[9] suggesting that clarifying the level and type of pro-inflammatory mediators secreted during sepsis development may provide a better understanding of the immune status of preterm neonates.

Since the inflammatory process is a key step in sepsis development, many studies have evaluated inflammatory mediators that may predict or enable early sepsis diagnosis in preterm neonates. Nevertheless, it has been shown that evaluated inflammatory mediators vary among preterm neonates, and further studies are necessary to resolve their role.[10] Therefore, in the present study, we evaluated (in cord blood and venous blood plasma) the levels of some chemokines, such as interleukin-8 (IL-8), monocyte chemotactic protein 1 (MCP-1), macrophage inflammatory protein 1α (MIP-1α), and their potential predictive role in early diagnosis of sepsis in preterm neonates, along with some standard laboratory analyses.

Material and Methods

Study Population

This study was performed on newborns who were hospitalized at the Pediatric Internal Diseases Clinic, Clinical Center of Nis, Serbia. It involved a total of 101 neonates born at 36 weeks of GA. Due to maternal pregnancy-induced hypertension and premature rupture of membranes (PROMs), 21 premature neonates were excluded from the study. Furthermore, by using exclusion criteria, premature neonates with congenital malformations, laboratory-confirmed TORCH (toxoplasma, rubella virus, cytomegalovirus, herpes simplex virus-II), presence of any systemic disease, and premature neonates born to mothers with signs of infection (cervicovaginitis, chorioamnionitis, urinary tract infection, and fever during delivery) were excluded from the current study.

Sepsis Definition and Study Group Allocation

Sepsis is usually defined as a systemic inflammatory response with life-threatening organ dysfunction in the presence of suspected or proven infection, while neonatal sepsis is a clinical syndrome characterized by signs and symptoms in neonates, caused by invasion of pathogens. [11] Inclusion criteria for neonatal sepsis, in our study, were adopted according to the Criteria published by the International Pediatric Sepsis Consensus Conference.[12]

According to the infant's age, all enrolled participants in the study were classified into two groups (Group 1: <32 weeks and Group 2: 32-36 weeks of GA).[13] Also, both groups were divided into EOS (first sepsis episode occurs < 72 h of life) and LOS (first sepsis episode occurs >72 h of life), according to the time when the first sepsis episode appeared.[14]

Neonatal and Maternal Data

By using maternal and infant medical records, all neonatal and maternal data were retrospectively obtained. These data included neonatal weight and length, GA, sex, delivery mode, Apgar score at 1 minute after birth, low growth for GA, respiratory distress syndrome (RDS), pregnancy-induced hypertension, periventricular and intraventricular hemorrhage, and PROM. Low growth for GA was determined as weight and length less than the 10th percentile for GA.[15]

Blood Samples and Laboratory Data

IL-8, MCP-1, and MIP-1α were detected simultaneously in venous and cord blood samples using the ELISA technique, according to the manufacturer's instructions. To perform this analysis, we used a 96-well flat-bottom plate kit, Express Assay Format Human Cytokine Group (Bio-Rad, Hercules, USA). Following microplate reading, the results were estimated using the BioPlex 2200 system (Bio-Rad, Hercules, USA), according to the analytical methodology given by the manufacturer's instructions.

Statistical Analysis

The normality of the data was assessed by using Shapiro-Wilk and Kolmogorov-Smirnov tests. Non-normally distributed data are expressed as minimum-maximum (median), and comparisons between groups were evaluated using the Kruskal-Wallis and/or Mann-Whitney tests. Categorical variables are expressed as frequencies and compared using the chi-square test. Normally distributed data are expressed as mean ± SD and compared by using ANOVA. All statistical tests were two-sided and performed at a significance level of P=0.05. Statistical analysis was performed using SPSS Statistics in a Windows environment.

Results

Overall, 80 preterm infants were included in the study (out of 101 total preterm infants recruited), according to the inclusion criteria. Only seven infants (8.75%) were born before 32 GA, while 73 infants (91.25%) were born between 32 and 36 GA (Table 1). Other clinical and demographic features of the preterm infants and mothers enrolled in our study are shown in Table 1.

Table 1.

Clinical characteristics of the study population.

Characteristics	n (%), N=101	n (%), N=80
Prematurity-before 32 weeks of gestational age	8 (7.9%)	7 (8.75%)
Prematurity-32-36 weeks of gestational age	93 (92.1%)	73 (91.25%)
Birth by cesarean section	40 (39.6%)	28 (35%)
Low weight for gestational age	12 (11.9%)	7 (8.75%)
Low growth for gestational age	10 (9.9%)	5 (6.3)
Pregnancy-induced hypertension	14 (13.9%)	/
PROMs	9 (8.9%)	/
PDA	23 (22.8%)	22 (27.5)
RDS	32 (31.7%)	31 (38.8%)
Periventricular and intraventricular hemorrhage	8 (7.9%)	7 (8.75%)

PROMs: premature rupture of membranes; PDA: patent ductus arteriosus; RDS: respiratory distress syndrome.

As shown in Table 2, 21 of the 80 preterm infants developed sepsis. Regarding GA, in Group 1 (infants <32 weeks of GA), 2 infants (28.6%) demonstrated EOS, 1 infant with LOS (14.3%), and 4 infants (57.2%) without septic episodes. On the other hand, in Group 2 (infants 32-36 weeks of GA), 8 infants (11%) developed EOS, 10 infants (13.7%)

developed LOS, and 55 infants (75.3%) did not develop sepsis (Table 2). There was no significant difference in sepsis incidence between the two groups (Group 1 and Group 2) and the control group (infants without sepsis development) (P>0.05). However, we should take into account that Group 1 had only 3 preterm infants who developed sepsis, and results obtained from this group should be used with caution due to the small number of participants included in this group. Moreover, clinical variables (birth weight, length, total number of leukocytes, percentage of neutrophils, lymphocytes, monocytes, sex, and Apgar score) and C-reactive protein (CRP) concentration in venous blood plasma showed no statistical significance when sepsis groups (EOS and LOS) were compared to the control group (Table 2). Nevertheless, venous blood plasma procalcitonin (PCT) concentration showed statistical significance (P<0.05) when EOS and LOS were compared, as well as when LOS and the control group were compared (P<0.001). Additionally, significantly higher (P<0.001) PCT concentrations were detected when EOS and the control group were compared (Table 2).

Table 2.

Values of some clinical and laboratory variables and their comparison among subjects by sepsis subgroups

Variable	EOS	LOS	NS	*P-value*
<32 GW	2 (28.6%)	1 (14.3%)	4 (57.2%)	0.256
32-36 GW	8 (11%)	10 (13.7%)	55 (75.3%)	
Normal growth for GA	11 (14.7%)	10 (13.3%)	54 (72%)	1
Low growth for GA	0 (0%)	0 (0%)	5 (100%)	
Female	5 (13.9%)	5 (13.9%)	26 (72.2%)	1
Male	5 (11.4%)	6 (13.6%)	33 (75%)	
Apgar score min-max (median)	4-9 (8)	8-9 (8)	4-9 (8)	0.227
Leukocytes (x10^9/L), min-max (median)	10-37.8 (17.2)	11.1-31.5 (17.97)	10.1-31.2 (19)	0.721
Neutrophils (%), min-max (median)	18-71.1 (61.45)	35.8-68.1 (58.7)	22.4-80.3 (59.7)	0.48
Monocytes (%), mean ± SD	7.49±1.4	7.47±1.44	7.72±1.69	0.846
Lymphocytes (%), mean ± SD	33.75±15.64	37.76±11.24	32.12±12.19	0.753
CRP (mg/L), min–max (median)	0-15.4 (6.42)	0.5-5.3 (2.2)	0-55.8 (1.3)	0.082
PCT (ng/mL), min–max (median)	4.85-26.59 (10.43)	3.13-16.9 (6.66)	0-4.79 (1.18)	EOS vs. LOS: <0.05 Early vs. NS: <0.001 LOS vs. NS <0.001

GW: gestational week, GA: gestational age, NS: no sepsis
CRP: C-reactive protein, PCT: procalcitonin.

To further profile potential chemokines involved in neonatal sepsis, we next measured the levels of IL-8, MCP-1, and MIP-1α in cord blood and venous blood plasma. Since there were only 3 enrolled cases in Group 1 (infants <32 weeks of GA), we focused on analyzing the named chemokines in Group 2 (infants 32-36 weeks of GA), which recruited 18 preterm infants. IL-8 concentrations in cord blood and venous blood plasma were significantly higher (P<0.001) in sepsis groups (EOS and LOS) than in the control group (Figure 1). Additionally, IL-8 concentrations in cord blood differed significantly (P=0.02) between sepsis groups (EOS and LOS), while IL-8 concentrations in venous blood plasma did not differ significantly (P=0.06) between sepsis groups (EOS and LOS). Significantly higher levels of IL-8 (P<0.001) were observed in cord blood compared to the venous blood plasma in each group of preterm infants individually (Figure 1).

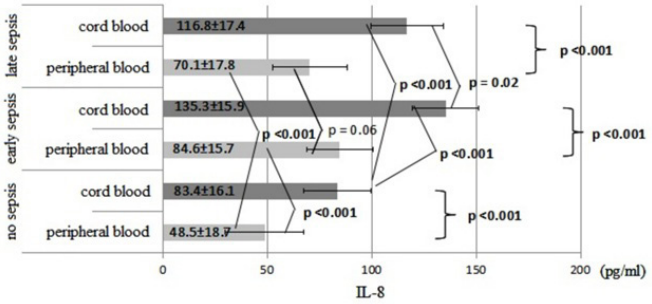

Figure 1. *Levels of IL-8 (pg/mL) in cord blood and peripheral venous blood among sepsis subgroups and the control group. IL-8 levels were evaluated as described in the Materials and Methods section. Data were presented as mean ± SD. Abbreviations: no sepsis – neonates without sepsis development; early sepsis – neonates who developed sepsis in the first 72 h of life; late sepsis – neonates who developed sepsis after 72 h of life.*

As shown in Figure 2, MCP-1 concentration in venous blood plasma did not significantly differ between sepsis groups (EON and LOS) and the control group (P>0.05). Significantly higher (P<0.001) MCP-1 values in cord blood were observed in sepsis groups (EON and LOS) compared to the control group of preterm infants. However, MCP-1 concentrations (in cord blood and venous blood plasma) did not differ significantly (P>0.05) between EON and LOS preterm infants. Significantly higher levels of MCP-1 (P<0.001) were detected in venous blood plasma than in cord blood in each group of preterm infants individually, including the LOS group (P=0.001) (Figure 2).

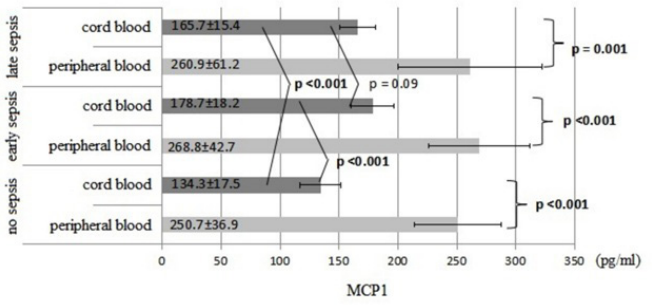

Figure 2. *Levels of MCP-1 (pg/mL) in cord blood and peripheral venous blood among sepsis subgroups and the control group. MCP-1 levels were evaluated as described in the Materials and Methods section. Data were presented as mean ± SD. Abbreviations: no sepsis – neonates without sepsis development; early sepsis – neonates who developed sepsis in the first 72 h of life; late sepsis – neonates who developed sepsis after 72 h of life.*

On the other hand, levels of MIP-1α in venous blood plasma showed no significant difference (P>0.05) between sepsis groups (EON and LOS), while MIP-1α levels in cord blood significantly differed (P=0.048) comparing EOS with the LOS group (Figure 3). Furthermore, concentrations of MIP-1α in cord blood were significantly higher (P<0.001) in sepsis groups (EOS and LOS) compared to the control group. Comparing each group individually, significantly higher values of MIP-1α (P<0.001) in cord blood than in venous blood plasma were found only in the control group of preterm infants (Figure 3).

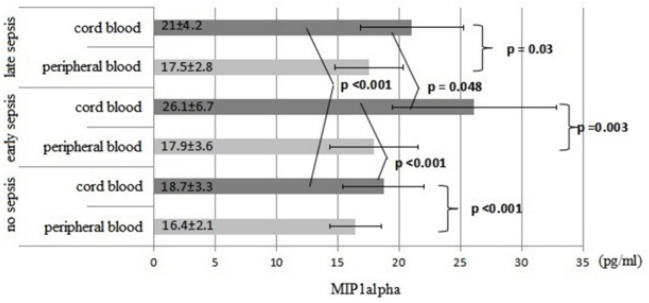

Figure 3. *Levels of MIP-1alpha (pg/mL) in cord blood and peripheral venous blood among sepsis subgroups and the control group.*
MIP-1alpha levels were evaluated as described in the Materials and Methods section. Data were presented as mean ± SD. Abbreviations: no sepsis – neonates without sepsis development; early sepsis – neonates who developed sepsis in the first 72 h of life; late sepsis – neonates who developed sepsis after 72 h of life.

Discussion

Following pathogen entry, immune cells usually produce several pro-inflammatory cytokines, chemokines, and other inflammatory mediators to eliminate the pathogen. All these released mediators induce the development of systemic inflammation in adults and infants.[16] At the same time, many studies have well documented adult sepsis,[17-19] studies involving neonatal sepsis are often limited, with conflicting results about potentially inflammatory mediators involved in sepsis prediction in premature infants.

To improve outcomes among preterm neonates with sepsis development, early detection and appropriate treatment are crucial. In the present study, we evaluated representative chemokines (IL-8, MCP-1, and MIP-1α) that may be involved in predicting sepsis development. Since there are different levels of immune system maturity in preterm neonates due to fetal development,[20] we especially focused on preterm neonates who are younger or older than 32 weeks of GA. Given that different levels of immune system maturity could result from heterogeneity in the immune response during sepsis,[21] we evaluated specific immune mediators (CRP and PCT) to improve prediction of sepsis development in preterm neonates. Current study results showed no significant differences in some clinical variables (birth weight, length, sex, and Apgar score) when comparing sepsis (EOS and LOS) and control (without sepsis development) groups. These results may indicate consistent participant enrollment and precise inclusion of preterm neonates in our study. This is in line with previous reports,[22,23] which allows more accurate estimation of predictive factors for sepsis development in preterm neonates.[24] Nevertheless, since the EOS group contains 7 participants (only 3 participants with sepsis development), results obtained from this group should be used with caution.

CRP, an acute phase protein, is the most frequently used for diagnosis of neonatal sepsis. The synthesis of this pentameric protein is stimulated mainly by IL-6 and TNF-α.[20] CRP levels obtained in our study did not differ significantly between sepsis groups (EOS and LOS) compared to the control group of premature neonates, suggesting that CRP may not be useful for early diagnosis or prediction of neonatal sepsis development. Taking into account that the half-life of CRP is 24-48 h and it needs 12 h to reach an elevated level,[25] this may partially clarify the findings in our study. Recent studies showed that CRP sensitivity for diagnosis of EOS is around 50% with high positive results.[26,27] In line with this, a previous report indicated that measuring CRP levels for LOS detection is not accurate enough for selecting neonates for further investigation or treatment.[28] A recent study[29] showed that the sensitivity of CRP to detect LOS is 62%, indicating that CRP is not a useful tool in the early diagnosis of neonatal sepsis.[21]

PCT is another acute-phase reactant protein that cannot be detected in normal human plasma. Increased levels of PCT are secreted in response to circulating bacterial toxins.[20] Our study results showed significantly increased PCT venous blood levels in the sepsis group (EOS and LOS) compared to the control group. Furthermore, markedly elevated venous blood PCT levels were detected in the EOG group compared to the LOS group, indicating that PCT plasma levels may serve as a potential biomarker for sepsis prediction. Similar observations were reported earlier, showing that increased PCT levels occur in fetal inflammatory response.[30] Since elevated PCT levels occur 2-4 h after bacterial infection and remain increased for the next 24 h,[31] it may be used as a useful biomarker for early diagnosis of neonatal sepsis, which corresponds with our study results. These findings are in line with an earlier meta-analysis which demonstrated PCT as a potential biomarker for early sepsis detection.[32] However, it should be noted that newborns, physiologically, have increased levels of PCT on the first day after birth and return to normal values 48 h after birth, indicating that levels of PCT fluctuate within three days after birth and the diagnostic value of PCT, especially for EOS detection, is still controversial.[16] The neonatal immune system is not fully developed[33] and is associated with delayed maturation of different parts of the immune system, which may lead to altered cytokine and chemokine production.[25] IL-8 is a pro-inflammatory chemokine that is produced during inflammation by immune and non-immune cells. This chemokine has a great ability to attract and stimulate neutrophils to sites of inflammation and to promote macrophage and monocyte growth and differentiation.[34] Our study results found that IL-8 concentrations in cord blood and venous blood plasma were markedly elevated in sepsis groups (EOS and LOS) compared to the control group of preterm infants, as well as in cord blood plasma in the EOS group when compared with the LOS group. Furthermore, IL-8 levels in

cord blood plasma were notably increased compared to venous blood plasma in each group of preterm infants individually. These observations may indicate that IL-8 levels in cord blood plasma, rather than in venous blood plasma, could better predict sepsis development in preterm infants. In line with our results are previous reports demonstrating that increased IL-8 production in neonates leads to enhanced activation of neutrophils and T cell activation during infection,[35] as well as a study indicating increased IL-8 levels in infants with proven LOS.[36] Similar results were confirmed in previous studies,[37, 38] while some reports documented decreased IL-8 levels in preterm neonates.[24,39] Although the reason for these conflicting results remains unclear, it is well known that some factors can modulate cytokine and chemokine production, including sepsis definition (clinical or proven), GA, or different microorganisms (which may induce various cytokine and chemokine secretion).[24] Elevated IL-8 levels were also observed in cord blood of preterm neonates, without sepsis development. Similar modified cytokine and chemokine levels were shown in other reports, but the functional significance of these findings still needs to be clarified.[40] In addition, our results showed that cord blood levels of MCP-1 and MIP-1α notably differ in sepsis groups (EOS and LOS) compared to the control group, as well as when EOS was compared with the LOS group of preterm neonates. Moreover, significantly different levels of MCP-1 and MIP-1α were observed in each group of preterm infants individually. In contrast, venous blood levels of MCP-1 and MIP-1α showed no significant difference in sepsis groups (EON and LOS) compared to the control group or in each group of preterm neonates individually. Such observations suggest that cord blood levels of MCP-1 and MIP-1α may be credible predictors for sepsis development in preterm neonates. Growing evidence indicates that levels of pro-inflammatory cytokines and chemokines increase rapidly following exposure to bacterial antigens, much earlier than elevated CRP levels.[41] Previous reports demonstrated that increased levels of neutrophil and monocyte/macrophage chemoattractants in preterm neonates could be linked with intrauterine inflammation,[42-44] which correlates with results obtained in our study. In line with previous studies, neutrophils and macrophages secrete various cytokines and chemokines to eliminate pathogens following pathogen entry, which finally may result in the development of systemic inflammation in adults and newborns.[41] Although chemokine secretion is required for host defense against bacterial infection, overproduction of these soluble inflammatory mediators has been documented to play an essential role in sepsis development,[42,43] which corresponds with our study results. Furthermore, a depleted number of monocytes in preterm neonates, with an essential role in phagocytosis and secretion of pro-inflammatory cytokines and chemokines, could have a harmful effect during infection and sepsis development[45] and needs to be considered for sepsis prediction in preterm neonates.[43]

From a clinical perspective, evaluating IL-8, MCP-1, and MIP-1α in cord blood may benefit sepsis prediction in preterm neonates, especially for late-onset sepsis, together with certain biochemical parameters. However, these observations do not exclude the role of other chemokines in sepsis development. Therefore, larger prospective studies together with multicenter studies are required to validate the clinical utility and reproducibility before any of these parameters can be routinely used into sepsis prediction algorithms.

In summary, results obtained in our study showed an evident imbalance in chemokine production, with highly elevated production of pro-inflammatory chemokines (IL-8, MCP-1, and MIP-1α), which may contribute to sepsis development in preterm neonates. We have also shown that determination of IL-8 levels (from cord blood and venous blood plasma), as well as MCP-1 and MIP-1α levels in cord blood, has predictive potential for sepsis development in preterm neonates. Assessment of PCT levels in venous blood plasma may serve as a helpful factor, together with cord blood levels of IL-8, MCP-1 and MIP-1α, for earlier detection of potential sepsis development in preterm neonates. Nevertheless, additional studies involving a larger number of cohorts and preterm neonates are required for the identification of specific markers to gain more insight into the prediction of sepsis in preterm neonates and to avoid needless antibiotic therapy and severe infectious disease.

Author Contributions

Jelena Vucic: writing – original draft, conceptualization, methodology, Supervision.
Karin Vasic: writing – review and editing, investigation, methodology, formal analysis.
Sandra Stankovic: writing – review and editing, methodology, investigation.
Voja Pavlovic: writing – review and editing, conceptualization, investigation.

Funding

This study did not receive any specific grant from funding agencies in the public, commercial, or not-for-profit sectors.

Ethical Statement

The study was approved by the Ethics Committee, Medical Faculty in Nis (35144/2017), and written informed consent was obtained from the parents for all recruited premature neonates prior to study participation.

Conflict of interest

The authors declare that they have no conflicts of interest.

References

1. Kim F, Polin RA, Hooven TA. Neonatal sepsis. BMJ. 2020 Oct 1;371:m3672. doi: 10.1136/bmj.m3672. PMID: 33004379.
2. Kuzniewicz MW, Mukhopadhyay S, Li S, Walsh EM, Puopolo KM. Time to Positivity of Neonatal Blood Cultures for Early-onset Sepsis. Pediatr Infect Dis J. 2020 Jul;39(7):634-

640. doi: 10.1097/INF.0000000000002632. PMID: 32379197.
3. Zasada M, Lenart M, Rutkowska-Zapała M, Stec M, Czyz O, Mól N, Siedlar M, Kwinta P. Inflammasome function in monocyte subsets and a risk of late-onset sepsis in preterm very low birth weight neonates. Minerva Pediatr (Torino). 2022 Apr;74(2):121-131. doi: 10.23736/S2724-5276.18.05034-X. Epub 2018 Jan 29. PMID: 29381011.
4. Miller JE, Higgins LD, Dong Y, Collins JE, Bean JF, Seitz AL, Katz JN, Jain NB. Association of Strength Measurement with Rotator Cuff Tear in Patients with Shoulder Pain: The Rotator Cuff Outcomes Workgroup Study. Am J Phys Med Rehabil. 2016 Jan;95(1):47-56. doi: 10.1097/PHM.0000000000000329. PMID: 26098921; PMCID: PMC4713123.
5. Hsu HE, Abanyie F, Agus MSD, Balamuth F, Brady PW, Brilli RJ, Carcillo JA, Dantes R, Epstein L, Fiore AE, Gerber JS, Gokhale RH, Joyner BL Jr, Kissoon N, Klompas M, Lee GM, Macias CG, Puopolo KM, Sulton CD, Weiss SL, Rhee C. A National Approach to Pediatric Sepsis Surveillance. Pediatrics. 2019 Dec;144(6):e20191790. doi: 10.1542/peds.2019-1790. PMID: 31776196; PMCID: PMC6889946.
6. Wurzel D, Neeland MR, Anderson J, Abo YN, Do LAH, Donato CM, Bines JE, Toh ZQ, Higgins RA, Jalali S, Cole T, Subbarao K, McMinn A, Dohle K, Haeusler GM, McNab S, Alafaci A, Overmars I, Clifford V, Lee LY, Daley AJ, Buttery J, Bryant PA, Burgner D, Steer A, Tosif S, Konstantinov IE, Duke T, Licciardi PV, Pellicci DG, Crawford NW. A case report describing the immune response of an infant with congenital heart disease and severe COVID-19. Commun Med (Lond). 2021 Nov 15;1:47. doi: 10.1038/s43856-021-00047-7. PMID: 35602234; PMCID: PMC9053208.
7. Marchant EA, Kan B, Sharma AA, van Zanten A, Kollmann TR, Brant R, Lavoie PM. Attenuated innate immune defenses in very premature neonates during the neonatal period. Pediatr Res. 2015 Nov;78(5):492-7. doi: 10.1038/pr.2015.132. Epub 2015 Jul 17. PMID: 26186294; PMCID: PMC5059157.
8. Goswami S, Gupta R, Ramji S. Flow Cytometry: An Important Diagnostic Tool in Critically Ill Preterm Neonates with Suspected Sepsis. Am J Perinatol. 2022 Apr;39(6):616-622. doi: 10.1055/s-0040-1718370. Epub 2020 Sep 29. PMID: 32992350.
9. Segura-Cervantes E, Mancilla-Ramírez J, González-Canudas J, Alba E, Santillán-Ballesteros R, Morales-Barquet D, Sandoval-Plata G, Galindo-Sevilla N. Inflammatory Response in Preterm and Very Preterm Newborns with Sepsis. Mediators Inflamm. 2016;2016:6740827. doi: 10.1155/2016/6740827. Epub 2016 May 16. PMID: 27293317; PMCID: PMC4884838.
10. Collins A, Weitkamp JH, Wynn JL. Why are preterm newborns at increased risk of infection? Arch Dis Child Fetal Neonatal Ed. 2018 Jul;103(4):F391-F394. doi: 10.1136/archdischild-2017-313595. Epub 2018 Jan 30. PMID: 29382648; PMCID: PMC6013388.
11. Celik IH, Hanna M, Canpolat FE, Mohan Pammi. Diagnosis of neonatal sepsis: the past, present and future. Pediatr Res. 2022 Jan;91(2):337-350. doi: 10.1038/s41390-021-01696-z. Epub 2021 Nov 2. PMID: 34728808; PMCID: PMC8818018.
12. Goldstein B, Giroir B, Randolph A; International Consensus Conference on Pediatric Sepsis. International pediatric sepsis consensus conference: definitions for sepsis and organ dysfunction in pediatrics. Pediatr Crit Care Med. 2005 Jan;6(1):2-8. doi: 10.1097/01.PCC.0000149131.72248.E6. PMID: 15636651.
13. Bogale A, Borko UD, Abreha S, Balta B. Determinants of mortality among preterm neonates admitted at Wolaita Sodo University Comprehensive Specialized Hospital, southern Ethiopia: An unmatched case-control study. PLoS One. 2024 Dec 2;19(12):e0314632. doi: 10.1371/journal.pone.0314632. PMID: 39621711; PMCID: PMC11611175.
14. Kucova P, Kantor L, Fiserova K, Lasak J, Röderova M, Kolar M. Bacterial Pathogens and Evaluation of a Cut-Off for Defining Early and Late Neonatal Infection. Antibiotics (Basel). 2021 Mar 9;10(3):278. doi: 10.3390/antibiotics10030278. PMID: 33803288; PMCID: PMC7998728.
15. Fenton TR, Merlino Barr S, Elmrayed S, Alshaikh B. Expected and Desirable Preterm and Small Infant Growth Patterns. Adv Nutr. 2024 Jun;15(6):100220. doi: 10.1016/j.advnut.2024.100220. Epub 2024 Apr 24. PMID: 38670164; PMCID: PMC11251411.
16. Yadav P, Yadav SK. Progress in Diagnosis and Treatment of Neonatal Sepsis: A Review Article. JNMA J Nepal Med Assoc. 2022 Mar 11;60(247):318-324. doi: 10.31729/jnma.7324. PMID: 35633256; PMCID: PMC9226748.
17. Kurul Ş, Beckers FLM, Vermeulen MJ, Suurland J, Hasbek JE, Ramakers CRB, Simons SHP, Reiss IKM, Taal HR. Inflammation, sepsis severity and neurodevelopmental outcomes of late-onset sepsis in preterm neonates. Pediatr Res. 2023 Dec;94(6):2026-2032. doi: 10.1038/s41390-023-02742-8. Epub 2023 Jul 19. PMID: 37468719.
18. Shah J, Balasubramaniam T, Yang J, Shah PS. Leukopenia and Neutropenia at Birth and Sepsis in Preterm Neonates of <32 Weeks' Gestation. Am J Perinatol. 2022 Jul;39(9):965-972. doi: 10.1055/s-0040-1721133. Epub 2020 Nov 23. PMID: 33231269.
19. Ebenebe CU, Hesse F, Blohm ME, Jung R, Kunzmann S, Singer D. Diagnostic accuracy of interleukin-6 for early-onset sepsis in preterm neonates. J Matern Fetal Neonatal Med. 2021 Jan;34(2):253-258. doi: 10.1080/14767058.2019.1606194. Epub 2019 Apr 29. PMID: 30966828.
20. Bethou A, Bhat BV. Neonatal Sepsis-Newer Insights. Indian J Pediatr. 2022 Mar;89(3):267-273. doi: 10.1007/s12098-021-03852-z. Epub 2021 Jun 25. PMID: 34170492.
21. Cantey JB, Lee JH. Biomarkers for the Diagnosis of Neonatal Sepsis. Clin Perinatol. 2021 Jun;48(2):215-227. doi: 10.1016/j.clp.2021.03.012. PMID: 34030810.
22. Mota RB, Soares P, Guimarães H. Assessment of a score's performance in predicting positive culture studies in preterm neonates with clinical suspicion of sepsis. J Mother Child. 2022 Apr 1;25(2):119-122. doi: 10.34763/jmotherandchild.20212502.d-21-00019. PMID: 34786899; PMCID: PMC8976589.
23. Rao JG, Sarangi R, Das R, Nanda D, Jena PP, Krishnegowda VK. Outcomes and antimicrobial usage in preterm neonates < 34 weeks gestation with culture-negative neonatal sepsis: a prospective observational study. BMC Infect Dis. 2025 Dec 6;26(1):44. doi: 10.1186/s12879-025-12288-1. PMID: 41353525; PMCID: PMC12797939.
24. Hibbert J, Strunk T, Simmer K, Richmond P, Burgner D, Currie A. Plasma cytokine profiles in very preterm infants with late-onset sepsis. PLoS One. 2020 May 14;15(5):e0232933. doi: 10.1371/journal.pone.0232933. PMID: 32407417; PMCID: PMC7224469.

25. Glaser MA, Hughes LM, Jnah A, Newberry D. Neonatal Sepsis: A Review of Pathophysiology and Current Management Strategies. Adv Neonatal Care. 2021 Feb 1;21(1):49-60. doi: 10.1097/ANC.0000000000000769. PMID: 32956076.
26. Yochpaz S, Friedman N, Zirkin S, Blumovich A, Mandel D, Marom R. C-reactive protein in early-onset neonatal sepsis - a cutoff point for CRP value as a predictor of early-onset neonatal sepsis in term and late preterm infants early after birth? J Matern Fetal Neonatal Med. 2022 Dec;35(23):4552-4557. doi: 10.1080/14767058.2020.1856068. Epub 2020 Dec 6. PMID: 33280469.
27. Macallister K, Smith-Collins A, Gillet H, Hamilton L, Davis J. Serial C-Reactive Protein Measurements in Newborn Infants without Evidence of Early-Onset Infection. Neonatology. 2019;116(1):85-91. doi: 10.1159/000497237. Epub 2019 May 21. PMID: 31112949.
28. Balayan S, Chauhan N, Chandra R, Kuchhal NK, Jain U. Recent advances in developing biosensing based platforms for neonatal sepsis. Biosens Bioelectron. 2020 Dec 1;169:112552. doi: 10.1016/j.bios.2020.112552. Epub 2020 Aug 25. PMID: 32931992.
29. Brown JVE, Meader N, Wright K, Cleminson J, McGuire W. Assessment of C-Reactive Protein Diagnostic Test Accuracy for Late-Onset Infection in Newborn Infants: A Systematic Review and Meta-analysis. JAMA Pediatr. 2020 Mar 1;174(3):260-268. doi: 10.1001/jamapediatrics.2019.5669. Erratum in: JAMA Pediatr. 2020 Jun 1;174(6):625. doi: 10.1001/jamapediatrics.2020.0950. PMID: 32011640; PMCID: PMC7042944.
30. Kordek A, Łoniewska B, Podraza W, Nikodemski T, Rudnicki J. Usefulness of estimation of blood procalcitonin concentration versus C-reactive protein concentration and white blood cell count for therapeutic monitoring of sepsis in neonates. Postepy Hig Med Dosw (Online). 2014 Dec 21;68:1516-23. doi: 10.5604/17322693.1133101. PMID: 25531715.
31. Sharma D, Farahbakhsh N, Shastri S, Sharma P. Biomarkers for diagnosis of neonatal sepsis: a literature review. J Matern Fetal Neonatal Med. 2018 Jun;31(12):1646-1659. doi: 10.1080/14767058.2017.1322060. Epub 2017 May 7. PMID: 28427289.
32. Wacker C, Prkno A, Brunkhorst FM, Schlattmann P. Procalcitonin as a diagnostic marker for sepsis: a systematic review and meta-analysis. Lancet Infect Dis. 2013 May;13(5):426-35. doi: 10.1016/S1473-3099(12)70323-7. Epub 2013 Feb 1. PMID: 23375419.
33. Eichberger J, Resch E, Resch B. Diagnosis of Neonatal Sepsis: The Role of Inflammatory Markers. Front Pediatr. 2022 Mar 8;10:840288. doi: 10.3389/fped.2022.840288. PMID: 35345614; PMCID: PMC8957220.
34. Lisowska KA. The Role of Interleukin-8 (IL-8) in Treatment-Resistant Depression: A Review of Mechanisms, Biomarker Potential, and Therapeutic Implications. Int J Mol Sci. 2025 Oct 16;26(20):10092. doi: 10.3390/ijms262010092. PMID: 41155383; PMCID: PMC12562488.
35. Gibbons D, Fleming P, Virasami A, Michel ML, Sebire NJ, Costeloe K, Carr R, Klein N, Hayday A. Interleukin-8 (CXCL8) production is a signatory T cell effector function of human newborn infants. Nat Med. 2014 Oct;20(10):1206-10. doi: 10.1038/nm.3670. Epub 2014 Sep 21. PMID: 25242415.
36. Lusyati S, Hulzebos CV, Zandvoort J, Sukandar H, Sauer PJ. Cytokines patterns in newborn infants with late onset sepsis. J Neonatal Perinatal Med. 2013;6(2):153-63. doi: 10.3233/NPM-1364112. PMID: 24246518.
37. Chen X, Zhang X, Xue R, Mi L, Liu Y, Zhang G, Bu J, Bei F. Intrauterine inflammation exposure may increase the risk of late-onset sepsis in premature infants: a retrospective cohort study. Ital J Pediatr. 2025 Jul 10;51(1):218. doi: 10.1186/s13052-025-02040-5. PMID: 40640885; PMCID: PMC12247326.
38. Gustafsson A, Johansson E, Henckel E, Olin A, Rodriguez L, Brodin P, Lange S, Bohlin K. Antisecretory factor in breastmilk is associated with reduced incidence of sepsis in preterm infants. Pediatr Res. 2024 Feb;95(3):762-769. doi: 10.1038/s41390-023-02909-3. Epub 2023 Nov 24. PMID: 38001236; PMCID: PMC10899102.
39. Strunk T, Hibbert J, Doherty D, Nathan E, Simmer K, Richmond P, Currie A, Burgner D. Impaired Cytokine Responses to Live Staphylococcus epidermidis in Preterm Infants Precede Gram-positive, Late-onset Sepsis. Clin Infect Dis. 2021 Jan 27;72(2):271-278. doi: 10.1093/cid/ciaa063. PMID: 31960030.
40. Lindner U, Tutdibi E, Binot S, Monz D, Hilgendorff A, Gortner L. Levels of cytokines in umbilical cord blood in small for gestational age preterm infants. Klin Padiatr. 2013 Mar;225(2):70-74. doi: 10.1055/s-0033-1334879. Epub 2013 Mar 22. PMID: 23526611.
41. Sugitharini V, Prema A, Berla Thangam E. Inflammatory mediators of systemic inflammation in neonatal sepsis. Inflamm Res. 2013 Dec;62(12):1025-34. doi: 10.1007/s00011-013-0661-9. Epub 2013 Sep 8. PMID: 24013483.
42. Otsubo Y, Hashimoto K, Kanbe T, Sumi M, Moriuchi H. Association of cord blood chemokines and other biomarkers with neonatal complications following intrauterine inflammation. PLoS One. 2017 May 22;12(5):e0175082. doi: 10.1371/journal.pone.0175082. PMID: 28531215; PMCID: PMC5439663.
43. Anderson J, Thang CM, Thanh LQ, Dai VTT, Phan VT, Nhu BTH, Trang DNX, Trinh PTP, Nguyen TV, Toan NT, Harpur CM, Mulholland K, Pellicci DG, Do LAH, Licciardi PV. Immune Profiling of Cord Blood From Preterm and Term Infants Reveals Distinct Differences in Pro-Inflammatory Responses. Front Immunol. 2021 Nov 1;12:777927. doi: 10.3389/fimmu.2021.777927. PMID: 34790206; PMCID: PMC8591285.
44. Morajker G, Patil AA, Ranya Raghavendra P, Datar A, Nair S, Dandekar Jain P, Balasubramanian H, Haribalakrishna A, Goyal M, Kabra NS. Urinary immune biomarkers for late-onset sepsis in preterm very low birth weight neonates - a diagnostic accuracy study. J Perinat Med. 2025 Oct 7;54(3):630-636. doi: 10.1515/jpm-2025-0342. PMID: 41052967.
45. de Jong E, Strunk T, Burgner D, Lavoie PM, Currie A. The phenotype and function of preterm infant monocytes: implications for susceptibility to infection. J Leukoc Biol. 2017 Sep;102(3):645-656. doi: 10.1189/jlb.4RU0317-111R. Epub 2017 Jun 19. PMID: 28630102.

***Corresponding author**: Voja Pavlovic, e-mail: vojapav@yahoo.com*

International Journal of Biomedicine 16(3) (2026) 346-351
http://dx.doi.org/10.21103/Article16(3)_OA3

ORIGINAL ARTICLE

INTERNATIONAL JOURNAL OF BIOMEDICINE

Integrated Immunomorphological and Molecular Profiling Predicts Response to Neoadjuvant Therapy in Breast Cancer

S.V. Vtorushin[1,2], N.A. Tarabanovskaya[1], N.V. Krakhmal[1,2], S.S. Naumov[1,2], N.V. Litviakov[1,2]

[1]*Cancer Research Institute, Tomsk National Research Medical Center of the Russian Academy of Sciences, Tomsk, Russian Federation*
[2]*Siberian State Medical University, Tomsk, Russian Federation*

Abstract

Background: To investigate whether integrating assessment of the tumor immune microenvironment with molecular genetic alterations improves prediction of response to neoadjuvant systemic therapy in patients with invasive breast cancer.
Methods and Results: This retrospective study included 23 patients with invasive breast cancer treated at the Cancer Research Institute, Tomsk National Research Medical Center, from 2023 to 2025. All patients received neoadjuvant systemic therapy followed by surgery. Pathological response was assessed using the Residual Cancer Burden (RCB) system. Pretreatment tumor specimens were analyzed for stromal tumor-infiltrating lymphocytes, immune cell subsets and ratios, immune phenotype, immunosuppressive index, and copy number alterations in genes associated with chemotherapy response and drug resistance. Pathologic complete response (pCR; RCB-0) was achieved in 17 patients (73.9%), and a favorable pathological response (RCB-0/I) was observed in 19 patients (82.6%). Individual immune cell populations showed limited predictive value, whereas integrated immune parameters demonstrated stronger associations with treatment response. Patients with a favorable response had significantly higher CD8/FOXP3 ratios (4.07 vs. 1.72, p = 0.0002), lower FOXP3/CD8 ratios (0.25 vs. 0.58, p = 0.002), and lower CD68-positive macrophage infiltration (42 vs. 66.5 cells/HPF, p = 0.023). An inflamed immune phenotype and a low immunosuppressive index were associated with the highest probability of achieving pCR. Although no individual copy number alteration independently predicted treatment response, alterations involving TUBB3, ERBB2, and TOP2A were significantly associated with distinct tumor immune microenvironment characteristics.
Conclusions: Integrated assessment of the tumor immune microenvironment provides greater predictive value for neoadjuvant treatment response than evaluation of individual immune biomarkers alone. The observed associations between genomic alterations and immune microenvironment characteristics suggest that molecular alterations may influence therapeutic sensitivity through immune remodeling. Integrated immunomorphological and molecular profiling represents a promising strategy for predicting treatment response and personalizing neoadjuvant therapy in breast cancer. (**International Journal of Biomedicine. 2026;16(3):346-351.**)

Keywords: breast cancer • neoadjuvant therapy • pathological complete response • tumor immune microenvironment • immune profiling • copy number alterations • predictive biomarkers • personalized medicine

For citation: Vtorushin SV, Tarabanovskaya NA, Krakhmal NV, Naumov SS, Litviakov NV. Integrated Immunomorphological and Molecular Profiling Predicts Response to Neoadjuvant Therapy in Breast Cancer. International Journal of Biomedicine. 2026;16(3):346-351. doi:10.21103/Article16(3)_OA3

Abbrevations

BC, breast cancer; **pCR,** pathological complete response; **NAT,** neoadjuvant therapy; **TME,** tumor microenvironment; **TILs,** tumor-infiltrating lymphocytes; **sTILs,** stromal tumor-infiltrating lymphocytes; **CNA,** copy number alterations; **TNBC,** triple negative breast cancer; **IHC,** immunohistochemistry; **RCB,** residual cancer burden

Introduction

Breast cancer (BC) remains the most common malignant tumor in women worldwide and one of the leading causes of cancer-related mortality.[1] In recent years, neoadjuvant systemic therapy has become an essential component of treatment for patients with localized and locally advanced BC, particularly in triple-negative and HER2-positive subtypes. This approach not only reduces tumor burden and increases the feasibility of breast-conserving surgery but also provides

a unique opportunity to assess tumor sensitivity to systemic treatment in vivo.[2]

Pathologic complete response (pCR) is one of the key endpoints used to evaluate the efficacy of neoadjuvant therapy (NAT). Achievement of pCR is associated with improved disease-free and overall survival, especially in patients with biologically aggressive BC subtypes.[3,4] However, marked intratumoral heterogeneity leads to substantial variability in treatment response, even among tumors within the same molecular subtype. This highlights the need for additional biomarkers that can more accurately predict therapeutic sensitivity.

Growing evidence indicates that the tumor microenvironment (TME) plays a critical role in modulating the response to systemic therapy. Among its components, tumor-infiltrating lymphocytes (TILs) have been extensively investigated as predictive biomarkers in BC. Higher levels of stromal TILs are associated with an increased probability of achieving pCR, particularly in triple-negative BC (TNBC) and HER2-positive BC.[5,6]

Importantly, not only the density of immune infiltration but also its qualitative composition and spatial organization are of major biological and clinical relevance. A predominance of CD8-positive cytotoxic T lymphocytes reflects an active antitumor immune response, whereas accumulation of FOXP3-positive regulatory T cells and macrophage components contributes to the formation of an immunosuppressive microenvironment and may reduce the efficacy of systemic therapy.[7,8] Therefore, integral immune parameters that reflect the balance between effector and suppressive immune components may provide greater predictive value than individual immune markers alone.

In addition to immune microenvironmental features, molecular genetic alterations of tumor cells may also influence treatment response. Copy number alterations (CNA) in genes involved in DNA repair, drug transport, cell-cycle regulation, and microtubule dynamics may contribute to both direct sensitivity or resistance to cytotoxic therapy and tumor-immune microenvironment interactions.[9,10] However, the relationship between molecular genetic alterations and immune contexture in BC treated with NAT remains insufficiently characterized.

Despite the growing amount of data on immune and molecular predictors of treatment response, their integrated assessment remains an unresolved issue. The development of combined immunomorphological and molecular approaches may improve risk stratification and help identify patients with a higher probability of achieving a favorable response to NAT.

This study aimed to investigate the associations between immune TME parameters, molecular-genetic characteristics, and the efficacy of neoadjuvant systemic therapy in patients with BC.

Materials and Methods

Study Design and Patients

This retrospective study included 23 female patients with invasive BC who underwent examination and treatment at the Department of General Oncology, Cancer Research Institute, Tomsk National Research Medical Center (Tomsk, Russian Federation) between January 2023 and December 2025. All patients received neoadjuvant systemic therapy followed by surgical treatment. The median age at diagnosis was 46 years (range, 25-68 years). Before treatment initiation, all patients underwent a comprehensive clinical evaluation, including mammography, breast and regional lymph node ultrasonography, and histopathological confirmation of the diagnosis using ultrasound-guided core needle biopsy. Clinical staging was established according to the American Joint Committee on Cancer (AJCC) TNM Classification, 8th edition. The study cohort predominantly consisted of patients with cT2 tumors (69.6%) and clinically node-negative disease (cN0, 73.9%). Histological grading revealed grade 2 tumors in 65.2% of cases and grade 3 tumors in 34.8%. According to molecular subtype, the cohort included 9 cases (39.1%) of TNBC, 7 cases (30.4%) of triple-positive tumors, 5 cases (21.7%) of luminal B/HER2-negative tumors, and 2 cases (8.7%) of HER2-positive tumors.

Neoadjuvant Treatment and Response Assessment

Neoadjuvant treatment consisted of anthracycline-, taxane- and platinum-based chemotherapy regimens with anti-HER2 targeted therapy administered to patients with HER2-positive disease according to contemporary clinical guidelines. Depending on tumor subtype and treatment protocol, patients received four to eight treatment cycles. Following completion of NAT, all patients underwent surgical treatment. Breast-conserving surgery was performed in 8 patients (34.8%), whereas modified mastectomy was required in 15 (65.2%). Sentinel lymph node biopsy was performed in 6 patients (26.1%), while one patient underwent axillary lymph node dissection. Postoperative systemic treatment was administered according to molecular subtype, residual tumor burden, nodal status, and current clinical recommendations.

Pathological response was evaluated using the Residual Cancer Burden (RCB) classification; pCR was defined as the absence of residual invasive carcinoma in both the breast and regional lymph nodes (RCB-0). Favorable treatment response included RCB-0 and RCB-I, whereas RCB-II and RCB-III were classified as unfavorable responses.

Immunohistochemistry

Immunohistochemistry (IHC) analysis was performed on pretreatment core biopsy specimens. Tissue samples were fixed in 10% neutral buffered formalin, routinely processed, embedded in paraffin, and sectioned at a thickness of 3-4 μm. Immunohistochemical staining was performed on the Leica BOND-MAX automated staining platform (Leica Biosystems, Germany) using the Bond Polymer Refine Detection system. The following primary antibodies were used: CD4 (clone 4B12), CD8 (clone 4B11), FOXP3 (clone 236A/E7) and CD68 (clone KP1). PD-L1 expression was evaluated separately on the Ventana BenchMark platform (Roche Diagnostics, USA) using the SP142 assay.

Stromal tumor-infiltrating lymphocytes (sTILs) were assessed on hematoxylin and eosin stained slides according to the recommendations of the International Immuno-

Oncology Biomarker Working Group (formerly International TILs Working Group). Only stromal lymphocytes within the borders of the invasive tumor were evaluated.

The numbers of CD4, CD8, FOXP3, and CD68-positive cells were assessed separately in the stromal and intratumoral compartments. Positive cells were counted in five representative high-power fields (HPFs; ×400 magnification), and the mean number of positive cells per HPF was calculated.

To characterize the immune microenvironment, the CD8/FOXP3, FOXP3/CD8 and CD4/CD8 ratios were additionally calculated. Furthermore, tumors were classified according to immune phenotype and an immunosuppressive index was determined as previously described.

Molecular Genetic Analysis

Molecular genetic analysis was performed using pretreatment tumor biopsy specimens. Genomic DNA was isolated using the QIAamp DNA Mini Kit (Qiagen, Hilden, Germany) according to the manufacturer's instructions. DNA quality and integrity were evaluated using the TapeStation System (Agilent Technologies, Santa Clara, CA, USA), whereas DNA purity was assessed spectrophotometrically using a NanoDrop 2000instrument (Thermo Fisher Scientific, Waltham, MA, USA).

Genome-wide CNAs were analyzed using the Affymetrix CytoScan HD Array (Affymetrix, Santa Clara, CA, USA). Sample preparation, hybridization, washing, staining, and scanning were performed according to the manufacturer's protocol using the GeneChip®Scanner 3000 7G system. Raw data were processed using Chromosome Analysis Suite (ChAS), version 4.0 (Affymetrix, USA). Copy number gains and losses were identified according to the manufacturer's analytical algorithms.

Genes associated with chemotherapy sensitivity, drug resistance, DNA repair, and cell-cycle regulation were evaluated, including *BRCA1, XRCC1, ERCC1, TYMS, ABCB1, ABCC1, ABCC5, ABCG2, ERBB2, TOP2A, CCND1, ESR1, CYP19A1, EGFR, TUBB3*, and *TAP2*. Copy number status was classified as gain, loss, or normal copy number. Molecular findings were subsequently correlated with clinicopathological parameters, immune microenvironment characteristics, and treatment response.

Statistical Analysis

Statistical analyses were performed using STATISTICA for Windows, version 10.0 (StatSoft Inc., Tulsa, OK, USA). The normality of data distribution was assessed using the Shapiro-Wilk test. Continuous variables are presented as median and interquartile range (IQR) and were compared using the Mann-Whitney U test. Categorical variables were compared using Pearson's χ^2 test or Fisher's exact test as appropriate. All statistical tests were two-sided, and a P value <0.05 was considered statistically significant.

The baseline clinicopathological characteristics of the study cohort are presented in Table 1. Most patients had cT2 tumors (69.6%) and clinically node-negative disease (73.9%). TNBC represented the largest molecular subtype (39.1%), followed by triple-positive (30.4%), Luminal B/HER2-negative (21.7%), and HER2-positive tumors (8.7%).

Table 1. Clinicopathological characteristics of the study cohort (n = 23)

Characteristic	Value
Age, years	
Median (range)	46 (25-68)
Histological type	
Invasive carcinoma of no special type (NST)	22 (95.7%)
Special histological subtype	1 (4.3%)
Histological grade	
Grade 1	-
Grade 2	15 (65.2%)
Grade 3	8 (34.8%)
Clinical tumor stage (cT)	
cT1	4 (17.4%)
cT2	16 (69.6%)
cT3	2 (8.7%)
Multicentric disease	1 (4.3%)
Clinical nodal status (cN)	
cN0	17 (73.9%)
cN1	5 (21.7%)
cN3	1 (4.3%)
Molecular subtype	
Triple-negative breast cancer	9 (39.1%)
Triple-positive breast cancer	7 (30.4%)
Luminal B/HER2-negative breast cancer	5 (21.7%)
HER2-positive breast cancer	2 (8.7%)
Ki-67 (%)	
Median (range)	60 (23–98)
Lymphovascular invasion	
Absent	10 (43.5%)
Present	13 (56.5%)
Response to neoadjuvant therapy (RCB)	
RCB-0 (pathologic complete response)	17 (73.9%)
RCB-I (minimal residual disease)	2 (8.7%)
RCB-II–III (moderate/extensive residual disease)	4 (17.4%)

Results

Response to Neoadjuvant Therapy

Among the 23 patients included in the study, pCR with RCB-0 was achieved in 17 (73.9%) patients. Minimal residual disease (RCB-I) was observed in 2 patients (8.7%), whereas 4 patients (17.4%) demonstrated moderate or extensive residual disease (RCB-II and RCB-III). Overall, a favorable pathological response (RCB-0/I) was achieved in 19 patients (82.6%).

Immune Microenvironment and Treatment Response

The composition of the immune TME differed between patients with favorable and unfavorable responses to NAT (Table 2).

Table 2. Immune tumor microenvironment parameters according to pathological response to neoadjuvant therapy

Parameter	RCB-0/I (n=19)	RCB-II/III (n=4)	p
CD8/FOXP3 ratio	4.07 (2.8-5.9)	1.72 (1.2–2.4)	0.0002
FOXP3/CD8 ratio	0.25 (0.16-0.36)	0.58 (0.42–0.81)	0.002
CD68+ cells, cells/HPF	42 (31-58)	66.5 (59–79)	0.023
Stromal TILs, %	24 (15-35)	13.5 (10–18)	0.18
CD8+ cells, cells/HPF	54 (38-71)	30 (22–38)	0.16
CD4+ cells, cells/HPF	44 (30-56)	31.5 (24–38)	0.19
FOXP3+ cells, cells/HPF	14 (9-18)	19.5 (16–24)	0.24
CD4/CD8 ratio	0.81 (0.65-1.02)	1.05 (0.91–1.22)	0.13

Representative immunohistochemical staining patterns of the evaluated immune cell populations are shown in Figure 1.

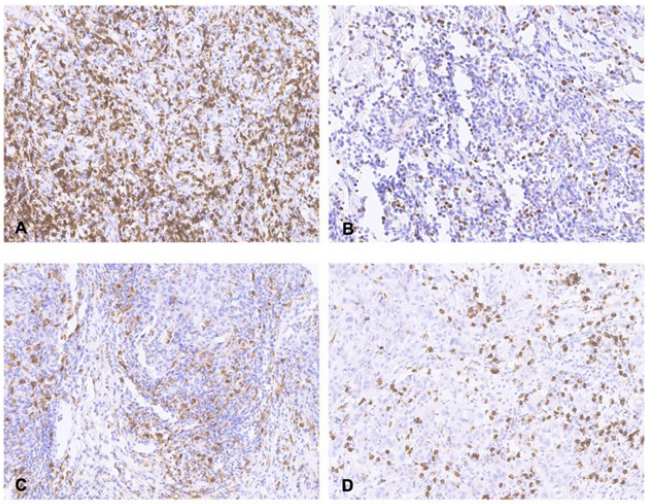

Fig. 1. *Representative immunohistochemical staining of immune cell populations in pretreatment breast cancer biopsy specimens. (A) CD8-positive cytotoxic T lymphocytes; (B) FOXP3-positive regulatory T lymphocytes; (C) CD68-positive macrophages; (D) CD4-positive T lymphocytes. Original magnification ×200.*

Patients achieving a favorable response exhibited higher levels of sTILs than those with residual disease (median, 24% vs. 13.5%; $p = 0.18$). Similarly, the numbers of CD8-positive cytotoxic T lymphocytes (54 vs. 30 cells/HPF; $p = 0.16$) and CD4-positive T lymphocytes (44 vs. 31.5 cells/HPF; $p = 0.19$) were higher in responders, whereas FOXP3-positive regulatory T cells were more abundant in non-responders (19.5 vs. 14 cells/HPF; $p = 0.24$).

The most pronounced difference was observed for CD68-positive macrophages. Patients with unfavorable treatment response demonstrated significantly higher numbers of CD68-positive cells than responders (66.5 vs. 42 cells/HPF; $p = 0.023$).

Analysis of immune cell ratios revealed marked differences between treatment response groups. The CD8/FOXP3 ratio was significantly higher in patients with favorable response (4.07 vs. 1.72; $p = 0.0002$), whereas the reciprocal FOXP3/CD8 ratio was significantly increased in patients with residual disease (0.58 vs. 0.25; $p = 0.002$). No significant difference was observed for the CD4/CD8 ratio ($p = 0.13$). PD-L1 expression assessed using the SP142 assay did not differ significantly between the two groups (median IC score, 1.2% vs. 0.7%; $p = 0.27$).

Immune Phenotype and Immunosuppressive Index

Based on the integrated assessment of immune cell distribution, 12 tumors (52.2%) were classified as inflamed whereas the remaining 11 tumors (47.8%) exhibited non-inflamed immune phenotypes, including immune-excluded, desert/excluded, immune-desert and excluded/inflamed patterns (Table 3).

Patients with an inflamed immune phenotype demonstrated a markedly higher frequency of pCR than those with non-inflamed tumors (91.7% vs. 54.5%). Although this difference did not reach statistical significance, a strong trend toward improved pathological response was observed (Fisher's exact test, $p = 0.069$).

Table 3. Association between tumor immune phenotype and pathological response to neoadjuvant therapy

Tumor immune phenotype	pCR (n = 17)	Residual disease (n = 6)	Total (n = 23)
Inflamed	11 (91.7%)	1 (8.3%)	12
Non-inflamed*	6 (54.5%)	5 (45.5%)	11

Fisher's exact test: P = 0.069
**Non-inflamed tumors included the immune-excluded, desert/excluded, immune-desert and excluded/inflamed phenotypes.*

The immunosuppressive index showed a significant association with treatment efficacy. A low immunosuppressive index (scores 0-1) was observed in 15 of 17 patients (88.2%) achieving pCR, whereas a high immunosuppressive index (scores 2-3) predominated among patients with residual disease (4 of 6; 66.7%) (Fisher's exact test, $p = 0.027$) (Table 4).

Table 4. Immunosuppressive index according to pathological response

Immunosuppressive index	pCR (n = 17)	Residual disease (n = 6)	Total (n = 23)
Low (scores 0-1)	15 (88.2%)	2 (11.8%)	17
High (scores 2-3)	2 (33.3%)	4 (66.7%)	6

Fisher's exact test: P = 0.027

The distribution of immune phenotypes also differed across molecular subtypes. HER2-positive and triple-positive tumors were predominantly characterized by an inflamed immune phenotype, whereas Luminal B/HER2-negative tumors more frequently exhibited non-inflamed immune phenotypes.

Copy Number Alterations and their Association with the Immune Microenvironment

Genome-wide copy number analysis identified recurrent alterations involving *TOP2A*(48%), *ABCC5*(43%), *ERBB2*(39%), *BRCA1* (39%) and *TUBB3* (35%). No individual CNA was significantly associated with pathological response to NAT. Because no direct associations with treatment response were identified, additional analyses were performed to evaluate relationships between genomic alterations and the immune microenvironment. Tumors harboring *TUBB3* CNA exhibited significantly lower sTILs levels than tumors without these alterations (10% vs. 25%; $p = 0.038$). Likewise, CD8-positive T cell density was significantly reduced in the presence of *TUBB3* alterations (23 vs. 59.5 cells/HPF; $p = 0.030$). Conversely, CNAs involving *ERBB2* and *TOP2A* were associated with increased numbers of FOXP3-positive regulatory T cells (17 vs. 10.5 cells/HPF; $p = 0.047$ and 19 vs. 12 cells/HPF; $p = 0.039$, respectively).

Discussion

The present study demonstrates that the immune TME plays a central role in determining the response to neoadjuvant systemic therapy in BC. Although a pCR was achieved in 73.9% of patients, treatment efficacy was associated not with individual immune cell populations but with the overall

functional organization of the immune microenvironment. This observation supports the concept that the balance between antitumor immune activation and local immunosuppression is a more informative predictor of therapeutic response than the absolute density of individual immune cell subsets.[5-8]

Among the evaluated immune parameters, sTILs tended to be more abundant in patients achieving a favorable pathological response, which is consistent with numerous studies demonstrating the predictive value of TILs in patients receiving NAT, particularly in TNBC and HER2-positive cases of BC.[5,6,11] However, the lack of statistical significance in the present study is most likely attributable to the limited sample size rather than the absence of a biological association.

Importantly, immune cell ratios demonstrated substantially greater discriminatory ability than individual immune cell populations. The CD8/FOXP3 ratio was significantly higher in responders, whereas the reciprocal FOXP3/CD8 ratio was increased in tumors with residual disease. These findings indicate that the functional balance between cytotoxic and immunosuppressive immune compartments provides a more robust estimate of antitumor immune competence than isolated quantification of CD8-positive or FOXP3-positive cells. This observation is consistent with the current understanding that coordinated interactions between immune cell populations, rather than individual immune subsets, determine the effectiveness of antitumor immunity and therapeutic response.[7,8,11]

Another important finding was the association between increased CD68-positive macrophage infiltration and an unfavorable response to NAT. Tumor-associated macrophages are recognized as major regulators of tumor progression, immune evasion, angiogenesis, and resistance to systemic therapy. Previous studies have demonstrated that macrophage-rich TME promote immunosuppressive signaling, inhibit cytotoxic T cell activity, and contribute to resistance to chemotherapy and immunotherapy.[8] Our findings further support the clinical relevance of macrophage-associated immune suppression in BC.

An integrated assessment of the immune TME provided additional prognostic information beyond individual immune biomarkers. Patients with an inflamed immune phenotype demonstrated the highest frequency of pCR, whereas non-inflamed tumors were substantially more likely to exhibit residual disease after neoadjuvant treatment. Similarly, a low immunosuppressive index was significantly associated with pCR. Collectively, these observations emphasize that the spatial organization and functional architecture of the immune TME represent clinically relevant determinants of therapeutic sensitivity rather than merely descriptive histopathological features.

One of the most interesting observations of the present study was the relationship between CNA and immune microenvironment characteristics. Although none of the investigated genomic alterations demonstrated an independent association with pathological response, several alterations were significantly associated with immune composition. In particular, *TUBB3* copy number alterations were associated with reduced sTILs density and decreased CD8-positive T cell infiltration, whereas alterations involving *ERBB2* and *TOP2A* were associated with increased FOXP3-positive regulatory T cell infiltration. These findings suggest that genomic alterations may influence treatment response indirectly through remodeling of the immune microenvironment rather than solely through modulation of intrinsic tumor sensitivity to cytotoxic agents. Such an interpretation is consistent with the emerging concept that genomic and immune tumor characteristics should be considered complementary components of an integrated predictive model rather than independent biomarkers.[9,10]

The present study has several limitations. First, the relatively small sample size limited the statistical power of subgroup analyses. Second, the cohort included different molecular subtypes of BC treated with subtype-specific neoadjuvant regimens, which may have influenced immune composition and treatment response. Finally, the retrospective design precludes definitive conclusions regarding causal relationships between genomic alterations, immune remodeling, and therapeutic efficacy. Nevertheless, the present findings support the concept that integrated immunomorphological and molecular profiling provides a more comprehensive characterization of tumor biology than evaluation of isolated biomarkers. Future prospective studies involving larger and molecularly homogeneous patient cohorts are warranted to validate these observations and to establish clinically applicable predictive models incorporating both immune TME characteristics and genomic alterations.

Conclusion

The present study demonstrates that the tumor immune microenvironment is a major determinant of response to neoadjuvant systemic therapy in BC. Among the evaluated biomarkers, integrated immune parameters - including the CD8/FOXP3 ratio, immune phenotype and immunosuppressive index - provided greater predictive value than the absolute density of individual immune cell populations, highlighting the importance of the functional organization of the antitumor immune response. Although individual CNAs were not independently associated with pathological response, significant associations between alterations involving *TUBB3*, *ERBB2,* and *TOP2A* and distinct immune microenvironment characteristics suggest that genomic alterations may contribute to therapeutic sensitivity through modulation of the immune landscape. These findings support the concept that genomic and immune characteristics represent complementary rather than independent determinants of treatment response.

Collectively, our results indicate that integrated immunomorphological and molecular profiling may improve prediction of neoadjuvant treatment efficacy and provide a biologically meaningful framework for patient stratification and personalized therapeutic decision-making in BC. Further prospective studies in larger, molecularly homogeneous cohorts are warranted to validate these findings and establish clinically applicable predictive models.

Ethical Considerations

The study was conducted in accordance with the ethical principles of the Declaration of Helsinki and was approved by the Local Ethics Committee of the Cancer Research Institute (Protocol No. 16, December 2023). Due to the retrospective study design and the use of anonymized archival tissue samples and clinical data, the requirement for informed consent was waived.

Competing Interests

The authors declare that they have no competing interests.

References

1. Siegel RL, Giaquinto AN, Jemal A. Cancer statistics, 2024. CA Cancer J Clin. 2024 Jan-Feb;74(1):12-49. doi: 10.3322/caac.21820. PMID: 38230766.
2. Loibl S, Poortmans P, Morrow M, Denkert C, Curigliano G. Breast cancer. Lancet. 2021 May 8;397(10286):1750-1769. doi: 10.1016/S0140-6736(20)32381-3. PMID: 33812473.
3. Cortazar P, Zhang L, Untch M, Mehta K, Costantino JP, Wolmark N, Bonnefoi H, Cameron D, Gianni L, Valagussa P, Swain SM, Prowell T, Loibl S, Wickerham DL, Bogaerts J, Baselga J, Perou C, Blumenthal G, Blohmer J, Mamounas EP, Bergh J, Semiglazov V, Justice R, Eidtmann H, Paik S, Piccart M, Sridhara R, Fasching PA, Slaets L, Tang S, Gerber B, Geyer CE Jr, Pazdur R, Ditsch N, Rastogi P, Eiermann W, von Minckwitz G. Pathological complete response and long-term clinical benefit in breast cancer: the CTNeoBC pooled analysis. Lancet. 2014 Jul 12;384(9938):164-172. doi: 10.1016/S0140-6736(13)62422-8. PMID: 24529560.
4. Spring LM, Fell G, Arfe A, Sharma C, Greenup R, Reynolds KL, Smith BL, Alexander B, Moy B, Isakoff SJ, Parmigiani G, Trippa L, Bardia A. Pathologic complete response after neoadjuvant chemotherapy and impact on breast cancer recurrence and survival: A comprehensive meta-analysis. Clin Cancer Res. 2020 Jun 15;26(12):2838-2848. doi: 10.1158/1078-0432.CCR-19-3492. PMID:32046998. PMCID: PMC7299787.
5. Xia G, Zhang Z, Jiang Q, Wang H, Wang J. Predictive value of stromal tumor-infiltrating lymphocytes in patients with breast cancer treated with neoadjuvant chemotherapy: A meta-analysis. Medicine (Baltimore). 2024 Feb 9;103(6):e36810. doi: 10.1097/MD.0000000000036810. PMID: 38335394.
6. Ladoire S, Arnould L, Apetoh L, Coudert B, Martin F, Chauffert B, Fumoleau P, Ghiringhelli F. Pathologic complete response to neoadjuvant chemotherapy of breast carcinoma is associated with the disappearance of tumor-infiltrating FOXP3+ regulatory T cells. Clin Cancer Res. 2008 Apr 15;14(8):2413-2420. doi: 10.1158/1078-0432.CCR-07-4491. PMID: 18413832.
7. Binnewies M, Roberts EW, Kersten K, Chan V, Fearon DF, Merad M, Coussens LM, Gabrilovich DI, Ostrand-Rosenberg S, Hedrick CC, Vonderheide RH, Pittet MJ, Jain RK, Zou W, Howcroft TK, Woodhouse EC, Weinberg RA, Krummel MF. Understanding the tumor immune microenvironment (TIME) for effective therapy. Nat Med. 2018 May;24(5):541-550. doi: 10.1038/s41591-018-0014-x. PMID: 29686425.
8. Myers SP, Sevilimedu V, Barrio AV, Tadros AB, Mamtani A, Robson ME, Morrow M, Lee MK. Pathologic complete response after neoadjuvant systemic therapy for breast cancer in BRCA mutation carriers and noncarriers. NPJ Breast Cancer. 2024 Jul 26;10(1):63. doi: 10.1038/s41523-024-00674-y. PMID:39060255.
9. Symmans WF, Peintinger F, Hatzis C, Rajan R, Kuerer H, Valero V, Assad L, Poniecka A, Hennessy B, Green M, Buzdar AU, Hortobagyi GN, Pusztai L. Measurement of residual breast cancer burden to predict survival after neoadjuvant chemotherapy. J Clin Oncol. 2007 Oct 1;25(28):4414-4422. doi: 10.1200/JCO.2007.10.6823. PMID: 17785706.
10. Dieci MV, Radosevic-Robin N, Fineberg S, van den Eynden G, Ternes N, Penault-Llorca F, Pruneri G, D'Alfonso TM, Demaria S, Castaneda C, Sanchez J, Badve S, Michiels S, Bossuyt V, Rojo F, Singh B, Nielsen T, Viale G, Kim SR, Hewitt S, Wienert S, Loibl S, Rimm D, Symmans F, Denkert C, Adams S, Loi S, Salgado R; International Immuno-Oncology Biomarker Working Group on Breast Cancer. Update on tumor-infiltrating lymphocytes (TILs) in breast cancer, including recommendations to assess TILs in residual disease after neoadjuvant therapy and in carcinoma in situ: A report of the International Immuno-Oncology Biomarker Working Group on Breast Cancer. Semin Cancer Biol. 2018 Oct;52(Pt 2):16-25. doi: 10.1016/j.semcancer.2017.10.003. PMID: 29024776.
11. Schlam I, Loi S, Salgado R, Swain SM. Tumor-infiltrating lymphocytes in HER2-positive breast cancer: potential impact and challenges. ESMO Open. 2025 Feb;10(2):104120. doi: 10.1016/j.esmoop.2024.104120. PMID:39826475.

Corresponding author: *Nadezhda V. Krakhmal - krakhmal@mail.ru*

International Journal of Biomedicine 16(3) (2026) 352-356
http://dx.doi.org/10.21103/Article16(3)_OA4

ORIGINAL ARTICLE

INTERNATIONAL JOURNAL OF BIOMEDICINE

Ultrasound Evaluation of Lower Limb Arteries in Non-Diabetic Controls and Diabetic Patients

Adel Alzahrani[1*], Omar Alserihy[1], Asma Alkhaldi[1], Khadijah Alshuqyfii[1], Ahmed Monis[1], Yaser Khojah[1], Nawaf Alsaedi[1], Reem T. Alturki[2], Salahaden R Sultan[3,4]

[1]*Department of Diagnostic Radiology and Medical Imaging, King Abdullah Medical City, Makkah, Saudi Arabia*
[2]*Department of Radiological Sciences, College of Applied Medical Sciences, King Saud University, Riyadh, Saudi Arabia*
[3]*Department of Radiologic Sciences, Faculty of Applied Medical Sciences, King Abdulaziz University, Jeddah, Saudi Arabia*
[4]*Department of Radiology, King Abdulaziz University Hospital, King Abdulaziz University, Jeddah, Saudi Arabia*

Abstract

Background: Diabetes mellitus is associated with an increased risk of lower extremity arterial disease. Ultrasound imaging enables non-invasive assessment of both arterial morphology and hemodynamics. This study aimed to compare lower limb arterial morphology and hemodynamic characteristics assessed using ultrasound between asymptomatic diabetic patients and non-diabetic controls.

Methods and Results: This study included 71 participants comprising 38 diabetic patients and 33 non-diabetic controls. Duplex ultrasound examinations of the popliteal, anterior, and posterior tibial arteries were performed using a high-resolution ultrasound system. B-mode ultrasound was used to measure wall thickness, and Doppler imaging was used to assess flow velocity (FV), resistive index (RI), and acceleration time (AT). Comparisons between groups were performed using the Mann–Whitney U test, with statistical significance set at $P \leq 0.05$.

A total of 406 arterial segments were evaluated. Diabetic patients demonstrated significantly greater wall thickness compared with controls (median 0.71 mm [IQR 0.33] vs. 0.62 mm [IQR 0.30]; $P < 0.001$). Doppler ultrasound revealed significantly higher RI values in diabetic patients (median 0.98 [IQR 0.03] vs. 0.94 [IQR 0.07]; $P = 0.008$) and prolonged AT (median 110 ms [IQR 37] vs. 103 ms [IQR 33.75]; $P = 0.04$). No significant difference in FV was observed between groups ($P = 0.76$).

Conclusion: Diabetic patients exhibit structural and hemodynamic alterations in lower limb arteries, characterized by increased arterial wall thickness, elevated vascular resistance, and prolonged systolic acceleration time. These findings suggest that triplex ultrasound-derived parameters may be useful pre-clinical markers of diabetes-associated vascular impairment and could facilitate earlier identification of lower extremity arterial disease.(**International Journal of Biomedicine. 2026;16(3):352-356.**)

Keywords: diabetes mellitus • peripheral artery disease • hemodynamics • vascular imaging • ultrasound

For citation: Alzahrani A, Alserihy O, Alkhaldi A, Alshuqyfii K, Monis A, Khojah Y, Alsaedi N, Alturki RT, Sultan SR. Ultrasound Evaluation of Lower Limb Arteries in Non-Diabetic Controls and Diabetic Patients International Journal of Biomedicine. 2026;16(3):352-356. doi:10.21103/Article16(3)_OA4

Introduction

Diabetes mellitus (DM) is a chronic metabolic disorder that has emerged as one of the leading global health challenges due to its increasing prevalence and its profound impact on morbidity and mortality.[1] The disease is characterized by persistent hyperglycemia causing metabolic and vascular dysfunction.[2] Vascular complications remain a major cause of disability and death among diabetic patients, accounting for a substantial proportion of hospitalizations and reduced quality of life. [3,4]

Diabetes-related vascular complications arise from chronic hyperglycemia-induced endothelial dysfunction and oxidative stress, with advanced glycation end-products

and inflammation accelerating atherosclerosis and vascular damage.[5,6] Peripheral artery disease (PAD) is a major macrovascular complication of diabetes and a manifestation of systemic atherosclerosis, leading to partial or complete occlusion of lower-extremity arteries and impaired tissue perfusion. [7] PAD is associated with impaired wound healing and diabetic foot ulceration, and it increases the risk of chronic limb-threatening ischemia, lower extremity amputation, and mortality.[8,9] Vascular alteration, including increased arterial stiffness and impaired arterial compliance, may develop early in the course of dysglycaemia and may precede the clinical manifestation of diabetes and its vascular complications.[10,11] Therefore, early detection of these subclinical vascular alterations is essential for timely intervention, risk stratification, and prevention of disease progression and its associated complications.

Duplex ultrasound is a non-invasive imaging modality for PAD, offering non-invasive assessment of lower limb arterial circulation.[12] B-mode ultrasound enables measurement of intima–media thickness (IMT), a recognized marker of subclinical atherosclerosis and vascular remodeling. In contrast, Doppler ultrasound provides quantitative hemodynamic parameters such as blood flow velocity and volume, resistive index (RI), and acceleration time (AT), allowing for the assessment of both structural and functional vascular abnormalities.[13,14] The present study aimed to investigate structural and hemodynamic differences in the lower limb arteries of patients with diabetes mellitus compared with non-diabetic controls using B-mode and Doppler ultrasound imaging, through measuring intima-media thickness, flow volume, RI, and AT in the popliteal, anterior tibial, and posterior tibial arteries.

Methods

Study Design and Participants

This observational pilot study was ethically approved on 10.12.2023 by the Institute Review Board of Research Ethics Committee at King Abdullah Medical City (IRB No 23-1177). The study design adhered to the principles outlined in the Declaration of Helsinki and the International Conference of Harmonization of Good Clinical Practice. Adult participants referred to the ultrasound department for lower limb arterial assessment were prospectively recruited. The diabetic group comprised asymptomatic patients with type 2 diabetes mellitus (T2DM) of ≤5 years duration and without clinical evidence or a history of diabetes-related vascular complications or peripheral arterial disease. Healthy age- and BMI-matched non-diabetic volunteers served as controls. Ultrasound assessment of the lower limb arteries was performed by an experienced vascular sonographer.

Ultrasound Assessment and Data Acquisition

Lower limb ultrasound examinations were performed on all participants to evaluate the popliteal, anterior tibial, and posterior tibial arteries using a high-resolution EPIQ ultrasound imaging system (Philips Healthcare, Andover, MA, USA) equipped with a high-frequency linear transducer. Image quality was optimized by adjusting key parameters, including depth, focus point, overall gain, time-gain compensation, and dynamic range, to achieve high-resolution B-mode images. Longitudinal views of all arteries were acquired for comprehensive assessment. B-mode and Doppler ultrasound imaging were used to measure intima-media thickness, flow velocity, resistive index (RI), and acceleration time (AT) for all arteries depicted via ultrasound with Doppler angle correction of 60° (Figure 1). During ultrasound imaging, participants were positioned supine. A sufficient amount of gel was applied, and the transducer was placed on the artery to be assessed.

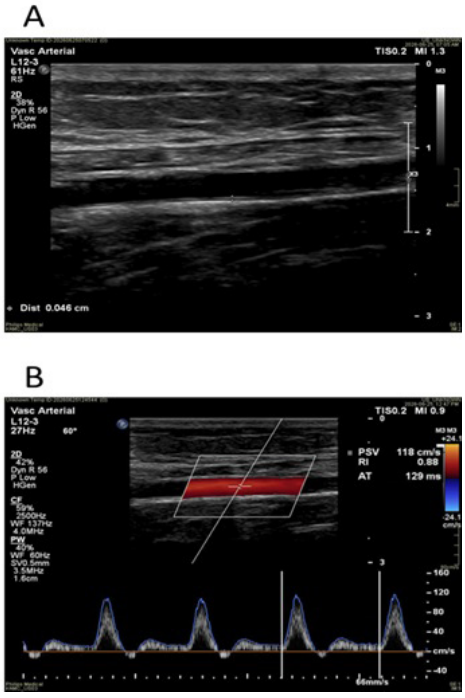

Figure 1. *Ultrasound measurement of lower limb arterial parameters. B-mode measurement of wall thickness (A). Doppler measurements of peak systolic velocity (PSV), resistive index (RI), and acceleration time (AT).*

Statistical Analysis

Statistical analysis was conducted using SPSS Statistics (Version 21.0, IBM Corp., Armonk, NY, USA). The Mann–Whitney U test was employed to assess differences in intima–media thickness, flow velocity, RI and AT of the lower limb arteries between non-diabetic controls and diabetic patients. Statistical significance was defined as a P-value ≤ 0.05.

Results

A total of 406 lower limb arteries from 71 participants were evaluated using duplex ultrasound, comprising 33 non-diabetic controls and 38 patients with T2DM. Overall, the cohort had a mean age of 61.4 ± 16.0 years and a mean BMI of 29.6 ± 7.3 kg/m². The control group included 23 females and 10 males, with a mean age of 60.0 years and a mean BMI of 29.2 kg/m². The diabetic group consisted of 12 females and 26 males, with a mean age of 62.7 years and a mean BMI of 29.7 kg/m². Of the 71 patients included in this study, 36 were male (10 control and 26 diabetic), and 35 were female (23

control and 12 diabetic). Lower limb arterial wall thickness measured by B-mode ultrasound was significantly greater in the diabetic group compared with the control group (control: median 0.62 mm, interquartile range [IQR] 0.30 mm; diabetic: median 0.71 mm, IQR 0.33 mm; $Z = -4.20$, $P < 0.001$, n=383; Figure 2A). RI and AT assessed using Doppler ultrasound, also differed significantly between groups, with diabetic patients demonstrating higher RI and delayed AT values than controls (RI, control: median 0.94, IQR 0.07; diabetic: median 0.98, IQR 0.03; $Z = -2.65$, $P = 0.008$, n=405, Figure 2B; AT, control: median 103 ms, IQR 33.75 ms; diabetic: median 110 ms, IQR 37 ms; $Z = -2.02$, $P = 0.04$, n=405, Figure 2C). No significant difference in flow velocity was observed between the control and diabetic groups ($Z = -0.30$, $P = 0.76$, n=406, Figure 2D).

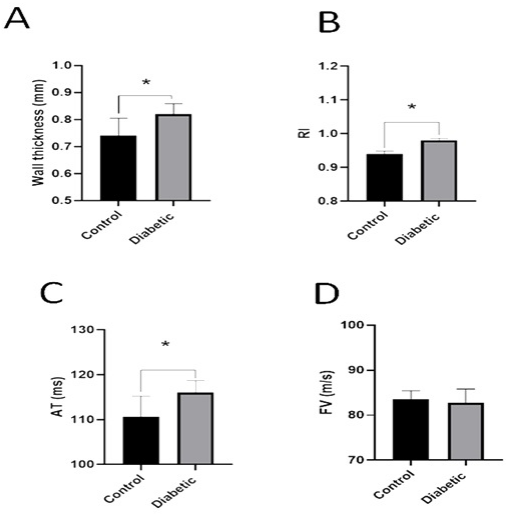

*Figure 2. Comparison of lower limb arterial intima–media thickness (IMT, A), resistive index (RI, B), acceleration time (AT, C), and flow velocity (FV, D) between control and diabetic groups. Data are presented as median and interquartile range (IQR). *P ≤ 0.05 using the Mann–Whitney U test.*

Discussion

This study investigated the structural and hemodynamic characteristics of lower limb arteries in diabetic patients compared with non-diabetic controls using ultrasound imaging, encompassing B-mode imaging and Doppler spectral analysis. Our findings demonstrate that diabetic patients exhibit significantly increased IMT, higher RI, and prolonged systolic AT, with no significant difference in mean flow volume was identified between groups. These findings indicate that DM is associated with morphological and hemodynamic alterations in the lower limb arteries, and support the utility of ultrasound as a useful modality for detecting subclinical arterial abnormalities in diabetic patients.

The increased arterial wall thickness observed in the present study is consistent with the progressive vascular remodeling associated with hyperglycemia, which promotes oxidative stress and inflammation, increases advanced glycation end-product formation, and impairs endothelial function, thereby stimulating smooth muscle cell proliferation and extracellular matrix accumulation, which contribute to arterial wall thickening and stiffening.[15–17] These extend previous observations to the lower limb arteries, which are particularly susceptible to diabetic macroangiopathy and play a central role in the development of peripheral arterial disease, critical limb ischemia, and diabetic foot complications.[18,19] Similar findings have been reported, with progressive increases in the wall thickness of the dorsalis pedis and posterior tibial arteries with increasing duration of T2DM, and a significant positive association between diabetes duration and artery wall thickness.[20] The greater wall thickness identified across multiple arterial segments, despite the relatively short duration of diabetes and absence of overt vascular complications in our cohort, suggests that diabetes-related macrovascular changes are diffuse in nature and may be detectable even in asymptomatic individuals. Collectively, these findings underscore the potential role of duplex ultrasound as a sensitive, non-invasive tool for the early identification of subclinical diabetic vasculopathy.

The significantly higher RI and prolonged AT observed in diabetic patients indicate the presence of early hemodynamic alterations associated with diabetic vasculopathy. RI is a Doppler-derived parameter reflecting downstream vascular resistance and vascular compliance, and elevated RI in diabetic patients is consistent with increased peripheral vascular impedance.[21] Several studies reported a progressive increase in the pulsatility index (PI) and RI of the peripheral arteries with increasing diabetes duration.[20,22,23] In addition, the significantly prolonged AT observed in the present study provides complementary evidence of impaired arterial hemodynamics. AT represents the interval between the onset of systolic flow and the attainment of peak systolic velocity on spectral Doppler waveform analysis, thereby serving as an indirect marker of arterial compliance, proximal flow impedance, and downstream vascular resistance.[24] The clinical utility of AT has been established across multiple vascular territories, where pedal acceleration time has emerged as a reliable Doppler parameter for assessing lower limb ischemia and peripheral arterial disease.[25–27] The prolonged AT identified in the diabetic cohort supports the presence of early functional vascular abnormalities and highlights the potential value of Doppler waveform analysis for detecting subclinical lower extremity vascular impairment. Together, RI and AT appear to be sensitive for detecting early lower limb vascular dysfunction and may represent practical quantitative markers for incorporation into routine duplex ultrasound surveillance of diabetic patients.

Several limitations of the present study should be acknowledged. The relatively small sample size and single-center design may have limited the generalizability of the findings. The cross-sectional nature of the study and the need for a longitudinal study are warranted to characterize further and assess vascular alterations associated with diabetes. In addition, incorporating clinical variables such as glycemic control, medication use, and the presence of microvascular

complications in future studies would provide a more comprehensive understanding of the factors influencing lower limb vascular remodeling and hemodynamic impairment.

Conclusion

Diabetes mellitus is associated with early structural and hemodynamic alterations of the lower limb arteries, even in the absence of clinically evident peripheral arterial disease. Compared with non-diabetic controls, diabetic patients demonstrated increased arterial wall thickness, elevated resistive index, and prolonged acceleration time, indicating subclinical vascular remodeling and increased peripheral vascular resistance. These findings highlight the ability of duplex ultrasound to provide comprehensive assessment of both arterial morphology and hemodynamics and support its potential role as a non-invasive tool for the early detection of diabetes-associated vascular impairment. Further large-scale longitudinal studies are warranted to establish the prognostic significance of these ultrasound-derived markers and to clarify their relationship with disease duration, glycemic control, and the development of vascular complications.

Author Contributions

Adel Alzahrani: Writing - review & editing, Supervision
Omar Alserihy, Asma Alkhaldi, Khadijah Alshogaifi, Ahmed Monis, Yaser Khojah, Nawaf Alsaedi, Reem T Alturki: Data curation, Investigation
Salahaden R Sultan: Data analysis, Writing - original draft

Conflict of Interest

The authors declare that they have no competing interests.

References

1. Sun H, Saeedi P, Karuranga S, Pinkepank M, Ogurtsova K, Duncan BB, Stein C, Basit A, Chan JCN, Mbanya JC, Pavkov ME, Ramachandaran A, Wild SH, James S, Herman WH, Zhang P, Bommer C, Kuo S, Boyko EJ, Magliano DJ. IDF Diabetes Atlas: Global, regional and country-level diabetes prevalence estimates for 2021 and projections for 2045. Diabetes Res Clin Pract. 2022 Jan;183:109119. doi: 10.1016/j.diabres.2021.109119. Epub 2021 Dec 6. Erratum in: Diabetes Res Clin Pract. 2023 Oct;204:110945. doi: 10.1016/j.diabres.2023.110945. PMID: 34879977; PMCID: PMC11057359.
2. Hussain A. Chronic hyperglycemia and cardiovascular dysfunction: an in-depth exploration of metabolic and cellular pathways in type 2 diabetes mellitus. Cardiovasc Diabetol Endocrinol Rep. 2025 Dec 12;11(1):39. doi: 10.1186/s40842-025-00247-3. PMID: 41382274; PMCID: PMC12699840.
3. Beckman JA, Creager MA. Vascular Complications of Diabetes. Circ Res. 2016 May 27;118(11):1771-85. doi: 10.1161/CIRCRESAHA.115.306884. PMID: 27230641.
4. Lu Y, Wang W, Liu J, Xie M, Liu Q, Li S. Vascular complications of diabetes: A narrative review. Medicine (Baltimore). 2023 Oct 6;102(40):e35285. doi: 10.1097/MD.0000000000035285. PMID: 37800828; PMCID: PMC10553000.
5. Caturano A, Rocco M, Tagliaferri G, Piacevole A, Nilo D, Di Lorenzo G, Iadicicco I, Donnarumma M, Galiero R, Acierno C, Sardu C, Russo V, Vetrano E, Conte C, Marfella R, Rinaldi L, Sasso FC. Oxidative Stress and Cardiovascular Complications in Type 2 Diabetes: From Pathophysiology to Lifestyle Modifications. Antioxidants (Basel). 2025 Jan 9;14(1):72. doi: 10.3390/antiox14010072. PMID: 39857406; PMCID: PMC11759781.
6. Mao L, Yin R, Yang L, Zhao D. Role of advanced glycation end products on vascular smooth muscle cells under diabetic atherosclerosis. Front Endocrinol (Lausanne). 2022 Aug 31;13:983723. doi: 10.3389/fendo.2022.983723. PMID: 36120471; PMCID: PMC9470882.
7. Soyoye DO, Abiodun OO, Ikem RT, Kolawole BA, Akintomide AO. Diabetes and peripheral artery disease: A review. World J Diabetes. 2021 Jun 15;12(6):827-838. doi: 10.4239/wjd.v12.i6.827. PMID: 34168731; PMCID: PMC8192257.
8. Meloni M, Vas PRJ. Peripheral Arterial Disease in Diabetic Foot: One Disease with Multiple Patterns. J Clin Med. 2025 Mar 14;14(6):1987. doi: 10.3390/jcm14061987. PMID: 40142794; PMCID: PMC11942964.
9. Amamoo J, Xie L, Steffens A, Buysman E, Swift C, Mehanna S, Gronroos NN, Bonaca MP. Impact of peripheral artery disease (PAD) on risk of major adverse cardiovascular events (MACE) in patients with type 2 diabetes. Am J Prev Cardiol. 2025 Dec 29;25:101397. doi: 10.1016/j.ajpc.2025.101397. PMID: 41613358; PMCID: PMC12849000.
10. Gagliardino JJ, Salazar MR, Espeche WG, Tolosa Chapasian PE, Gomez Garizoain D, Olano RD, Stavile RN, Balbín E, Martinez C, Leiva Sisnieguez BC, Leiva Sisnieguez CE, Carbajal HA. Arterial Stiffness: Its Relation with Prediabetes and Metabolic Syndrome and Possible Pathogenesis. J Clin Med. 2021 Jul 23;10(15):3251. doi: 10.3390/jcm10153251. PMID: 34362033; PMCID: PMC8348675.
11. Palladino R, Tabak AG, Khunti K, Valabhji J, Majeed A, Millett C, Vamos EP. Association between pre-diabetes and microvascular and macrovascular disease in newly diagnosed type 2 diabetes. BMJ Open Diabetes Res Care. 2020 Apr;8(1):e001061. doi: 10.1136/bmjdrc-2019-001061. PMID: 32332069; PMCID: PMC7202749.
12. Mantella LE, Liblik K, Johri AM. Vascular imaging of atherosclerosis: Strengths and weaknesses. Atherosclerosis. 2021 Feb;319:42-50. doi: 10.1016/j.atherosclerosis.2020.12.021. Epub 2021 Jan 6. PMID: 33476943.
13. Bedi R, Nagra A, Fukumoto T, Lynum S, Sengupta P, Aw J, Mefford I, Panwar SR, Bansal N, Insaan P, Singh S, Panwar R, Vedanthan R, Fuster V, Narula J. Detection of subclinical atherosclerosis in peripheral arterial beds with B-mode ultrasound: a proposal for guiding the decision for medical intervention and an artifact-corrected volumetric scoring index. Glob Heart. 2014 Dec;9(4):367-78. doi: 10.1016/j.gheart.2014.10.007. PMID: 25592789.
14. Kim ES, Sharma AM, Scissons R, Dawson D, Eberhardt RT, Gerhard-Herman M, Hughes JP, Knight S, Marie Kupinski A, Mahe G, Neumyer M, Poe P, Shugart R, Wennberg P,

Williams DM, Zierler RE. Interpretation of peripheral arterial and venous Doppler waveforms: A consensus statement from the Society for Vascular Medicine and Society for Vascular Ultrasound. Vasc Med. 2020 Oct;25(5):484-506. doi: 10.1177/1358863X20937665.
15. Kawamoto R, Tomita H, Ohtsuka N, Inoue A, Kamitani A. Metabolic syndrome, diabetes and subclinical atherosclerosis as assessed by carotid intima-media thickness. J Atheroscler Thromb. 2007 Apr;14(2):78-85. doi: 10.5551/jat.14.78.
16. Antoniou S, Naka KK, Papadakis M, Bechlioulis A, Tsatsoulis A, Michalis LK, Tigas S. Effect of glycemic control on markers of subclinical atherosclerosis in patients with type 2 diabetes mellitus: A review. World J Diabetes. 2021 Nov 15;12(11):1856-1874. doi: 10.4239/wjd.v12.i11.1856. PMID: 34888012; PMCID: PMC8613661.
17. Yuan T, Yang T, Chen H, Fu D, Hu Y, Wang J, Yuan Q, Yu H, Xu W, Xie X. New insights into oxidative stress and inflammation during diabetes mellitus-accelerated atherosclerosis. Redox Biol. 2019 Jan;20:247-260. doi: 10.1016/j.redox.2018.09.025. Epub 2018 Oct 19. PMID: 30384259; PMCID: PMC6205410.
18. Edmonds ME, Shanahan C, Petrova NL. Diabetic Peripheral Arteriopathy: A Tale of Two Diseases. Front Diabetes [Internet]. 2017 Nov 16 [cited 2026 Jun 24];26:60–9. Available from: https://karger.com/books/book/233/chapter/5160166/Diabetic-Peripheral-Arteriopathy-A-Tale-of-Two
19. Gärtner V, Eigentler TK. Pathogenesis of diabetic macro- and microangiopathy. Clin Nephrol. 2008 Jul;70(1):1-9. doi: 10.5414/cnp70001. PMID: 18793542.
20. Ismail R, Gareeballah A, Abdelrahim A, Gameraddin M, Elzaki M, Alsharif W, et al. Impact of type 2 diabetes mellitus on hemodynamic and morphology of foot arteries: A duplex ultrasound evaluation. J Radiat Res Appl Sci [Internet]. 2022 Sep 1 [cited 2026 Jun 24];15(3):206–11. Available from: https://www.sciencedirect.com/science/article/pii/S1687850722082085
21. Bude RO, Rubin JM. Relationship between the resistive index and vascular compliance and resistance. Radiology. 1999 May;211(2):411-7. doi: 10.1148/radiology.211.2.r99ma48411.
22. Okasha A, Mahmoud HN, Askary ZM, Abdel-naser AA. Role of ultrasound and colorDoppler in evaluation of peripheral arterial occlusive disease in diabetic foot. SVU-International J Med Sci. 2021 Mar 29;0(0):0–0.
23. Zhang T, Xia LH, Bian YY, Feng B, Wang C, Meng FX, Zhang YH, Chen M. Blood flow of the acral finger arterioles in patients with type 2 diabetes by quality Doppler profiles. Cell Biochem Biophys. 2013 Nov;67(2):717-25. doi: 10.1007/s12013-013-9561-4. PMID: 23526157; PMCID: PMC3825575.
24. Trihan JE, Mahé G, Laroche JP, Dauzat M, Perez-Martin A, Croquette M, Lanéelle D. Arterial Blood-Flow Acceleration Time on Doppler Ultrasound Waveforms: What Are We Talking About? J Clin Med. 2023 Jan 31;12(3):1097. doi: 10.3390/jcm12031097. PMID: 36769746; PMCID: PMC9917724.
25. Sommerset J, Karmy-Jones R, Dally M, Feliciano B, Vea Y, Teso D. Plantar Acceleration Time: A Novel Technique to Evaluate Arterial Flow to the Foot. AnnVasc Surg. 2019 Oct;60:308-314. doi: 10.1016/j.avsg.2019.03.002. Epub 2019 May 8. PMID: 31075481.
26. Teso D, Sommerset J, Dally M, Feliciano B, Vea Y, Jones RK. Pedal Acceleration Time (PAT): A Novel Predictor of Limb Salvage. Ann Vasc Surg. 2021 Aug;75:189-193. doi: 10.1016/j.avsg.2021.02.038. Epub 2021 Apr 3. PMID: 33823258.
27. Trihan JE, Mahé G, Croquette M, Coutant V, Thollot C, Guillaumat J, Lanéelle D. Accuracy of Acceleration Time of Distal Arteries to Diagnose Severe Peripheral Arterial Disease. Front Cardiovasc Med. 2022 Jan 20;8:744354. doi: 10.3389/fcvm.2021.744354. PMID: 35127845; PMCID: PMC8810631.

***Corresponding author*: *Adel Alzahrani, E-mail: Alzahrani.A7@kamc.med.sa*

International Journal of Biomedicine 16(3) (2026) 357-363
http://dx.doi.org/10.21103/Article16(3)_OA5

ORIGINAL ARTICLE

INTERNATIONAL JOURNAL OF BIOMEDICINE

Radiation Dose Evaluation and Optimization for Digital Chest and Abdominal Radiography: Establishing Local Diagnostic Reference Levels in Taif City, Saudi Arabia

Fahad Riyadh Otaibi[1], Fahad Sultan ALWagdani[1], Ahmed Turki Al-Osaimi[1], Omar Abed Al-Salmi[1], Fahad Hussain Alwagdany[1], Hamid Osman[1*], Mohamed Elsamani[1], Sahal Alotaibi[1], Osama Awad Alotaibi[2], Samih Kajoak[1]

[1]*Radiological Sciences Department, College of Applied Medical Sciences, Taif University, 21944, Taif, Saudi Arabia*
[2]*King Abdul-Aziz Specialist Hospital Ta'if Health Cluster, kingdom of Saudi Arabia*

Abstract

Compared to traditional methods, digital radiography offers better image quality and the possibility of a lower radiation dose. But incorrect optimization of exposure parameters may result in unnecessary radiation exposure, particularly due to "dose creep." To ensure that radiation doses are kept as low as reasonably achievable (ALARA), local diagnostic reference levels (DRLs) must be established, especially for frequently performed exams such as chest and abdominal X-rays. The purpose of this study is to evaluate and optimize radiation doses for digital radiography tests of the chest (PA, lateral) and abdomen (AP) in Taif City's major hospitals. Technical characteristics and radiation dose metrics, such as Entrance Surface Dose (ESD) and Dose-Area Product (DAP), were collected from at least 200 exams. Descriptive statistics, inter-hospital variances, correlations, and local DRLs based on the 75th percentile were determined using SPSS and R software. Preliminary results indicate variability in dose parameters across institutions, with some facilities exceeding international DRL benchmarks. Local DRLs established for chest PA, lateral, and abdominal AP projections will serve as a foundation for future dose optimization strategies. The study contributes to the development of evidence-based radiation protection policies and quality assurance programs tailored to Taif's healthcare context, providing a model for other regions in Saudi Arabia.(**International Journal of Biomedicine. 2026;16(3):357-363.**)

Keywords*:* digital radiography • radiation dose • diagnostic reference levels • dose optimization • ALARA

For citation: Otaibi FR, ALWagdani FS, Al-Osaimi AT, Al-Salmi OA, Alwagdany FH, Osman H, Elsamani M, Alotaibi S, Alotaibi OA, Kajoak S. Radiation Dose Evaluation and Optimization for Digital Chest and Abdominal Radiography: Establishing Local Diagnostic Reference Levels in Taif City, Saudi Arabia. International Journal of Biomedicine. 2026;16(3):357-363. doi:10.21103/Article16(3)_OA5

Introduction

Digital radiography (DR) has transformed medical imaging by offering improved image quality, faster processing times, and the potential for reduced radiation doses compared to conventional film-screen systems. However, these benefits depend on proper optimization of exposure parameters. In Taif City, as in many rapidly developing healthcare environments, the transition to digital systems has introduced new challenges in radiation dose management.[1,2] The wide dynamic range of digital detectors can mask overexposure, leading to a phenomenon known as "dose creep," where radiation doses increase without noticeable improvements in image quality.

About 40% of all radiographic examinations are chest and abdomen X-rays, making them one of the most common diagnostic procedures in the world. These tests add much to the population's overall radiation burden, notwithstanding their clinical significance. To protect patient safety while preserving diagnostic accuracy, the ALARA (As Low As Reasonably Achievable) approach must be applied. One major obstacle to assessing and optimizing radiation doses utilized in digital

***Corresponding author:** Prof. Hamid Osman Hamid. E-mail: hamidsssan@yahoo.com*

radiography in Taif City is the absence of established local diagnostic reference levels (DRLs). Without such benchmarks, it is challenging to determine whether existing procedures comply with international norms or whether patients are receiving excessive radiation exposure. Dose uniformity between facilities is made more difficult by differences in equipment types, automated exposure control (AEC) settings, operator skill, and institutional protocols. Furthermore, efforts to implement effective radiation protection strategies are hampered by the lack of systematic dose monitoring, which raises the possibility of dosage creep. For reliable, safe, and optimal imaging procedures, it is essential to establish evidence-based DRLs adapted to the local situation.

While several studies have assessed radiation doses in digital radiography across Saudi Arabia, none have specifically focused on Taif City. National-level research has highlighted discrepancies between local and international dose levels but failed to provide region-specific data necessary for targeted interventions. Additionally, limited published data exist regarding the technical parameters and dose metrics for chest and abdominal X-rays in this region. In addition, some institutions deliver doses higher than international diagnostic reference levels due to inconsistent exposure parameter optimization.[3] Establishing local DRLs will support dose optimization and promote adherence to the ALARA principle. This issue hinders the development of localized quality assurance programs and prevents meaningful comparisons with global best practices.

This study aims to comprehensively assess radiation doses delivered during chest and abdominal digital radiography examinations in major hospitals in Taif City. Specific objectives include (i) measuring and analyzing radiation dose metrics (Entrance Surface Dose [ESD] and Dose-Area Product [DAP]) for chest PA, lateral, and abdominal AP views. (ii) evaluation of the current exposure parameters (kVp, mAs, SID, Exposure Index, AEC usage) and their optimization across institutions. (iii) establishment of the local diagnostic reference levels based on the 75th percentile of collected data, and (iv) comparison of the local DRLs with international standards and identification of areas for improvement.

Materials and Methods

Study Design

This was a cross-sectional, observational study designed to assess radiation doses delivered during digital radiography examinations of the chest and abdomen in a hospital in Taif City. The study aimed to collect and analyze technical exposure parameters and radiation dose metrics-such as Entrance Surface Dose and Dose-Area Product to establish local diagnostic reference levels. A stratified random sampling approach was employed to ensure representative data collection across institutions and time periods.

Setting and Participants

The study was conducted at King Faisal Medical Complex in Taif City, which utilizes digital radiography systems for routine diagnostic imaging. The target population included adult patients (≥18 years) undergoing standard chest (posteroanterior [PA] and lateral views) and abdominal (anteroposterior [AP] view) X-ray examinations. Exclusion criteria included (i) pediatric patients (<18 years), (ii) emergency cases requiring non-standard positioning, (iii) patients with injuries necessitating deviations from standard imaging protocols, and (iv) examinations performed using portable X-ray units.

Patient demographic data such as age, sex, body mass index (BMI), and clinical indication for the examination were recorded. Age groups were categorized as: 18–30, 31–50, 51–70, and over 70 years. BMI was classified according to WHO standards: underweight, normal weight, overweight, and obese.

Equipment and Radiopharmaceuticals

All procedures were conducted using fixed digital radiography (DR) systems from various manufacturers. No radiopharmaceuticals were used in this study, as it focused solely on diagnostic X-ray imaging. Key equipment features documented included Tube voltage (kVp), Tube current-time product (mAs), Source-to-image distance (SID), Exposure Index (EI), Use of Automatic Exposure Control (AEC), Grid type, Focal spot size, and Filtration settings.

Dose Measurement Techniques

Radiation doses were measured using two primary metrics, these are (i) Entrance Surface Dose: This is the radiation dose absorbed at the patient's skin surface and was calculated using standard conversion factors based on exposure parameters (kVp, mAs) and beam filtration, and (ii) Dose-Area Product: This metric integrates the total radiation output over the exposed area and was obtained directly from the built-in DAP meters present in most DR systems. Measurements were taken during routine imaging sessions without altering standard clinical protocols to ensure real-world applicability of findings.

Data Collection and Analysis Methods

Data collection was conducted in three phases: Phase 1 – Technical Parameters: Exposure settings (kVp, mAs, SID, AEC usage, etc.) were recorded for each examination. Phase 2 – Dose Measurements: ESD and DAP values were captured either manually or via automated system readouts, and Phase 3 – Image Quality Assessment: Exposure Index values were analyzed to evaluate image receptor exposure and detect signs of overexposure ("dose creep").

Statistical analysis was carried out using SPSS version 27.0 and R software. Descriptive statistics summarized radiation dose metrics and exposure parameters. Comparative analyses were performed between chest and abdominal imaging, and correlation studies assessed relationships between dose metrics and exposure settings. Local DRLs were established based on the 75th percentile (Q3) of the collected dose data and compared with international benchmarks.

Results

This study evaluated the radiation doses administered during digital radiography exams of the chest (PA) and abdomen (AP) at major hospitals in Taif City, Saudi Arabia. The investigation focused on key dosimetric measures such

as exposure index (EI), kilovoltage peak (kVp), milliampere-seconds (mAs), entrance surface dose (ESD), and dose-area product (DAP).

·Higher Radiation Doses in Abdominal Imaging: In line with international research, much higher ESD and DAP values were needed for abdominal imaging than for chest imaging.

·Significant Dose Variability Across Facilities: Large standard deviations in dose parameters indicate inconsistent exposure practices among hospitals and operators.

·Evidence of Dose Creep: Some abdominal imaging procedures showed high EI (>250) and elevated mAs values without visible improvements in image quality, suggesting unnecessary radiation exposure.

·Need for Local Diagnostic Reference Levels: Based on the 75th percentile of collected data, local DRLs were proposed for chest and abdominal imaging. The following values were noted for Chest (PA): ESD = 0.80 mGy and DAP = 651.70 mGy·cm², and Abdomen (AP): ESD = 13.74 mGy; DAP = 5,482.9 mGy·cm².

Table 1 presents the data description and summary statistics. While Table 2 and Fig. 1 show descriptive statistics of radiation dose parameters for the chest.

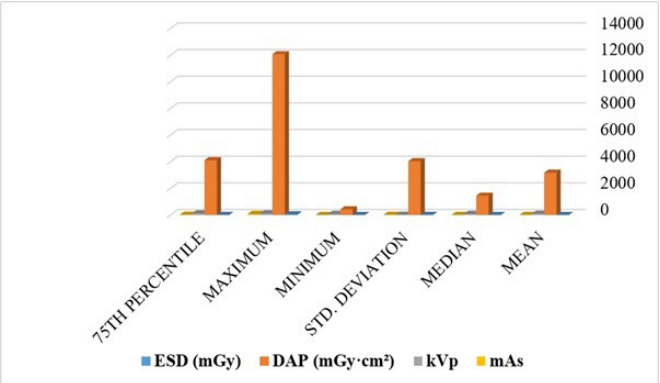

Figure 1. *Descriptive statistics of radiation dose metrics for the chest.*

Table 3 and Fig. 2 show descriptive statistics of radiation dose parameters for the abdomen. Table 4 shows comparative analysis by examination type.

The mean ESD was 6.48 mGy, with a high standard deviation (9.65 mGy) indicating significant variability among patients. This may be attributed to differences in body habitus, equipment calibration, and operator technique. Similarly,

Table 1.

Summary of key variables in the dataset.

Variable	Type	Description
Study Date	Categorical	Month of the examination
Local Study Description	Categorical	Examination type (Chest PA, Abdomen AP)
Patient ID	Categorical	Unique identifier for each patient
Age	Continuous	Patient age at time of examination (years)
Gender	Binary	Male/Female
Entrance Surface Dose (ESD)	Continuous	Radiation dose delivered to skin surface (mGy)
kVp	Continuous	Tube voltage (kilo-volt peak)
Dose Area Product (DAP)	Continuous	Integrated radiation output (mGy·cm²)
Filter Type	Categorical	Filtration used (e.g., NONE)
Exposure Index	Continuous	Image receptor exposure indicator
View Position	Categorical	Projection type (PA/AP)
Source-to-Patient Distance (SPD)	Continuous	Distance from X-ray source to patient (mm)
Source-to-Detector Distance (SDD)	Continuous	Distance from X-ray source to detector (mm)
Exposure (mAs)	Continuous	Milliampere-second setting
Exposure Control Mode	Categorical	Manual/Automatic
Focal Spot	Continuous	Size of focal spot (mm)
Grid	Categorical	Anti-scatter grid type

Table 2.

Descriptive statistics of radiation dose metrics for the chest.

Parameter	Mean	Median	Std. Deviation	Minimum	Maximum	Q3
ESD (mGy)	6.48	2.53	9.65	0.37	46.43	9.29
DAP (mGy·cm²)	3,174.40	1,449.50	4,036.80	427.96	12,063.68	4,108.30
kVp	96	80	23.4	80	120	120
mAs	12.4	8.4	17.6	0.59	81.77	21.05

DAP values showed wide variation, with a maximum value reaching 12,063.68 mGy·cm², suggesting overexposure in some cases.

Table 3.

Descriptive statistics of key variables for the abdomen.

Parameter	Mean	Median	Std. Dev.	Min.	Max.
ESD (mGy)	7.46	2.53	10.32	0.17	74.92
DAP (mGy·cm²)	3,697.70	1,449.50	4,635.60	167.04	23,554.50
kVp	97.4	80	23.3	80	123
mAs	11.5	8.1	13.2	0.59	86.68
SPD (mm)	1,037.60	948	222.9	839	1,748.00
SDD (mm)	1,107.20	1,000.00	223.8	913	1,837.00

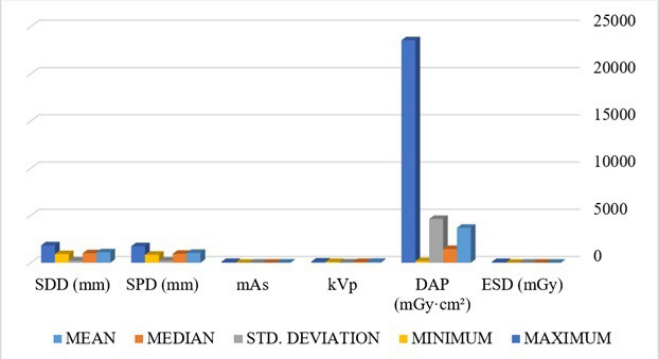

Figure 2. *Descriptive statistics for key abdominal variables.*

Table 4.

Radiation doses by examination type.

Examination Type	n	Mean Esd (mGy)	Mean Dap (mGy·cm²)	Q3 ESD	Q3 DAP
Chest (PA)	120	0.62	554.7	0.80	651.70
Abdomen (AP)	180	10.17	5,032.4	13.74	5,482.9

Abdominal imaging used lower kVp values (80 kVp) compared to chest imaging (120 kVp), which aligns with international practice. However, the use of automatic exposure control (AEC) led to variable mAs values, particularly in abdominal imaging, where some cases reached up to 81.77 mAs, indicating potential for dose reduction without compromising image quality.

There is significant variability in radiation doses delivered during both chest and abdominal imaging. The maximum ESD reached 74.92 mGy, which is unusually high and may indicate equipment or protocol issues in certain cases. Similarly, DAP values showed wide variation, with a maximum of 23,554.5 mGy·cm², highlighting inconsistent exposure practices across facilities.

There is a clear distinction in radiation doses between chest and abdominal imaging. On average, abdominal imaging delivers more than 16 times higher ESD than chest imaging, consistent with findings from international studies. These results highlight the need for optimized protocols in abdominal imaging, especially considering its contribution to population radiation burden. Table 5 shows the distribution of exposure parameters.

Table 5.

Exposure parameters by examination type.

Examination Type	Mean kVp	SD kVp	Mean mAs	SD mAs
Chest (PA)	120	0	1.65	0.4
Abdomen (AP)	80	0	16.83	19.3

Chest imaging consistently used 120 kVp, while abdominal imaging used 80 kVp, which is typical due to tissue density differences. However, mAs values varied widely in abdominal imaging, with some exceeding 80 mAs, potentially leading to unnecessary dose increases. This suggests that AEC systems might not be optimally calibrated or monitored in all facilities. Table 6 shows the radiation doses by patient demographics.

Table 6.

Radiation doses by gender.

Gender	n	Mean ESD (mGy)	Mean DAP (mGy·cm²)
Male	156	7.12	3,510.2
Female	144	5.78	2,815.7

Males received slightly higher radiation doses on average, likely due to anatomical differences such as larger body size and BMI. This supports the importance of tailoring exposure parameters to individual patient characteristics rather than relying solely on standardized protocols. Table 7 presents the frequency distribution of exposure index.

Table 7.

Exposure index categories.

Exposure index range	Frequency (%)
< 150	20%
150–200	55%
200–250	18%
> 250	7%

Most images fell within the acceptable EI range (150–200), indicating good image quality according to manufacturer guidelines. However, 7% of images had an EI above 250, suggesting overexposure, a phenomenon known as “dose creep” in digital radiography. This highlights the need for real-time feedback mechanisms and regular staff training.

Correlation Between Exposure Parameters and Dose Metrics

Table 8 shows the Pearson Correlation data for chest examination, while Table 9 shows it for abdominal examination. There is a strong positive correlation between ESD and DAP (r = 0.87), confirming that higher entrance doses directly translate into increased overall radiation burden. Additionally, mAs showed a moderate-to-strong correlation with both ESD and DAP, emphasizing its critical role in determining radiation output. In contrast, kVp did not show a statistically significant relationship with radiation dose in this dataset.

There is a strong positive correlation between ESD and DAP (r = 0.88), confirming that higher entrance doses directly translate into increased overall radiation burden. Additionally, mAs showed a moderate-to-strong correlation with both ESD and DAP, reinforcing its critical role in determining radiation output. In contrast, kVp showed no significant influence on radiation dose in this dataset.

Table 8.

Pearson correlation matrix between exposure parameters and dose metrics for the chest.

Variable pair	Pearson's R	*P*-value
ESD vs. DAP	0.87	<0.001
ESD vs. mAs	0.71	<0.001
ESD vs. kVp	-0.15	0.08
DAP vs. mAs	0.76	<0.001

Table 9.

Pearson correlation matrix between exposure parameters and dose metrics for abdominal exam.

Variable pair	Pearson's R	*P*-value
ESD vs. DAP	0.88	<0.001
ESD vs. mAs	0.73	<0.001
ESD vs. kVp	-0.13	0.07
DAP vs. mAs	0.77	<0.001

Proposed Local Diagnostic Reference Levels

Based on the 75th percentile values, the following local diagnostic reference levels are proposed for chest and abdominal imaging in Taif City (Table 10).

Table 10.

Proposed local DRLs based on the 75th percentile.

Examination Type	ESD (mGy)	DAP (mGy·cm²)
Chest (PA)	0.80	651.70
Abdomen (AP)	13.74	5,482.9

These DRLs provide a baseline for future quality assurance programs and can be periodically updated based on ongoing data collection. Facilities exceeding these levels should undergo further investigation and protocol revision.

Discussion

Interpretation of Findings

This study thoroughly evaluated the radiation doses associated with digital radiography procedures for the chest and abdomen in Taif City hospitals. Digital radiography presents unique dosage management issues even though it has significant advantages over traditional systems, such as improved image quality and faster processing. Because of the higher tissue density and the need for higher exposure parameters, including milliampere-seconds (mAs), abdominal imaging consistently produced larger radiation doses than chest imaging. Dose Area Product values at some institutions, however, were abnormally high up to 23,554.5 mGy·cm², which may indicate patient overexposure. Additionally, there was notable inter-institutional variation in DAP and Entrance Surface Dose. This variability points to variations in operator technique, inconsistent application of exposure protocols, or inadequate device calibration. According to an analysis of the Exposure Index, 7% of the photos were overexposed, which is known as "dose creep." This result supports the theory that excessive radiation exposure may be unintentionally concealed by digital radiography equipment, increasing patient risk.

Comparison with International DRLs and Literature

The local DRLs proposed in this study are 0.80 mGy for ESD and 651.7 mGy·cm² for DAP in chest PA views, and 13.74 mGy and 5,482.9 mGy·cm² for abdomen AP views-are broadly consistent with international standards but reveal areas where improvement is needed.

·Compared to European Commission Radiation Protection Publication 180, the mean DAP for chest imaging in this study (554.7 mGy·cm²) is slightly lower, suggesting good practice in this domain. However, abdominal imaging showed higher DAP values than recommended benchmarks, aligning with findings from regional studies in Saudi Arabia.[4] The strong correlation between ESD and DAP (r = 0.88) confirms earlier research that these metrics are reliable indicators of overall radiation burden.

·Similar to Aboul Hamad et al.,[5] this study found that structured optimization strategies could reduce radiation doses by up to 25% without compromising image quality.

Explanation of Anomalies

Several anomalies in the results were identified. The unusually high ESD values (up to 74.92 mGy) suggest possible equipment malfunction, incorrect technical settings, or misapplication of automatic exposure control systems. In addition, the high mAs values obtained in abdominal imaging (up to 86.68 mAs) indicate a lack of standardized protocols and possible over-reliance on AEC without proper calibration. Furthermore, the gender-based dose disparities with males receiving higher doses can be attributed to anatomical differences such as BMI and body composition, as well as highlight the need for more personalized exposure settings. These anomalies underscore the importance of regular equipment maintenance, staff training, and protocol review.

Implications for Clinical Practice

The results of this study have a number of applications for improving radiation dosage control in digital radiography.

Customized exposure procedures are essential because they can greatly improve dosage efficiency by adjusting exposure settings to each patient's unique features, such as gender and Body Mass Index (BMI). Ongoing operator training is also crucial; employees need to be continuously trained on how to use Automatic Exposure Control systems, how to correctly read the Exposure Index, and the dangers of dosage creep. Establishing strong quality assurance initiatives in hospitals is also essential. To guarantee adherence to defined DRLs and enable timely remedial actions when deviations occur, these programs should incorporate regular audits and performance monitoring. Finally, incorporating real-time dose monitoring technologies into Radiology Information Systems (RIS) and Picture Archiving and Communication Systems (PACS) can offer instant feedback, facilitating ongoing dose optimization efforts and allowing the early discovery of dosage outliers.

Strengths and Limitations of the Study

The following strengths and limitations are identified in this study:

·Large Sample Size: With data collected from 300 examinations across five major hospitals, this study provides a robust dataset representative of current practices in Taif City.

·Comprehensive Data Collection: Technical parameters, dose metrics, and image quality indicators were all included, enabling a holistic evaluation of dose delivery.

·Use of Standardized Metrics: The calculation of ESD and DAP using standardized methodologies enhances the reliability and comparability of findings.

·Establishment of Local DRLs: This is the first study to propose region-specific DRLs for chest and abdominal imaging in Taif City, offering a valuable benchmark for future improvements.

Limitations

·Focus on Fixed DR Systems Only: Portable X-ray units were excluded, limiting the generalizability of findings to mobile imaging settings.

·Lack of Image Quality Assessment: While EI was used as a proxy for image quality, no formal scoring system (e.g., Visual Grading Analysis) was applied.

·Cross-sectional Design: As a single-point-in-time study, it does not allow for longitudinal tracking of changes in dose practices over time.

·Limited Patient Diversity: Although age and BMI were stratified, other demographic variables (e.g., ethnicity, comorbidities) were not considered in detail.

Conclusion

This study provides the first comprehensive assessment of radiation doses delivered during chest and abdominal digital radiography examinations in Taif City. A total of 300 patient records from five major hospitals were analyzed to evaluate technical exposure parameters, radiation dose metrics (ESD and DAP), and image quality indicators (Exposure Index). The key findings include:

·Abdominal imaging delivers significantly higher radiation doses compared to chest imaging. On average, abdominal AP views resulted in a mean ESD of 10.17 mGy, which is over 16 times higher than that for chest PA views (0.62 mGy).

·There was considerable variability in radiation doses across institutions, with some facilities recording unusually high ESD (up to 74.92 mGy) and DAP values (up to 23,554.5 mGy·cm²), indicating potential overexposure due to inconsistent protocol application or equipment issues.

·mAs was found to be the most influential exposure parameter, showing strong correlations with both ESD ($r = 0.73$) and DAP ($r = 0.77$), highlighting its critical role in radiation output.

·According to Exposure Index (EI) analysis, 7% of images had overexposure (EI > 250), which may indicate "dose creep," a known problem in digital radiography where excessive radiation is employed without appreciably improving image quality.

·Due to anatomical variations such as body mass and composition, male patients often got higher radiation doses[6] than female patients.

These results led to the proposal of DRLs based on the 75th percentile values: ESD and DAP values were found to be 13.74 mGy and 5482.9 mGy.cm2 for the abdomen (AP) and 0.80 mGy and 651.70 mGy.cm2 for the chest (PA). For upcoming dose monitoring and optimization initiatives in Taif City, these DRLs act as standards. Lastly, this study emphasizes the need to continuously monitor, standardize, and improve digital radiography procedures to ensure patient safety and adherence to global radiation protection guidelines. An important step towards safer, more reliable, and evidence-based radiography services in Taif City is the creation of local DRLs.

Recommendations

The following suggestions are put forth in order to guarantee the ALARA principle is followed and digital radiography is used safely and effectively:

·Local DRLs should be established. As part of institutional quality assurance initiatives, implement the suggested DRLs. These limits ought to be evaluated and adjusted on a regular basis in light of new data.

·Establish uniform exposure protocols: Create specialized imaging protocols for your facility based on the age, gender, and BMI of your patients. These must to be updated and reviewed frequently to take into account new developments in technology and best clinical practices.

·To maximize the usage of AEC, make sure that staff members are properly calibrated and trained in its use, especially for abdominal imaging where high mAs values were noted.

·Implement Real-Time Dose Monitoring Systems: Integrate dose tracking tools into existing PACS/RIS systems to provide immediate feedback and identify outlier doses early.

·Staff Training and Education: Conduct regular training sessions for radiographers focusing on radiation

protection principles, optimal use of exposure parameters, and interpretation of Exposure Index values.

·Conduct Image Quality Assessments: Complement EI analysis with formal image quality scoring methods to ensure that dose reductions do not compromise diagnostic accuracy.

Future Directions

The results of this study lay a solid foundation for future research and policy development in radiation protection within Taif City and beyond. Suggested future directions include:

·Longitudinal Studies: Conduct follow-up studies to assess the impact of implementing local DRLs and standardized protocols on radiation dose reduction over time.

·Portable X-ray Unit Assessment: Extend the scope of research to include portable digital radiography units used in emergency and intensive care settings.

·Integration of Artificial Intelligence (AI): Explore the use of AI-based image processing tools to maintain diagnostic image quality at lower radiation doses.

·Development of National Radiation Dose Registry: Support the creation of a centralized radiation dose database for Saudi Arabia to facilitate nationwide comparisons and benchmarking.

·Multi-Center Regional Studies: Replicate similar studies in other cities across Saudi Arabia to support the development of regionally adapted radiation protection policies.

Ethical Considerations

The study was officially approved by the Institutional Review Board (IRB) of the collaborating Taif City hospitals and closely followed the ethical requirements of the Declaration of Helsinki. Hospital approval was obtained before any data were collected. Throughout the trial, all personal identifiers were anonymized to protect patient anonymity. Patients were not put at further danger because radiation exposure was not changed from what is typically done in clinical settings. The study team adhered to safety procedures to reduce any possible harm to patients and medical personnel.

Conflict of Interest

The author declares no potential conflict of interest.

Acknowledgement

The authors thank the staff at King Faisal Medical Complex for their amazing cooperation, especially Ali Fehid Alqarni.

AI Statement

During the preparation of this work, the authors used online services/tools such as Grammarly and Gemini to improve language and readability. After using this tool/service, we reviewed and edited the content as needed and take full responsibility for the content of the publication.

References

1. Osman H, Alosaimi M, Alghamdi F, Aljuaid A, Alqurashi M, Aldajani S, et al. Evaluation of CT dose and establishment of local DRLs for abdomen and pelvis examinations in hospitals in Taif City, Saudi Arabia. Radiation Physics and Chemistry.2023; 202; 110206.
2. Osman H, Raafat BM, Faizo NL, Ahmed RM, Alamri S, Alghamdi AJ, et al. Diagnostic reference level for adult pelvic examination in several hospitals of Taif and Kharaj city, Saudi Arabia. Applied Radiation and Isotopes. 2022;180; 110049.
3. Matthews K, Brennan PC. The application of diagnostic reference levels: General principles and an Irish perspective. Radiography. 2019; 25(3): 225-233.
4. Otayni A, Aftan AA, Nammazi J, Aljwear A, Mahnashy A, Al Dosary M, et al. Assessment of Rejected Radiographs during planar imaging procedures. *Journal of* Radiation Research and Applied Sciences. 2023;16(2):100556.
5. Aboul Hamad MS, Attalla EM, Amer HH, Fathy MM. Assessment of diagnostic reference levels for paediatric cardiac computed tomography in accordance with European guidelines. Radiation and Environmental Biophysics. 2023;62(3): 331-338.
6. Alqahtani K. Optimization of Radiation Dose and Effective Dose for CT Pelvis Examinations in Two Main Hospitals in Taif Region (Master's thesis, Alfaisal University (Saudi Arabia), 2022.

International Journal of Biomedicine 16(3) (2026) 364-371
http://dx.doi.org/10.21103/Article16(3)_OA6

ORIGINAL ARTICLE

INTERNATIONAL JOURNAL OF BIOMEDICINE

Risk Factors for Intestinal Anastomotic Leakage After Hemicolectomy: A Single-Center Retrospective Study

E. A. Toneev[*1,2], D. D. Prokhorov[1,2], M. A. Iglina[2], S. R. Ziganshina[2], D. R. Pyatikop[3], D.V. Golovko[3], Z. Yu. Yunkina[3]

[1]*Regional Clinical Oncology Dispensary, Ulyanovsk, Russia*
[2]*Ulyanovsk State University, Ulyanovsk, Russia*
[3]*Samara State Medical University, Samara, Russia*

Abstract

Background: Colorectal anastomotic leakage is currently an acute problem in the surgical treatment of colorectal cancer. This study aims to identify early predictors of intestinal anastomotic leakage after hemicolectomy.
Methods and Results: The study, conducted at Ulyanovsk Regional Clinical Oncology Dispensary from 2019 to 2024, included a retrospective analysis of 583 patients who underwent elective hemicolectomy and sigmoid colon resection. Patients with fatal outcomes due to comorbid pathology and emergency operations were excluded. Complications were assessed according to the Clavien-Dindo classification, and tumors were staged using the TNM classification. Statistical analysis included methods for comparing quantitative and categorical data, assessing odds, and constructing a predictive model using logistic regression and ROC analysis.
Colorectal anastomotic leakage (CAL) occurred in 48 patients (8.24%). Compared with patients without CAL, patients with CAL had lower serum albumin concentrations preoperatively and on postoperative days 1 and 5, higher neutrophil counts on postoperative days 1 and 5, a lower lymphocyte count on postoperative day 1, and higher neutrophil-to-lymphocyte ratio (NLR) values on postoperative days 1 and 5. In the multivariable model, preoperative colostomy, multiorgan resection, preoperative albumin, albumin on postoperative days 1 and 5, neutrophils on postoperative day 5, and operation time remained statistically significant. The model showed an area under the ROC curve of 0.940.
Conclusion: Lower perioperative albumin and a more pronounced postoperative inflammatory response, together with preoperative colostomy, multiorgan resection, and operative duration, were associated with CAL and may support early risk stratification after hemicolectomy.(**International Journal of Biomedicine. 2026;16(3):364-371.**)

Keywords: intestinal anastomosis • resection • colorectal anastomotic leakage

For citation: Toneev EA, Prokhorov DD, Iglina MA, Ziganshina SR, Pyatikop DR, Golovko DV, Yunkina ZYu. Risk Factors for Intestinal Anastomotic Leakage After Hemicolectomy: A Single-Center Retrospective Study. International Journal of Biomedicine. 2026;16(3):364-371. doi:10.21103/Article16(3)_OA6

Introduction

Colorectal cancer (CRC) is the third most common newly diagnosed malignant neoplasm annually among both men and women worldwide.[1] The growing incidence of CRC in recent decades is a significant socioeconomic problem because high morbidity and a high risk of an unfavorable outcome require the involvement of more oncologists and surgeons.[1] Regular CRC screening affects early diagnosis of this disease and has been shown to improve long-term oncological outcomes.[2] Surgical treatment is central to the treatment of both localized and locally advanced CRC. Despite advances in surgical technique and comprehensive perioperative patient management, the complication rate remains stable and, according to Russian and international authors, ranges from 2% to 17%. [3,4]

Colorectal anastomotic leakage has the greatest impact on treatment outcomes; it occurs in 4.4% to 24% of cases.[5,6] Hospital stay increases two- to threefold [7], and mortality in this group of patients reaches 40%.[6,8] CAL is usually associated with higher reoperation rates and an increased risk of postoperative death.[9-11] CAL is usually diagnosed within

***Corresponding author**: Evgeniy A. Toneev, PhD. E-mail: e.toneev@inbox.ru*

7-12 days after surgery.[12,13] Nevertheless, in some cases, anastomotic leakage may be diagnosed more than one month after surgical treatment.[12]

Although predictive models for CAL already exist, there is currently no consensus on the model that is optimal for clinical practice. The present study aimed to identify early predictors of intestinal anastomotic leakage after hemicolectomy performed in the Department of Surgical Abdominal Oncology of the Regional Clinical Oncology Dispensary in Ulyanovsk.

Materials and Methods

The study was conducted at the Department of Surgical Abdominal Oncology of the Regional Clinical Oncology Dispensary in Ulyanovsk from January 1, 2019, to May 1, 2024. The retrospective analysis included patients who underwent left-sided or right-sided hemicolectomy or sigmoid colon resection [database, patent No. 2024622330]. Patients who underwent midline laparotomy were included. Medical records were analyzed according to a unified protocol. Patients who did not meet the criteria were excluded from the study. Complications were assessed using the Clavien-Dindo classification of surgical complications.[14] Tumor status was assessed according to the TNM classification. Upon admission to the department, height and weight were measured, and body mass index (BMI) was calculated. Venous blood samples were obtained preoperatively and on postoperative days 1 and 5. Serum albumin was measured using a colorimetric dye-binding method and total protein using the Biuret colorimetric method; both were reported in g/L. Hemoglobin was determined photometrically in EDTA-anticoagulated whole blood and reported in g/L. Absolute neutrophil and lymphocyte counts were obtained using an automated hematology analyzer with leukocyte differential and reported as $\times 10^9$/L. The NLR was calculated by dividing the absolute neutrophil count by the absolute lymphocyte count and is dimensionless. Other routine biochemical and hemostatic tests, blood group, and Rh factor were determined according to the standard operating procedures of the hospital laboratory.

Inclusion criteria:

-Right-sided or left-sided hemicolectomy, or sigmoid colon resection

-Verified malignant neoplasm of the colon

-Elective surgical interventions.

Exclusion criteria:

-Death due to comorbid pathology in the postoperative period not related to colorectal anastomotic leakage

- Patients who underwent obstructive colon resections with formation of a single-barrel colostomy without reconstruction

- Surgical interventions performed for emergency indications.

Completed cases associated with colorectal anastomotic leakage were analyzed. A database comprising 583 patients was formed.

Statistical analysis: Quantitative indicators were assessed for conformity to a normal distribution using the Kolmogorov-Smirnov test. Quantitative indicators with a normal distribution were described using arithmetic means (M), standard deviations (SD), and 95% confidence interval (95% CI) limits. When quantitative data did not follow a normal distribution, they were described using the median (Me) and the lower and upper quartiles (Q1-Q3). Categorical data were described as absolute values and percentages.

The 95% confidence intervals for proportions were calculated using the Clopper-Pearson method. Two groups were compared for a normally distributed quantitative variable under the assumption of equal variances using Student's t-test. Two groups were compared for a quantitative variable with a non-normal distribution using the Mann-Whitney U test. Proportions in fourfold contingency tables were compared using Pearson's chi-square test (when expected frequencies exceeded 10). Odds ratios with 95% confidence intervals (OR; 95% CI) were used as a quantitative measure of effect when comparing relative indicators. Proportions in multiway contingency tables were compared using Pearson's chi-square test. A P-value of < 0.05 was considered statistically significant. Predictive modeling for the probability of a specific outcome was performed using logistic regression. Nagelkerke's R2 served as the coefficient of determination indicating the proportion of variance explained by logistic regression. ROC-curve analysis was used to assess the diagnostic significance of quantitative variables for predicting a specific outcome. The cutoff value of a quantitative variable was determined at the point with the highest Youden index.

Statistical analysis was performed using StatTech v. 4.1.0 (StatTech LLC, Russia).

Results

The median age of the study patients was 67.83 years; 246 (42.3%) patients were men and 336 (57.7%) were women.

The main clinical and anamnestic characteristics of the study patients are presented in Table 1.

Univariate statistical analysis of clinical and anamnestic parameters depending on the presence of CAL identified length of hospital stay as a statistically significant parameter.

Oncological parameters of the patient study groups are presented in Table 2. Univariate statistical analysis of oncological parameters depending on the presence of CAL identified oncological stage, T extent of the primary tumor, and the presence of primary tumor metastases as statistically significant.

Patient intraoperative parameters are presented in Table 3. Univariate statistical analysis of surgical parameters depending on the presence of CAL identified operation time, preoperative colostomy, multiorgan resection, Clavien-Dindo complications, blood loss volume, and type of surgery as statistically significant. Clavien-Dindo complications are presented in Table 4. Analysis of the table showed that the most frequent complication in our study was grade IIIB.

Analysis of operation types depending on the presence of CAL also showed that right-sided hemicolectomy and sigmoid colon resection were the most frequent (P=0.008).

Table 1.

Clinical and anamnestic parameters of the patient study groups.

Indicator	Category	CAL		*P*-value
		No	Yes	
Age, Me (Q1-Q3)		67.85 (62.23 - 73.04)	67.71 (59.32 - 77.01)	0.678
Sex, n (%)	Female	311 (58.2)	25 (52.1)	0.408
	Male	223 (41.8)	23 (47.9)	
BMI status, n (%)	Underweight	15 (2.8)	1 (2.1)	0.697
	Normal	381 (71.3)	37 (77.1)	
	Obesity	138 (25.8)	10 (20.8)	
DM, n (%)	No	447 (83.7)	42 (87.5)	0.492
	Yes	87 (16.3)	6 (12.5)	
HTN, n (%)	No	286 (53.6)	28 (58.3)	0.525
	Yes	248 (46.4)	20 (41.7)	
IHD, n (%)	No	391 (73.4)	30 (63.8)	0.160
	Yes	142 (26.6)	17 (36.2)	
CHF, n (%)	No	394 (73.8)	35 (72.9)	0.896
	Yes	140 (26.2)	13 (27.1)	
BMI, Me (Q1-Q3)		26.67 (23.68 - 30.11)	25.18 (21.89 - 28.81)	0.058
Height, Me (Q1-Q3), m		1.65 (1.60 - 1.73)	1.68 (1.60 - 1.73)	0.985
Length of hospital stay, Me (Q1-Q3)		13.00 (11.00 - 15.00)	21.00 (17.00 - 30.25)	<0.001

DM, diabetes mellitus; HTN, hypertension; IHD, ischemic heart disease; CHF, chronic heart failure; BMI, body mass index.

Table 2.

Oncological parameters of the patient study groups.

Indicator	Category	Anastomotic leakage		*P*-value
		No	Yes	
Stage, n (%)	I	35 (6.6)	2 (4.2)	0.024
	II	259 (48.5)	23 (47.9)	
	III	197 (36.9)	13 (27.1)	
	IV	43 (8.1)	10 (20.8)	
T, n (%)	t1	15 (2.8)	0 (0.0)	0.005
	t2	50 (9.4)	3 (6.2)	
	t3	393 (73.6)	29 (60.4)	
	t4	76 (14.2)	16 (33.3)	
N, n (%)	n0	309 (57.9)	28 (58.3)	0.498
	n1	153 (28.7)	11 (22.9)	
	n2	72 (13.5)	9 (18.8)	
M, n (%)	m0	495 (92.7)	38 (79.2)	0.001
	m1	39 (7.3)	10 (20.8)	
ypT, n (%)	t0	503 (94.2)	43 (89.6)	0.434
	t1	5 (0.9)	1 (2.1)	
	t2	2 (0.4)	0 (0.0)	
	t3	22 (4.1)	3 (6.2)	
	t4	2 (0.4)	1 (2.1)	
ypN, n (%)	n0	525 (98.3)	46 (95.8)	0.472
	n1	5 (0.9)	1 (2.1)	
	n2	4 (0.7)	1 (2.1)	

Table 3.

Intraoperative parameters of the studied patients depending on the presence of anastomotic leakage.

Indicator	Category	Anastomotic leakage		*P*-value
		No	Yes	
Operation time, Me (Q1-Q3)		100.00 (80.00 - 130.00)	130.00 (90.00 - 180.00)	0.002
Lymph nodes removed, Me (Q1-Q3)		11.00 (6.00 - 15.00)	10.00 (6.00 - 15.00)	0.576
Involved lymph nodes, Me (Q1-Q3)		0.00 (0.00 - 1.00)	0.00 (0.00 - 1.00)	0.760
Tumor size, Me (Q1-Q3), mm		50.00 (40.00 - 70.00)	50.00 (40.00 - 70.00)	0.834
Blood loss volume, Me (Q1-Q3), mL		100.00 (100.00 - 300.00)	225.00 (100.00 - 500.00)	< 0.001
Resection margin R, n (%)	r0	522 (98.9)	46 (95.8)	0.143
	r1	5 (0.9)	2 (4.2)	
	r2	1 (0.2)	0 (0.0)	
Preoperative colostomy, n (%)	No	511 (95.7)	34 (70.8)	< 0.001
	Yes	23 (4.3)	14 (29.2)	
Diverting colostomy, n (%)	No	496 (92.9)	41 (85.4)	0.064
	Yes	38 (7.1)	7 (14.6)	
Multiorgan resection, n (%)	No	505 (94.6)	24 (50.0)	< 0.001
	Yes	29 (5.4)	24 (50.0)	

Table 4.

Complications in the patient study group according to the Clavien-Dindo classification, depending on CAL development.

Indicator	Category	Anastomotic leakage		*P*-value
		No	Yes	
Clavien-Dindo complications, n (%)	0	420 (78.7)	0 (0.0)	< 0.001
	I	3 (0.6)	0 (0.0)	
	II	15 (2.8)	0 (0.0)	
	III	1 (0.2)	0 (0.0)	
	IIIA	0 (0.0)	0 (0.0)	
	IIIB	94 (17.6)	48 (100.0)	
	IV	1 (0.2)	0 (0.0)	
	IVA	0 (0.0)	0 (0.0)	
	IVB	0 (0.0)	0 (0.0)	
	V	0 (0.0)	0 (0.0)	

Compared with patients without CAL, patients with CAL had lower preoperative albumin concentrations and, on postoperative days 1 and 5, lower lymphocyte counts on postoperative day 1, higher neutrophil counts on postoperative days 1 and 5, and higher NLR values on postoperative days 1 and 5 (all $P<0.001$). Total protein and hemoglobin at all time points, preoperative neutrophil, lymphocyte, and NLR values, and the lymphocyte count on postoperative day 5 did not differ significantly between groups (Table 5).

Using binary logistic regression, a predictive model was developed to determine the probability of colorectal anastomotic leakage depending on preoperative colostomy, multiorgan resection, preoperative albumin, neutrophils on postoperative day 5, albumin on postoperative day 1, albumin on postoperative day 5, and operation time.

The area under the ROC curve was 0.940 +/- 0.024, with a 95% CI of 0.892-0.987. The resulting model was statistically significant ($P<0.001$) (Figure 1).

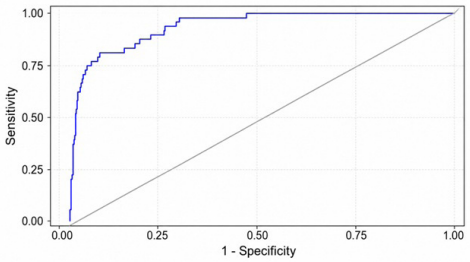

Figure 1. *ROC Curve Depicting the Relationship Between the Probability of Colorectal Anastomotic Leakage and the Logistic Function Value (P).*

Table 5.

Laboratory parameters of the studied patients depending on the presence of anastomotic leakage.

Indicator	Category	CAL		*P*-value
		No	Yes	
Preoperative albumin, Me (Q1-Q3)		37.50 (34.42 - 40.70)	33.40 (31.70 - 35.67)	< 0.001
Albumin on postoperative day 1, Me (Q1-Q3)		37.20 (34.50 - 40.92)	31.85(29.68 - 33.83)	< 0.001
Albumin on postoperative day 5, Me (Q1-Q3)		38.59 (33.82 - 41.97)	31.50 (30.30 - 34.50)	< 0.001
Preoperative total protein, Me (Q1-Q3)		70.50 (66.70 - 73.80)	70.70 (67.50 - 73.28)	0.811
Total protein on postoperative day 1, Me (Q1-Q3)		59.30 (55.30 - 63.60)	59.45 (56.33 - 65.17)	0.540
Total protein on postoperative day 5, Me (Q1-Q3)		58.10 (54.00 - 62.65)	57.00 (52.35 - 61.77)	0.268
Preoperative hemoglobin, M +/- SD (95% CI)		113.61 ± 21.38 (111.80 - 115.43)	108.77 ± 20.09 (102.94 - 114.61)	0.131
Hemoglobin on postoperative day 1, Me (Q1-Q3)		111.00 (98.00 - 125.00)	107.00 (99.75 - 116.25)	0.305
Hemoglobin on postoperative day 5, Me (Q1-Q3)		108.00 (96.00 - 121.00)	104.00 (95.75 - 116.00)	0.307
Preoperative neutrophils, Me (Q1-Q3)		4.50 (3.40 - 5.83)	4.69 (3.74 - 6.21)	0.234
Neutrophils on postoperative day 1, Me (Q1-Q3)		7.60 (5.60 - 10.10)	9.90 (6.99 - 12.40)	< 0.001
Neutrophils on postoperative day 5, Me (Q1-Q3)		4.67 (3.40 - 6.24)	6.46 (4.50 - 9.72)	< 0.001
Preoperative lymphocytes, Me (Q1-Q3)		1.70 (1.39 - 2.20)	1.67 (1.29 - 2.03)	0.438
Lymphocytes on postoperative day 1, Me (Q1-Q3)		1.40 (1.00 - 1.80)	1.08 (0.80 - 1.30)	< 0.001
Lymphocytes on postoperative day 5, Me (Q1-Q3)		1.50 (1.14 - 1.90)	1.21 (1.00 - 1.88)	0.054
Preoperative NLR, Me (Q1-Q3)		2.52 (1.82 - 3.68)	3.00 (2.15 - 4.07)	0.140
NLR on postoperative day 1, Me (Q1-Q3)		5.37 (3.39 - 8.52)	9.37 (5.69 - 13.35)	< 0.001
NLR on postoperative day 5, Me (Q1-Q3)		3.11 (2.24 - 4.58)	5.09 (2.72 - 8.04)	< 0.001

NLR, neutrophil-to-lymphocyte ratio (dimensionless). Albumin, total protein, and hemoglobin are reported in g/L; absolute neutrophil and lymphocyte counts are reported in ×10⁹/L.

Table 6.

Logistic regression.

Predictors	Unadjusted		Adjusted	
	COR; 95% CI	*P*-value	AOR; 95% CI	*P*-value
Preoperative colostomy: yes	8.478; 3.951 - 18.192	< 0.001	20.937; 6.424 - 68.238	< 0.001
Multiorgan resection: yes	16.655; 8.406 - 32.983	< 0.001	156.867; 37.450 - 657.208	< 0.001
Preoperative albumin	0.785; 0.717 - 0.859	< 0.001	0.792; 0.689 - 0.910	0.001
Albumin day 1	0.801; 0.748 - 0.857	< 0.001	0.792; 0.695 - 0.902	< 0.001
Albumin day 5	0.833; 0.783 - 0.885	< 0.001	0.905; 0.825 - 0.992	0.032
Neutrophils day 5	1.174; 1.094 - 1.259	< 0.001	1.134; 1.027 - 1.251	0.012
Operation time	1.008; 1.003 - 1.013	0.004	0.991; 0.982 - 1.000	0.048

The cutoff value of the logistic function P corresponding to the highest Youden index was 0.143. Leakage was predicted when the logistic function P was greater than or equal to this value. The sensitivity and specificity of the model were 80.9% and 92.5%, respectively.

The resulting regression model was statistically significant (P<0.001). Based on the Nagelkerke coefficient of determination, the model explained 60.7% of the observed variance in the presence of leakage.

Preoperative colostomy was associated with substantially higher adjusted odds of CAL (AOR = 20.937; 95% CI: 6.424-68.238; P<0.001) compared with no preoperative colostomy.

Multiorgan resection was also associated with substantially higher adjusted odds of CAL (AOR = 156.867;

95% CI: 37.450-657.208; *P*<0.001) compared with standard resection.

For preoperative albumin, each 1 g/L increase was associated with lower adjusted odds of CAL (AOR = 0.792; 95% CI: 0.689-0.910; *P*=0.001) (Table 6). Thus, lower preoperative albumin was associated with greater risk.

Albumin on postoperative days 1 and 5 showed the same direction of association. Each 1 g/L increase was associated with lower adjusted odds of CAL on day 1 (AOR = 0.792; 95% CI: 0.695-0.902; P<0.001) and day 5 (AOR = 0.905; 95% CI: 0.825-0.992; *P*=0.032).

For the neutrophil count on postoperative day 5, each 1 $\times 10^9$/L increase was associated with higher adjusted odds of CAL (AOR = 1.134; 95% CI: 1.027-1.251; *P*=0.012).

Operation time showed a small but statistically significant association with CAL. In unadjusted analysis, each additional minute was associated with higher odds (COR = 1.008; 95% CI: 1.003-1.013; *P*=0.004), whereas after adjustment the direction reversed (AOR = 0.991; 95% CI: 0.982-1.000; *P*=0.048). This reversal suggests confounding or model instability and warrants cautious interpretation.

Discussion

Colorectal anastomotic leakage is currently an acute problem in the surgical treatment of colorectal cancer. The issue of early predictors and prediction of CAL remains debated.

International authors have noted an association between CAL and patient sex.[15,16] These studies report an increased risk of CAL in male patients and link it to androgen activity and the subsequent characteristics of intestinal microcirculation after hormonal exposure. In our study, no statistically significant parameters related to patients' sex were identified. According to the study by Yu et al.,[17] taller patient height predisposes to CAL due to smaller pelvic dimensions, particularly the pelvic inlet and intertuberous distance. This parameter was not statistically significant in our study.

Previous studies have associated advanced tumor stage and metastatic disease with CAL. [18,19] In our cohort, CAL was more frequent among patients with stage IV disease (20.8% vs. 8.1%), T4 tumors (33.3% vs. 14.2%), and distant metastases (M1: 20.8% vs. 7.3%); stage, T category, and M category were statistically significant in univariate analysis. In contrast, measured tumor size did not differ between the groups (median 50 mm in both groups).

Preoperative colostomy was associated with an increased risk of CAL. A previous colostomy was most often created for acute intestinal obstruction; therefore, this variable may identify a clinically more compromised subgroup with prior surgical trauma and impaired nutritional or inflammatory status. Consistent with this interpretation, the CAL group in our cohort had lower perioperative albumin concentrations but a stronger postoperative inflammatory response, reflected by higher neutrophil counts and NLR values rather than a uniform reduction in all laboratory parameters.[20]

Noteworthy are the results regarding the effect of BMI on the risk of colorectal anastomotic leakage. International colleagues note that BMI >30 kg/m^2 is considered an independent risk factor for CAL.[21,22] In our study, this parameter was not significant, apparently because patients with obesity were compensated, and this pathological condition therefore did not have a negative effect.

International sources identify poor nutrition and malnutrition as predictors of CAL.[23] Although low BMI was not statistically significant in our study, the direction of the albumin changes was consistent and clinically relevant: patients who developed CAL had lower median serum albumin preoperatively (33.40 vs. 37.50 g/L) and on postoperative days 1 (31.85 vs. 37.20 g/L) and 5 (31.50 vs. 38.59 g/L). Accordingly, odds ratios below 1 for albumin indicate that higher albumin concentrations were associated with lower odds of CAL, whereas lower albumin concentrations were associated with higher risk.

The surgeon's vigilance is important for early diagnosis of CAL, because delayed diagnosis is associated with an unfavorable prognosis. Inflammatory markers and clinical signs of peritonitis should therefore be monitored carefully.[24] In our study, the NLR was higher in patients who developed CAL on postoperative day 1 (median 9.37 vs. 5.37) and day 5 (5.09 vs. 3.11; both *P*<0.001). This upward change in NLR, rather than the absolute level alone, may help identify patients who require timely additional imaging to verify the complication.

The cellular components showed the same directional pattern: neutrophil counts were higher in the CAL group on postoperative day 1 (9.90 vs. 7.60 $\times 10^9$/L) and day 5 (6.46 vs. 4.67 $\times 10^9$/L), whereas the lymphocyte count was lower on postoperative day 1 (1.08 vs. 1.40 $\times 10^9$/L). The day-5 lymphocyte count was also numerically lower, but the difference did not reach statistical significance (*P*=0.054). Total protein and hemoglobin did not differ significantly at any assessed time point, and preoperative neutrophil, lymphocyte, and NLR values were not significant. Because an automated leukocyte differential is simple and inexpensive, these directional changes may help surgeons suspect CAL even in settings with limited diagnostic resources.

Longer operation time may indicate more complex surgical manipulations, which are already associated with a higher expected risk of postoperative complications. Our study demonstrated the influence of operation time on the risk of CAL development, which is confirmed by multiple international and Russian studies.[25-28]

International colleagues note that intraoperative blood loss greater than 100 mL increases the risk of CAL.[29] Our analysis confirms this effect: in the CAL group, the median blood loss was 225 mL, significantly higher than in the group with a favorable postoperative period, where it was 100 mL.

The authors also identified an association between CAL and multiorgan resection during surgery. Expansion of the surgical procedure leads to greater trauma to the body and an increased risk of postoperative complications.[30]

Conclusion

In our study, the incidence of colorectal anastomotic leakage was 48 cases (8.24%). In univariate analyses,

CAL was associated with advanced oncological stage, T category, M category, longer operation time and hospital stay, preoperative colostomy, multiorgan resection, Clavien-Dindo complications, greater blood loss, type of surgery, lower albumin concentrations preoperatively and on postoperative days 1 and 5, higher neutrophil counts on postoperative days 1 and 5, a lower lymphocyte count on postoperative day 1, and higher NLR values on postoperative days 1 and 5. In the multivariable model, preoperative colostomy, multiorgan resection, preoperative albumin, albumin on postoperative days 1 and 5, neutrophils on postoperative day 5, and operation time remained statistically significant. These findings support combined assessment of nutritional and inflammatory markers for early postoperative risk stratification.

Author Contributions

Eugene A. Toneev: Conceptualization, Methodology, Investigation, Formal Analysis, Writing—Review and Editing, Supervision and Project Administration.
Daniil D. Prokhorov: Conceptualization, Methodology, Investigation, Data Curation, Formal Analysis, Writing—Original Draft Preparation, Review and Editing.
Marina A. Iglina: Investigation, Data Curation.
Syumbel R. Ziganshina: Investigation, Data Curation, Writing—Original Draft Preparation.
Daniil R. Pyatikop: Investigation, Data Curation, Writing—Original Draft Preparation.
Daria V. Golovko: Investigation, Data Curation, Writing—Original Draft Preparation.
Zainap Yu. Yunkina: Investigation, Data Curation, Writing—Original Draft Preparation.
All authors have read and approved the final version of the manuscript.

Information on Support Sources

This work was carried out in accordance with the research plan of the T.Z. Biktimirov Faculty of Medicine, Institute of Medicine, Ecology and Physical Culture, Ulyanovsk State University, Ulyanovsk, Russia. The authors received no financial support from pharmaceutical companies.

Conflict of Interest

The authors declare no conflict of interest.

Ethical Statement

The study was conducted in accordance with the ethical principles of the Declaration of Helsinki and was approved by the Ethics Committee of the Regional Clinical Oncology Dispensary and Ulyanovsk State University, Ulyanovsk. The study involved a retrospective analysis of routinely collected medical records and no study-specific intervention. The procedure for obtaining or waiving individual informed consent followed the decision of the approving ethics committee and applicable regulations.

References

1. Bray F, Ferlay J, Soerjomataram I, Siegel RL, Torre LA, Jemal A. Global cancer statistics 2018: GLOBOCAN estimates of incidence and mortality worldwide for 36 cancers in 185 countries. CA Cancer J Clin. 2018 Nov;68(6):394-424. doi: 10.3322/caac.21492. Epub 2018 Sep 12. Erratum in: CA Cancer J Clin. 2020 Jul;70(4):313. doi: 10.3322/caac.21609. PMID: 30207593.
2. Lauby-Secretan B, Vilahur N, Bianchini F, Guha N, Straif K; International Agency for Research on Cancer Handbook Working Group. The IARC Perspective on Colorectal Cancer Screening. N Engl J Med. 2018 May 3;378(18):1734-1740. doi: 10.1056/NEJMsr1714643. Epub 2018 Mar 26. PMID: 29580179; PMCID: PMC6709879.
3. 2015 European Society of Coloproctology Collaborating Group. Predictors for Anastomotic Leak, Postoperative Complications, and Mortality After Right Colectomy for Cancer: Results From an International Snapshot Audit. Dis Colon Rectum. 2020 May;63(5):606-618. doi: 10.1097/DCR.0000000000001590. PMID: 32032201.
4. Rasulov AO, Malikhov AG, Rakhimov OA, Kozlov NA, Malikhova OA. Immediate results of right-sided hemicolectomy with complete mesocolic excision and D3 lymph node dissection in treatment of cancer of the right colon. Pirogov Russian Journal of Surgery. 2017;(8):79-86. (In Russ.).
5. Darbishgadjiev ShO, Baulin AA, Zimin YuI, Baulin VA, Baulina O.A. Results of surgical treatment of colorectal cancer. Health and Education Millennium. 2018;20(4):42-46. (In Russ.). doi:10.26787/nydha-2226-7425-2018-20-4-42-46.
6. Yanushkevich SV, Yanushkevich VYu. Protection of an anastomosis in rectal cancer surgery. Surgery News. 2017;25(4):412-420. (In Russ.). doi.org:10.18484/2305-0047.2017.4.412.
7. Rencuzogullari A, Benlice C, Valente M, Abbas MA, Remzi FH, Gorgun E. Predictors of Anastomotic Leak in Elderly Patients After Colectomy: Nomogram-Based Assessment From the American College of Surgeons National Surgical Quality Program Procedure-Targeted Cohort. Dis Colon Rectum. 2017 May;60(5):527-536. doi: 10.1097/DCR.0000000000000789. PMID: 28383453.
8. Boström P, Haapamäki MM, Matthiessen P, Ljung R, Rutegård J, Rutegård M. High arterial ligation and risk of anastomotic leakage in anterior resection for rectal cancer in patients with increased cardiovascular risk. Colorectal Dis. 2015 Nov;17(11):1018-27. doi: 10.1111/codi.12971. PMID: 25851151.
9. Branagan G, Finnis D; Wessex Colorectal Cancer Audit Working Group. Prognosis after anastomotic leakage in colorectal surgery. Dis Colon Rectum. 2005 May;48(5):1021-6. doi: 10.1007/s10350-004-0869-4. PMID: 15789125.
10. Mirnezami A, Mirnezami R, Chandrakumaran K, Sasapu K, Sagar P, Finan P. Increased local recurrence and reduced survival from colorectal cancer following anastomotic leak: systematic review and meta-analysis. Ann Surg. 2011 May;253(5):890-9. doi: 10.1097/SLA.0b013e3182128929. PMID: 21394013.
11. Phillips B. Reducing Gastrointestinal Anastomotic Leak Rates: Review of Challenges and Solutions. Open Access Surg. 2016, 5, 5-14.

12. Hyman N, Manchester TL, Osler T, Burns B, Cataldo PA. Anastomotic leaks after intestinal anastomosis: it's later than you think. Ann Surg. 2007 Feb;245(2):254-8. doi: 10.1097/01.sla.0000225083.27182.85. PMID: 17245179; PMCID: PMC1876987.
13. Kanellos I, Vasiliadis K, Angelopoulos S, Tsachalis T, Pramateftakis MG, Mantzoros I, Betsis D. Anastomotic leakage following anterior resection for rectal cancer. Tech Coloproctol. 2004 Nov;8 Suppl 1:s79-81. doi: 10.1007/s10151-004-0119-8. PMID: 15655652.
14. Clavien PA, Barkun J, de Oliveira ML, Vauthey JN, Dindo D, Schulick RD, de Santibañes E, Pekolj J, Slankamenac K, Bassi C, Graf R, Vonlanthen R, Padbury R, Cameron JL, Makuuchi M. The Clavien-Dindo classification of surgical complications: five-year experience. Ann Surg. 2009 Aug;250(2):187-96. doi: 10.1097/SLA.0b013e3181b13ca2. PMID: 19638912.
15. Park JS, Choi GS, Kim SH, Kim HR, Kim NK, Lee KY, Kang SB, Kim JY, Lee KY, Kim BC, Bae BN, Son GM, Lee SI, Kang H. Multicenter analysis of risk factors for anastomotic leakage after laparoscopic rectal cancer excision: the Korean laparoscopic colorectal surgery study group. Ann Surg. 2013 Apr;257(4):665-71. doi: 10.1097/SLA.0b013e31827b8ed9. PMID: 23333881.
16. Verduin WM, Warps AK, van den Helder R, Doodeman HJ, Houdijk APJ; INfluences of Fat And MUscle in colorectal Surgery Collaborative. Visceral Fat and Anastomotic Leakage After Colon Cancer Resection. Dis Colon Rectum. 2021 Feb 1;64(2):163-170. doi: 10.1097/DCR.0000000000001779. PMID: 33394767.
17. Yu ZL, Liu XH, Liu HS, Ke J, Zou YF, Cao WT, Xiao J, Zhou ZY, Lan P, Wu XJ, Wu XR. Impact of pelvic dimensions on anastomotic leak after anterior resection for patients with rectal cancer. Surg Endosc. 2021 May;35(5):2134-2143. doi: 10.1007/s00464-020-07617-1. Epub 2020 May 14. PMID: 32410082.
18. Sciuto A, Merola G, De Palma GD, Sodo M, Pirozzi F, Bracale UM, Bracale U. Predictive factors for anastomotic leakage after laparoscopic colorectal surgery. World J Gastroenterol. 2018 Jun 7;24(21):2247-2260. doi: 10.3748/wjg.v24.i21.2247. PMID: 29881234; PMCID: PMC5989239.
19. Zhu QL, Feng B, Lu AG, Wang ML, Hu WG, Li JW, Mao ZH, Zheng MH. Laparoscopic low anterior resection for rectal carcinoma: complications and management in 132 consecutive patients. World J Gastroenterol. 2010 Sep 28;16(36):4605-10. doi: 10.3748/wjg.v16.i36.4605.
20. Awad S, El-Rahman AIA, Abbas A, Althobaiti W, Alfaran S, Alghamdi S, Alharthi S, Alsubaie K, Ghedan S, Alharthi R, Asiri M, Alzahrani A, Alotaibi N, Shoma A, Sheishaa MSA. The assessment of perioperative risk factors of anastomotic leakage after intestinal surgeries; a prospective study. BMC Surg. 2021 Jan 7;21(1):29. doi: 10.1186/s12893-020-01044-8. PMID: 33413244; PMCID: PMC7789647.
21. Watanabe J, Tatsumi K, Ota M, Suwa Y, Suzuki S, Watanabe A, Ishibe A, Watanabe K, Akiyama H, Ichikawa Y, Morita S, Endo I. The impact of visceral obesity on surgical outcomes of laparoscopic surgery for colon cancer. Int J Colorectal Dis. 2014 Mar;29(3):343-51. doi: 10.1007/s00384-013-1803-9. Epub 2013 Dec 3. PMID: 24297037.
22. Cakir H, Heus C, Verduin WM, Lak A, Doodeman HJ, Bemelman WA, Houdijk AP. Visceral obesity, body mass index and risk of complications after colon cancer resection: A retrospective cohort study. Surgery. 2015 May;157(5):909-15. doi: 10.1016/j.surg.2014.12.012. Epub 2015 Feb 21. PMID: 25708142.
23. Kwag SJ, Kim JG, Kang WK, Lee JK, Oh ST. The nutritional risk is a independent factor for postoperative morbidity in surgery for colorectal cancer. Ann Surg Treat Res. 2014 Apr;86(4):206-11. doi: 10.4174/astr.2014.86.4.206. Epub 2014 Mar 25. PMID: 24783180; PMCID: PMC3996723.
24. Gray M, Marland JRK, Murray AF, Argyle DJ, Potter MA. Predictive and Diagnostic Biomarkers of Anastomotic Leakage: A Precision Medicine Approach for Colorectal Cancer Patients. J Pers Med. 2021 May 25;11(6):471. doi: 10.3390/jpm11060471. PMID: 34070593; PMCID: PMC8229046.
25. Telem DA, Chin EH, Nguyen SQ, Divino CM. Risk factors for anastomotic leak following colorectal surgery: a case-control study. Arch Surg. 2010 Apr;145(4):371-6; discussion 376. doi: 10.1001/archsurg.2010.40. PMID: 20404288.
26. Choi DH, Hwang JK, Ko YT, Jang HJ, Shin HK, Lee YC, Lim CH, Jeong SK, Yang HK. Risk factors for anastomotic leakage after laparoscopic rectal resection. J Korean Soc Coloproctol. 2010 Aug;26(4):265-73. doi: 10.3393/jksc.2010.26.4.265. Epub 2010 Aug 31. PMID: 21152228; PMCID: PMC2998006.
27. Huh JW, Kim HR, Kim YJ. Anastomotic leakage after laparoscopic resection of rectal cancer: the impact of fibrin glue. Am J Surg. 2010 Apr;199(4):435-41. doi: 10.1016/j.amjsurg.2009.01.018. Epub 2009 May 28. PMID: 19481197.
28. Khasanov AG, Sufiyarov IF, Bakirov ER, Yamalova GR. Failure of colonic anastomotic sutures. Medical Bulletin of Bashkortostan. 2020;15(1(85)):75-79. EDN WHOIZL. (In Russ.).
29. Kawada K, Hasegawa S, Hida K, Hirai K, Okoshi K, Nomura A, Kawamura J, Nagayama S, Sakai Y. Risk factors for anastomotic leakage after laparoscopic low anterior resection with DST anastomosis. Surg Endosc. 2014 Oct;28(10):2988-95. doi: 10.1007/s00464-014-3564-0. Epub 2014 May 23. Erratum in: Surg Endosc. 2014 Oct;28(10):2996-7. PMID: 24853855; PMCID: PMC4186976.
30. Pommergaard HC, Gessler B, Burcharth J, Angenete E, Haglind E, Rosenberg J. Preoperative risk factors for anastomotic leakage after resection for colorectal cancer: a systematic review and meta-analysis. Colorectal Dis. 2014 Sep;16(9):662-71. doi: 10.1111/codi.12618. PMID: 24655784.

International Journal of Biomedicine 16(3) (2026) 372-377
http://dx.doi.org/10.21103/Article16(3)_OA7

ORIGINAL ARTICLE

INTERNATIONAL JOURNAL OF BIOMEDICINE

Ginsenoside Rg3 Induces Apoptosis While Attenuates Collagen Metabolism in Human Vocal Cord Scar Fibroblasts In Vitro

Yan Qin[1], Kang Wang[1], Zhi-Mao Zhang [1], Ting Wu[2], Long Zhang[1], Jun Liu[1*]

[1]*Department of Otorhinolaryngology Head and Neck Surgery, Yichang Central People's Hospital ,The First College of Clinical Medical Science, China Three Gorges University, 443000, Yichang, China*

[2]*Department of Otorhinolaryngology Head and Neck Surgery, Nanjing Tongren Hospital, School of Medicine, Southeast University, 211102, Nanjing, China*

Abstract

Background: This study aimed to investigate the effects of ginsenoside Rg3 on apoptosis and collagen metabolism in human vocal cord scar fibroblasts (HVCSFs) and the molecular mechanisms involved.
Methods and Results: HVCSFs were cultured in vitro and treated with different concentrations of ginsenoside Rg3. Cell proliferation inhibition rate was detected by CCK-8 assay. Cell apoptosis was analyzed by flow cytometry and Calcein/PI live/dead cell staining. Cell invasion ability was detected by Transwell assay. Expression levels of apoptosis-related protein caspase-3 and Collagen Type I, Collagen Type III (Col I, Col III) were detected by Western blot and Quantitative real-time polymerase chain reaction (qPCR). HVCSFs were cultured in vitro and exposed to increasing concentrations of ginsenoside Rg3. Rg3 treatment dose-dependently inhibited HVCSFs proliferation, as shown by the CCK-8 assay ($P<0.0001$). Flow cytometry and Calcein/PI live/dead staining consistently revealed a significant induction of apoptosis upon Rg3 exposure ($P<0.0001$). Cell invasion was also effectively suppressed, as assessed by the Transwell assay ($P<0.001$, $P<0.0001$). At the protein level, Western blot analysis demonstrated that Rg3 upregulated caspase 3 expression ($P<0.01$, $P<0.001$) while downregulating both Col I and Col III ($P<0.05$, $P<0.01$). Correspondingly, qPCR results showed elevated mRNA levels of caspase 3 ($P<0.05$, $P<0.01$, $P<0.0001$) and reduced mRNA levels of Col I and Col III ($P<0.05$, $P<0.0001$) in response to Rg3 treatment.
Conclusions. Ginsenoside Rg3 may promote the apoptosis of HVCSFs through activating the caspase-3-dependent apoptotic pathway and inhibiting the expression of Col I and Col III, thereby improving vocal cord scar fibrosis. This study provides experimental evidence for ginsenoside Rg3 as a potential anti-vocal cord scar drug.(**International Journal of Biomedicine. 2026;16(3):372-377.**)

Keywords: ginsenoside Rg3 • vocal cord scar • fibroblasts • apoptosis • collagen metabolism

For citation: Qin Y, Wang K, Zhang Z-M, Wu T, Zhang L, Liu J. Ginsenoside Rg3 Induces Apoptosis While Attenuates Collagen Metabolism in Human Vocal Cord Scar Fibroblasts In Vitro. International Journal of Biomedicine. 2026;16(3):372-377. doi:10.21103/Article16(3)_OA7

Introduction

Vocal fold scarring refers to the pathological fibrosis of the extracellular matrix within the lamina propria, leading to impaired vibratory function and voice disorders.[1,2] It is commonly caused by surgical trauma (e.g., vocal fold resection),[3] prolonged intubation, chronic inflammation, or radiation therapy. Scar tissue disrupts the viscoelastic properties of the vocal folds, resulting in symptoms such as hoarseness, vocal fatigue, reduced vocal range, and breathiness. Although various clinical interventions have been tested for the treatment of voice disorders and vocal fold paralysis,[4-8] satisfactory restoration of vocal fold function remains elusive. Current therapeutic options are limited, necessitating the development of novel approaches to promote vocal fold healing and functional recovery.

Ginsenoside Rg3, a bioactive compound enriched from steamed or heated Panax ginseng roots, exhibits multiple pharmacological effects, including anti-angiogenic, anti-tumor, and anti-fibrotic properties.[9-11] Previous studies have demonstrated that ginsenoside Rg3 inhibits fibroblast proliferation and migration while inducing apoptosis, thereby modulating the expression of proteins and mRNA levels associated with proliferation, apoptosis, and migration.[12,13]

Additionally, ginsenoside Rg3 has been shown to suppress fibroblast proliferation, angiogenesis, and collagen synthesis via the TGF-β1/Smad and ERK signaling pathways.[14] Histologically, the composition and distribution of the extracellular matrix (ECM) in the lamina propria are essential for maintaining the viscoelastic properties required for vocal fold vibration. The ECM comprises hyaluronic acid (HA), collagen, elastin, fibronectin, and other components.[7,15] Specifically, HA maintains viscoelasticity and functions as a shock absorber, collagen provides structural support, and elastin preserves vocal fold vibration through its intrinsic elasticity.

This study aims to verify whether ginsenoside Rg3 can reduce human vocal fold scarring and explore the underlying mechanisms by which ginsenoside Rg3 regulates scar formation in human vocal folds.

Materials and Methods

Chemicals

Ginsenoside Rg3 (purity ≥99.5%) was obtained from Wuhan Jingbiao Technology Co., Ltd. (Wuhan, China). Rg3 powder was dissolved in dimethyl sulfoxide (DMSO) to prepare a stock solution, which was then sterilized by filtration through a 0.22 μm polyethersulfone (PES) membrane filter. The stock solution was serially diluted with complete cell culture medium to achieve final Rg3 concentrations of 10, 20, 40, 80, and 160 μg/mL. The final concentration of DMSO in all treatment groups was maintained at 0.05% (v/v). A vehicle control group containing 0.05% DMSO without Rg3 was used as the negative control.

Cell culture

Human vocal cord scar fibroblasts (HVCSFs) were obtained from iCell Bioscience Inc. (Shanghai, China). Cells were maintained in high-glucose Dulbecco's Modified Eagle Medium (DMEM; HyClone, China) supplemented with 10% fetal bovine serum (FBS; Solarbio, China) and cultured at 37°C in a humidified atmosphere containing 5% CO_2. The medium was refreshed every 2–3 days, and cells were passaged when reaching 80–90% confluence.

Cell viability assay

Cell viability was evaluated using the Cell Counting Kit-8 assays (CCK-8; Bioswamp Life Science, China) according to the manufacturer's instructions. Briefly, HVCSFs were seeded in 96-well plates at a density of 3×10^3 cells per well in 100 μL of complete medium and incubated at 37°C in a humidified atmosphere with 5% CO_2 for 24 h to allow complete attachment. The medium was then replaced with fresh medium containing Rg3 at final concentrations of 0 (vehicle control), 10, 20, 40, 80, and 160 μg/mL. At designated time points (24, 48, and 72 h post-treatment), 10 μL of CCK-8 reagent was added to each well, and plates were incubated for an additional 1–4 h at 37°C. The absorbance at 450 nm was measured using a microplate reader (Allsheng, China). Cell viability was calculated using the following formula: Cell viability (%) = [(OD_control - OD_treated) / (OD_control - OD_blank)] × 100%. Each treatment group was assayed in quintuplicate, and experiments were repeated independently at least three times.

Flow Cytometry

Cell cycle analysis: HVCSFs (1×10^7 per group) were harvested, washed with PBS, and fixed in 75% ethanol at -20°C for at least 24 h. After washing twice with PBS, cells were stained with 0.5 mL PI/RNase Staining Buffer (BD Biosciences, USA) for 15 min at room temperature in the dark. DNA content was analyzed using a flow cytometer (ACEA NovoCyte, China), and cell cycle distributions were determined using NovoExpress software (ACEA Biosciences, China).

Apoptosis detection: Cell apoptosis was assessed using an Annexin V-FITC/PI Apoptosis Detection Kit (BD Biosciences, USA). After 48 h of treatment, HVCSFs were collected and resuspended in 1× Annexin V Binding Buffer. Annexin V-FITC (5 μL) and PI (5 μL) were added according to the manufacturer's instructions. After incubation for 15 min at room temperature in the dark, cells were analyzed by flow cytometry (ACEA NovoCyte, China). Data were analyzed using NovoExpress software (Allsheng, China).

Calcein-AM/Propidium Iodide (PI) staining

Cell viability was evaluated using the Calcein-AM/PI Double Staining Kit (C2015S, Beyotime Biotechnology, China) according to the manufacturer's instructions. Briefly, treated HVCSFs were washed twice with PBS and incubated with a working solution containing Calcein-AM (2 μM) and PI (4.5 μM) at 37°C for 30 min in the dark. After incubation, cells were washed once with PBS to remove excess dye and immediately visualized under an inverted fluorescence microscope (Nikon Ts2/Ts2-FL, Japan) equipped with appropriate filter sets. Calcein-AM-positive live cells (green fluorescence, excitation/emission = 494/517 nm) and PI-positive dead cells (red fluorescence, excitation/emission = 535/617 nm) were captured using NIS-Elements software (Nikon, Japan). Representative images from at least three independent experiments were recorded.

Transwell assay

Cell invasion assay: HVCSFs (2×10^4 cells in 200 μL serum-free DMEM) were seeded into the upper chamber of a Matrigel-coated Transwell insert (8 μm pore size; BD Biosciences, USA). The lower chamber contained 600 μL DMEM with 10% FBS as a chemoattractant. After 24h incubation at 37°C, invaded cells were fixed with 4% paraformaldehyde and stained with 0.1% crystal violet. Invaded cells were quantified by counting five random fields per insert under an inverted microscope (Nikon, Japan).

Cell migration assay: Transwell chambers (8 μm pore size; Corning, USA) were pre-hydrated with PBS for 5 min. HVCSFs (1×10^5 cells in 0.5 mL medium with 1% FBS) were seeded into the upper chamber, while the lower chamber contained 0.75 mL complete medium with 10% FBS. After 24 h incubation at 37°C, non-migrated cells were removed from the upper surface. Migrated cells were fixed with 4% paraformaldehyde (20 min, RT), stained with 0.5% crystal violet (30 min), and counted under 200× magnification (five random fields per chamber).

Quantitative real-time PCR (qPCR)

Total RNA of HVCSFs was extracted using TRIzol Reagent (Ambion, USA) and quantified with a Nano-300 micro-spectrophotometer (Aosheng, China). Genomic DNA

was removed using 5× gDNA digester Mix (YEASEN, China) at 42°C for 2 min. First-strand cDNA was synthesized using Hifair® III 1st Strand cDNA Synthesis SuperMix (YEASEN, China) in a 20 μL reaction containing 15 μL digested RNA and 5 μL 4× SuperMix at 25°C for 5 min, 55°C for 15 min, and 85°C for 5 min. qCR was performed on a CFX-Connect 96 system (Bio-Rad, USA) using Hieff® qPCR SYBR® Green Master Mix (No Rox) (YEASEN, China). Each 20 μL reaction contained 10 μL Master Mix, 0.5 μL each primer (10 μM), 1 μL cDNA, and 8 μL DNase/RNase-free water. The cycling conditions were: 95°C for 3 min, followed by 40 cycles of 95°C for 5 s, 56°C for 10 s, and 72°C for 25 s. Melting curve analysis was performed to verify specificity. GAPDH served as the internal reference, and relative expression of Collagen Type(Col)I, Col III, and Caspase-3 was calculated using the $2^{-\triangle\triangle ct}$ method. qPCR primer sequences are listed in Table 1.

Table 1.

The information on the primers used of qPCR

Gene	Sequence	Size of amplified fragment (bp)
Col I-F	5'-GAGATGGTGTTGATGGTCCC-3'	100
Col I-R	3'-GCAGCAAAGTTCCCAGTAAGA-5'	
Col III-F	5'-TGCCCACAGCCTTCTACAC-3'	111
Col III-R	3'-GCCAGGGTCACCATTTCT-5'	
Caspase-3-F	5'-GGTTCATCCAGTCGCTTT-3'	99
Caspase-3-R	3'-ATTCTGTTGCCACCTTTC-5'	
GAPDH-F	5'-GGGAAACTGTGGCGTGAT-3'	299
GAPDH-R	3'-GAGTGGGTGTCGCTGTTGA-5'	

Western Blotting

Protein samples were extracted from HVCSFs using RIPA lysis buffer (Bioswamp, China) supplemented with protease and phosphatase inhibitors (Bioswamp, China), followed by centrifugation at 12,000×g for 15 min at 4°C. Protein concentrations were determined using the BCA protein assay kit (Bioswamp, China) according to the manufacturer's instructions, with absorbance measured at 562 nm. Equal amounts of protein (20 μg per lane) were mixed with 5× loading buffer (Bioswamp, China), denatured by boiling for 10 min, and separated on 10% SDS-PAGE gels prepared using a one-step PAGE gel preparation kit (Bioswamp, China). Electrophoresis was performed at a constant voltage of 300 V for 20 min using rapid electrophoresis buffer (Bioswamp, China). Proteins were then transferred to PVDF membranes (Bioswamp, China) using rapid transfer buffer (Bioswamp, China) at 400 mA for 15–30 min in a wet transfer system. After blocking with protein-free rapid blocking solution (Bioswamp, China) for 10 min at room temperature, membranes were incubated with primary antibodies against Col I, Col III, Caspase-3, or GAPDH (1:1000, Bioswamp, China) diluted in primary antibody dilution buffer (Bioswamp, China) for 1 h at room temperature. Following three washes with PBST (5 min each), membranes were incubated with HRP-conjugated secondary antibodies (goat anti-rabbit IgG, 1:20000, Biosharp, China; goat anti-mouse IgG, 1:20000, Bioswamp, China) for 1 h at room temperature, washed three times with PBST (5 min each), and visualized using Super ECL Plus chemiluminescence detection kit (Bioswamp, China). Immunoreactive bands were captured using a fully automated chemiluminescence analyzer (Tanon-5200, China), and band intensities were quantified with ImageJ software.

Statistical analysis

All experiments were independently conducted in triplicate to ensure reproducibility. Each data represents the mean value derived from three independent replicates, and results are presented as mean ± standard deviation (SD). Differences among multiple groups were analyzed using one-way analysis of variance (ANOVA) followed by post-hoc Tukey's honestly significant difference (HSD) test for multiple comparisons. Differences with a *P*-value of <0.05 were considered statistically significant (*$P < 0.05$, ** $P < 0.01$, *** $P < 0.001$,****$P < 0.0001$). All analyses were performed using GraphPad Prism 10.4.2 (GraphPad Software, USA).

Results

Ginsenoside Rg3 exhibits concentration-dependent inhibition of the proliferation of HVCSFs and promotion of their apoptosis.

We treated HVCSFs with 0, 10, 20, 40, 80, and 160 μg/mL Ginsenoside Rg3, detected the cell proliferation inhibition rate using the CCK-8 method, analyzed the apoptosis situation by flow cytometry and Calcein/PI live/dead cell staining, tested the invasion ability of cells by Transwell assay, and detected the expression level of apoptosis-related protein caspase-3 by Western blot and qPCR. CCK-8 showed that after 24 hours, with the increase in drug concentration, the inhibition rate further rose from approximately 19.98% to 44.55% (Figure 1A) (P <0.0001), while following a 48-hour exposure to the drug, the inhibition rate elevated from 40.32% to 61.80% (Figure 1A)(P <0.0001). Flow cytometry and Calcein/PI indicated that with the increase of Ginsenoside Rg3 concentration, the apoptosis of HVCSFs increased (Figure 1B-C) (P < 0.0001). Transwell assay showed that with the increase of Ginsenoside Rg3 concentration, the number of invaded cells gradually decreased (figure 2A) ($P_{10\ \mu g/mL}$=0.0896, $P_{20\ \mu g/mL}$<0.0001, $P_{40\ \mu g/mL}$<0.0001, $P_{80\ \mu g/mL}$=<0.0001, $P_{160\ \mu g/mL}$<0.0001) the number of migrated cells also revealed a similar trend(figure 2B) ($P_{10\ \mu g/mL}$=0.0518, $P_{20\ \mu g/mL}$<0.0001, $P_{40\ \mu g/mL}$<0.0001, $P_{80\ \mu g/mL}$=<0.0001, $P_{160\ \mu g/mL}$<0.0001)qPCR indicated that Ginsenoside Rg3 upregulated the expression of caspase-3 in a concentration-dependent manner(figure 3A)($P_{10\ \mu g/mL}$=0.0089, $P_{20\ \mu g/mL}$=0.0064, $P_{40\ \mu g/mL}$=0.0047, $P_{80\ \mu g/mL}$=0.0021, $P_{160\ \mu g/mL}$=0.0005), Western blot results showed that Ginsenoside Rg3 also enhanced the expression of caspase-3 protein(figure 3B-C) ($P_{10\ \mu g/mL}$=0.8259, $P_{20\ \mu g/mL}$=0.0234, $P_{40\ \mu g/mL}$=0.0096, $P_{80\ \mu g/mL}$<0.0001, $P_{160\ \mu g/mL}$<0.0001).

Ginsenoside Rg3 inhibits the excessive deposition of extracellular matrix in HVCSFs.

In normal vocal cords, Col I is the main type of collagen, providing high strength and tensile resistance, maintaining the

mechanical stability of the vocal cords, and enabling them to withstand vibrations and tension during speech. Col III usually coexists with Col I to form a finer fiber network, increasing the elasticity and flexibility of the tissue, and facilitating the adaptability of vocal cord vibrations. The mRNA transcription levels of the genes encoding these two types of collagens (Col I and Col III) were typically detected using qPCR. The results showed that after Rg3 treatment, Col I mRNA levels in HVCSFs were significantly downregulated. This inhibitory effect was also dose-dependent (Figure 3 A) ($P_{10\ \mu g/mL}$=0.0082, $P_{20\ \mu g/mL}$=0.0104, $P_{40\ \mu g/mL}$=0.0064, $P_{80\ \mu g/mL}$=0.0037, $P_{160\ \mu g/mL}$=0.0015) and the mRNA level trend of Col III was similar to that (figure 3 A) ($P_{10\ \mu g/mL}$=0.0062, $P_{20\ \mu g/mL}$=0.0033, $P_{40\ \mu g/mL}$=0.0021, $P_{80\ \mu g/mL}$=0.0304, $P_{160\ \mu g/mL}$=0.0011). We performed the Western blot experiment, and the results showed that a higher concentration of Rg3 significantly inhibited the Col I protein level in HVCSFs (Figure 3 B-C) ($P_{10\ \mu g/mL}$=0.1217, $P_{20\ \mu g/mL}$=0.0466, $P_{40\ \mu g/mL}$=0.0188, $P_{80\ \mu g/mL}$<0.0001, $P_{160\ \mu g/mL}$<0.0001), while the Col III protein level exhibited a similar trend (figure 3 B-C) ($P_{10\ \mu g/mL}$=0.0998, $P_{20\ \mu g/mL}$=0.0606, $P_{40\ \mu g/mL}$=0.0339, $P_{80\ \mu g/mL}$<0.0001, $P_{160\ \mu g/mL}$<0.0001).

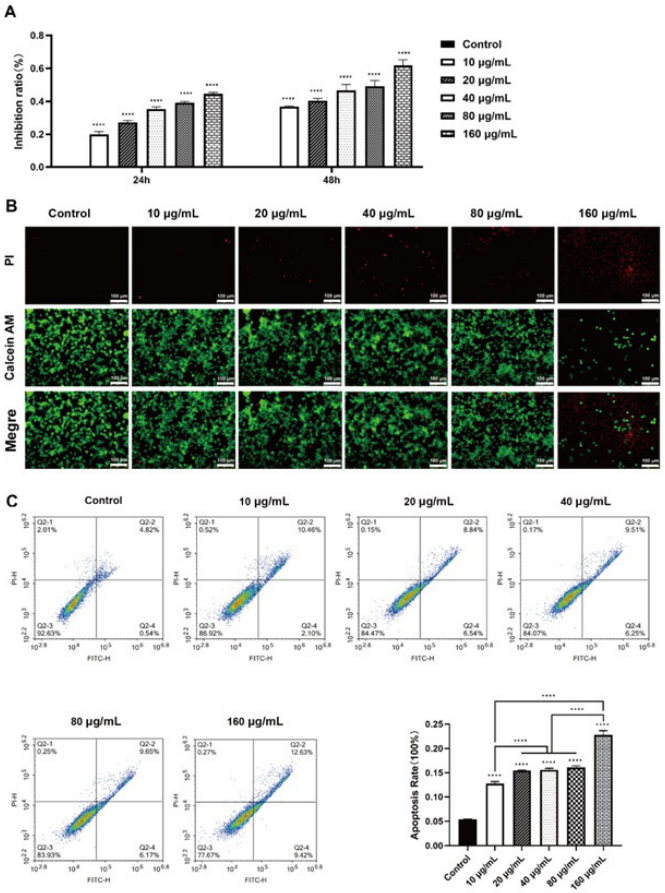

Figure1. *Rg3 inhibited the proliferation of Human vocal cord scar fibroblasts (HVCSFs) and promoted their apoptosis. A: The inhibition ratio of constructed with the Cell Counting Kit-8 assays(CCK-8) results after Rg3 treatment for 24 h and 48h, B: Fluorescence images of HVCSFs dual-stained with calcein AM (green) and PI (red) at 48 h after Rg3 treatment (10×, Scale bar =100* **μm**), *C: Flow cytometry analysis of apoptosis and the corresponding apoptosis rates in HVCSFs were obtained after 48 h after Rg3 treatment (****P < 0.0001).*

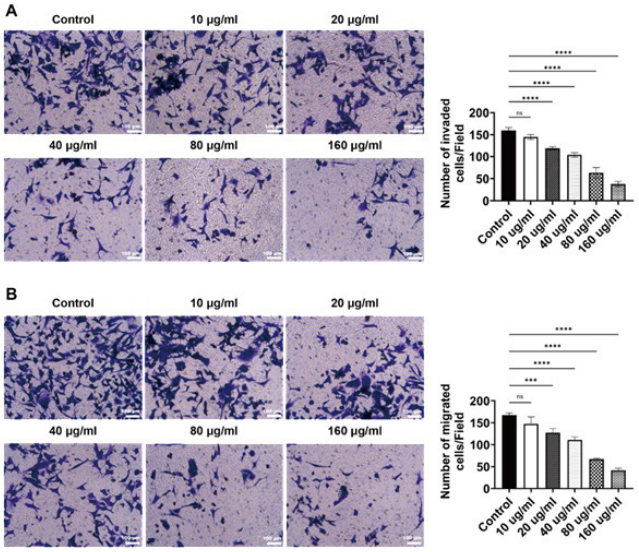

Figure 2. *The migration and invasion abilities of HVCSFs were assayed in Transwell chambers after Rg3 treatment, A: the Transwell invaded, B: the Transwell migrated (200×, Scale bar =100* μm, *** *P < 0.001,**** P< 0.0001).*

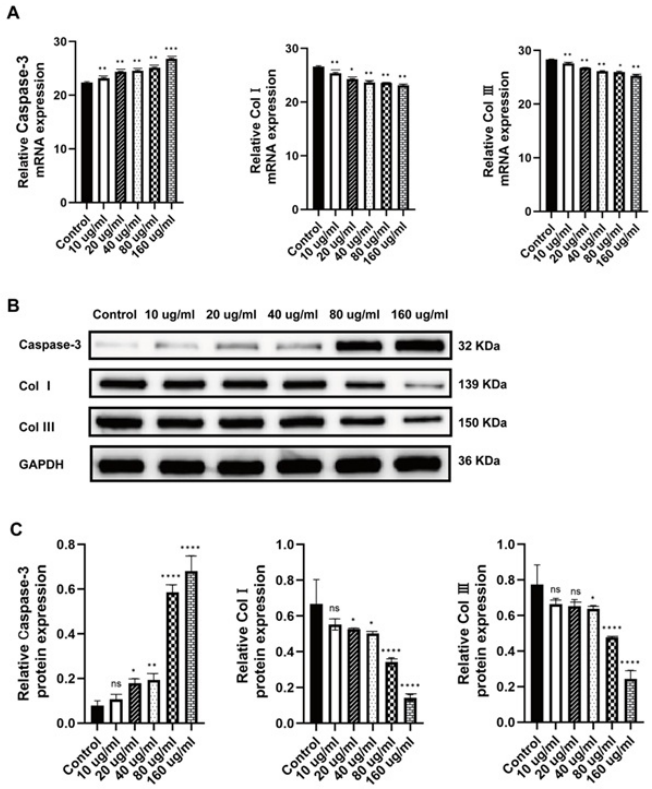

Figure 3. *Effects of Rg3 on Collagen Type (Col) I, Col III, and Caspase-3 signaling activities in cultured HVCSFs. A: It showed mRNA relative expression levels of Col I, Col III, and Caspase-3 in HVCSFs at treated with different concentrations of Rg3 (10, 20, 40, 80, and 160 μg/mL). B: Protein levels of Col I, Col III, and Caspase-3 in HVCSFs at treated with different concentrations of Rg3. C: Densitometric analysis of (B). (*P< 0.05, ** P < 0.01, *** P < 0.001,**** P < 0.0001).*

Discussion

The present study demonstrated that ginsenoside Rg3 exerts significant inhibitory effects on the proliferation of human vocal fold scar fibroblasts (HVFSFs), while promoting their apoptosis in a concentration-dependent manner. Additionally, Rg3 effectively suppressed the excessive deposition of Col I and Col III, key ECM components that contribute to vocal fold fibrosis. These findings suggest that Rg3 may serve as a potential therapeutic agent for vocal fold scarring by modulating fibroblast activity and collagen metabolism.

The results of this study indicate that ginsenoside Rg3 has a dual regulatory effect on HVCSFs, providing important clues for a deeper understanding of its therapeutic mechanism. Firstly, Rg3 dose-dependently inhibited the proliferation of HVCSFs and significantly promoted cell apoptosis. The Caspase (Cysteine-dependent aspartate-directed proteases) family is a core molecule in the apoptotic signaling pathway. Among them, Caspase-3 is regarded as the key executor of apoptosis, and its activation marks an irreversible "dead end" in the process of cell apoptosis.[16] Western blot and qPCR analyses confirmed that the expression of the apoptotic execution molecule caspase-3 was significantly upregulated after Rg3 treatment, suggesting that Rg3 may actively induce the programmed death of over-proliferating vocal cord scar fibroblasts by activating the caspase-3-dependent apoptotic pathway. Furthermore, the regulatory effect of Rg3 on collagen metabolism is particularly significant. The study found that treatment with Rg3 significantly reduced the expression levels of Col I and Col III, which are the main ECM components that are excessively deposited in the vocal cord scar tissue. By inhibiting the synthesis of these key collagen molecules, Rg3 effectively alleviated the excessive deposition of the extracellular matrix, which is crucial for restoring the normal structure and vibration characteristics of the vocal cord.

The results of this study indicate that ginsenoside Rg3 exerts dual regulatory effects on HVFSFs, providing important insights into its therapeutic mechanism. Firstly, Rg3 dose-dependently inhibited HVFSFs proliferation and significantly promoted cell apoptosis. The caspase (cysteine-dependent aspartate-directed protease) family serves as a core component of apoptotic signaling pathways, with caspase-3 regarded as the key executioner of apoptosis; its activation marks an irreversible commitment to cell death.[16] Western blot and qPCR analyses confirmed that caspase-3 expression was significantly upregulated following Rg3 treatment, suggesting that Rg3 may actively induce programmed cell death in over-proliferating vocal fold scar fibroblasts through activation of the caspase-3-dependent apoptotic pathway. Furthermore, the regulatory effect of Rg3 on collagen metabolism is particularly noteworthy. Rg3 treatment significantly reduced the expression levels of Col I and Col III, which are the main ECM components excessively deposited in vocal fold scar tissue. By inhibiting the synthesis of these key collagen molecules, Rg3 effectively alleviated excessive ECM deposition, which is crucial for restoring the normal structural architecture and vibratory characteristics of the vocal folds.

Although this discussion focuses on the caspase-3 pathway, intracellular signaling networks are complex and highly interconnected. Caspase-3 activation is frequently regulated by multiple upstream signaling pathways, including Bcl-2 family proteins[17] (modulating the mitochondrial apoptosis pathway) and the Fas/FasL system [18] (regulating the death receptor-mediated apoptosis pathway). Concurrently, Rg3 may exert anti-fibrotic effects synergistically with caspase-3 pathway activation by modulating other classical fibrosis-related pathways, such as TGF-β/Smad,[14] MAPK (mitogen-activated protein kinase),[12,19] and PI3K/Akt (phosphatidylinositol 3-kinase/protein kinase B).[20-22] For instance, Rg3 may inhibit TGF-β1 expression or receptor activation, thereby attenuating pro-fibrotic signaling[23] - an effect that may occur independently of or in synergy with its pro-apoptotic actions. Future studies should comprehensively elucidate the complete signaling network through which Rg3 exerts its effects in HVFSFs.

Conclusion

In conclusion, our findings highlight ginsenoside Rg3 as a promising candidate for anti-fibrotic therapy in vocal fold scarring, given its dual ability to induce fibroblast apoptosis and suppress pathological collagen deposition. Further in vivo studies and clinical trials are warranted to validate its therapeutic potential.

Acknowledgements

This work was supported by the Yichang Medical and Health Research Project(A23-1-024)

Author Contributions

Conceived and designed the experiments: Jun Liu, Long Zhang. Performed the experiments: Yan Qin, Kang Wang, Zhi-Mao Zhang. Analyzed the data: Ting Wu. Contributed reagents/materials/analysis tools: Kang Wang, Zhi-Mao Zhang, Wu Ting. Writing the paper: Yan Qin, Jun Liu, Long Zhang.

References

1. Yang Y, Xu X, Zhuang P. Explore the Pattern of Biomechanical Alterations in Vocal Fold Scar and Its Objective Quantitative Assessment Method. J Voice. 2024 Jul 24:S0892-1997(24)00212-1. doi: 10.1016/j.jvoice.2024.07.003. Epub ahead of print. PMID: 39054187.
2. Miura R, Matsuzaki H, Suzuki H, Makiyama K, Oshima T. Effect of a Single Injection of Basic Fibroblast Growth Factor into the Vocal Folds: A 36-Month Clinical Study. J Voice. 2023 May;37(3):444-451. doi: 10.1016/j.jvoice.2021.01.015. Epub 2021 Feb 9. PMID: 33573843.
3. Vontela S, Balouch B, Bress E, Brennan MJ, Alnouri G, Martha VV, Sataloff RT. Vocal Fold Paresis and Voice Outcomes following Vocal Fold Mass Excision. J Voice. 2024 Jan;38(1):225-230. doi: 10.1016/j.jvoice.2021.07.014. Epub

2021 Aug 30. PMID: 34474936.
4. Kang HT, Park KN, Lee SW. Regenerative Effect of a 532-nm Diode Laser on Vocal Fold Scar in a Rabbit Model. J Voice. 2026 Jan;40(1):160-166. doi: 10.1016/j.jvoice.2023.09.004. Epub 2023 Oct 29. PMID: 37903688.
5. Svistushkin MV, Kotova S, Shpichka A, Starostina S, Shekhter A, Bikmulina P, Nikiforova A, Zolotova A, Royuk V, Kochetkov PA, Timashev S, Fomin V, Vosough M, Svistushkin V, Timashev P. Stem cell therapy for vocal fold regeneration after scarring: a review of experimental approaches. Stem Cell Res Ther. 2022 May 3;13(1):176. doi: 10.1186/s13287-022-02853-9. PMID: 35505357; PMCID: PMC9066721.
6. John M, Nabizath A, Krishnakumar S, Menon U, Menon D, Nair M. Injectable Tissue Adhesive Microgel Composite Containing Antifibrotic Drug for Vocal Fold Scarring. ACS Appl Bio Mater. 2024 Aug 19;7(8):5237-5246. doi: 10.1021/acsabm.4c00422. Epub 2024 Jul 15. PMID: 39007499.
7. Pierce JL, Olson B, Merrill RM, Pierce J, Isom A, Torrecillas V, McCrary H, Aylward A, Smith ME, Ben Christensen M. Amniotic Fluid as a Potential Treatment for Vocal Fold Scar in a Rabbit Model. J Voice. 2025 Jan 3:S0892-1997(24)00445-4. doi: 10.1016/j.jvoice.2024.12.015. Epub ahead of print. PMID: 39755523.
8. Halder N, Perkerson R, Kanekiyo T, Rutt AL. Compatibility of Hepatocyte Growth Factor, Adipose-Derived Mesenchymal Stem Cells, and Dermal Fillers for the Treatment of Vocal Fold Scar. Stem Cell Rev Rep. 2025 May;21(4):1131-1133. doi: 10.1007/s12015-025-10862-3. Epub 2025 Feb 28. PMID: 40019729.
9. Wu L, Bai L, Dai W, Wu Y, Xi P, Zhang J, Zheng L. Ginsenoside Rg3: A Review of its Anticancer Mechanisms and Potential Therapeutic Applications. Curr Top Med Chem. 2024;24(10):869-884. doi: 10.2174/1115680266283661240226052054. PMID: 38441023.
10. Yao ZW, Zhu H. Pharmacological mechanisms and drug delivery systems of ginsenoside Rg3: A comprehensive review. Pharmacol Res. 2025 Jun;216:107799. doi: 10.1016/j.phrs.2025.107799. Epub 2025 May 23. PMID: 40414584.
11. Tian ZF, Hu RY, Wang Z, Wang YJ, Li W. Molecular mechanisms behind the inhibitory effects of ginsenoside Rg3 on hepatic fibrosis: a review. Arch Toxicol. 2025 Feb;99(2):541-561. doi: 10.1007/s00204-024-03941-w. Epub 2024 Dec 27. PMID: 39729114.
12. Chen Y, Peng Y, Li P, Jiang Y, Song D. Ginsenoside Rg3 induces mesangial cells proliferation and attenuates apoptosis by miR-216a-5p/MAPK pathway in diabetic kidney disease. Aging (Albany NY). 2024 Jun 7;16(11):9933-9943. doi: 10.18632/aging.205907. Epub 2024 Jun 7. PMID: 38850526; PMCID: PMC11210261.
13. Yun E, Kwon BS, Kim J, Lee A. Ginsenoside Rg3 attenuates pulmonary fibrosis by inhibiting endothelial to mesenchymal transition. Anim Cells Syst (Seoul). 2023 Aug 4;27(1):159-170. doi: 10.1080/19768354.2023.2244549. PMID: 37554358; PMCID: PMC10405771.
14. Tang M, Bian W, Cheng L, Zhang L, Jin R, Wang W, Zhang Y. Ginsenoside Rg3 inhibits keloid fibroblast proliferation, angiogenesis and collagen synthesis in vitro via the TGFβ/Smad and ERK signaling pathways. Int J Mol Med. 2018 Mar;41(3):1487-1499. doi: 10.3892/ijmm.2018.3362. Epub 2018 Jan 4. PMID: 29328420; PMCID: PMC5819908.
15. Naba A. Mechanisms of assembly and remodelling of the extracellular matrix. Nat Rev Mol Cell Biol. 2024 Nov;25(11):865-885. doi: 10.1038/s41580-024-00767-3. Epub 2024 Sep 2. PMID: 39223427; PMCID: PMC11931590.
16. Eskandari E, Eaves CJ. Paradoxical roles of caspase-3 in regulating cell survival, proliferation, and tumorigenesis. J Cell Biol. 2022 Jun 6;221(6):e202201159. doi: 10.1083/jcb.202201159. Epub 2022 May 12. PMID: 35551578; PMCID: PMC9106709.
17. Liang Z, Chen Y, Gu R, Guo Q, Nie X. Asiaticoside Prevents Oxidative Stress and Apoptosis in Endothelial Cells by Activating ROS-dependent p53/Bcl-2/Caspase-3 Signaling Pathway. Curr Mol Med. 2023;23(10):1116-1129. doi: 10.2174/1566524023666221024120825. PMID: 36284389.
18. Wang Z, Tan Y, Xu F. Zonisamide improves Fas/FasL-mediated apoptosis and inflammation in a degenerative cervical myelopathy rat model. Tissue Cell. 2023 Apr;81:102024. doi: 10.1016/j.tice.2023.102024. Epub 2023 Jan 13. PMID: 36669388.
19. Choi RJ, Mohamad Zobir SZ, Alexander-Dann B, Sharma N, Ma MKL, Lam BYH, Yeo GSH, Zhang W, Fan TP, Bender A. Combination of Ginsenosides Rb2 and Rg3 Promotes Angiogenic Phenotype of Human Endothelial Cells via PI3K/Akt and MAPK/ERK Pathways. Front Pharmacol. 2021 Feb 10;12:618773. doi: 10.3389/fphar.2021.618773. PMID: 33643049; PMCID: PMC7902932.
20. Wan J, Cheng W, Xing X, He Y, Tang P, Feng Y, Liu S, Lu X, Zhong L. A SERS-Based Dual-Parameter Monitoring Nanoprobe of ROS and PI3K/Akt during Ginsenoside Rg3-Induced Cell Apoptosis. Biosensors (Basel). 2023 Jan 31;13(2):212. doi: 10.3390/bios13020212. PMID: 36831977; PMCID: PMC9953484.
21. Tao D, Li F, Zhang X, Guo H, Yang R, Yang Y, Zhang L, Shen Z, Teng J, Chen P, He B. 20(R)-ginsenoside Rg3 protects against focal cerebral ischemia–reperfusion injury by suppressing autophagy via PI3K/Akt/mTOR signaling pathway. Neuropharmacology. 2025 Feb 1;263:110226. doi: 10.1016/j.neuropharm.2024.110226. Epub 2024 Nov 16. PMID: 39557153.
22. Wang X, He R, Geng L, Yuan J, Fan H. Ginsenoside Rg3 Alleviates Cisplatin Resistance of Gastric Cancer Cells Through Inhibiting SOX2 and the PI3K/Akt/mTOR Signaling Axis by Up-Regulating miR-429. Front Genet. 2022 Mar 3;13:823182. doi: 10.3389/fgene.2022.823182. PMID: 35309116; PMCID: PMC8927288.
23. Xu H, Miao H, Chen G, Zhang G, Hua Y, Wu Y, Xu T, Han X, Hu C, Pang M, Tan L, Liu B, Zhou Y. 20(S)-ginsenoside Rg3 exerts anti-fibrotic effect after myocardial infarction by alleviation of fibroblasts proliferation and collagen deposition through TGFBR1 signaling pathways. J Ginseng Res. 2023 Nov;47(6):743-754. doi: 10.1016/j.jgr.2023.06.007. Epub 2023 Jul 3. PMID: 38107395; PMCID: PMC10721484.

***Corresponding author:** *Jun Liu. Department of Otorhinolaryngology Head and Neck Surgery, Yichang Central People's Hospital, The First College of Clinical Medical Science, China Three Gorges University. No.183 Yiling Avenue, Yichang City, Hubei Province, China. 443003. E-mail: dsgxliujun@163.com.*

International Journal of Biomedicine 16(3) (2026) 378-382
http://dx.doi.org/10.21103/Article16(3)_OA8

ORIGINAL ARTICLE

INTERNATIONAL JOURNAL OF BIOMEDICINE

Digital Platform for the Prediction of 3D Visual and 3D Ultrastructural Morphology of the Urinary Tract

Boris A. Berdichevskiy[1], Grigory V. Zubik

Tyumen State Medical University, Ministry of Health of the Russian Federation, Tyumen, Russia

Abstract

Background: Inflammatory diseases of the urinary system remain a significant clinical challenge in urology, and current diagnostic methods are limited in their ability to assess morphological and functional changes at the molecular and ultrastructural levels. The development of comprehensive digital tools integrating functional imaging with ultrastructural analysis is necessary to improve diagnosis and monitoring.

Methods and Results: This pilot study included 8 patients divided into two groups: inflammatory kidney diseases (n=4) and bladder inflammation (n=4). Data from PET/CT scans using ^{18}F-FDG and ^{11}C-choline were integrated with 3D anatomical reconstruction and 3D ultrastructural analysis performed by scanning and transmission electron microscopy. A clear relationship was established between the SUVmax of radiopharmaceuticals and the 3D anatomical and 3D ultrastructural changes reflecting bacterial inflammation activity. Clinical navigation schemes were developed enabling physicians to retrospectively assess the probable 3D visual and ultrastructural state of the urinary system using digital PET/CT indicators.(**International Journal of Biomedicine. 2026;16(3):378-382.**)

Keywords: digital imaging • PET/CT • scanning electron microscopy • urinary tract inflammation

For citation: Berdichevskiy BA, Zubik GV. Digital Platform for the Prediction of 3D Visual and 3D Ultrastructural Morphology of the Urinary Tract. International Journal of Biomedicine. 2026;16(3):378-382. doi:10.21103/Article16(3)_OA8

Introduction

Inflammatory diseases of the urinary system remain among the most prevalent and clinically significant challenges in urology.[1–3] Despite a broad spectrum of available diagnostic modalities—including laboratory testing, ultrasonography, computed tomography (CT), and magnetic resonance imaging (MRI)—accurate quantitative and qualitative assessment of morphological and functional changes at the molecular and ultrastructural levels remains a considerable challenge for the practicing clinician.[4] The limited resolution of conventional imaging technologies and the lack of an integrated analytical approach diminish the effectiveness of early detection of pathological alterations and longitudinal monitoring of inflammatory disease activity.[5] Over the past decades, the advent of whole-body positron emission tomography/computed tomography (PET/CT) has opened new avenues for evaluating the metabolic activity of inflammatory processes in the kidneys and urinary bladder.[6,7] However, in routine clinical practice, the functional information provided by PET/CT is predominantly used to detect neoplastic pathologies, whereas the interpretation of inflammation-related changes in scanned organs remains insufficiently developed.[8–11] Contemporary three-dimensional (3D) reconstruction techniques, based on high-precision data from advanced and resource-intensive research modalities, enable the acquisition of detailed ultrastructural images of pathological alterations. This capability is critically important for a deeper understanding of the pathogenesis of inflammatory processes and for the accurate assessment of their activity.[12–15] In this context, multidisciplinary approaches that combine functional and ultrastructural 3D visualization are of considerable interest. One such approach is the integration of PET/CT diagnostic data with findings from ultrastructural and clinical investigations. [16-17] Given the growing demand for personalized medicine and precision diagnostics in inflammatory diseases, there is a pressing need to develop digital analytical platforms. Such platforms would enable clinicians—without requiring in-depth expertise in nuclear medicine, 3D technologies, or electron microscopy—to rapidly and reliably assess the 3D visual and 3D ultrastructural state of the kidneys and urinary bladder based on standardized uptake values (SUV) of radiopharmaceuticals.

Therefore, the development and implementation of a digital analytical platform will not only improve the accuracy of diagnosis and monitoring of inflammatory processes but also lay the groundwork for the creation of novel clinical navigation algorithms, ultimately enhancing treatment efficacy and patient quality of life.

Objective

This study aimed to develop a digital analytical platform capable of retrospectively assessing, based on whole-body PET/CT digital data, the probable 3D visual and 3D ultrastructural state of urinary system organs in patients with inflammatory diseases of the kidneys and urinary bladder.

Materials and Methods

Study Design and Patient Population

This pilot study was based on the results of a comprehensive examination of eight patients treated at the Urology Department of the Tyumen Regional Clinical Hospital No. 2 between 2020 and 2023. The study was conducted in accordance with the Declaration of Helsinki and approved by the institutional ethics committee. All participants provided written informed consent.

Group 1 comprised three women and one man, with a median age of 39.5 years (range: 28–42), who had undergone nephrectomy for the following indications: acute purulent pyelonephritis with multiple parenchymal carbuncles (n=1), chronic pyelonephritis resulting in malignant nephrogenic hypertension with a preserved contralateral kidney (n=1), and a non-functioning, secondarily shrunken pyelonephritic kidney (n=2). The inclusion criteria were as follows: a history of nephrectomy for one of the specified diagnoses, whole-body ^{18}F-FDG PET/CT performed before surgery, age over 18 years, and provision of informed consent. Exclusion criteria included: an unverified diagnosis underlying the nephrectomy, the presence of renal or urinary tract malignancy, and severe decompensated comorbidities.

In the first case, ^{18}F-FDG PET/CT was performed to investigate a potential oncological cause of fever of unknown origin; in the remaining three cases, the scan was undertaken to exclude oncological causes of persistent isolated urinary syndrome with microhematuria. For comparative analysis, we used whole-body ^{18}F-FDG PET/CT images from Patient I., a 42-year-old male with no nephrourological history, and ultrastructural examination data of a kidney specimen from Patient A., a 38-year-old male without nephrourological history, whose kidney was removed due to traumatic avulsion from the renal pedicle.

For each case in the study group, 3D anatomical reconstruction of the sectional renal anatomy was generated from the post-nephrectomy gross specimen using our proprietary computer software. Concurrently, 3D ultrastructural reconstruction of all nephron elements within a single integrated block was performed based on transmission electron microscopy (TEM) at ×10,000 magnification.

Group 2 consisted of three women and one man, with a median age of 41.5 years (range: 30–45), who presented with inflammatory diseases of the urinary bladder. All had previously undergone ^{11}C-choline PET/CT to rule out oncological causes of persistent isolated urinary syndrome with microhematuria. During hospitalization, all patients underwent cystoscopy with targeted biopsy under general anesthesia. For comparative analysis, we used whole-body ^{11}C-choline PET/CT images from Patient M., a 42-year-old female with no nephrourological history, and ultrastructural findings from the bladder wall of Patient Sh., a 29-year-old male without nephrourological history, whose tissue was obtained during surgical debridement and closure of a traumatic bladder rupture.

For each case in Group 2, 3D visual reconstruction of the bladder mucosa was generated from the cystoscopic findings using our proprietary computer software. Additionally, 3D ultrastructural reconstruction of all bladder wall elements within a single integrated block was performed based on scanning electron microscopy (SEM) at ×6,000 magnification.

PET/CT Imaging

Whole-body PET/CT was performed according to a standard protocol using a Biograph PET/CT scanner (Siemens, Germany) installed at the Radiology Center of the Tyumen Regional Oncology Center. Functional changes in the renal parenchyma and bladder wall were evaluated based on tissue affinity for the radiopharmaceuticals. Regions of interest were analyzed automatically for standardized uptake values (SUV) in minimal (SUVmin), average (SUVavg), and maximal (SUVmax) ranges within comparable tissue volumes (cm^3). Radiopharmaceuticals were synthesized on-site using a compact cyclotron (Scanditronix, Sweden).

Electron Microscopy

Scanning electron microscopy (SEM) was performed at the Tyumen Scientific Center, Siberian Branch of the Russian Academy of Sciences, using a Hitachi High-Tech SU3800/SU3900 scanning electron microscope (Japan). Transmission electron microscopy (TEM) was employed for ultrastructural analysis of nephron elements at ×10,000 magnification, while SEM was utilized for 3D ultrastructural reconstruction of bladder wall elements at ×6,000 magnification.

Integrated Data Analysis

Based on the results of high-technology and research-intensive investigations, we assessed the relationship between the maximal standardized uptake value (SUVmax), obtained non-invasively by PET/CT, and the characteristic 3D visual and 3D ultrastructural tissue manifestations of pathology, obtained invasively by scanning and transmission electron microscopy.

Results

The comprehensive investigations conducted in this pilot study established a clear relationship among patients with renal pathology between the standardized uptake value of ^{18}F-FDG (SUVmax) in the renal parenchyma, the corresponding 3D anatomical features of sectional kidney anatomy, and the 3D ultrastructural state of all nephron elements within a single integrated block, reflecting varying degrees of bacterial inflammatory activity.

The assessment of the 3D ultrastructural state of the nephron was based on the visual analysis of the following parameters: podocyte size, organelle density within the podocyte, the condition of the basement membrane, the

presence of pathological contents within the urinary space, and the structural integrity of the proximal and distal tubules (Figure 1).

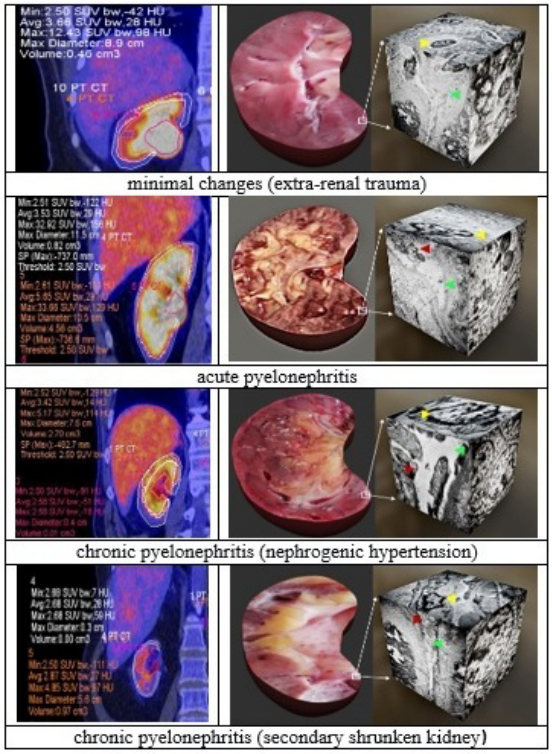

Figure 1. *Correlation of SUVmax values with the anatomical 3D reconstruction of the renal parenchyma and the segmented ultrastructural 3D reconstruction of the nephron.*

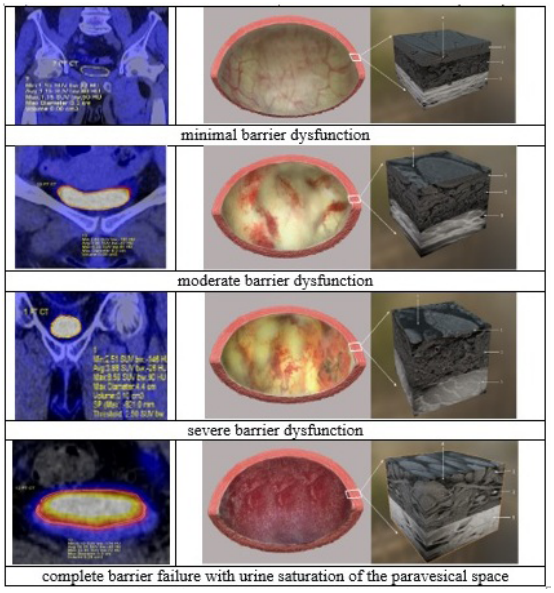

Figure 2. *Correlation of SUVmax values with the 3D cystoscopic view and the 3D ultrastructural condition of the bladder wall within a single integrated block.*

In Group 2, we analyzed a possible relationship between the SUVmax of ^{11}C-choline uptake in the bladder wall, the 3D cystoscopic appearance, and the 3D ultrastructural manifestations of impaired bladder barrier function, which leads to the saturation of the bladder wall layers with urine containing ^{11}C-choline. By assessing visual changes in cell size, the structural organization of superficial urothelial cells, and the presence and width of intercellular spaces, we evaluated the likelihood of urine penetration—containing not only ^{11}C-choline but also toxic peroxide enzymes and oxygen free radicals—into the deeper layers of the bladder wall (Figure 2).

Based on the relationships identified from multilevel imaging, we developed a clinical navigation scheme for practicing urologists. Using this scheme, a urologist—without specialized expertise in nuclear medicine or 3D ultrastructural analysis—can retrospectively determine, by referencing the affinity of the renal parenchyma for ^{18}F-FDG (SUVmax), the probable 3D anatomical state of the renal parenchyma and the 3D ultrastructural changes in all nephron elements within a single integrated block characteristic of bacterial inflammation at ×10,000 magnification (Figure 3).

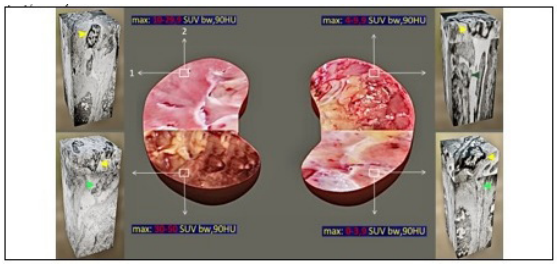

Figure 3. *Clinical navigation scheme of the probable 3D ultrastructural state of the nephron at 10,000× magnification and the 3D anatomical structure of the renal parenchyma based on the digital PET/CT standardized uptake value (SUV) of 18F-FDG.*

A similar clinical navigation scheme was developed to assess the likelihood of impaired bladder barrier function as one cause of recurrent cystitis. Using this scheme, a physician without specialized training in nuclear medicine or ultrastructural research methods can retrospectively determine, based on the digital values of bladder wall affinity for ^{11}C-choline, the probable 3D cystoscopic appearance and the 3D ultrastructural state of all bladder wall elements within a single integrated block (Figure 4).

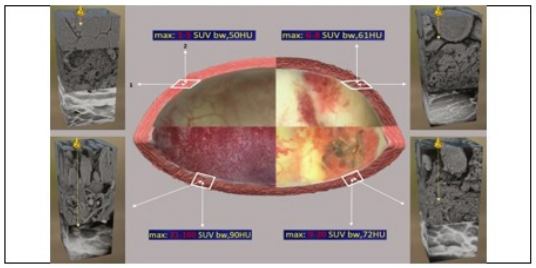

Figure 4. *Clinical navigation scheme of the probable 3D cystoscopic view of the mucosa and the 3D ultrastructural condition of the bladder wall's barrier functions at 6000× magnification, based on the digital standardized uptake value (SUV) of 11C-choline from PET/CT results.*

Discussion

This pilot study, which investigated the PET/CT-based molecular, cellular, and ultrastructural characteristics of the renal parenchyma and bladder wall elements, resulted in the development of a digital analytical platform. This platform enables the modeling of the probable 3D visual appearance and 3D ultrastructural state of the urinary system organs in the setting of inflammatory diseases, using data from ^{18}F-FDG and ^{11}C-choline PET/CT. The findings indicate a close relationship between the standardized uptake values of the radiopharmaceuticals (SUVmax) and the 3D ultrastructural manifestations of inflammation in both the renal parenchyma and the bladder wall.

Specifically, varying degrees of bacterial inflammatory activity within the renal parenchyma were associated with distinct changes in the digital SUVmax values for ^{18}F-FDG, which correlated with the severity of structural alterations in the nephron—the fundamental functional unit of the kidney. In the context of clinical and laboratory manifestations of bacterial cystitis, the digital SUVmax value for ^{11}C-choline reflected the integrity of the bladder's barrier function, specifically its capacity to prevent toxic urinary products—including enzymes, peroxides, and free radicals—from penetrating the deeper layers of the bladder wall.

These data support the feasibility and clinical relevance of integrating functional imaging with multilevel morphological analysis. The multidisciplinary approach implemented within our developed digital platform enhances the understanding of the pathogenesis of inflammatory diseases, which is essential for accurate diagnosis and monitoring and cannot be achieved by other currently available examination methods. This is particularly pertinent given the increasing demand for integrating digital technologies and artificial intelligence into routine clinical practice, ultimately contributing to improved clinical outcomes and enhanced quality of life for our patients.

Study Limitations

The present study has several limitations. This is a pilot investigation, and further research is required before widespread clinical implementation can be considered. An additional limitation is the absence of a comprehensive statistical analysis. A significant practical limitation at present is the high cost and limited availability of PET/CT imaging. Consequently, the results presented herein should be regarded as preliminary and require validation in larger studies with expanded sample sizes, a comparative design, and robust statistical analysis.

Conclusion

In this pilot study, we developed a digital analytical platform that enables the assessment of the probable 3D visual and 3D ultrastructural state of the urinary system organs in the setting of urological inflammatory diseases, based on PET/CT tissue affinity values for radiopharmaceuticals. The proposed clinical navigation schemes allow urologists to model, in an accessible and intuitive format, the probable condition of the kidneys and urinary bladder without the need for resource-intensive, high-technology investigations, thereby facilitating more accurate diagnosis and personalized treatment.

The limitations and shortcomings of our work are related to the pilot nature of the study, and larger-scale clinical investigations are required to confirm the efficacy of the proposed approach definitively.

Conflict of Interest

The authors have declared no conflict of interest.

Author Contributions

Boris A. Berdichevskiy: Conceptualization, Methodology, Supervision, Project administration, Writing – review & editing.
Grigory V. Zubik: Investigation, Data curation, Formal analysis, Software, Writing – original draft.
All authors have read and approved the final version of the manuscript.

References

1. Tandogdu Z, Wagenlehner FM. Global epidemiology of urinary tract infections. Curr Opin Infect Dis. 2016 Feb;29(1):73-9. doi: 10.1097/QCO.0000000000000228. PMID: 26694621.
2. Öztürk R, Murt A. Epidemiology of urological infections: a global burden. World J Urol. 2020 Nov;38(11):2669-2679. doi: 10.1007/s00345-019-03071-4. Epub 2020 Jan 10. PMID: 31925549.
3. Johnson JR, Russo TA. Acute Pyelonephritis in Adults. N Engl J Med. 2018 Jan 4;378(1):48-59. doi: 10.1056/nejmcp1702758. Erratum in: N Engl J Med. 2018 Mar 15;378(11):1069. doi: 10.1056/NEJMx180009. PMID: 29298155.
4. Dubbs SB, Sommerkamp SK. Evaluation and Management of Urinary Tract Infection in the Emergency Department. Emerg Med Clin North Am. 2019 Nov;37(4):707-723. doi: 10.1016/j.emc.2019.07.007. Epub 2019 Aug 19. PMID: 31563203.
5. Hanssen O, Lovinfosse P, Weekers L, Hustinx R, Jouret F. La tomographie par émission de positons au 18F-FDG en pathologie rénale non oncologique : indications actuelles et perspectives [^{18}F-FDG positron emission tomography in non-oncological renal pathology: Current indications and perspectives]. Nephrol Ther. 2019 Nov;15(6):430-438. French. doi: 10.1016/j.nephro.2018.11.007. Epub 2019 Apr 11. PMID: 30982747.
6. Solav S, Savale S, Patil AM. Localization of acute pyelonephritis in pyrexia of unknown origin using FDG PET/CT. Asia Ocean J Nucl Med Biol. 2020 Winter;8(1):79-83. doi: 10.22038/aojnmb.2019.14242. PMID: 32064288; PMCID: PMC6994777.
7. Dondi F, Pisani AR, Lucarelli NM, Gazzilli M, Talin A, Albano D, Rubini D, Maggialetti N, Rubini G, Bertagna F. Correlation between Kidney Uptake at [18F]FDG PET/

CT and Renal Function. J Pers Med. 2023 Dec 28;14(1):40. doi: 10.3390/jpm14010040. PMID: 38248741; PMCID: PMC10817585.
8. Berdichevsky B A, Berdichevsky V B, Sapozhevnikova E V, Pavlova I V, Boldyrev A L, Gonyaev A R, Korabelnikov M A, Zubik G V. [PET/CT MOLECULAR CELL IMAGING OF ACUTE PYELONEPHRITIS IN THE DIAGNOSIS OF FEVER OF UNKNOWN ORIGIN]. Urologiia. 2024 Sep;(4):75-80. Russian. PMID: 39563587.
9. Moghrabi S, Abdlkadir AS, Al-Hajaj N, Gnanasegaran G, Kumar R, Syed G, Bozkurt MF, Shukri S, Obeidat S, Khalaf A, Shahait M, Al-Nabhani K, Al-Ibraheem A. A New Era for PET/CT: Applications in Non-Tumorous Renal Pathologies. J Clin Med. 2024 Aug 7;13(16):4632. doi: 10.3390/jcm13164632. PMID: 39200774; PMCID: PMC11355182.
10. Peng Z, Shan H, Yang X, Li S, Tang D, Cao Y, Shao Q, Huo W, Yang Z. Weakly supervised learning-based 3D bladder reconstruction from 2D ultrasound images for bladder volume measurement. Med Phys. 2024 Feb;51(2):1277-1288. doi: 10.1002/mp.16638. Epub 2023 Jul 24. PMID: 37486288.
11. Miyaki T, Kawasaki Y, Hosoyamada Y, Amari T, Kinoshita M, Matsuda H, Kakuta S, Sakai T, Ichimura K. Three-dimensional imaging of podocyte ultrastructure using FE-SEM and FIB-SEM tomography. Cell Tissue Res. 2020 Feb;379(2):245-254. doi: 10.1007/s00441-019-03118-3. Epub 2019 Nov 22. PMID: 31758252.
12. Zhai XY, Birn H, Jensen KB, Thomsen JS, Andreasen A, Christensen EI. Digital three-dimensional reconstruction and ultrastructure of the mouse proximal tubule. J Am Soc Nephrol. 2003 Mar;14(3):611-9. doi: 10.1097/01.asn.0000051725.00406.0c. PMID: 12595496.
13. Amparore D, Pecoraro A, Piramide F, Verri P, Checcucci E, De Cillis S, Piana A, Burgio M, Di Dio M, Manfredi M, Fiori C, Porpiglia F. Three-dimensional imaging reconstruction of the kidney's anatomy for a tailored minimally invasive partial nephrectomy: A pilot study. Asian J Urol. 2022 Jul;9(3):263-271. doi: 10.1016/j.ajur.2022.06.003. Epub 2022 Jun 20. PMID: 36035345; PMCID: PMC9399544.
14. Ademola BL, Atanda AT, Aji SA, Abdu A. Clinical, morphologic and histological features of chronic pyelonephritis: An 8-year review. Niger Postgrad Med J. 2020 Jan-Mar;27(1):37-41. doi: 10.4103/npmj.npmj_109_19. PMID: 32003360.
15. Limkar AR, Sharma SM, Ricke WA. High-resolution ex vivo nanoCT reveals 3D architecture of the adult male mouse lower urogenital tract. PLoS One. 2025 Sep 18;20(9):e0326004. doi: 10.1371/journal.pone.0326004. PMID: 40966215; PMCID: PMC12445489.
16. Berdichevskiy BA, Zubik GV, et al. Method for diagnosing the state of renal parenchyma after nephrectomy based on ultrastructural 3D visualization of nephron elements in a single integrated block. Russian Federation Patent No. 2861061 C1. Filed: May 16, 2025; Published: April 28, 2026.
17. Berdichevskiy BA, Zubik GV, et al. Method for block 3D visualization of the bladder urothelial barrier state. Russian Federation Patent No. 2860636 C1. Filed: March 5, 2025; Published: April 21, 2026.

Corresponding author: *Professor Boris A. Berdichevsky, Dr. Sci., Department of Pediatric Surgery with the Course of Urology and Andrology, Tyumen State Medical University, Tyumen, Russia. E-mail: doktor_bba@mail.ru*

International Journal of Biomedicine 16(3) (2026) 383-387
http://dx.doi.org/10.21103/Article16(3)_OA9

ORIGINAL ARTICLE

INTERNATIONAL JOURNAL OF BIOMEDICINE

Impact of Magnets Inserted into Overdentures on the Periodontal Indices

Snežana V. Brković[1], Srđan D. Poštić[1], Veljko D. Ilić[2], Branimir D. Stošić [3,4], Pavle D. Ilić[5]

[1]*Clinic of Dental Prosthetic, University School of Dental Medicine, University of Belgrade, Belgrade, Serbia*
[2]*General and Oral Histology and Embriology, University School of Dental Medicine, University of Belgrade, Belgrade, Serbia*
[3]*Endodontics, University of Travnik, Faculty of Pharmacy and Health, Travnik, Federation of Bosnia and Hercegovina*
[4]*Šabac Health Center, Šabac, Serbia*
[5]*University of Belgrade, University School of Dental Medicine, Belgrade, Serbia*

Abstract

Background: Preserving teeth with compromised periodontal support when using tooth-supported removable dentures (overdentures—ODs) presents challenges related to periodontal tissue condition and denture retention.
The aim of the study was to assess the effects of inserting magnets into the OD base on periodontal tissue indices around abutment teeth (AT) beneath ODs.
Methods and Results: The 136 vital canines/premolars were included in the study. Experimental group (EG) involved 48 partially edentulous patients with 96 AT's in lower jaw while upper had complete denture, assuming subgroups: A) split mouth samples of 24 patients/24 teeth with magnets inserted in denture base around AT on one jaw side, while the contralateral side presented by 24 AT without magnets; B) 24 patients in whom magnets were placed around 48 AT on both sides of a mandibular OD. The control group comprised 20 individuals with healthy dental arches, each with one pair of canines/premolars (a total of 40 teeth). All patients were followed for one year, with the assessment of the plaque index (PI; Silness & Loe) and the gingival index (GI; Loe & Silness). Significant decrease of PI and GI values was noted in the EG subgroup B between the base time point [PI = 0.875 (0.4687-1.0312), GI =1.000 (0.359-1.578)] and 12 months recall (PI = 0.375 (0.2500-0.7500), GI = 0.750 (0.187-1.156)] ($P < 0.01$ in both cases).
Conclusion: The inserted magnets of OD significantly improved PI and GI values around experimental abutment teeth after 12 months. (**International Journal of Biomedicine. 2026;16(3):383-387.**)

Keywords: overdenture • magnet • plaque index • gingival index • long-term study

For citation: Brković SV , Poštić SD , Ilić VD[2], Stošić BD, Ilić PD. Impact of Magnets Inserted into Overdentures on the Periodontal Indices. International Journal of Biomedicine. 2026;16(3):383-387. doi:10.21103/Article16(3)_OA9

Introduction

The acrylic resin overdenture (OD) prosthesis is an appropriate treatment for partially edentulous patients who have a small number of remaining teeth with poor periodontal prognosis.[1] The remaining teeth for OD must be adequately prepared to achieve better adhesion than with conventional dentures.[2,3] The additional retention for OD is nowadays achieved by dental implants as the standard protocol in prosthetic rehabilitation. Furthermore, remaining teeth that are properly positioned and sufficiently stable can serve as abutments for telescopic (double) crowns, particularly when there is a high risk of osteoporosis.[4]Although ODs have been widely used, meaningful clinical problems are still related to the periodontal disease [5,6] as well as jaw osteoporosis.[7,8] With that in mind, some authors have attempted to apply a magnetic field (MF) to prevent alveolar bone loss after tooth extraction [5,9] a finding recently confirmed in bone and cartilage tissues.[10] The promising studies on the animal models [11-13] as well as human [14] regarding periodontal tissue preservation directed the aim of this study to measure the influence of MF on the periodontal health of abutment teeth (AT) under OD, comparing the

periodontal indices' values between abutment teeth with and without magnets. The null hypothesis was that periodontal tissues around teeth adjacent to magnets inserted into ODs have a periodontal health status similar to that of the control teeth (without magnets) beneath overdentures.

Materials and Methods

The Study Protocol

The 136 vital lower canines/premolars of patients were included in the study. Experimental group (EG) involved 48 subjects with maximally reduced tooth number, 96 abutment teeth overall, assuming two subgroups: A) split mouth samples of 24 patients/24 teeth with magnets inserted in denture base around AT on one jaw side, while the contralateral side presented by 24 AT without magnets; B) 24 patients in whom magnets were placed around 48 AT on both sides of a mandibular OD. The control group comprised 20 individuals with healthy dental arches, each with one pair of canines/premolars (a total of 40 teeth). All patients were followed for one year, with the assessment of the plaque index (PI; Silness & Loe) and the gingival index (GI; Loe & Silness).[15]

Before the study, patients were trained to follow an adequate oral hygiene regimen. This study included only lower canine/premolar abutments, which in EG showed poor periodontal status and reduced alveolar bone. Participants had to agree to wear the dentures continuously during the daytime and refrain from wearing them at night. All dentures were fabricated in the laboratory (Clinic of Dental Prosthetics, School of Dental Medicine, Belgrade University) by the same dental technicians using standardized materials and methodology. The measurements were taken by the same person (the first author of the study).

Magnets' Insertion into the Patient's Overdentures

Acupuncture micromagnets (AKMA R, Institute of Mihajlo Pupin, Belgrade, Serbia) were incorporated into the bases of the ODs (Fig 1) near the remaining AT with casting caps (Fig 2). All AT had metal copings that met the well-fitting criteria. Magnets were implanted at the beginning of the study. The used static magnet discs were spherical and consisted mostly of barium ferrite, with a concentrated magnetic flux density of 60 mT, attested by the Military Medical Academy, Belgrade (attest number: 1600-2/83). Magnet discs were plan-convex in shape, with a diameter of 3.0 mm and a height of 1.4mm. The subjects were assessed for periodontal health status to determine the PI and GI. According to the manufacturer's data (Mihajlo Pupun Institute), magnets exposed the biological homogeneous field with an effect of 5.0 mm along the axis and 8.0 mm to the sides. The plain surface of the magnet disc (south pole) was inward oriented, and the convex surface (north pole, i.e., therapeutic pole) outward to the gingival tissue. There would be no harmful magnetic influence due to the following of the International Commission on Non-Ionizing Radiation Protection (ICNIRP) parameters.[16] The index recordings were performed by the same operator at baseline and 12 months after magnet insertion. The PI value was measured after patients rinsed their mouths and dried (standard erythrosin disclosing tablets, Buttler Gum toothbrush, Sunstar Americas Inc., Chicago, USA). Dental plaque was detected by dental probe graded from 0 to 3 according to the following criteria: 0 - no dental plaque at the gingival third of the tooth crown; 1 - dental plaque present in very thin layers close to the gingival margin visible only by disclosing tablet; 2 - moderate presence of plaque in the gingival sulcus/pocket - visible by naked eye and 3 - large amount of dental plaque by completely saturated gingival sulcus/pocket and interdental space. The GI was characterized by the following values: 1 (0.1 to 1.0) - insignificant; 2 (1.1 to 2.0) - moderate, and 3 (2.1 to 3.0) - intensive gingival inflammation.

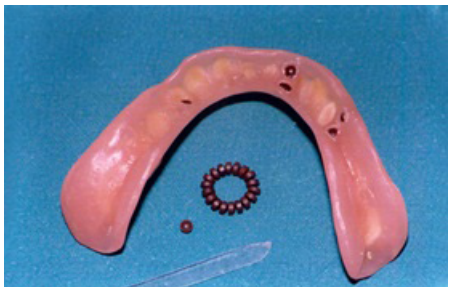

Fig. 1. *Suitable position of magnets in the OD base.*

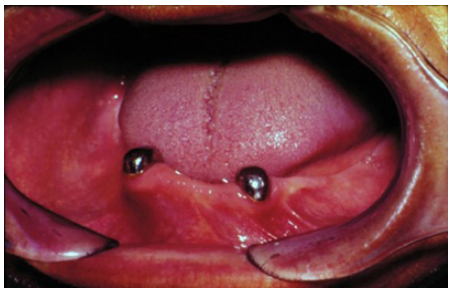

Fig. 2. *Abutment teeth prepared with casting caps.*

Statistical analysis was performed using SPSS Statistics for Windows, Version 11.5 (SPSS Inc., Chicago, IL). The results are presented as median (Me) and interquartile range (IQR [Q1; Q3]). A nonparametric repeated-measures ANOVA was used. A *P*-value <0.05 was considered statistically significant.

Results

PI values decreased significantly after 12 months in Subgroup B ($P<0.01$), but in Subgroup A, PI values increased insignificantly ($P>0.05$) (Table 1).

Table 1.

Plaque index values in the study subgroups at baseline and after 12 months.

	Baseline	12 months after	*P*-value
Subgroup A	0.632 (0.4531-1.2343)	0.687 (0.3125-0.9687)	>0.05
Subgroup B	0.875 (0.4687-1.0312)	0.375 (0.2500-0.7500)	<0.01

GI values showed similar changes. A statistically significant decrease after 12 months was observed in Subgroup B ($P<0.01$), whereas in Subgroup A, the PI value showed an insignificant increase ($P>0.05$) (Table 2).

Table 2.

Gingival index values in the study subgroups at baseline and after 12 months.

	Baseline	12 months after	*P*-value
Subgroup A	1.37 (1.118-1.625)	1.12 (0.687-1.484)	>0.05
Subgroup B	1.000 (0.359-1.578)	0.750 (0.187-1.156)	<0.01

Discussion

The study we conducted is somewhat unique, as it used the stated methodology of inserting magnets into the OD base and examining their effects on abutment tissues. Namely, the present study demonstrated that the magnetic field (MF) has a beneficial effect on periodontal tissues surrounding OD-worn teeth, as evidenced by more favorable PI and GI index values after 12 months in patients in whom magnets were placed around 48 AT on both sides of a mandibular OD. Thus, exposure to a constant MF has a positive effect on the two indicators of periodontal tissue status investigated. However, this improvement could be explained not only by the magnet›s influence but also by the combined effect of prior education on oral hygiene among the patients.

This study was inspired by the promising results of bioelectrical potential in bone tissue reported by Dr. Zachary Bert Friedenberg in 1966. Since then, many researchers have begun to examine the magnetic influence on various osteopathological entities.[14,17-19] ODs were chosen for this study instead of classical full /partial dentures due to their well-known positive effect on the periodontal tissue.[1-6] The encouragement of micromagnet implementation in the denture base led to positive results in our microbiological study, given its bacteriostatic effect.[20]

Due to the decrease in MF with distance to the third power ($1/r^3$), our magnet discs were inserted into the acrylic base as close as possible to the gingival tissue to achieve better results.

To the best of the authors' knowledge, this is the first study in the literature to investigate the influence of MF on periodontal health under OD. Thus, the results of the present study cannot be compared with those of similar studies. According to (WHO) standards [16] defined by ICNIRP, the MF obtained was classified as «safe» for human tissue treatments with no consequences for an indefinite period. Advantages of static over variable MF include easier control over a continuum, greater power stability, and no need for subject check-ups.

As the patients were highly motivated to preserve their remaining teeth, they eagerly accepted this treatment and underwent regular check-ups over the 12-month period. It is emphasized that there were no cases of fractured OD during the study, owing to the small dimensions of magnets precisely incorporated into the denture base. Dentures were fabricated at the University Clinic for Prosthodontics by the same person, a senior, very skilled technician, using conventional materials. This uniformity enabled a reliable statistical analysis of the data.

Low PI is explained by the reduction in microbes under MF in this study, as confirmed in our recent microbiological study.[20] Favorable GI under MF might be due to the accelerated metabolism of both inflamed and healthy tissues. Namely, the permeability of the cell membrane is increased, and so is cell metabolism.[11,22] More precisely, a beneficial bacteriostatic effect and improved vascularisation of tissues beneath the OD are also observed.

As the findings of the clinical periodontal indices/ tests were favorable, indicating improvement in PI and GI, the clinical procedure of this experiment, i.e., the insertion of magnets into OD, should be applied in everyday dental practice.

The results of some longitudinal [3,5] and our studies [19] should encourage investigators to apply MF in the oral environment and to use it for alveolar bone preservation for longer than one year, especially where remaining teeth are present. However, the literature suggests that magnets may not substitute for antibiotics in the treatment of bacterial infections in some dental treatments and adjunct periodontal surgery.

Moreover, we should keep in mind the upcoming technologies for measuring periodontal tissue load. Hence, the relatively new technique, the stereooptics method, was used to evaluate the resistance of periodontal supporting tissues around remaining teeth under OD. Namely, some authors used that model to study the distribution of occlusal stress on casts of a partially edentulous lower jaw with copings, yielding highly precise data using the digital image correlation method and ARAMIS software.[21]

Bearing in mind the huge increase in the use of implants under the overdenture, the finite element-simulated method on the newly designed model showed that the new design of customized mandible implant (sinewave plate), which showed an advantage over the standard method, could also be a novelty for application in prosthetic science, commonly used straight implant design regarding periodontal tissue condition.[22]

Overall, the results on periodontal condition relied on standardized indices and tests and may be considered reliable. In this study, it was expected that the periodontal condition of the teeth under OD prostheses would remain the same or even worsen after 1 year of therapy. However, PI and GI values around the teeth without MF influence were higher than expected, as reported in Tables 1 and 2. Moreover, teeth under static MF influence remained stable in their alveoli, with a favorable periodontal status, indicating long-term survival.

Conclusion

The null hypothesis that tissues adjacent to magnets had the same periodontal health as teeth without magnets was rejected, as MF showed a positive influence on PI and GI around remaining abutment teeth after 12 months following AT

with magnets. Hence, the presence of the static MF enhances the strength and resistance of periodontal supporting tissues around remaining teeth under OD. Additional use of magnets with OD is a simple, safe procedure widely accepted by patients and should be recommended to preserve the alveolar bone and stimulate other supporting tissues.

Clinical Implications

The results of this study showed beneficial effects of the magnetic field (improved periodontal indices) beneath the partial overdenture around preserved remaining teeth. The recommendation for the geriatric population is obvious: to include the remaining teeth, even with a poor periodontal prognosis, to reshape them and keep them as abutment teeth for a further overdenture with magnets inserted into their bases.

Author Contributions

Snežana V. Brković: Conceptualization, Methodology, Investigation, Data curation and interpretation, Writing – original draft.
Srđan D. Poštić: Investigation, Data curation and interpretation, Writing – review and editing.
Veljko D. Ilić: Data curation and interpretation, Writing – original draft.
Branimir D. Stošić: Data curation and interpretation
Pavle D. Ilić: Investigation, Data curation, Writing – review and editing.
All authors have approved the final article.

Ethical Statement

With the patients' written consent for the study, approval was obtained from the Ethics Committee of the School of Dental Medicine, Belgrade University (protocol number 572/1).

Conflict of Interests

The authors have declared no conflict of interest.

Statement of Generative AI Use

AI was not used in this study.

Sources of Funding

This research was granted by the Ministry of Science and Technology of Serbia, contract number 451-03-34/2026-03/200129, dated 05.02.2026

References

1. Pawar RS, Raipure PE, Kulkarni RS, Tagore M, Ganesan R. Fabrication of custom overdenture attachments using indigenously made parallelometer: A technique. J Indian Prosthodont Soc. 2019;19(1):83-87. doi: 10.4103/jips.jips_282_18. PMID: 30745759; PMCID: PMC6340085.
2. Mercouriadis-Howald A, Rollier N, Tada S, McKenna G, Igarashi K, Schimmel M. Loss of natural abutment teeth with cast copings retaining overdentures: a systematic review and meta-analysis. J Prosthodont Res. 2018; Oct;62(4):407-415. doi: 10.1016/j.jpor.2018.05.002. Epub 2018 Jun 8. PMID: 29891420.
3. Ettinger RL, Qian F. Longitudinal Assessment of Denture Maintenance Needs in an Overdenture Population. J Prosthodont. 2019;28(1):22-29. doi: 10.1111/jopr.12735. Epub 2018 Jan 29. PMID: 29380448.
4. Milić-Lemić A, Sredojević S, Radović K, Stamenković D, Miličić B, Popovac A, Stančić I. Retention force of overdenture retained with telescopic crowns – a comparison of polyether ether ketone and zirconia ceramic telescopic crowns. Srp Arh Celok Lek. 2020;148(7-8):410-16. DOI: https://doi.org/10.2298/SARH190923025M.
5. Bertl K, Tangl S, Rybaczek T, Berger B, Traindl-Prohazka M, Schuller-Götzburg P, Grossschmidt K. Prevalence and severity of periodontal disease in a historical Austrian population. J Periodontal Res. 2020;55(6):931-945. doi: 10.1111/jre.12785. Epub 2020 July 13. PMID: 32658361; PMCID: PMC7689777.
6. Aldhohrah T, Mashrah MA, Wang Y. Effect of 2-implant mandibular overdenture with different attachments and loading protocols on peri-implant health and prosthetic complications: A systematic review and network meta-analysis. J Prosthet Dent. 2022;127(6):832-44. doi: 10.1016/j.prosdent.2020.12.016. Epub 2021 Feb 3. PMID: 33546861.
7. Elawady D, Adam MA, Allam H, Mahmoud II, Alqutaibi AY, Shon AA. Single Implant-Retained Mandibular Overdentures: A Literature Review. Cureus. 2024,18;16(1):e52486. doi: 10.7759/cureus.52486. PMID: 38371006; PMCID: PMC10874113.
8. Helmy MH, Alqutaibi AY, El-Ella AA, Shawky AF. Effect of implant loading protocols on failure and marginal bone loss with unsplinted two-implant-supported mandibular overdentures: systematic review and meta-analysis. Int J Oral Maxillofac Surg. 2018; 47:642–650.
9. Yalamolu SSS, Bathala LR, Tammineedi S, Pragallapati SHLP, Vadlamudi C. Prosthetic journey of magnets: a review. J Med Life. 2023; Apr;16(4):501-506. doi: 10.25122/jml-2020-0012. PMID: 37305814; PMCID: PMC10251383.
10. Ribeiro TP, Flores M, Madureira S, Zanotto F, Monteiro FJ, Laranjeira MS. Magnetic Bone Tissue Engineering: Reviewing the Effects of Magnetic Stimulation on Bone Regeneration and Angiogenesis. Pharmaceutics. 2023; Mar 23;15(4):1045. doi: 10.3390/pharmaceutics15041045. PMID: 37111531; PMCID: PMC10143200.
11. Bambini F, Santarelli A, Putignano A, Procaccini M, Orsini G, Di Iorio D, et al. Use of supercharged cover screw as static magnetic field generator for bone healing, 2nd part: In vivo enhancement of bone regeneration in rabbits. J Biol Regul Homeost Agents. 2017;31(2):481-5. PMID: 28685556.
12. Zhang J, Meng X, Ding C, Shang P. Effects of static magnetic fields on bone microstructure and mechanical properties in mice. Electromagn Biol Med. 2018;37(2):76-83.

doi: 10.1080/15368378.2018.1458626. Epub 2018, PMID: 29617158.
13. Marycz K, Kornicka K, Röcken M. Static Magnetic Field (SMF) as a Regulator of Stem Cell Fate - New perspectives in regenerative medicine arising from an underestimated tool. Stem Cell Rev Rep. 2018;14(6):785-92. doi: 10.1007/s12015-018-9847-4. PMID: 30225821.
14. He Z, Selvamurugan N, Warshaw J, Partridge NC. Pulsed electromagnetic fields inhibit human osteoclast formation and gene expression via osteoblasts. Bone. 2018;106:194-203. doi: 10.1016/j.bone.2017.09.020. Epub 2017 Sep 28. PMID: 28965919.
15. Mueller H.-P. Periodontology (2nd ed.). Thieme. (2015). Retrieved from https://www.perlego.com/book/917726/periodontology-the-essentials-pdf (Original work published 2015).
16. Hardell L, Nilsson M, Koppel T, Carlberg M. Aspects on the International Commission on Non-Ionizing Radiation Protection (ICNIRP) 2020 Guidelines on Radiofrequency Radiation. Journ Cancer Sci Clinic Therapeutics 5 (2021): 250-285.
17. Poštić SD, Vujasinović-Stupar N, Asotić M, Rakočević Z. Systemic non-malignant osteoporosis and reduction of edentulous alveolar ridges. Sanamed. 2014;9(1):13-23.
18. Bi Y, Aldhohrah T, Mashrah MA, Su Y, Yang Z, Guo X, et al. Effects of attachment type and number of dental implants supporting mandibular overdenture on peri-implant health: A systematic review and network meta-analysis. J Prosthodont Res. 2022;30;66(3):357-73. doi: 10.2186/jpr.JPR_D_21_00073. Epub 2021 Sep 30. PMID: 34588403.
19. Elawady D, Adam MA, Allam H, Mahmoud II, Alqutaibi AY, Shon AA. Single Implant-Retained Mandibular Overdentures: A Literature Review. Cureus. 2024, 18;16(1):e52486. doi: 10.7759/cureus.52486. PMID: 38371006; PMCID: PMC10874113.
20. Brkovic S, Postic S, Ilic D. Influence of the magnetic field on microorganisms in the oral cavity. J Appl Oral Sci. 2015;23(2):179-86. doi: 10.1590/1678-775720140243. PMID: 26018310; PMCID: PMC4428463.
21. Poštić SD, Milošević M, Maneski T, Mladenovic, Brkovic S, Trifkovic B. Optical stereometric analysis of an experimental partially-edentulous mandible. AIME. 2022;14(6). doi:10.1177/16878132221106648.
22. Zhu F, Hou D, Zhou C, Chen Z, Cao Y, Ji L, Zou J, Xu Y. Precise extraction of impacted supernumerary tooth in the maxillary anterior region with a digital guide plate: A case report. Medicine (Baltimore). 2022 May 20;101(20):e29275. doi: 10.1097/MD.0000000000029275. PMID: 35608429; PMCID: PMC9276383.

***Corresponding author:** Dr. Srđan D. Poštić, PhD. University School of Dental Medicine in Beograd, Rankeova street 4, University of Belgrade, 11000 Belgrade, Serbia. E-mail: srdjan.postic@stomf.bg.ac.rs*

International Journal of Biomedicine 16(3) (2026) 388-394
http://dx.doi.org/10.21103/Article16(3)_CR1

CASE REPORT

INTERNATIONAL JOURNAL OF BIOMEDICINE

Sacroiliitis in Systemic Lupus Erythematosus–Systemic Sclerosis Overlap Syndrome: A Therapeutic Challenge

Mousa A. Albalwi

Department of Internal Medicine, Faculty of Medicine, University of Tabuk, Tabuk, Saudi Arabia

Abstract

Axial skeletal involvement is rare in systemic lupus erythematosus (SLE) and systemic sclerosis (SSc) and is not typically recognized in their overlap. We describe a 35-year-old woman with a 4-year history of SLE–SSc overlap who developed inflammatory low-back pain and progressive dyspnea. High-resolution computed tomography showed new usual-interstitial-pneumonia-pattern interstitial lung disease (ILD); sacroiliac magnetic resonance imaging confirmed bilateral active sacroiliitis; HLA-B27 was negative. After methotrexate withdrawal, mycophenolate, and nintedanib, rituximab was given for progressive ILD and produced both pulmonary stabilization and resolution of axial symptoms, allowing nonsteroidal anti-inflammatory drug discontinuation. Rituximab may offer dual benefit in overlap-associated sacroiliitis with ILD. (**International Journal of Biomedicine. 2026;16(3):388-394.**)

Keywords: **i**nterstitial lung disease • rituximab • MRI • connective tissue diseases

For citation: Albalwi MA. Sacroiliitis in Systemic Lupus Erythematosus–Systemic Sclerosis Overlap Syndrome: A Therapeutic Challenge. International Journal of Biomedicine. 2026;16(3):388-394. doi:10.21103/Article16(3)_CR1

Abbreviations

ANA, antinuclear antibody; **ASAS**, Assessment of SpondyloArthritis International Society; **CTD**, connective tissue disease; **HRCT**, high-resolution computed tomography; **ILD**, interstitial lung disease; **MRI**, magnetic resonance imaging; **NSAIDs**, nonsteroidal anti-inflammatory drugs; **SLE**, systemic lupus erythematosus; **SSc**, systemic sclerosis; **UIP**, usual interstitial pneumonia.

Introduction

Systemic lupus erythematosus (SLE) and systemic sclerosis (SSc) are chronic, multisystem autoimmune connective tissue diseases (CTDs) characterized by distinct yet partially overlapping immunopathogenic features, including loss of self-tolerance, autoantibody production, and tissue injury mediated by immune complex deposition, vasculopathy, and fibrosis.[1] Although each disease has a well-defined clinical phenotype, a subset of patients fulfills classification criteria for both entities simultaneously or sequentially, a condition referred to as SLE–SSc overlap syndrome. Reported prevalence estimates vary considerably depending on case definition and cohort, ranging from approximately 6.8% to 14% of patients with SSc in contemporary series, with patients typically being younger at diagnosis and more frequently exhibiting limited cutaneous SSc, anti–U1-RNP positivity, and antiphospholipid antibodies than those with isolated SSc.[2,3] Clinically, overlap patients often present with Raynaud phenomenon, inflammatory polyarthritis, gastroesophageal reflux, skin thickening, cytopenias, and variable degrees of renal and pulmonary involvement.[2,3] Interstitial lung disease (ILD), particularly when manifesting as a nonspecific interstitial pneumonia or, less commonly, a usual interstitial pneumonia (UIP) pattern, represents a major source of morbidity and mortality in SSc and occurs less frequently but with comparable clinical impact in SLE.[2]

Musculoskeletal manifestations are highly prevalent in both SLE and SSc, affecting 70–95% of patients with SLE and the majority of those with SSc over the disease course, with inflammatory arthralgia or arthritis commonly presenting first.[4,5] In SLE, articular involvement predominantly takes the form of a symmetric, non-erosive polyarthritis affecting the small joints of the hands, wrists, and knees (Jaccoud's arthropathy being a recognized variant), whereas in SSc, inflammatory arthritis, tendon friction rubs, flexion contractures, and acro-osteolysis are more characteristic.[4,5] In contrast, axial skeletal involvement—including sacroiliitis—remains distinctly uncommon and is not generally regarded as a characteristic feature of either disease or their overlap

phenotype.[5] The true prevalence of sacroiliitis in SLE is poorly defined, largely because the sacroiliac joints have historically been considered outside the spectrum of lupus arthropathy and are rarely imaged in routine practice. A case–control magnetic resonance imaging (MRI) study reported a significantly higher frequency of sacroiliac joint inflammation in patients with SLE than in age- and sex-matched controls, with elevated C-reactive protein concentrations identified as a risk factor for acute sacroiliitis.[6] A separate cohort study found inflammatory back pain in approximately 16% of SLE patients, of whom a subset demonstrated active sacroiliitis on MRI independent of HLA-B27 status.[7] Isolated case reports have documented bilateral sacroiliitis in juvenile and adult SLE as well as in SLE overlap syndromes with dermatomyositis, supporting the existence of a distinct "lupoid sacroarthropathy" phenotype that appears to reflect disease-intrinsic autoimmune inflammation rather than coexisting spondyloarthritis.[8-10] By contrast, sacroiliitis in SSc and in SLE–SSc overlap has been reported only exceptionally.[5,11] When sacroiliitis occurs in a patient with an established CTD, especially in the absence of HLA-B27 positivity, a family history of spondyloarthritis, or other defining spondyloarthritis features such as psoriasis, uveitis, inflammatory bowel disease, dactylitis, or enthesitis, the diagnostic differential becomes broad and includes infectious, mechanical, degenerative, and—most importantly—primary autoimmune etiologies that must be distinguished from seronegative spondyloarthropathy.[8-12] The 2009 Assessment of SpondyloArthritis International Society (ASAS) classification criteria for axial spondyloarthritis require the presence of chronic back pain (duration ≥3 months) beginning before age 45, together with imaging evidence of sacroiliitis plus one spondyloarthritis feature, or HLA-B27 positivity plus two such features.[12,13] Patients whose presentations lie outside these criteria, as in the present case, represent a diagnostic challenge and may reflect a mechanism of synovio-entheseal autoimmune activation rather than classic enthesis-driven spondyloarthritis.[14]

Management decisions in this population are further complicated by the presence of progressive ILD, which constrains the safe use of nonsteroidal anti-inflammatory drugs (NSAIDs), high-dose corticosteroids, and several conventional synthetic disease-modifying antirheumatic drugs (csDMARDs). Methotrexate, although effective for inflammatory arthritis in both SLE and SSc, is generally avoided or withdrawn once ILD develops due to concerns regarding pulmonary toxicity and confounding of disease monitoring. Mycophenolate mofetil is widely regarded as a first-line immunosuppressive agent for CTD-associated ILD, and the tyrosine kinase inhibitor nintedanib has been shown in the SENSCIS trial to reduce the annual rate of decline in forced vital capacity in patients with SSc-associated ILD,[15] When pulmonary progression continues despite combination immunosuppressive and antifibrotic therapy, B-cell–directed therapy with rituximab has increasingly been employed as a rescue strategy and has demonstrated efficacy in stabilizing or improving lung function across a range of CTD-ILDs, including SSc, inflammatory myositis, and lupus.[16,17] Beyond its pulmonary effects, rituximab may also exert a meaningful impact on extra-pulmonary inflammatory disease activity, including articular and axial manifestations, by depleting autoreactive B cells and modulating the synovio-entheseal immune milieu.[14,17,18]

Against this background, we report a case of MRI-confirmed bilateral active sacroiliitis arising in a patient with established SLE–SSc overlap who subsequently developed progressive ILD. The case addresses an important but underappreciated clinical intersection: the recognition of atypical axial manifestations in CTD overlap, the therapeutic limitations imposed by concurrent organ-threatening pulmonary disease, and the observation that B-cell depletion with rituximab—pursued primarily for pulmonary indications—may also provide meaningful benefit for inflammatory axial symptoms. To our knowledge, bilateral sacroiliitis in SLE–SSc overlap has not previously been described alongside a response of axial symptoms to rituximab, and the case therefore illustrates a clinically relevant but under-recognized musculoskeletal phenotype within the autoimmune overlap spectrum and provides a potential management framework when conventional options are restricted by pulmonary disease.

Case Presentation

Patient Information

A 35-year-old woman of Middle Eastern descent with a 4-year history of SLE–SSc overlap syndrome was evaluated in the rheumatology outpatient clinic for new inflammatory low-back pain of approximately three months' duration and progressively worsening exertional dyspnea. Her disease had originally been diagnosed after she presented with a 12-month history of triphasic Raynaud phenomenon, symmetric inflammatory polyarthralgia, and morning stiffness exceeding one hour, photosensitive malar rash, and gradually progressive skin tightening of the fingers and hands. At that initial evaluation, she met the 2019 European Alliance of Associations for Rheumatology/American College of Rheumatology (EULAR/ACR) classification criteria for SLE and the 2013 ACR/EULAR classification criteria for SSc, resulting in a diagnosis of SLE–SSc overlap syndrome. She had been started on hydroxychloroquine 400 mg daily, low-dose prednisolone, and methotrexate titrated to 15 mg weekly with folic acid supplementation, with reasonable control of her arthritis and skin findings. Her other initial manifestations included recurrent gastroesophageal reflux managed with proton pump inhibitor therapy, mild dysphagia for solids, and inflammatory polyarthritis involving the metacarpophalangeal and proximal interphalangeal joints bilaterally, associated with mild-to-moderate skin thickening of the fingers and distal forearms (modified Rodnan skin score in the mild-to-moderate range). She had no history of digital ulceration, scleroderma renal crisis, cardiac involvement, seizures, psychosis, lupus nephritis, serositis, or hematologic cytopenias. Importantly, she had no personal or family history of psoriasis, inflammatory bowel disease, anterior uveitis, reactive arthritis, or ankylosing spondylitis, and no prior axial symptoms or morning back stiffness. She was a non-smoker,

consumed no alcohol, and had no known occupational, environmental, or pharmacological exposures associated with pulmonary fibrosis. She was married, had two children, and worked in a sedentary administrative role. Her family history was negative for autoimmune disease, and she had no known drug allergies.

Baseline evaluation performed two years earlier, including transthoracic echocardiography, showed no evidence of pulmonary hypertension, and high-resolution computed tomography (HRCT) of the chest at that time demonstrated no interstitial lung disease. Baseline pulmonary function testing was within normal reference ranges. Serologic testing had revealed a strongly positive antinuclear antibody with a speckled pattern (titer 1:1280; negative <1:80), elevated anti-double-stranded DNA antibody by *Crithidia luciliae* immunofluorescence assay (titer 1:160; negative <1:10), and a markedly positive anti-Scl-70 (anti-topoisomerase I) antibody (>220 U/mL; negative <7 U/mL). Anti-centromere, anti-RNA polymerase III, anti-U1-RNP, anti-Sm, anti-Ro/SSA, anti-La/SSB, anti-Jo-1, and anti-PM-Scl antibodies were negative. Antiphospholipid antibodies (lupus anticoagulant, anti-cardiolipin, and anti-β2-glycoprotein I) and rheumatoid factor were negative. Complement C3 and C4 levels were within normal limits. Baseline complete blood count, serum creatinine, liver enzymes, creatine kinase, thyroid function, and urinalysis were unremarkable, and inflammatory markers (erythrocyte sedimentation rate and C-reactive protein) were mildly elevated, consistent with active inflammatory arthritis.

Diagnostic Assessment

The patient described her back pain as insidious in onset, localized to the lower back and bilateral buttock regions with occasional alternating buttock pain, worse in the second half of the night and on awakening, associated with morning stiffness lasting more than 60 minutes, improving with movement but not with rest, and only partially responsive to as-needed analgesia. The pain had progressed over approximately three months and had begun to interfere with sleep and daily activities. These features fulfilled the ASAS expert criteria for inflammatory back pain. Concurrently, she reported progressive exertional dyspnea (New York Heart Association functional class II–III), a dry nonproductive cough, reduced exercise tolerance, and intermittent fatigue. She denied fever, weight loss, hemoptysis, chest pain, or orthopnea. On physical examination during the current evaluation, she was afebrile and hemodynamically stable with normal oxygen saturation at rest on room air. Cardiovascular examination was unremarkable with no evidence of right heart strain. Respiratory examination revealed fine bibasilar inspiratory (Velcro-like) crackles without wheeze. Peripheral joint examination revealed no active synovitis, swelling, or effusion; mild residual skin thickening was noted over the fingers and distal forearms, with no new digital ulcers, pitting scars, or telangiectasias. Spinal examination demonstrated preserved lumbar range of motion without spinal tenderness, but reproducible pain was elicited during sacroiliac joint provocation maneuvers (positive FABER/Patrick test and sacroiliac compression test bilaterally). There was no evidence of enthesitis, dactylitis, or peripheral inflammatory arthritis. Ophthalmologic history and examination were negative for anterior uveitis, and there were no cutaneous findings suggestive of psoriasis.

Magnetic resonance imaging of the sacroiliac joints, performed with dedicated short tau inversion recovery (STIR), T1, and post-gadolinium sequences, demonstrated bilateral subchondral bone-marrow edema involving both iliac and sacral surfaces with corresponding post-contrast enhancement, findings consistent with active sacroiliitis as defined by ASAS criteria (Figure 1); no definite structural changes such as erosions, sclerosis, or ankylosis were identified. High-resolution computed tomography of the chest revealed new bilateral, predominantly basal and subpleural reticulation with traction bronchiectasis and early honeycombing, radiographic features consistent with a usual interstitial pneumonia (UIP) pattern (Figure 2). Plain radiographs of the sacroiliac joints and lumbar spine were unremarkable.

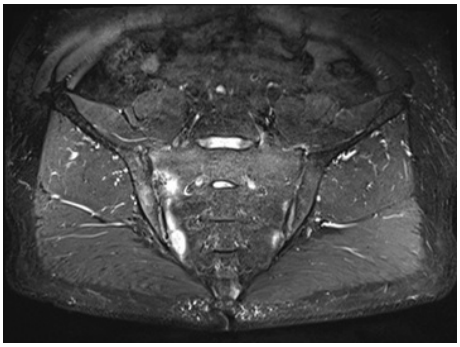

Figure 1. *Coronal T2 fat-suppressed MRI showing bilateral subchondral bone marrow edema of the sacroiliac joints, right greater than left, consistent with active inflammatory sacroiliitis.*

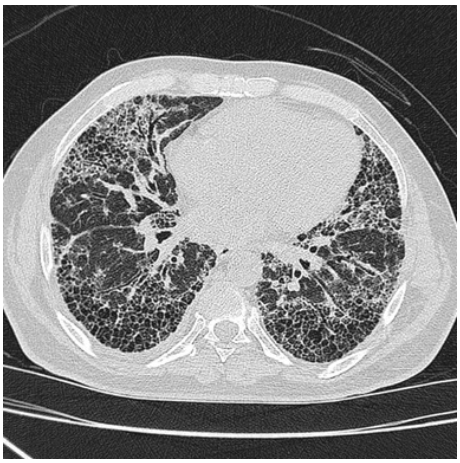

Figure 2. *High-resolution chest CT showing basal and subpleural honeycombing with traction bronchiectasis, consistent with a Usual Interstitial Pneumonia (UIP) pattern.*

HLA-B27 testing by flow cytometry was negative. Repeat serologic panel demonstrated persistent high-titer ANA, persistently positive anti-Scl-70 antibody, and low-titer anti-dsDNA antibody; complement levels remained normal. Routine laboratory studies, including complete blood count, renal function, liver enzymes, creatine kinase, and

urinalysis, were within normal reference ranges. Inflammatory markers (erythrocyte sedimentation rate and C-reactive protein) were mildly elevated. Screening for tuberculosis (interferon-gamma release assay), hepatitis B, hepatitis C, and human immunodeficiency virus was negative prior to subsequent escalation of immunosuppression. Transthoracic echocardiography was repeated and showed preserved biventricular function with no evidence of pulmonary hypertension. Pulmonary function testing demonstrated a restrictive pattern with reduced diffusing capacity for carbon monoxide, consistent with the radiographic findings of new-onset ILD. Taking together the clinical features (inflammatory back pain without defining spondyloarthritis features), imaging findings (bilateral active sacroiliitis), and negative HLA-B27 status in the absence of psoriasis, uveitis, inflammatory bowel disease, or family history of spondyloarthritis, the sacroiliitis was judged most consistent with an atypical musculoskeletal manifestation of the underlying SLE–SSc overlap syndrome rather than a concurrent axial spondyloarthritis. Infectious, tuberculous, and mechanical etiologies were considered and excluded.

Therapeutic Interventions

Methotrexate at a stable weekly dose of 15 mg subcutaneously had previously yielded satisfactory control of inflammatory arthritis and stabilization of skin thickening over the preceding two years. Following confirmation of new-onset ILD on HRCT, methotrexate was discontinued in view of its potential to cause or confound pulmonary toxicity. Hydroxychloroquine 400 mg daily was continued for its established benefit in SLE-related skin and articular disease, and low-dose prednisolone was maintained at the lowest effective dose, with subsequent taper to minimize long-term glucocorticoid exposure given the coexistence of SSc. Mycophenolate mofetil was initiated and gradually escalated, over several weeks, to 1500 mg twice daily as tolerated. The patient underwent vaccination review, pneumococcal and influenza immunization, and standard tuberculosis screening prior to and during immunosuppressive escalation. Despite adequate dosing and good adherence to mycophenolate, her ILD progressed both clinically (worsening exertional dyspnea and reduced exercise tolerance) and radiographically (increased extent of fibrotic reticulation and honeycombing on follow-up HRCT) over a period of several months. The antifibrotic agent nintedanib was added at 150 mg twice daily, with gradual dose titration to manage gastrointestinal side effects, in accordance with the evidence-based established by the SENSCIS trial for SSc-associated ILD.[15]

Concurrent with the evolution of her pulmonary disease, the patient continued to experience inflammatory low-back pain characterized by nocturnal worsening, prolonged morning stiffness, and improvement with movement. NSAIDs were prescribed intermittently and in the lowest effective doses under proton-pump inhibitor cover, with partial symptomatic benefit; however, their use was deliberately minimized given concerns about SSc-associated gastrointestinal dysmotility, gastroesophageal reflux, and the well-recognized renal and cardiovascular risks of chronic NSAID therapy in patients with active connective-tissue disease. Low-dose oral glucocorticoids provided only modest additional benefit and were not escalated due to the risk of precipitating scleroderma renal crisis in the setting of anti-Scl-70 positivity. Referral for physiotherapy with a structured program of spinal mobility and posture-focused exercises was made, and the patient was counseled on sleep ergonomics.

Given the continued progression of ILD despite optimized mycophenolate mofetil and nintedanib, and after multidisciplinary discussion involving rheumatology, pulmonology, and the patient herself, rituximab was initiated as rescue B-cell–depleting therapy in accordance with the evidence supporting its use in refractory CTD-ILD.[16,17] The patient received induction therapy with two intravenous infusions of rituximab 1 g, administered two weeks apart, with standard premedication (intravenous corticosteroid, antihistamine, and paracetamol), and screening for hepatitis B, hepatitis C, and tuberculosis was performed prior to each infusion. Serum immunoglobulin levels were checked at baseline and were within normal limits. The patient tolerated both infusions without infusion-related reactions, allergic events, or infectious complications. Mycophenolate mofetil and nintedanib were continued during and after rituximab induction, and hydroxychloroquine was maintained.

Outcomes

Following rituximab induction, the patient demonstrated stabilization of her interstitial lung disease, with no further clinical deterioration in exertional dyspnea, cough, or exercise tolerance, and no progression of fibrotic changes on subsequent follow-up HRCT. In parallel, she reported a pronounced and progressive reduction in inflammatory axial pain, with the resolution of nocturnal symptoms, the disappearance of prolonged morning stiffness, and the restoration of unimpaired spinal mobility during daily activities. Within several weeks of the second infusion, her axial symptoms had diminished sufficiently to allow complete discontinuation of NSAIDs, which she has not required since. Peripheral joint examination remained free of synovitis, and there was no recurrence of inflammatory arthritis. Inflammatory markers normalized, and serum complement levels remained within the reference range. Rituximab maintenance was planned every six months based on clinical response, B-cell repopulation status, and tolerability, in accordance with published protocols for CTD-ILD.[16,17] At the most recent follow-up, the patient remained clinically stable on combination mycophenolate mofetil, nintedanib, hydroxychloroquine, and maintenance rituximab, with no respiratory decline, no recurrence of axial symptoms, and no serious adverse events attributable to therapy.

Discussion

The present case illustrates a distinctly atypical presentation of bilateral active sacroiliitis in a patient with SLE–SSc overlap syndrome complicated by progressive ILD. While peripheral inflammatory arthritis is a well-recognized manifestation in both SLE and SSc, axial skeletal involvement remains rare and under-characterized.[4,5] Published reports describing sacroiliitis in SLE are sparse and consist predominantly of isolated case observations and small case

series. Yilmaz and colleagues, in a cross-sectional study of 281 adult SLE patients, reported inflammatory back pain in approximately 16% and demonstrated active sacroiliitis on MRI in a subset, with the majority of affected patients being HLA-B27 negative.[7] Kayacan Erdogan and colleagues, in a case–control MRI study of 63 SLE patients compared with matched controls, found a significantly higher prevalence of sacroiliitis in patients with SLE and identified elevated C-reactive protein as a risk factor for acute sacroiliitis, supporting the concept of disease-intrinsic inflammatory involvement of the sacroiliac joints rather than a chance coexistence of spondyloarthritis.[6] Tanatar and colleagues described a 16-year-old girl with juvenile SLE who developed bilateral sacroiliitis confirmed by MRI and was ultimately classified as having juvenile spondyloarthritis after exclusion of infection.[8] Gupta and Dhanota reported an adolescent male with SLE and bilateral symmetric active sacroiliitis on MRI in the absence of HLA-B27, which they interpreted as a rare disease-intrinsic manifestation of SLE.[9] Chandrasekhara and colleagues described a case of SLE–dermatomyositis overlap who subsequently developed symptomatic bilateral sacroiliitis and introduced the concept of "lupoid sacroarthropathy."[10] Tarhan and colleagues similarly documented an SLE patient with coexisting ankylosing spondylitis.[11] In contrast to these predominantly lupus-centric reports, the coexistence of sacroiliitis with SLE–SSc overlap appears exceptional. To our knowledge, the present case is among the few published descriptions of MRI-confirmed bilateral active sacroiliitis in this specific overlap phenotype. The consistent features across the published cases—young adult or adolescent patient, bilateral active inflammation on MRI, absence of HLA-B27, and lack of defining spondyloarthritis features—closely parallel the findings in our patient and strengthen the argument that axial inflammation can occur as a disease-intrinsic manifestation within the autoimmune CTD spectrum.[6-11]

In our patient, the absence of HLA-B27 positivity, the lack of personal or family history of psoriasis, inflammatory bowel disease, uveitis, or reactive arthritis, and the absence of enthesitis, dactylitis, or characteristic radiographic changes together substantially reduced the pre-test probability of a concurrent axial spondyloarthritis. The observation of bilaterally symmetric active sacroiliitis on MRI in a patient with serologically active SLE–SSc overlap, along with a rising inflammatory marker profile, is therefore most plausibly interpreted as a rare but genuine musculoskeletal manifestation of the underlying autoimmune overlap, rather than a coincidental seronegative spondyloarthropathy. This interpretation accords with the growing body of evidence from cohort studies and case reports suggesting that sacroiliitis may represent an under-recognized facet of the SLE musculoskeletal phenotype.[6,7,10] It should, however, be acknowledged that the ASAS MRI definition of active sacroiliitis is not disease-specific and that bone-marrow edema may occasionally be observed in mechanical, infectious, and degenerative conditions, as well as in asymptomatic individuals.[12,13] In the present case, alternative etiologies including infection, tuberculosis (which remains relevant in our regional context), and mechanical pathology were actively excluded, and the coincidence of axial inflammation with clinically and serologically active CTD supports autoimmune pathogenesis. The exact mechanism underlying sacroiliac inflammation in SLE and related overlap syndromes remains incompletely understood. Still, it has been proposed that autoimmune activation at the synovio-entheseal interface, immune complex deposition, type I interferon–driven inflammation, and possibly B-cell–dependent pathways—mechanisms that differ fundamentally from the enthesis-driven, IL-17/IL-23–polarized pathogenesis typical of HLA-B27–associated axial spondyloarthritis.[14]

Therapeutic decision-making in this case was substantially shaped by the presence of progressive ILD, which constrained the use of several agents otherwise useful in axial inflammatory disease. NSAIDs, the mainstay of symptomatic therapy in axial spondyloarthritis, were restricted by concerns about SSc-related gastrointestinal dysmotility and renal risk. TNF-α inhibitors, widely used in classic axial spondyloarthritis, are generally avoided in SLE because of the risk of inducing lupus-like phenomena and worsening autoantibody profiles, and evidence supporting IL-17 inhibitors in this population is limited.[9] Methotrexate, although beneficial for the patient's arthritis and skin disease, was withdrawn after ILD developed, and mycophenolate mofetil was initiated as a broader-spectrum immunosuppressant with established efficacy in CTD-ILD. When pulmonary disease progressed despite optimized mycophenolate dosing, nintedanib was added based on the SENSCIS trial, which demonstrated a significant reduction in the rate of decline in forced vital capacity in patients with SSc-ILD treated with this tyrosine kinase inhibitor.[15] The subsequent introduction of rituximab was driven primarily by continued pulmonary progression; growing evidence supports the efficacy of B-cell depletion in CTD-associated ILD, including SSc-ILD, with sustained complete B-cell depletion correlating with stabilization or improvement in pulmonary function.[16,17] Notably, in the present case, rituximab was associated not only with stabilization of ILD but also with marked improvement in inflammatory axial symptoms, enabling complete discontinuation of NSAIDs. Although rituximab is not established as a standard therapy for sacroiliitis, there is biological plausibility for its efficacy in axial inflammation of autoimmune origin: B cells contribute to autoantibody production, antigen presentation, and local pro-inflammatory cytokine release, and B-cell involvement has been documented in the pathogenesis of ankylosing spondylitis.[14,18] The parallel temporal improvement in pulmonary and axial symptoms in our patient, while subject to the limitations inherent in single-patient observations, raises the possibility that B-cell–directed therapy may offer dual benefit in overlap patients with atypical autoimmune sacroiliitis and coexisting ILD. This observation is hypothesis-generating and warrants systematic evaluation in larger CTD-ILD cohorts with dedicated musculoskeletal phenotyping.

Several important limitations of this report should be acknowledged. As a single-patient observation, causal inferences regarding the effect of rituximab on axial symptoms cannot be drawn, and spontaneous fluctuations in inflammatory sacroiliitis, the contribution of ongoing

mycophenolate therapy, regression-to-mean effects, and placebo effects cannot be entirely excluded. Follow-up MRI of the sacroiliac joints after rituximab was not systematically performed, thereby precluding objective imaging confirmation of the resolution of bone marrow edema. Additionally, although the clinical and serological profile strongly supported a CTD-associated sacroiliitis, the absence of a universally accepted diagnostic framework for "lupus-associated" or "CTD-associated" sacroiliitis introduces some degree of diagnostic uncertainty. The strengths of the report include longitudinal follow-up, careful exclusion of alternative etiologies, objective imaging documentation of active sacroiliitis using standard ASAS-compliant MRI criteria, and temporal correlation of both pulmonary and axial outcomes with therapy. Taken together, this case underscores the importance of systematically reassessing new axial symptoms in patients with CTD overlap, maintaining a broad differential diagnosis that includes rare disease-intrinsic manifestations, and tailoring treatment strategies to account for concurrent organ-threatening disease. Clinicians should remain alert to axial musculoskeletal manifestations that fall outside the traditional phenotypes of classic spondyloarthritis or isolated CTD and consider the potential dual therapeutic benefit of B-cell depletion in carefully selected patients with overlap syndromes complicated by progressive ILD.

Conclusion

Sacroiliitis is an uncommon but clinically relevant manifestation in systemic lupus erythematosus–systemic sclerosis overlap. In patients with concurrent interstitial lung disease, therapeutic options may be limited. This case demonstrates that rituximab can stabilize interstitial lung disease and may also provide meaningful improvement in inflammatory axial symptoms. Early recognition of atypical musculoskeletal manifestations and individualized treatment strategies are essential in managing overlap syndromes.

Patient Perspective

"Before my back pain started, I had already been living with joint swelling, Raynaud's, and skin changes for several years. When I developed new pain in my lower back — worst at night and in the mornings — I was worried something had changed in my disease. The breathlessness that came at the same time made everything harder. Being told I had lung disease on top of what I already had, and that my sacroiliac joints were inflamed, was difficult to process. I had to stop methotrexate, which had been helping my joints, and start new medications. The back pain continued for some time, and I used painkillers that I knew were not ideal for my stomach.

After starting rituximab, the change was noticeable. My breathing became more stable, and the back pain — which had been affecting my sleep and daily movement — gradually resolved. I was able to stop the painkillers completely. I feel that my condition is now under better control, and I am grateful that the treatment addressed both problems at the same time. I hope sharing my experience helps other patients and doctors recognize these less common complications early."

Author Contributions

The author confirms sole responsibility for the conception, investigation, design, and writing of the manuscript.

Acknowledgments

The author wishes to thank the patient for her consent to the publication of this case.

Funding

This research received no external funding.

Ethics Statement

Ethical review and approval were waived for this study because it is a single-case report. Written informed consent has been obtained from the patient for the publication of this paper.

Conflicts of Interest

The author declares no conflict of interest.

References

1. Kaul A, Gordon C, Crow MK, Touma Z, Urowitz MB, van Vollenhoven R, Ruiz-Irastorza G, Hughes G. Systemic lupus erythematosus. Nat Rev Dis Primers. 2016 Jun 16;2:16039. doi: 10.1038/nrdp.2016.39. PMID: 27306639.
2. Alharbi S, Ahmad Z, Bookman AA, Touma Z, Sanchez-Guerrero J, Mitsakakis N, Johnson SR. Epidemiology and Survival of Systemic Sclerosis-Systemic Lupus Erythematosus Overlap Syndrome. J Rheumatol. 2018 Oct;45(10):1406-1410. doi: 10.3899/jrheum.170953. Epub 2018 Jul 15. PMID: 30008448.
3. Bass RD, Moore DF, Steen VD. Prevalence and Characteristics of Patients With Systemic Sclerosis Fulfilling the 2019 EULAR/American College of Rheumatology Classification Criteria for Systemic Lupus Erythematosus. Arthritis Care Res (Hoboken). 2024 Mar;76(3):311-317. doi: 10.1002/acr.25235. Epub 2023 Dec 19. PMID: 37691427.
4. Grossman JM. Lupus arthritis. Best Pract Res Clin Rheumatol. 2009 Aug;23(4):495-506. doi: 10.1016/j.berh.2009.04.003. PMID: 19591780.
5. Jacques T, Sudoł-Szopińska I, Larkman N, O'Connor P, Cotten A. Musculoskeletal Manifestations of Non-RA Connective Tissue Diseases: Scleroderma, Systemic Lupus Erythematosus, Still's Disease, Dermatomyositis/Polymyositis, Sjögren's Syndrome, and Mixed Connective Tissue Disease. Semin Musculoskelet Radiol. 2018 Apr;22(2):166-179. doi: 10.1055/s-0038-1639473. Epub 2018 Apr 19. PMID: 29672805.
6. Kayacan Erdogan E, Gokcen N, Badak SO, Bicakci YK, Arslan D. Sacroiliitis in systemic lupus erythematosus : The

rates of involvement of the forgotten joint. Z Rheumatol. 2021 Jun;80(5):447-455. English. doi: 10.1007/s00393-020-00879-z. Epub 2020 Sep 18. PMID: 32945953.
7. Yilmaz N, Yazici A, Özulu TÜrkmen B, Karalok I, Yavuz Ş. Sacroiliitis in Systemic Lupus Erythematosus Revisited. Arch Rheumatol. 2020 Jan 8;35(2):254-258. doi: 10.46497/ArchRheumatol.2020.7514. PMID: 32851375; PMCID: PMC7406165.
8. Tanatar A, Topal U, GÜl KaradaĞ Ş, SÖnmez HE, Aktay Ayaz N. Coexistence of Juvenile Systemic Lupus Erythematosus and Juvenile Spondyloarthropathy: A Case Report and Review of the Literature. Arch Rheumatol. 2020 Jan 8;35(1):132-136. doi: 10.5606/ArchRheumatol.2020.7468. PMID: 32637929; PMCID: PMC7322298.
9. Gupta V, Dhanota DS. Symptomatic Bilateral Sacroiliitis in a Patient with Juvenile Systemic Lupus Erythematosus: A Rare Association. Mediterr J Rheumatol. 2023 Mar 31;34(1):105-107. doi: 10.31138/mjr.34.1.105. PMID: 37223595; PMCID: PMC10201104.
10. Chandrasekhara PK, Jayachandran NV, Thomas J, Narsimulu G. Systemic lupus erythematosus and dermatomyositis with symptomatic bilateral sacroiliitis: an unusual and interesting association. Mod Rheumatol. 2009;19(1):84-6. doi: 10.1007/s10165-008-0120-6. Epub 2008 Sep 11. PMID: 18784900.
11. Tarhan F, Argın M, Can G, Özmen M, Keser G. Coexistence of systemic lupus erythematosus and ankylosing spondylitis: another case report and review of the literature. Eur J Rheumatol. 2014 Mar;1(1):39-43. doi: 10.5152/eurjrheum.2014.008. Epub 2014 Mar 1. PMID: 27708869; PMCID: PMC5042260.
12. Rudwaleit M, van der Heijde D, Landewé R, Listing J, Akkoc N, Brandt J, Braun J, Chou CT, Collantes-Estevez E, Dougados M, Huang F, Gu J, Khan MA, Kirazli Y, Maksymowych WP, Mielants H, Sørensen IJ, Ozgocmen S, Roussou E, Valle-Oñate R, Weber U, Wei J, Sieper J. The development of Assessment of SpondyloArthritis international Society classification criteria for axial spondyloarthritis (part II): validation and final selection. Ann Rheum Dis. 2009 Jun;68(6):777-83. doi: 10.1136/ard.2009.108233. Epub 2009 Mar 17. Erratum in: Ann Rheum Dis. 2019 Jun;78(6):e59. doi: 10.1136/ard.2009.108233corr1. PMID: 19297344.
13. Sieper J, Poddubnyy D. Axial spondyloarthritis. Lancet. 2017 Jul 1;390(10089):73-84. doi: 10.1016/S0140-6736(16)31591-4. Epub 2017 Jan 20. PMID: 28110981.
14. Wilbrink R, Spoorenberg A, Verstappen GMPJ, Kroese FGM. B Cell Involvement in the Pathogenesis of Ankylosing Spondylitis. Int J Mol Sci. 2021 Dec 11;22(24):13325. doi: 10.3390/ijms222413325. PMID: 34948121; PMCID: PMC8703482.
15. Distler O, Highland KB, Gahlemann M, Azuma A, Fischer A, Mayes MD, Raghu G, Sauter W, Girard M, Alves M, Clerisme-Beaty E, Stowasser S, Tetzlaff K, Kuwana M, Maher TM; SENSCIS Trial Investigators. Nintedanib for Systemic Sclerosis-Associated Interstitial Lung Disease. N Engl J Med. 2019 Jun 27;380(26):2518-2528. doi: 10.1056/NEJMoa1903076. Epub 2019 May 20. PMID: 31112379.
16. Xu L, Wang F, Luo F. Rituximab for the treatment of connective tissue disease-associated interstitial lung disease: A systematic review and meta-analysis. Front Pharmacol. 2022 Oct 28;13:1019915. doi: 10.3389/fphar.2022.1019915. PMID: 36386239; PMCID: PMC9650441.
17. Al Tabaa O, Ghossan R, Combier A, Steelandt A, Thomas M, Avouac J, Allanore Y. Sustained complete B cell depletion is associated with rituximab efficacy in connective tissue disorders-associated interstitial lung disease. RMD Open. 2023 Feb;9(1):e002832. doi: 10.1136/rmdopen-2022-002832. PMID: 36754549; PMCID: PMC9923347.
18. Schett G, Müller F, Taubmann J, Mackensen A, Wang W, Furie RA, Gold R, Haghikia A, Merkel PA, Caricchio R, D'Agostino MA, Locatelli F, June CH, Mougiakakos D. Advancements and challenges in CAR T cell therapy in autoimmune diseases. Nat Rev Rheumatol. 2024 Sep;20(9):531-544. doi: 10.1038/s41584-024-01139-z. Epub 2024 Aug 6. PMID: 39107407.

***Corresponding author*: *Mousa A. Albalwi, MD, MPH. Department of Internal Medicine, Faculty of Medicine, University of Tabuk, Tabuk, Saudi Arabia. E-mail: Mousa.Albalwi@ut.edu.sa*

International Journal of Biomedicine 16(3) (2026) 395-397
http://dx.doi.org/10.21103/Article16(3)_CR2

CASE REPORT

INTERNATIONAL JOURNAL OF BIOMEDICINE

When One Antibody Disappears, and Others Emerge: A Six-Year Evolution of Antiphospholipid Antibodies in a Pregnant Woman with Systemic Lupus Erythematosus

Ina Toska[1*], Rexhep Shkurti[1], Ervin Rapushi[2], Anila Mitre[3]

[1]*University of Tirana, Faculty of Natural Sciences, Department of Biotechnology, Tirana, Albania*
[2]*University of Medicine, Tirana, Albania*
[3]*University of Tirana, Faculty of Natural Sciences, Department of Biology, Tirana, Albania*

Abstract

Antiphospholipid antibodies (aPL) are frequently detected in patients with systemic autoimmune diseases, particularly in systemic lupus erythematosus (SLE), and are associated with thrombotic events and adverse pregnancy outcomes. Although persistent aPL positivity is crucial for antiphospholipid syndrome (APS) classification, increasing evidence suggests that aPL profiles may evolve over time. Longitudinal observations documenting the transition between antiphospholipid antibody specificities remain limited.
We report the case of a 33-year-old woman with SLE diagnosed in 2019, who initially presented with persistent high-titer anti-β2GPI IgM (confirmed on repeat testing after 12 weeks) positivity. Lupus anticoagulant (LAC) and anti-β2GPI IgG were initially negative. During her first pregnancy in 2024, anti-β2GPI antibodies became negative, while LAC activity increased from 42.3 to 48.3 sec and anticardiolipin IgM antibodies became positive (60.6 U/mL). The pregnancy resulted in a preterm birth at 36 weeks of gestation. During the second pregnancy, in March 2026, LAC activity further increased to 55.1 sec, and both aCL IgM and IgG antibodies became positive. Throughout the six-year follow-up period, the patient remained free of arterial or venous thrombotic events and remained on stable treatment with hydroxychloroquine, methylprednisolone, and low-dose aspirin.
This case demonstrates a remarkable longitudinal evolution of the aPL profile in a woman with SLE, characterized by the disappearance of high-titer anti-β2GPI IgM antibodies and subsequent emergence of LAC and aCL antibodies. These findings emphasize the dynamic nature of antiphospholipid autoimmunity and support the importance of long-term monitoring of aPL profiles in patients with SLE, particularly during reproductive years. (**International Journal of Biomedicine. 2026;16(3):395-397.**)

Keywords: antiphospholipid antibodies • lupus anticoagulant • aCL antibodies • systemic lupus erythematosus

For citation: Toska I, Shkurti R, Rapushi E, Mitre A. When One Antibody Disappears, and Others Emerge: A Six-Year Evolution of Antiphospholipid Antibodies in a Pregnant Woman with Systemic Lupus Erythematosus. International Journal of Biomedicine. 2026;16(3):395-397. doi:10.21103/Article16(3)_CR2

Introduction

Systemic lupus erythematosus (SLE) is a chronic autoimmune disease characterized by immune dysregulation and the production of a spectrum of autoantibodies. Among them, antiphospholipid antibodies (aPL), including lupus anticoagulant (LAC), anticardiolipin antibodies (aCL), and anti-β2GPI antibodies (anti-β2GPI), are of particular clinical importance due to their association with thrombotic events and pregnancy morbidity.[1-3] Antiphospholipid antibodies are detected in up to 50% of patients with SLE, while approximately 20% of patients with APS have underlying SLE.[3]

Clinical practice and current APS classification criteria primarily focus on the presence and persistence of aPL.[1] In contrast, relatively little attention has been given to the longitudinal evolution of individual antibody profiles. Although persistent aPL positivity remains central in APS classification, increasing evidence suggests that antiphospholipid antibody profiles may evolve over time, with fluctuations in antibody titer, disappearance of previously detected antibodies, and

***Corresponding author:** Ina Toska, PhD(C)*
ina.toska@yahoo.com
ina_toska.fshnutdr@unitir.edu.al

emergence of new antibody specificities.[4,5] Understanding these temporal changes may be relevant in women of reproductive age, in whom alterations in aPL profiles could influence risk stratification and pregnancy management and long- term clinical surveillance.[2]

This case describes a woman with SLE who demonstrated a longitudinal six-year evolution of her antiphospholipid antibody profile. Initial high-titer anti-β2GPI IgM positivity was confirmed on repeat testing at least 12 weeks later. Her antiphospholipid antibody profile evolved, with the disappearance of anti-β2GPI antibodies and the subsequent emergence of lupus anticoagulant and anticardiolipin antibodies during follow-up.

Case Presentation

A 33-year-old woman was diagnosed with SLE in 2019 based on clinical findings and immunological abnormalities, including positive antinuclear antibodies (ANA), positive anti-double-stranded DNA antibodies (anti-dsDNA), and decreased complement levels (C3 and C4). She fulfilled the 2019 ACR/EULAR classification criteria for SLE. Following the diagnosis, she was treated with hydroxychloroquine, methylprednisolone, and low-dose aspirin with regular rheumatologic follow-up.

Initial antiphospholipid antibody testing performed at the time of SLE diagnosis revealed isolated high-titer anti-β2GPI IgM positivity >200 RU/mL (reference value < 20 RU/mL), while anti-β2GPI IgG and lupus anticoagulant were negative. The patient had no history of arterial or venous thrombosis, previous pregnancy losses, or family history of APS.

In July 2024, during her first trimester of pregnancy, laboratory reassessment demonstrated persistently decreased C3 and C4 levels. ENA profile (SSA positive, anti-Sm positive), ANA and anti-dsDNA remained positive. Lupus anticoagulant activity was measured at 42.3 sec, while both anti-β2GPI IgM and IgG were negative on repeat testing, indicating the disappearance of the previously detected high-titer anti-β2GPI IgM antibodies. Repeat testing in November 2024 showed further changes in antiphospholipid antibody profile. Lupus anticoagulant activity increased to 48.3 sec and anticardiolipin IgM antibodies became positive at 60.6 U/mL (reference value <12 U/mL). No thrombotic manifestations were observed. The patient's first pregnancy subsequently resulted in a preterm birth at 36 weeks of gestation.

In March 2026, during her second pregnancy, repeat antiphospholipid antibody testing revealed continued evolution of the antiphospholipid antibody profile. Lupus anticoagulant activity increased to 55.1 sec. Anticardiolipin antibodies were positive for both IgM and IgG, with values of 38.4 U/mL and 20.7 U/mL (reference value <12 U/mL), respectively.

Throughout the six-year follow-up period, the patient remained free of documented arterial or venous thrombotic events, and no major therapeutic modifications were introduced. Serial laboratory assessments demonstrated the longitudinal evolution of the antiphospholipid antibody profile, characterized by the disappearance of high-titer anti-β2GPI IgM antibodies and the subsequent emergence of lupus anticoagulant and anticardiolipin antibodies.

Disussion

This case report illustrates a remarkable longitudinal evolution of the antiphospholipid antibody profile in a woman with SLE over a six-year follow-up. The most notable finding was the transition from isolated high-titer anti-β2GPI IgM positivity at the time of diagnosis to the subsequent disappearance of anti-β2GPI antibodies and emergence of LAC and anticardiolipin antibodies during this period. These changes occurred despite stable treatment with hydroxychloroquine, methylprednisolone, and low-dose aspirin, with no documented thrombotic manifestations.

Antiphospholipid antibodies are frequently detected in SLE patients and are associated with an increased risk for thrombotic and obstetric complications.[2,3] Current classification criteria focus on the persistence of aPL positivity and require laboratory confirmation after at least 12 weeks.[1] Accumulating evidence suggests that the aPL profile is dynamic and may change throughout the disease's course. This case provides a clear illustration of this phenomenon.

Table 1.

Evolution of antiphospholipid antibody profile during follow-up.

Time point	Clinical status	LAC (sec)	aCL IgM (U/mL)	aCL IgG (U/mL)	Anti-β2GPI IgM (RU/mL)	Anti-β2GPI IgG (RU/mL)	Other findings
2019	SLE diagnosis	Neg	-	-	>200	Neg	ANA + anti-dsDNA + low C3/C4
07.2024	First pregnancy (1st trimester)	42.3	Neg	Neg	Neg	Neg	ANA + anti-dsDNA + low C3/C4, ENA +
11.2024	Follow-up during pregnancy	48.3	60.6	Neg	Neg	Neg	No thrombotic events
2025	Pregnancy outcome						Preterm birth at 36 weeks
03.2026	Second pregnancy (1st trimester)	55.1	38.4	20.7	Neg	Neg	Low C3/C4

LAC-lupus anticoagulant, aCL-anticardiolipin antibodies, anti-β2GPI-anti-beta-2 glycoprotein I, C3- complement component 3, C4-complement component 4, ENA-extractable nuclear antigen.

In longitudinal studies of SLE patients, similar fluctuations and serological transitions have been reported.[4] aPL may exhibit variable patterns over time, including seroconversion from positive to negative status and the appearance of new antibody specificities. These observations support the concept that antiphospholipid autoimmunity represents a dynamic process.[5]

The mechanism underlying these changes remains incompletely understood. Persistent immune dysregulation and ongoing B-cell activation in SLE may contribute to shifts in autoantibody profiles over time, although the factors driving longitudinal evolution remain unclear.[6] The transition observed in this patient, characterized by the disappearance of anti-β2GPI antibodies and subsequent emergence of LAC and aCL antibodies, may reflect the natural evolution of antiphospholipid autoimmunity rather than a stable antibody pattern.

The absence of arterial or venous thrombosis despite the longitudinal evolution of aPL profile is another noteworthy aspect. LAC is considered the strongest laboratory predictor of thrombotic and obstetric manifestations among antiphospholipid antibodies. The progressive increase in LAC activity observed in this patient may be clinically relevant despite the absence of thrombotic manifestations. However, not all individuals with positive aPL develop clinical APS. The occurrence of thrombosis is thought to depend on additional genetic, inflammatory, or environmental factors known as a "second hit" in susceptible individuals.[7] The present findings also highlight the importance of repeated testing, as a single negative result may not accurately reflect future risk and may fail to capture the dynamic evolution of aPL profile.

The longitudinal evolution of aPL antibody profiles remains incompletely understood. While fluctuations in aPL status have been reported, no consistent pattern of antibody evolution has been established. Factors such as previous births, the interpregnancy interval, hormonal changes, and environmental exposures have been suggested as potential modulators of aPL dynamics; however, robust evidence supporting these associations is still lacking.

This woman experienced two pregnancies during the follow-up period, with a preterm birth at 36 weeks of gestation during the first pregnancy. Pregnant women with SLE and aPL positivity have an increased risk for adverse obstetric outcomes.[2]

Although a direct relationship cannot be established from a single case, the emergence and progressive increase of LAC during pregnancy may be clinically relevant, given the well-recognized association between LAC positivity and adverse pregnancy outcomes. This observation further emphasizes the importance of close laboratory surveillance in pregnant women with SLE.

This report has some limitations. As a single case report, it cannot establish causal relationships between changes in antiphospholipid antibody profiles and pregnancy, hormonal influences, or other clinical factors. Furthermore, these findings cannot be generalized to all patients with SLE or APS. Nevertheless, the prolonged six-year follow-up with repeated laboratory assessments provides a unique opportunity to document the longitudinal evolution of antiphospholipid antibody profiles.

Conclusion

This case demonstrates a six-year longitudinal evolution of the aPL profile in a woman with SLE, characterized by the disappearance of high-titer anti-β2GPI IgM antibodies and the subsequent emergence of LAC and aCL antibodies. These changes occurred despite stable treatment and in the absence of thrombotic events. The findings support the concept that antiphospholipid autoimmunity may evolve over time and emphasize the value of long-term monitoring of aPL profiles in SLE patients, particularly during the reproductive years. Further research is warranted to identify the factors that drive the longitudinal evolution of antiphospholipid antibody profiles and to clarify their clinical significance.

Acknowledgments

The authors are grateful to the patient for kindly allowing them to publish her case.

Conflict of Interest

The authors declare that they have no competing interests.

References

1. Miyakis S, Lockshin MD, Atsumi T, Branch DW, Brey RL, Cervera R, et al. International consensus statement on an update of the classification criteria for definite antiphospholipid syndrome (APS). J Thromb Haemost. 2006 Feb;4(2):295-306. doi: 10.1111/j.1538-7836.2006.01753.x. PMID: 16420554.
2. Tektonidou MG, Andreoli L, Limper M, Amoura Z, Cervera R, Costedoat-Chalumeau N, et al. EULAR recommendations for the management of antiphospholipid syndrome in adults. Ann Rheum Dis. 2019 Oct;78(10):1296-1304. doi: 10.1136/annrheumdis-2019-215213. Epub 2019 May 15. PMID: 31092409; PMCID: PMC11034817.
3. Pons-Estel GJ, Andreoli L, Scanzi F, Cervera R, Tincani A. The antiphospholipid syndrome in patients with systemic lupus erythematosus. J Autoimmun. 2017 Jan;76:10-20. doi: 10.1016/j.jaut.2016.10.004. Epub 2016 Oct 21. PMID: 27776934.
4. Frodlund M, Walhelm T, Dahle C, Sjöwall C. Longitudinal Analysis of Anti-cardiolipin and Anti-β2-glycoprotein-I Antibodies in Recent-Onset Systemic Lupus Erythematosus: A Prospective Study in Swedish Patients. Front Med (Lausanne). 2021 Feb 24;8:646846. doi: 10.3389/fmed.2021.646846.
5. Chighizola CB, Willis R, Maioli G, Sciascia S, Andreoli L, Amengual O, et al. Deciphering the clinical significance of longitudinal antiphospholipid antibody titers. Autoimmun Rev. 2024 Mar;23(3):103510. doi: 10.1016/j.autrev.2023.103510.
6. Giannakopoulos B, Krilis SA. The pathogenesis of the antiphospholipid syndrome. N Engl J Med. 2013 Mar 14;368(11):1033-44. doi: 10.1056/NEJMra1112830. PMID: 23484830.
7. Meroni PL, Borghi MO, Raschi E, Tedesco F. Pathogenesis of antiphospholipid syndrome: understanding the antibodies. Nat Rev Rheumatol. 2011 Jun;7(6):330-9. doi: 10.1038/nrrheum.2011.52. Epub 2011 May 10. PMID: 21556027.

International Journal of Biomedicine 16(3) (2026) 398-400
http://dx.doi.org/10.21103/Article16(3)_CR3

CASE REPORT

INTERNATIONAL JOURNAL OF BIOMEDICINE

Demyelinating Sensorimotor Polyneuropathy in a Pediatric Patient with a *KIF1B* Variant: A Case Report

Armand Shehu[1], Anita Pilika[1], Aida Bushati[1], Kristi Aleksi[2*], Xhentila Doka[1], Era Kurti[1], Era Shehu[3]

[1]*Mother Teresa University Hospital, Tirane, Albania*
[2]*Faculty of Medicine, University of Medicine, Tirane, Albania*
[3]*Faculty of Medicine, Our Lady of Good Counsel University, Tirane, Albania*

Abstract

Sensorimotor polyneuropathies in childhood comprise a clinically and etiologically heterogeneous group of peripheral nerve disorders. They are commonly associated with progressive motor and sensory impairment, balance and gait disturbances, musculoskeletal deformities, reduced functional independence, and overall long-term disability. Herein, we present a diagnostically challenging case of a 13-year-old boy with a demyelinating electrophysiological profile, despite identification of a genetic variant previously associated with an axonal, non-demyelinating form of peripheral sensorimotor neuropathy. (**International Journal of Biomedicine. 2026;16(3):398-400.**)

Keywords: Charcot-Marie-Tooth • *KIF1B* • demyelinating sensorimotor polyneuropathy

For citation: Shehu A, Pilika A, Bushati A, Aleksi K, Doka X, Kurti E, Shehu E. Demyelinating Sensorimotor Polyneuropathy in a Pediatric Patient with a *KIF1B*: A Case Report. International Journal of Biomedicine. 2026;16(3):398-400. doi:10.21103/Article16(3)_CR3

Introduction

Sensorimotor neuropathies in childhood comprise a heterogeneous group of disorders affecting peripheral motor and sensory nerves. They cause progressive weakness, sensory loss, balance and gait impairment, musculoskeletal deformities, reduced functional independence, and overall long-term disability. Their etiology is broad and includes hereditary or acquired causes, such as traumatic, metabolic, toxic, nutritional, and immune-mediated causes.[1] In clinical practice, distinguishing inherited from acquired neuropathies is essential, as this directly influences diagnostic strategy, prognosis, genetic counseling, and management.

Case Presentation

In December 2023, a 13-year-old boy was referred to our Neuropediatric Service for evaluation. On clinical assessment, his general condition was stable; he was afebrile, with no vomiting, and was responsive and appropriately oriented for his biological age. Neurological examination revealed a mild articulation disorder. Also, both gross and fine motor functions were impaired; he was unable to run or walk quickly, had difficulty climbing stairs, fatigued easily, and could not rise from the floor without support, so Gowers' sign was positive. He was unable to write and had difficulty performing tasks such as opening a bottle cap. During sensory evaluation, he reported numbness in the hands and feet, as well as difficulty distinguishing cold from warm objects by touch. At musculoskeletal examination, deformity of the right talocrural joint, hammer-toe deformity of the great toes, and reduced muscle bulk in the upper limbs, thighs, and calves were observed. Deep tendon reflexes, including patellar and Achilles reflexes, were absent bilaterally. Spinal deformities were also noticed, including thoracic kyphoscoliosis, lumbar lordosis, and leftward trunk deviation. The child had started physiotherapy approximately 1.5 years ago and had also been wearing spinal braces. No abnormalities were detected on the rest of the physical examination, including the cardiac, pulmonary, and abdominal systems.

The parents reported that symptoms began at approximately 6 years of age and had worsened over time. The pregnancy and perinatal history were uneventful, and early childhood development was reported as unremarkable. Family history was unremarkable.

Results of the complete blood count, biochemical laboratory tests, echocardiogram, and electrocardiogram were within age-appropriate limits. Head magnetic resonance imaging was also unremarkable. Spinal X-ray findings supported the physical examination. Electroneuromyography (ENMG) revealed chronic demyelinating sensorimotor polyneuropathy, with markedly reduced motor conduction velocities and amplitudes, prolonged latencies, increased motor unit potential amplitude/duration, and a sparse interference pattern. Whole-exome sequencing (WES) with copy number calling was performed and identified a heterozygous variant of uncertain significance (VUS) in the *KIF1B* gene (Table 1).

Table 1.
Variant details.

Genomic coordinate (GRCh38)	chr1:10268208C>T
HGVS nomenclature	c.665C>T
ID Transcript	NM_001365951.3
Protein change	p.Thr222Met
Location	exon 7/49
Class / ACMG classification	class 3 / VUS
Function	missense

ACMG = American College of Medical Genetics and Genomics
HGVS = Human Genome Variation Society

Discussion

This case describes a 13-year-old boy with childhood-onset, slowly progressive, chronic sensorimotor polyneuropathy.

Hereditary vs. Acquired

The combination of neurological and musculoskeletal impairment, medical history, a long-standing childhood-onset course with gradual progression over several years, the electrophysiological findings, and the absence of relevant systemic abnormalities is not suggestive of an acquired disorder. Instead, these features support a hereditary sensorimotor neuropathy, probably within the Charcot–Marie–Tooth (CMT) disease spectrum.[2]

Demyelinating vs. Axonal

CMT represents a clinically and genetically heterogeneous group of inherited peripheral neuropathies characterized by chronic motor and sensory impairment. [3,4] Although the family history in this case was unremarkable, this does not exclude genetic etiology, because de novo variants may also occur. The electrophysiological findings are central to diagnostic interpretation. In CMT, nerve conduction assessment is commonly used to distinguish demyelinating types from axonal, non-demyelinating types. A median nerve conduction velocity below approximately 35 or 38 m/s, depending on authors, is generally used to support a demyelinating classification, whereas relatively preserved velocities with reduced amplitudes favor an axonal form.[3-5] In the present patient, the markedly slow nerve conduction velocities are therefore more consistent with a demyelinating CMT-like phenotype, while the reduced amplitudes observed do not exclude such a phenotype, as in long-standing demyelinating neuropathies, secondary axonal loss may occur.[4,6]

Meanwhile, WES identified a heterozygous VUS in the *KIF1B* gene. KIF1B encodes a kinesin motor protein involved in microtubule-based intracellular transport, including axonal transport of mitochondria and other cargoes important for neuronal function. Variants in *KIF1B* have been associated with CMT type 2A1 (CMT2A1), a rare autosomal dominant disease.[7] Given that this variant is of uncertain significance, it requires cautious interpretation since, according to ACMG/AMP principles, a VUS should not be used as definitive diagnostic evidence or as the sole basis for clinical decision-making.[8,9]

Conclusion

In conclusion, this case highlights the importance of careful phenotype–genotype correlation in genetic disorders and underscores the need for cautious interpretation of variants of uncertain significance in clinical practice. In the present patient, the phenotype is most consistent with a slowly progressive, childhood-onset hereditary sensorimotor neuropathy, with ENMG findings predominantly suggestive of nerve demyelination. Despite the chronic electrophysiological changes indicating axonal loss, the overall pattern does not align well with a classic axonal phenotype. Furthermore, although a heterozygous variant of uncertain significance in *KIF1B* was identified, this finding alone is insufficient to establish a diagnosis of CMT2A1.

Ethical Statement

Informed consent was obtained from the patient's parents for the publication of this report.

Conflicts of Interest

None.

References

1. Korinthenberg R, Trollmann R, Plecko B, Stettner GM, Blankenburg M, Weis J, Schoser B, Müller-Felber W, Lochbuehler N, Hahn G, Rudnik-Schöneborn S. Differential Diagnosis of Acquired and Hereditary Neuropathies in Children and Adolescents-Consensus-Based Practice Guidelines. Children (Basel). 2021 Aug 9;8(8):687. doi: 10.3390/children8080687. PMID: 34438578; PMCID: PMC8392610.

2. Bird TD. Charcot-Marie-Tooth Hereditary Neuropathy Overview. In: Adam MP, Feldman J, Mirzaa GM, et al., editors. GeneReviews®. Seattle (WA): University of Washington, Seattle; 1993-2025.

3. Banchs I, Casasnovas C, Albertí A, De Jorge L, Povedano M, Montero J, Martínez-Matos JA, Volpini V. Diagnosis of Charcot-Marie-Tooth disease. J Biomed Biotechnol. 2009;2009:985415. doi: 10.1155/2009/985415. Epub 2009 Oct 8. PMID: 19826499; PMCID: PMC2760395.

4. Nagappa M, Sharma S, Taly AB. Charcot Marie Tooth [Internet]. PubMed. Treasure Island (FL): StatPearls Publishing; 2024. Available from: https://www.ncbi.nlm.nih.gov/books/NBK562163/
5. Moss KR, Bopp TS, Johnson AE, Höke A. New evidence for secondary axonal degeneration in demyelinating neuropathies. Neurosci Lett. 2021 Jan 23;744:135595. doi: 10.1016/j.neulet.2020.135595. Epub 2020 Dec 24. PMID: 33359733; PMCID: PMC7852893.
6. Zhao C, Takita J, Tanaka Y, Setou M, Nakagawa T, Takeda S, Yang HW, Terada S, Nakata T, Takei Y, Saito M, Tsuji S, Hayashi Y, Hirokawa N. Charcot-Marie-Tooth disease type 2A caused by mutation in a microtubule motor KIF1Bbeta. Cell. 2001 Jun 1;105(5):587-97. doi: 10.1016/s0092-8674(01)00363-4. Erratum in: Cell 2001 Jul 13;106(1):127. PMID: 11389829.
7. KIF1B kinesin family member 1B [Homo sapiens (human)] - Gene - NCBI [Internet]. Nih.gov. 2026 [cited 2026 Jun 18]. Available from: https://www.ncbi.nlm.nih.gov/gene/23095?utm_source=chatgpt.com
8. Richards S, Aziz N, Bale S, Bick D, Das S, Gastier-Foster J, Grody WW, Hegde M, Lyon E, Spector E, Voelkerding K, Rehm HL; ACMG Laboratory Quality Assurance Committee. Standards and guidelines for the interpretation of sequence variants: a joint consensus recommendation of the American College of Medical Genetics and Genomics and the Association for Molecular Pathology. Genet Med. 2015 May;17(5):405-24. doi: 10.1038/gim.2015.30. Epub 2015 Mar 5. PMID: 25741868; PMCID: PMC4544753.
9. Mighton C, Abu-El-Haija A, Aggarwal V, Akkari YMN, Astbury C, Best DH, Conlin LK, Harrison SM, Jiang N, Kruszka P, McKnight D, Nguyen Dolphyn TT, Barquet Ramos F, Thomas CP, Bean LJH, Rehm HL; Laboratory Quality Assurance Committee. Points to consider for the reporting of variants of uncertain significance in germline genetic and genomic testing: A statement of the American College of Medical Genetics and Genomics (ACMG). Genet Med. 2026 Jul;28(7):102583. doi: 10.1016/j.gim.2026.102583. Epub 2026 Jun 12. PMID: 42287277.

***Corresponding author**: Kristi Aleksi. E-mail: kristialeksi1@gmail.com*

International Journal of Biomedicine 16(3) (2026) 401-405
http://dx.doi.org/10.21103/Article16(3)_CR4

CASE REPORT

INTERNATIONAL JOURNAL OF BIOMEDICINE

Diagnostic Reappraisal after 12-Year Follow-up of Pediatric Myopathy with Heterozygous *NEB* Variants and Dystrophy-Like Progression

Afërdita Tako[1], Mirela Tabaku[2*], Aida Bushati[3], Rovena Aliaj[1], Armand Shehu[1], Sindi Dizdari[1], Paskal Cullufi[3]

[1]*Department of Pediatrics, Mother Teresa University Hospital Center, Tirana, Albania*
[2]*Department of Pediatrics, Genetics Service, University of Medicine Tirana, Tirana, Albania*
[3]*Department of Pediatrics, University of Medicine Tirana, Tirana, Albania*

Abstract

Background: Mutations in the *NEB* gene are the most frequent genetic cause of autosomal recessive nemaline myopathy, a clinically heterogeneous congenital myopathy.
In pediatric myopathy, longitudinal observation is essential because the evolving phenotype may challenge an initially plausible molecular interpretation and reveal features requiring diagnostic reappraisal.
Case presentation: This report describes a 12-year clinical-genetic trajectory in a child with congenital-onset myopathy, persistent hyperCKemia, two heterozygous *NEB* variants, and later dystrophy-like progression. Clinical exome sequencing performed at 5 years of age identified two heterozygous *NEB* variants: the canonical splice-site variant c.10872+1G>C and the missense variant c.11333T>C (p.Ile3778Thr). The patient achieved independent ambulation at 20 months but later developed progressive weakness, Gowers' sign, scapular winging, distal muscle wasting, and progressive functional decline, ultimately losing independent ambulation at 12 years. Cardiac and respiratory assessments remained normal during follow-up.
Conclusions: This report describes a 12-year clinical-genetic trajectory in a child with congenital-onset myopathy, persistent hyperCKemia, two heterozygous *NEB* variants of unresolved phase, and later dystrophy-like progression. The longitudinal course highlights the importance of cautious interpretation of exome findings and supports ongoing diagnostic reappraisal when evolving features broaden the neuromuscular differential diagnosis. (**International Journal of Biomedicine. 2026;16(3):401-405.**)

Keywords: *NEB* • nemaline myopathy • pediatric myopathy • hyperCKemia • longitudinal follow-up • diagnostic reappraisal

For citation: Tako A, Tabaku M, Bushati A, Aliaj R, Shehu A, Dizdari S, Cullufi P. Diagnostic Reappraisal after 12-Year Follow-up of Pediatric Myopathy with Heterozygous NEB Variants and Dystrophy-Like Progression. International Journal of Biomedicine. 2026;16(3):401-405. doi:10.21103/Article16(3)_CR4

Introduction

Nemaline myopathy (NM) is a genetically heterogeneous congenital myopathy characterized by skeletal muscle weakness, hypotonia, and nemaline rods on muscle histopathology. Among the currently recognized disease genes, *NEB*, which encodes nebulin, is one of the most frequent causes of autosomal recessive NM. Nebulin is a large thin-filament protein involved in sarcomeric organization, thin-filament length regulation, and force generation, and *NEB*-related disease spans a broad clinical spectrum ranging from severe neonatal presentations to milder childhood phenotypes compatible with prolonged ambulation.[1-4]

The increasing use of next-generation sequencing has improved the diagnostic work-up of pediatric neuromuscular disorders. However, the clinical value of a molecular finding is maximized when it is interpreted together with the longitudinal phenotype. This is particularly relevant when a child with congenital-onset motor impairment later develops persistent hyperCKemia, calf pseudohypertrophy, Gowers' sign, scapular winging, and progressive loss of ambulation, a pattern that can overlap with muscular dystrophy.[3-6]

This report describes the 12-year longitudinal course of a child with two heterozygous *NEB* variants whose phenotype evolved from congenital-onset myopathy toward dystrophy-like progression with persistent hyperCKemia and loss of

ambulation. Rather than presenting the findings as definitive proof of *NEB* causality, the case illustrates how long-term clinical evolution may challenge an initially plausible molecular interpretation and support diagnostic reappraisal when the phenotype broadens.

Case Presentation

The patient was a boy born at term after an uncomplicated pregnancy and spontaneous vaginal delivery, with normal neonatal adaptation and no known family history of neuromuscular disease. Motor delay became evident from infancy. Head control was achieved at 4 months, independent sitting at 8 months, supported walking at 15 months, and independent ambulation at 20 months, indicating early motor impairment despite eventual acquisition of walking.

Initial neurological evaluation showed generalized hypotonia, absent deep tendon reflexes, paraspinal muscle atrophy, and mild gastrocnemius pseudohypertrophy. Cranial nerve function was preserved, and no persistent bulbar dysfunction was clearly documented during follow-up. Electromyography demonstrated a myopathic pattern.

Serial biochemical investigations provided consistent evidence of chronic muscle involvement. At the initial evaluation, serum AST was 100 U/L, ALT was 80 U/L, CK was 1500 U/L, and LDH was 800 U/L. These abnormalities persisted during follow-up; representative later values included AST 80 U/L, ALT 70 U/L, CK 1000 U/L, and LDH 700 U/L. Overall, CK remained approximately within the range of 1000-1500 U/L across the available longitudinal data.

Although the patient achieved independent ambulation, progressive motor deterioration became evident during childhood. He developed Gowers' sign, scapular winging, distal muscle wasting, and worsening weakness with increasing functional limitation. Within the available documentation, no clear contractures, scoliosis, or persistent facial or bulbar involvement were consistently recorded. Serial clinical cardiopulmonary evaluations remained reassuring, with no documented evidence of cardiac involvement or overt respiratory compromise. Independent ambulation was ultimately lost at age 12.

Clinical exome sequencing performed at 5 years of age identified two heterozygous *NEB* variants: c.10872+1G>C, a canonical splice-site variant, and c.11333T>C (p.Ile3778Thr), a missense variant. The diagnostic laboratory considered the findings supportive of possible NEB-associated disease and recommended parental testing to determine whether the variants were in trans. Parental segregation analysis was not performed; therefore, the phase of the variants remains unresolved. In addition, dedicated dystrophinopathy testing, including DMD deletion/duplication analysis, was not documented in the available initial diagnostic workup.

Differential diagnosis

At presentation, the combination of infantile hypotonia, delayed motor milestones, absent deep tendon reflexes, and a myopathic electromyographic pattern supported congenital myopathy. Over time, persistent CK elevation of approximately 1000-1500 U/L, mild calf pseudohypertrophy, Gowers' sign, progressive weakness, and childhood loss of ambulation broadened the clinical differential toward dystrophinopathy and other inherited muscular dystrophies.

The identification of two heterozygous NEB variants made NEB-associated disease a plausible molecular consideration for the early congenital-onset phenotype. However, because the phase was not established and the subsequent clinical course showed dystrophy-like progression, the case is best interpreted as a clinically informative overlap between features of congenital myopathy and a progressive dystrophic phenotype. This framing highlights that longitudinal follow-up can refine diagnosis, redirect differential thinking, and identify patients who may require additional evaluation beyond the initial exome result. The longitudinal clinical course is summarized in Table 1.

Table 1.

Twelve-year clinical and diagnostic timeline: Developmental, biochemical, molecular, and functional milestones documented during follow-up.

Age/period	Key finding	Clinical meaning
Infancy	Hypotonia; delayed milestones	Congenital-onset neuromuscular disease
20 months	Independent ambulation achieved	Early gain despite motor delay
Childhood	CK approximately 1000-1500 U/L; Gowers' sign; scapular winging	Progressive skeletal-muscle involvement
5 years	Two heterozygous NEB variants identified	Plausible NEB-related molecular consideration; allelic phase unresolved
12 years	Loss of independent ambulation	Major marker of dystrophy-like progression

Discussion

This case is characterized by a long clinical course in which congenital-onset features were followed by substantial dystrophy-like progression over 12 years. Infantile hypotonia, delayed motor milestones, absent reflexes, and a myopathic electromyographic pattern supported a congenital myopathy presentation and could fit within the broad *NEB*-associated disease spectrum. The later emergence of persistent marked hyperCKemia, Gowers' sign, scapular winging, distal wasting, and loss of independent ambulation shifted the interpretation toward a more complex clinicogenetic picture.

Published studies of *NEB*-associated NM emphasize broad phenotypic heterogeneity and variable motor, bulbar, respiratory, and skeletal muscle involvement. [1-4] The present case spans a long observation window from early motor delay to later functional decline, providing a clearer view of phenotypic evolution over time (Figure 1). This longitudinal dimension is clinically relevant: a child who initially achieves independent walking may still develop a progressive course that changes the diagnostic interpretation, surveillance priorities, and management questions.

Figure 1. *Longitudinal clinic-genetic timeline summarizing the major developmental, molecular, and functional milestones during the 12-year follow-up.*

The molecular findings are clinically relevant but should be interpreted cautiously. The canonical splice-site variant c.10872+1G>C represents the stronger molecular finding, whereas p.(Ile3778Thr) requires contextual interpretation in relation to the patient's phenotype and available variant literature. [7,10] Together, the two identified *NEB* variants provide a plausible but not definitive molecular explanation, as parental segregation analysis was not performed, and the allelic phase remains unresolved. Therefore, a confirmed biallelic *NEB*-related disorder cannot be established based on the available data. Key clinical and molecular features informing the diagnostic interpretation are summarized in Table 2.

Phenotype evolution remains central in pediatric neuromuscular disease. In a male patient with persistent hyperCKemia, calf pseudohypertrophy, progressive weakness, Gowers' sign, and childhood loss of ambulation, dystrophinopathy and other muscular dystrophies remain important clinical considerations. [8,9] In the present case, longitudinal follow-up revealed a dystrophy-like trajectory despite early features and molecular findings that initially pointed toward congenital myopathy.

This case underscores a key diagnostic principle in pediatric neuromuscular disorders: early genotype-phenotype correlation may remain provisional, particularly when longitudinal clinical evolution introduces atypical features for the initially suspected condition. In such scenarios, maintaining a dynamic diagnostic framework and reconsidering alternative etiologies is essential. Table 3 summarizes selected recent literature relevant to pediatric and *NEB*-associated nemaline myopathy, providing context for the longitudinal features observed in the present patient.

Table 2.

Clinical and molecular features informing diagnosis: Summary of the principal findings supporting possible NEB involvement and features broadening the neuromuscular differential diagnosis.

Domain	Features supporting possible NEB involvement	Features broadening the differential diagnosis
Early phenotype	Hypotonia, delayed milestones, myopathic EMG	Congenital myopathy presentation
Molecular findings	Two heterozygous NEB variants; one canonical splice-site allele	Missense variant requires contextual interpretation; allelic phase unresolved
Biochemistry	Persistent muscle enzyme elevation	CK, approximately 1000-1500 U/L, broadens the differential toward dystrophic disorders
Motor course	Early congenital myopathy-compatible presentation	Loss of ambulation at 12 years
Cardiorespiratory follow-up	No cardiac/respiratory involvement documented	Predominantly skeletal-muscle course

Table 3.

Selected literature context for interpreting the present longitudinal phenotype.

Study	Clinical context	Motor/CK profile	Interpretive value	Relevance to present case / limitation
Christophers et al., 2023 [2]	Pediatric NM systematic review	Broad heterogeneity	Frames pediatric NM variability	Supports heterogeneity but does not establish causality in an individual case
Amburgey et al., 2021 [9]	Cross-sectional NM study	Disability spectrum	Contrasts with marked decline	Useful comparator for severity, but cross-sectional design limits longitudinal inference
Moreno et al., 2023 [3]	NEB-specific cohort	Variable progression	Key NEB comparator	Relevant NEB cohort, although the present patient lacks a confirmed biallelic phase
Haidong et al., 2024 [10]	Clinicopathologic NM series	Pathology-informed cases	Shows value of orthogonal data	Highlights the limitation created by the absence of a muscle biopsy in the present case
Chalipat et al., 2024 [11]	Pediatric NEB case	Normal CK	Highlights CK contrast	Contrasts with persistent hyperCKemia in the present patient
Present case	12-year follow-up	CK of 1000-1500 U/L; loss of ambulation	Educational diagnostic reappraisal	Longitudinal observation, but causality remains limited by unresolved phase and incomplete dystrophy work-up

Clinical Implications

This case emphasizes that persistent hyperCKemia, Gowers' sign, calf pseudohypertrophy, scapular winging, and loss of ambulation should prompt diagnostic re-evaluation for dystrophinopathy or other muscular dystrophies, even when exome sequencing identifies plausible variants in a congenital myopathy gene. For similar patients, a longitudinal approach that combines repeated functional assessments, updated variant interpretations, and targeted re-evaluations as the phenotype evolves may be particularly informative. This longitudinal perspective may be useful for clinicians evaluating children with overlapping congenital myopathy and muscular dystrophy features.

Diagnostic Limitations

Several methodological constraints should be considered when interpreting this case. Parental segregation analysis was not performed; therefore, the allelic phase remained unresolved. Although clinical exome sequencing was performed, additional orthogonal investigations, including muscle biopsy, muscle MRI, RNA-based analysis, and targeted CNV-sensitive assessment of dystrophinopathy-associated genes, were not available. Therefore, the findings should be interpreted as a longitudinal clinical-genetic observation rather than as definitive proof of *NEB* causality. These limitations do not eliminate the clinical value of the report, but they define its appropriate interpretation.

Conclusion

This report documents a 12-year clinicogenetic follow-up of a child with congenital-onset myopathy, persistent hyperCKemia, two heterozygous *NEB* variants of unresolved phase, and subsequent dystrophy-like progression with loss of ambulation. The case highlights the importance of longitudinal phenotyping and cautious interpretation of molecular findings, particularly when evolving clinical features broaden the differential diagnosis toward muscular dystrophy. Longitudinal multidisciplinary reassessment remains particularly important in such complex neuromuscular presentations.

AI Statement

AI-assisted tools were used solely for language editing and manuscript formatting, based on scientific material provided by the authors.

Ethics Statement

Written informed consent for publication of the clinical details was obtained from the patient's parents/legal guardians. Ethical review and approval were waived because this study represents a retrospective descriptive case report without experimental intervention. The study was conducted in accordance with the Declaration of Helsinki and institutional ethical standards.

Author Contributions

Afërdita Tako contributed to conceptualization, literature review, patient evaluation and clinical follow-up.
Mirela Tabaku contributed to conceptualization, literature review, interpretation of clinical-genetic findings, manuscript drafting, and final manuscript revision.
Aida Bushati, Rovena Aliaj, Armand Shehu, Sindi Dizdari, and Paskal Cullufi contributed to clinical data collection, interpretation, and critical revision of the manuscript.
All authors reviewed and approved the final manuscript.

Funding

No funding was received for this study.

Conflict of Interest

The authors declare no conflict of interest.

Data Availability Statement

Data supporting the findings of this study are included within the article. Additional information is available from the corresponding author upon reasonable request.

References

1. Sewry CA, Laitila JM, Wallgren-Pettersson C. Nemaline myopathies: a current view. J Muscle Res Cell Motil. 2019 Jun;40(2):111-126. doi: 10.1007/s10974-019-09519-9. Epub 2019 Jun 21. PMID: 31228046; PMCID: PMC6726674.
2. Christophers B, Lopez MA, Gupta VA, Vogel H, Baylies M. Pediatric Nemaline Myopathy: A Systematic Review Using Individual Patient Data. J Child Neurol. 2022 Jun;37(7):652-663. doi: 10.1177/08830738221096316. Epub 2022 Jun 7. PMID: 36960434; PMCID: PMC10032635.
3. Moreno CAM, Artilheiro MC, Fonseca ATQSM, Camelo CG, de Medeiros GC, Sassi FC, de Andrade CRF, Donkervoort S, Silva AMS, Dalfior-Junior L, Abath-Neto OL, Reed UC, Bönnemann C, Zanoteli E. Clinical Manifestation of Nebulin-Associated Nemaline Myopathy. Neurol Genet. 2023 Jan 25;9(1):e200056. doi: 10.1212/NXG.0000000000200056. PMID: 36714460; PMCID: PMC9879277.
4. Ryan MM, Schnell C, Strickland CD, Shield LK, Morgan G, Iannaccone ST, Laing NG, Beggs AH, North KN. Nemaline myopathy: a clinical study of 143 cases. Ann Neurol. 2001 Sep;50(3):312-20. doi: 10.1002/ana.1080. PMID: 11558787.
5. Darras BT, Urion DK, Ghosh PS. Dystrophinopathies. 2000 Sep 5 [Updated 2022 Jan 20]. In: Adam MP, Bick S, Mirzaa GM, et al., editors. GeneReviews® [Internet]. Seattle (WA): University of Washington, Seattle; 1993-2026.
6. Fratter C, Dalgleish R, Allen SK, Santos R, Abbs S, Tuffery-Giraud S, Ferlini A. EMQN best practice guidelines

for genetic testing in dystrophinopathies. Eur J Hum Genet. 2020 Sep;28(9):1141-1159. doi: 10.1038/s41431-020-0643-7. Epub 2020 May 18. PMID: 32424326; PMCID: PMC7608854.
7. Pangalos C, Hagnefelt B, Lilakos K, Konialis C. First applications of a targeted exome sequencing approach in fetuses with ultrasound abnormalities reveals an important fraction of cases with associated gene defects. PeerJ. 2016 Apr 26;4:e1955. doi: 10.7717/peerj.1955. PMID: 27168972; PMCID: PMC4860337.
8. ClinVar. NM_001164508.2(NEB):c.11333T>C (p.Ile3778Thr), Variation ID: 435964. National Center for Biotechnology Information.
9. Amburgey K, Acker M, Saeed S, Amin R, Beggs AH, Bönnemann CG, et al. A Cross-Sectional Study of Nemaline Myopathy. Neurology. 2021 Mar 9;96(10):e1425-e1436. doi: 10.1212/WNL.0000000000011458. Epub 2021 Jan 4. PMID: 33397769; PMCID: PMC8055318.
10. Haidong L, Yin L, Ping C, Xianzhao Z, Qi Q, Xiaoli M, Zheng L, Wenhao C, Yaguang Z, Qianqian Q. Clinico-pathological and gene features of 15 nemaline myopathy patients from a single Chinese neuromuscular center. Acta Neurol Belg. 2024 Feb;124(1):91-99. doi: 10.1007/s13760-023-02333-8. Epub 2023 Jul 31. PMID: 37525074; PMCID: PMC10874337.
11. Chalipat S, Talewad S, Gupta A, Bahal M, Mane SV. Nemaline Myopathy With a Compound Heterozygous Mutation: A Case Report. Cureus. 2024 Jul 4;16(7):e63828. doi: 10.7759/cureus.63828. PMID: 39099920; PMCID: PMC11297552.

***Corresponding author:** *Assoc. Prof. Dr. Mirela Tabaku. Department of Pediatrics, Genetics Service, University of Medicine Tirana, Tirana, Albania. E-mail: mtabaku@yahoo.com.*

International Journal of Biomedicine 16(3) (2026) 406-409
http://dx.doi.org/10.21103/Article16(3)_CR5

CASE REPORT

INTERNATIONAL JOURNAL OF BIOMEDICINE

Food Noise, Intrusive Thoughts, and Depression - Improvement on Tirzepatide: A Case Report

Amirah Alhowiti

Department of Family and Community Medicine, Faculty of Medicine, University of Tabuk, KSA

Abstract

Tirzepatide (Mounjaro) is a dual long-acting glucose-dependent insulinotropic polypeptide receptor and glucagon-like peptide-1 receptor agonist. Tirzepatide was approved for the treatment of type 2 diabetes in the USA, Europe, and Asia. In addition, tirzepatide showed a substantial sustained weight loss and retarded the progression to type 2 diabetes. However, concerns about its association with depression, suicidality, and various compulsive disorders, including compulsive shopping, were raised. Food noise is common among patients with hyperactive autistic spectrum disorder, which is a common disorder affecting 1/100 of children worldwide. We reported a case of depression, intrusive thoughts, and food noise improvement following tirzepatide in a 34-year-old Saudi female. Tirzepatide (Mounjaro) could be repurposed for the treatment of intrusive thoughts and food noise in patients with high body mass index.(**International Journal of Biomedicine. 2026;16(3):406-409.**)

Keywords: tirzepatide • type 2 diabetes • body mass index • food noise

For citation: Alhowiti A. Food Noise, Intrusive Thoughts, and Depression - Improvement on Tirzepatide: A Case Report. International Journal of Biomedicine. 2026;16(3):406-409. doi:10.21103/Article16(3)_CR5

Introduction

GLP-1-like receptor agonists (RAs) and dual glucose-dependent insulinotropic polypeptide (GIP)/glucagon-like peptide 1 (GLP-1) agonists (twincretins) represent a paradigm shift in obesity treatment.[1] Glucagon-like peptide receptor agonists were approved for treating type 2 diabetes in 2005, and a new long-acting formulation appeared to reduce the need for frequent subcutaneous injections. GLP-1 is well known as a gut hormone and also acts as a neuropeptide, produced in select brainstem neurons. GLP-1 stimulates insulin secretion, slows digestion, and signals the brain to promote fullness. [2-4] GLP-1-like receptor agonists and twincretins had a low risk of hypoglycemia and significantly reduced major adverse cardiovascular events.[5]

Despite the above benefits, reports about safety concerns of GLP-1 agonists were received by the European Medicines Agency regarding the association with depression, warranting further investigations.[6] Tobaiqy et al.[7] stated that although psychiatric adverse events constitute only 1.2% of the total reports for semaglutide, liraglutide, and tripeptide. However, the severity and fatality rates in some reports require further assessment. On the other hand, existing evidence suggests that GLP-1 RAs could be of value in treating psychiatric disorders, including depression, major neurocognitive disorders, and alcohol use disorders.[8,9]

Evidence of food-noise improvement with GLP-1 agonist treatment is present. Food noise is a constant, persistent, insuppressible preoccupation with food, to the extent that patients feel their lives revolve around eating.[10] Food noise and repetitive behavior are common features in hyperactive autistic spectrum disorder, which is a common disorder affecting 1/100 of children worldwide.[11] Insights from social media reported the association of GLP-1 agonists with behavioral addictions, including compulsive shopping, and various psychological disorders.[12]

We reported a case of a substantial improvement in depression symptomatology, intrusive thoughts, and food noise following tirzepatide use.

Case Report

A 34-year-old Saudi female patient, a single teacher with a Master of Arts in Translation. She is the second of healthy parents and was diagnosed with depression in 2020 and started sertraline without improvement. Then she showed some improvement on fluoxetine, she reported food obsessions in the form of food noise and intrusive thoughts, she spends almost 10 hours/day thinking about which items of food she would like to eat during that day. In addition, she had very severe thoughts about hurting herself or other people, for example, jumping in front of the train, while

on fluoxetine, she still experienced frequent and severe bouts of low mood. This patient was also diagnosed with paranoia and reports of an impulse to spend more money on shopping.

The Patient Experience before Mounjaro, in Her Own Words

"I was overweight for as long as I can remember. And I have been feeling sad (depressed) since I was a pre-teen. I was prescribed Sertraline for over a year, and the only difference was complete numbness and fatigue. In 2023, I started on Fluoxetine and began to see a difference in my mood. I am still me, and I can finally function, but fatigue persists".

Six months previously, the patient started on tirzepatide 10 mg per day for morbid obesity; her body mass index (BMI) was 49, her weight was 123, and her Height was 157. The patient showed substantial improvement in depression, food noise, and intrusive thoughts.

The Patient Feelings following Mounjaro

"Months ago, I had to start Mounjaro because of my obesity, which started to affect my knees, so I had to take Mounjaro as a way to kickstart my weight loss journey. I noticed that Mounjaro hushed the voices in my head that had driven me to spend hours on end browsing food apps to see what I could eat. I didn't realize how much energy, time, and thought I was putting into choosing a meal. That's why I developed a habit of eating once a day, late at night, and in large quantities. Food noise almost completely disappeared.

Another major thing I noticed while taking Mounjaro was how easily I could identify intrusive thoughts and shush them out quickly, like never before. And the frequency with which I have these intrusive thoughts also differed. Intrusive thoughts are a rare occurrence. In relation to depression, while on Mounjaro, my depressive episodes are shorter than before and occur less frequently as well. Before, even on medication, I would still have periods of bad mood, fatigue, and dissociation for weeks or a month. Now they are far and few between, and maybe it's related to my cycle. Normally, ovulation periods and PMS are the worst.

I use Mounjaro now less as a weight loss drug and more as a mood stabilizer that helps my mind rest a bit and not waste time over what meal to eat next."

She is now following up at the family medicine clinic on tirzepatide (Mounjaro) and fluoxetine. Her current body mass index is 44. Importantly, the patient reported no body image distortion or guilt regarding her high body mass index. The fluoxetine dose was not escalated.

Discussion

We reported a case of improving food noise, obsession, and intrusive thoughts with tirzepatide (Mounjaro). Our findings were similar to Järvinen et al.,[13] who reported an improvement in severe obsessive food craving in a patient with hyperactive autistic spectrum disorder treated with liraglutide 2.4mg/day. There is an increasing awareness about the role of GLP-1 agonists in decreasing food-compulsive eating and addiction.[14] GLP-1 agonists were shown to affect cognitive processes and influence the reward process in the brain to influence various addictive behaviors, including alcohol dependence and recreational drug abuse. [15]

Hindbrain GLP-1 neurons, located primarily in the nucleus of the solitary tract, project directly to forebrain regions, including the paraventricular nucleus and other areas of the hypothalamus, to regulate satiety and suppress food-seeking behavior. [16,17]

Dysfunction in cortico-striatal-thalamic circuits mediates executive functioning, and poor behavioral inhibition was observed in patients with obsessive-compulsive disorder and hyperactivity.

A recent case report suggested the association of semaglutide with depression.[18] However, the case reported a male patient with a previous episode of depression, suggesting that his depressive symptomatology could be a relapse of previous depression. In addition, our patient is not a case of depression, but depression and compulsive disorder. Furthermore, we used tirzepatide, a dual-acting medication that stimulates both the GIP and GLP-1 receptors.

While gut enteroendocrine cells and brainstem preproglucagon (PPG) neurons both produce GLP-1, they regulate feeding via independent mechanisms. Optogenetic or chemogenetic activation of PPG neurons in the nucleus tractus solitarius profoundly suppresses eating and promotes satiation.[19]

The restricted and repetitive patterns of behavior in autism and obsessive-compulsive disorder share various features, including ritualized patterns of verbal and nonverbal behavior, highly restrictive routine, and resistance to change. Therefore, the diagnosis is extremely challenging and leads to overdiagnosis of obsessive-compulsive disorders among patients with autism. [20]

The American Psychiatric Association included restrictive behavior as a criterion for autism diagnosis. Repetitive behavior in patients with autism appears similar to arranging, ordering, and cleaning in compulsive disorders. [21] Importantly, 17.4% of patients with obsessive-compulsive disorders had autism. However, they are usually underdiagnosed due to phenotypical similarities. [22] Jiujias et al.[23] hypothesized that obsessions initiate anxiety and compulsions relieve anxiety; therefore, there is a bidirectional relationship. The relationship between anxiety and repetitive behavior in Autism is unclear. More differences between OCD and autism are in sensory processing and executive functioning. The accurate diagnosis of repetitive behavior in autism and OCD is highly important for the introduction of the treatment for a better outcome. [24]

Although antidepressant, antipsychotic, and stimulant drugs are used to treat autism with some success. However, they do not fully reverse all the symptoms of autism spectrum disorders. In addition, autism spectrum disorders are associated with other metabolic disorders, including diabetes and obesity. [25] Therefore, drugs that address all the behavioral and metabolic disorders, like GLP-1 agonists, are attractive.

Although the effects of GLP-1 agonists on mood disorders showed mixed results, the evidence was based on observational studies. [26] Our report is important because it is the second case report in the literature to show the substantial

improvement of compulsive/obsessive behavior and depression in a patient with morbid obesity. Therefore, GLP-1 agonists should be thought of as a treatment for patients with obsession/depression, in particular, food noise and intrusive thoughts.

Conclusion

Tirzepatide (Mounjaro) alleviates repetitive behavior and food noise in a patient with autism/obsessive-compulsive disorders. GLP-1 agonists could be considered a treatment for patients with high body mass index and repetitive behavior. Further larger studies investigating different GLP-1 agonists and doses are highly recommended.

Ethical Considerations

The patient provided written informed consent to publish case-associated data without identifying details.

Author Contribution Statement

The author confirms sole responsibility for the conception, design, and writing of the manuscript.

Conflict of Interest

The author has declared no conflict of interest.

References

1. FDA-Approved Drugs to Treat Overweight and Obesity. J Psychosoc Nurs Ment Health Serv. 2022 Aug;60(8):7-8. doi: 10.3928/02793695-20220615-79. Epub 2022 Aug 1. PMID: 35917244.
2. Nauck MA, Quast DR, Wefers J, Meier JJ. GLP-1 receptor agonists in the treatment of type 2 diabetes - state-of-the-art. Mol Metab. 2021 Apr;46:101102. doi: 10.1016/j.molmet.2020.101102. Epub 2020 Oct 14. PMID: 33068776; PMCID: PMC8085572.
3. Graaf Cd, Donnelly D, Wootten D, Lau J, Sexton PM, Miller LJ, Ahn JM, Liao J, Fletcher MM, Yang D, Brown AJ, Zhou C, Deng J, Wang MW. Glucagon-Like Peptide-1 and Its Class B G Protein-Coupled Receptors: A Long March to Therapeutic Successes. Pharmacol Rev. 2016 Oct;68(4):954-1013. doi: 10.1124/pr.115.011395. PMID: 27630114; PMCID: PMC5050443.
4. Zhao X, Wang M, Wen Z, Lu Z, Cui L, Fu C, Xue H, Liu Y, Zhang Y. GLP-1 Receptor Agonists: Beyond Their Pancreatic Effects. Front Endocrinol (Lausanne). 2021 Aug 23;12:721135. doi: 10.3389/fendo.2021.721135. PMID: 34497589; PMCID: PMC8419463.
5. Ma X, Liu Z, Ilyas I, Little PJ, Kamato D, Sahebka A, Chen Z, Luo S, Zheng X, Weng J, Xu S. GLP-1 receptor agonists (GLP-1RAs): cardiovascular actions and therapeutic potential. Int J Biol Sci. 2021 May 11;17(8):2050-2068. doi: 10.7150/ijbs.59965. PMID: 34131405; PMCID: PMC8193264.
6. McIntyre RS, Mansur RB, Rosenblat JD, Kwan ATH. The association between glucagon-like peptide-1 receptor agonists (GLP-1 RAs) and suicidality: reports to the Food and Drug Administration Adverse Event Reporting System (FAERS). Expert Opin Drug Saf. 2024 Jan;23(1):47-55. doi: 10.1080/14740338.2023.2295397. Epub 2023 Dec 19. PMID: 38087976.
7. Tobaiqy M, Elkout H. Psychiatric adverse events associated with semaglutide, liraglutide and tirzepatide: a pharmacovigilance analysis of individual case safety reports submitted to the EudraVigilance database. Int J Clin Pharm. 2024 Apr;46(2):488-495. doi: 10.1007/s11096-023-01694-7. Epub 2024 Jan 24. PMID: 38265519; PMCID: PMC10960895.
8. Chen X, Zhao P, Wang W, Guo L, Pan Q. The Antidepressant Effects of GLP-1 Receptor Agonists: A Systematic Review and Meta-Analysis. Am J Geriatr Psychiatry. 2024 Jan;32(1):117-127. doi: 10.1016/j.jagp.2023.08.010. Epub 2023 Aug 21. PMID: 37684186.
9. Cooper DH, Ramachandra R, Ceban F, Di Vincenzo JD, Rhee TG, Mansur RB, Teopiz KM, Gill H, Ho R, Cao B, Lui LMW, Jawad MY, Arsenault J, Le GH, Ramachandra D, Guo Z, McIntyre RS. Glucagon-like peptide 1 (GLP-1) receptor agonists as a protective factor for incident depression in patients with diabetes mellitus: A systematic review. J Psychiatr Res. 2023 Aug;164:80-89. doi: 10.1016/j.jpsychires.2023.05.041. Epub 2023 Jun 5. PMID: 37331261.
10. Hayashi D, Edwards C, Emond JA, Gilbert-Diamond D, Butt M, Rigby A, Masterson TD. What Is Food Noise? A Conceptual Model of Food Cue Reactivity. Nutrients. 2023 Nov 17;15(22):4809. doi: 10.3390/nu15224809. PMID: 38004203; PMCID: PMC10674813.
11. Zeidan J, Fombonne E, Scorah J, Ibrahim A, Durkin MS, Saxena S, Yusuf A, Shih A, Elsabbagh M. Global prevalence of autism: A systematic review update. Autism Res. 2022 May;15(5):778-790. doi: 10.1002/aur.2696. Epub 2022 Mar 3. PMID: 35238171; PMCID: PMC9310578.
12. Arillotta D, Floresta G, Papanti Pelletier GD, Guirguis A, Corkery JM, Martinotti G, Schifano F. Exploring the Potential Impact of GLP-1 Receptor Agonists on Substance Use, Compulsive Behavior, and Libido: Insights from Social Media Using a Mixed-Methods Approach. Brain Sci. 2024 Jun 20;14(6):617. doi: 10.3390/brainsci14060617. PMID: 38928616; PMCID: PMC11202225.
13. Järvinen A, Laine MK, Tikkanen R, Castrén ML. Beneficial Effects of GLP-1 Agonist in a Male With Compulsive Food-Related Behavior Associated With Autism. Front Psychiatry. 2019 Mar 1;10:97. doi: 10.3389/fpsyt.2019.00097. PMID: 30881319; PMCID: PMC6405420.
14. Andersen A, Lund A, Knop FK, Vilsbøll T. Glucagon-like peptide 1 in health and disease. Nat Rev Endocrinol. 2018 Jul;14(7):390-403. doi: 10.1038/s41574-018-0016-2. PMID: 29728598.
15. Vallöf D, Maccioni P, Colombo G, Mandrapa M, Jörnulf JW, Egecioglu E, Engel JA, Jerlhag E. The glucagon-like peptide 1 receptor agonist liraglutide attenuates the reinforcing properties of alcohol in rodents. Addict Biol. 2016 Mar;21(2):422-37. doi: 10.1111/adb.12295. Epub 2015 Aug 25. PMID: 26303264; PMCID: PMC5049632.
16. Fuccillo MV. Striatal Circuits as a Common Node for Autism Pathophysiology. Front Neurosci. 2016 Feb 9;10:27. doi: 10.3389/fnins.2016.00027. PMID: 26903795; PMCID: PMC4746330.
17. Cork SC, Richards JE, Holt MK, Gribble FM,

Reimann F, Trapp S. Distribution and characterisation of Glucagon-like peptide-1 receptor expressing cells in the mouse brain. Mol Metab. 2015 Aug 5;4(10):718-31. doi: 10.1016/j.molmet.2015.07.008. PMID: 26500843; PMCID: PMC4588458.

18. Manoharan SVRR, Madan R. GLP-1 Agonists Can Affect Mood: A Case of Worsened Depression on Ozempic (Semaglutide). Innov Clin Neurosci. 2024 Jun 1;21(4-6):25-26. PMID: 38938530; PMCID: PMC11208009.

19. Brierley DI, Holt MK, Singh A, de Araujo A, McDougle M, Vergara M, Afaghani MH, Lee SJ, Scott K, Maske C, Langhans W, Krause E, de Kloet A, Gribble FM, Reimann F, Rinaman L, de Lartigue G, Trapp S. Central and peripheral GLP-1 systems independently suppress eating. Nat Metab. 2021 Feb;3(2):258-273. doi: 10.1038/s42255-021-00344-4. Epub 2021 Feb 15. PMID: 33589843; PMCID: PMC7116821.

20. Paula-Pérez I. Differential diagnosis between obsessive compulsive disorder and restrictive and repetitive behavioural patterns, activities and interests in autism spectrum disorders. Rev Psiquiatr Salud Ment. 2013 Oct-Dec;6(4):178-86. English, Spanish. doi: 10.1016/j.rpsm.2012.07.005. Epub 2012 Sep 13. PMID: 23084795.

21. van Steensel FJ, Bögels SM, Perrin S. Anxiety disorders in children and adolescents with autistic spectrum disorders: a meta-analysis. Clin Child Fam Psychol Rev. 2011 Sep;14(3):302-17. doi: 10.1007/s10567-011-0097-0. PMID: 21735077; PMCID: PMC3162631.

22. American Psychiatric Association. Diagnostic and statistical manual of mental disorders: DSM-5-TR (5th ed., text rev. ed.). American Psychiatric Association. Diagnostic and Statistical Manual of Mental Disorders, Fifth Edition, Text Revision (DSM-5-TR). 18 March 2022. doi:10.1176/appi.books.9780890425787

23. Jiujias M, Kelley E, Hall L. Restricted, Repetitive Behaviors in Autism Spectrum Disorder and Obsessive-Compulsive Disorder: A Comparative Review. Child Psychiatry Hum Dev. 2017 Dec;48(6):944-959. doi: 10.1007/s10578-017-0717-0. PMID: 28281020.

24. O'Loghlen J, McKenzie M, Lang C, Paynter J. Correction: Repetitive Behaviors in Autism and Obsessive-Compulsive Disorder: A Systematic Review. J Autism Dev Disord. 2024 Aug;54(8):3194-3196. doi: 10.1007/s10803-024-06450-y. Erratum for: J Autism Dev Disord. 2025 Jul;55(7):2307-2321. doi: 10.1007/s10803-024-06357-8. PMID: 38954363; PMCID: PMC11300541.

25. Sachdeva P, Mehdi I, Kaith R, Ahmad F, Anwar MS. Potential natural products for the management of autism spectrum disorder. Ibrain. 2022 Jun 21;8(3):365-376. doi: 10.1002/ibra.12050. PMID: 37786737; PMCID: PMC10528773.

26. Herman RJ, Schmidt HD. Targeting GLP-1 receptors to reduce nicotine use disorder: Preclinical and clinical evidence. Physiol Behav. 2024 Jul 1;281:114565. doi: 10.1016/j.physbeh.2024.114565. Epub 2024 Apr 23. PMID: 38663460; PMCID: PMC11128349

***Correspondence**: Amirah Alhowiti. E-mail: aalhowiti@ut.edu.sa*

IJBM

INTERNATIONAL JOURNAL OF BIOMEDICINE

Instructions for Authors

International Journal of Biomedicine (IJBM) publishes peer-reviewed articles on the topics of basic, applied, and translational research on biology and medicine. International Journal of Biomedicine welcomes submissions of the following types of paper: Original Articles, Reviews, Viewpoints, Case Reports, and Brief Communications.

All research studies involving animals must have been conducted following animal welfare guidelines such as *the National Institutes of Health (NIH) Guide for the Care and Use of Laboratory Animals*, or equivalent documents. Studies involving human subjects or tissues must adhere to the *Declaration of Helsinki and Title 45, US Code of Federal Regulations, Part 46, Protection of Human Subjects*, and must have received approval of the appropriate institutional committee charged with oversight of human studies. Informed consent must be obtained.

Pre-submissions

Authors are welcome to send an abstract or draft manuscript to obtain a view from the Editor about the suitability of their paper. Our Editors will do a quick review of your paper and advise if they believe it is appropriate for submission to our journal. It will not be a full review of your manuscript.

Manuscript Submission

Manuscript submissions should conform to the guidelines set forth in the Recommendations for the Conduct, Reporting, Editing and Publication of Scholarly Work in Medical Journals (ICMJE Recommendations), available from www.ICMJE.org.

Original works will be accepted with the understanding that they are contributed solely to the Journal, are not under review by another publication, and have not previously been published except in abstract form.

All manuscripts must be submitted through the International Journal of Biomedicine`s online submission system (www.ijbm.org/submission.php). Manuscripts must be typed, double-spaced using a 14-point font, including references, figure legends, and tables. Leave 1-inch margins on all sides. Assemble the manuscript in this order: Title Page, Abstract, Keywords, Text (Introduction, Methods, Results, and Discussion), Acknowledgments, Sources of Funding, Disclosures, References, Tables, Figures, and Figure Legends. References, Figures, and Tables should be cited in numerical order according to first mention in the text.

The preferred order for uploading files is as follows: Cover letter, Full Manuscript PDF (PDF containing all parts of the manuscript including references, legends, figures and tables), Manuscript Text File (MS Word), Figures (each figure and its corresponding legend should be presented together), and Tables. Files should be labeled with appropriate and descriptive file names (e.g., SmithText.doc, Fig1.eps, Table3.doc). Text, Tables, and Figures should be uploaded as separate files. (Multiple figure files can be compressed into a Zip file and uploaded in one step; the system will then unpack the files and prompt the naming of each figure. See www.WinZip.com for a free trial.)

Authors who are unable to provide an electronic version or have other circumstances that prevent online submission must contact the Editorial Office prior to submission to discuss alternate options (editor@ijbm.org).

Cover Letter

The cover letter should be saved as a separate file for upload. In it, the authors should (1) state that the manuscript, or parts of it, have not been and will not be submitted elsewhere for publication; (2) state that all authors have read and approved the manuscript; and (3) disclose any financial or other relations that could lead to a conflict of interest. If a potential conflict exists, its nature should be stated for each author. When there is a stated potential conflict of interest a footnote will be added indicating the author's equity interest in or other affiliation with the identified commercial firms.

The corresponding author should be specified in the cover letter. All editorial communications will be sent to this author. A short paragraph telling the editors why the authors think their paper merits publication priority may be included in the cover letter.

Types of articles

Original articles

Original articles present the results of original research. These manuscripts should present well-rounded studies reporting innovative advances that further knowledge about a topic of importance to the fields of biology or medicine. These can be submitted as either a full-length article (no more than 6,000 words, 4 figures, 4 tables) or a Short Communication (no more than 2,500 words, 2 figures, 2 tables). An original

article may be Randomized Control Trial, Controlled Clinical Trial, Experiment, Survey, and Case-control or Cohort study.

Case Reports

Case reports describe an unusual disease presentation, a new treatment, a new diagnostic method, or a difficult diagnosis. The authors must make it clear what the case adds to the field of medicine and include an up-to-date review of all prior cases. These articles should be no more than 5,000 words with no more than 6 figures and 3 tables. Case Reports should consist of the following headings: Abstract (no more than 100 words), Introduction, Case Presentation, Discussion, and Conclusions. The number of authors for a clinical case description must not exceed seven. Those who contributed to the patient's care but did not contribute directly to the intellectual work of the manuscript should be listed in the acknowledgments section.

Reviews

Reviews analyze the current state of understanding on a particular subject of research in biology or medicine, the limitations of current knowledge, future directions to be pursued in research, and the overall importance of the topic. Reviews could be non-systematic (narrative) or systematic. Reviews can be submitted as a Mini-Review (no more than 2,500 words, 3 figures, and 1 table) or a long review (no more than 6,000 words, 6 figures, and 3 tables). Reviews should contain four sections: Abstract, Introduction, Topics (with headings and subheadings, and Conclusions and Outlook.

Viewpoints

Viewpoint articles include academic papers, which address any important topic in biomedicine from a personal perspective than standard academic writing. Maximum length is 1,200 words, ≤70 references, and 1 small table or figure.

Short Communications

Short communications are concise scientific papers (typically 1,500–2,500 words) that present novel, preliminary, or urgent findings without the length or depth of a full research article. Main body of text, excluding tables (<2), figures (<2), and references (<15), not to exceed 1,000 words. Short Communications should contain Abstract, Introduction, Materials and Methods, Results, and Conclusion.

Research Reporting Guidelines

Authors are encouraged to adhere to recognized research reporting guidelines for study types:

• Randomized trials: CONSORT (https://www.equator-network.org/reporting-guidelines/consort/)

• Observational studies: STROBE (https://www.equator-network.org/reporting-guidelines/strobe/)

• Systematic reviews: PRISMA (https://www.equator-network.org/reporting-guidelines/prisma/)

• Case reports: CARE (https://www.equator-network.org/reporting-guidelines/care/)

• Qualitative research: SRQR (https://www.equator-network.org/reporting-guidelines/srqr/)

• Diagnostic / prognostic studies: STARD (https://www.equator-network.org/reporting-guidelines/stard/)

• Animal pre-clinical studies: ARRIVE (https://www.equator-network.org/reporting-guidelines/improving-bioscience-research-reporting-the-arrive-guidelines-for-reporting-animal-research/)

• Study protocols: SPIRIT (https://www.equator-network.org/reporting-guidelines/spirit-2013-statement-defining-standard-protocol-items-for-clinical-trials/)

Genetic Nomenclature and Sequence Data

DNA sequence variants should be described in the text and tables according to HGVS (Human Genome Variation Society) nomenclature (varnomen.hgvs.org). DNA-level changes must be specified relative to a specific reference sequence, such as NCBI RefSeq or a Locus Reference Genomic (LRG) record. Tabular listings of the described sequence variants must include columns for DNA, RNA, and protein, and clearly indicate whether the changes were determined experimentally or predicted exclusively theoretically.

Nucleotide sequence data can be submitted to any of the three major collaborative databases:

• DNA Data Bank of Japan (DDBJ): http://www.ddbj.nig.ac.jp

• European Nucleotide Archive (ENA): ebi.ac.uk/ena

• GenBank: https://www.ncbi.nlm.nih.gov/genbank/

Manuscript Preparation

Title Page

The first page of the manuscript (title page) should include (1) a full title of the article, (2) a short title of less than 60 characters with spaces, (3) the authors' names, academic degrees, and affiliations, (4) the total word count of the manuscript (including Abstract, Text, References, Tables, Figure Legends), (5) the number of figures and tables, and (6) the name, email address, and complete address of corresponding author.

Disclaimers. An example of a disclaimer is an author's statement that the views expressed in the submitted article are his or her own and not an official position of the institution or funder.

Abstract

The article should include a brief abstract of no more than 200 words. Limit use of acronyms and abbreviations. Define at first use with acronym or abbreviation in parentheses. The abstract should be structured with the following headings: Background, Methods and Results, and Conclusions. The Background section should describe the rationale for the study. Methods and Results should briefly describe the methods and present the significant results. Conclusions should succinctly state the interpretation of the data. Authors should supply a list of up to four key words not appearing in the title, which will be used for indexing. The key words should be listed immediately after the Abstract. Use terms from the Medical Subject Headings (MeSH) list of Index Medicus when possible.

Main text in the IMRaD format

Introduction should describe the purpose of the study and its relation to previous work in the field; it should not include an extensive literature review.

Methods should be concise but sufficiently detailed to permit repetition by other investigators. Previously published methods and modifications should be cited by reference. A subsection on statistics should be included in the Methods section.

Results should present positive and relevant negative findings of the study, supported when necessary by reference to Tables and Figures.

Discussion should interpret the results of the study, with emphasis on their relation to the original hypotheses and to previous studies. The importance of the study and its limitations should also be discussed.

The IMRaD format does not include a separate Conclusion section. The conclusion is built into the Discussion. More information on the structure and content of these sections can be found in the Recommendations for the Conduct, Reporting, Editing and Publication of Scholarly Work in Medical Journals (ICMJE Recommendations), available from www.ICMJE.org.

Author Contributions, Acknowledgments, Sources of Funding, and Disclosures

CRediT (Contributor Roles Taxonomy) author statement should be provided during the submission process**.**

Acknowledgments : All contributors who do not meet the criteria for authorship should be listed in an acknowledgments section. Examples of those who might be acknowledged include a person who provided purely technical help, writing assistance, or a department chairperson who provided only general support. Authors should declare whether they had assistance with study design, data collection, data analysis, or manuscript preparation. If such assistance was available, the authors should disclose the identity of the individuals who provided this assistance and the entity that supported it in the published article.

Sources of Funding: All sources of financial support for the study should be cited on the title page, including federal or state agencies, nonprofit organizations, and pharmaceutical or other commercial sources.

Disclosure and conflicts of interest: All authors must disclose any financial or other relations that could lead to a conflict of interest. If a potential conflict exists, its nature should be stated for each author. All sources of financial support for the study should be cited, including federal or state agencies, nonprofit organizations, and pharmaceutical or other commercial sources. Please use ICMJE Form for Disclosure of Potential Conflicts of Interest (http://www.icmje.org/conflicts-of-interest/).

References

References should follow the standards summarized in the NLM's International Committee of Medical Journal Editors (ICMJE) Recommendations for the Conduct, Reporting, Editing and Publication of Scholarly Work in Medical Journals: Sample References webpage (www.nlm.nih.gov/bsd/uniform_requirements.html) and detailed in the NLM's Citing Medicine, available from www.ncbi.nlm.nih.gov/books/NBK7256/. MEDLINE abbreviations for journal titles (www.ncbi.nlm.nih.gov/nlmcatalog/journals) should be used.

References should be presented in the Vancouver style. The first six authors should be listed in each reference citation (if there are more than six authors, "et al" should be used following the sixth). Periods are not used in authors' initials or journal abbreviations. Examples of journal reference style:

Journal Article: Serruys PW, Ormiston J, van Geuns RJ, de Bruyne B, Dudek D, Christiansen E, et al. A Polylactide Bioresorbable Scaffold Eluting Everolimus for Treatment of Coronary Stenosis: 5-Year Follow-Up. J Am Coll Cardiol. 2016;67(7):766-76. doi: 10.1016/j.jacc.2015.11.060.

Book: Murray PR, Rosenthal KS, Kobayashi GS, Pfaller MA. *Medical Microbiology*. 4th ed. St. Louis: Mosby; 2002.

Chapter in Edited Book: Meltzer PS, Kallioniemi A, Trent JM. Chromosome alterations in human solid tumors. In: Vogelstein B, Kinzler KW, editors. *The Genetic Basis of Human Cancer*. New York: McGraw-Hill; 2002:93–113.

References should be numbered consecutively in the order in which they are first mentioned in the text. Identify references in text, tables, and legends by Arabic numerals in parentheses and listed at the end of the article in citation order.

Tables

Tables should be comprehensible without reference to the text and should not be repetitive of descriptions in the text. Every table should consist of two or more columns; tables with only one column will be treated as lists and incorporated into the text. All tables must be cited in the text and numbered in order of appearance. Tables should include a short title. Place explanatory matter in footnotes, not in the heading. Explain all nonstandard abbreviations in footnotes, and use symbols to explain information if needed. Each table submitted should be double-spaced, each on its own page. Each table should be saved as its own file as a Word Document. Explanatory matter and source notations for borrowed tables should be placed in the table footnote.

Figures and Legends

All illustrations (line drawings and photographs) are classified as figures. All figures should be cited in the text and numbered in order of appearance. Figures should be provided in .tiff, .jpeg or .eps formats. Color images must be at least 300 dpi. Gray scale images should be at least 300 dpi. Line art (black and white or color) and combinations of gray scale images and line art should be at least 1,000 dpi. The optimal size of lettering is 12 points. Symbols should be of a similar size. Figures should be sized to fit within the column (86 mm) or the full text width (180 mm). Line figures must be sharp, black and white graphs or diagrams, drawn professionally or with a computer graphics package. Legends should be supplied for each figure and should be brief and not repetitive of the text. Any source notation for borrowed figures should appear at the end of the legend. Figures should be uploaded as individual files.

Units of Measurement

Measurements of length, height, weight, and volume should be reported in metric units (meter, kilogram, or liter) or their decimal multiples. Temperatures should be in degrees Celsius. Blood pressures should be in millimeters of mercury. All measurements must be given in SI or SI-derived units. Drug concentrations may be reported in either SI or mass units, but the alternative should be provided in parentheses where appropriate

Style and Language

The journal accepts manuscripts written in English. Spelling should be US English only. The language of the manuscript must meet the requirements of academic

publishing. Reviewers may advise rejection of a manuscript compromised by grammatical errors. Non-native speakers of English may choose to use a copyediting service.

Abbreviations and Symbols

Use only standard abbreviations; use of nonstandard abbreviations can be confusing to readers. Avoid abbreviations in the title of the manuscript. The spelled-out abbreviation followed by the abbreviation in parenthesis should be used on first mention unless the abbreviation is a standard unit of measurement.

Drugs should be referred to by their generic names. If proprietary drugs have been used in the study, refer to these by their generic name, mentioning the proprietary name, and the name and location of the manufacturer, in parentheses.

Permissions

To use tables or figures borrowed from another source, permission must be obtained from the copyright holder, usually the publisher. Authors are responsible for applying for permission for both print and electronic rights for all borrowed materials and are responsible for paying any fees related to the applications of these permissions. This is necessary even if you are an author of the borrowed material. It is essential to begin the process of obtaining permission early, as a delay may require removing the copyrighted material from the article. The source of a borrowed table should be noted in a footnote and of a borrowed figure in the legend. It is essential to use the exact wording required by the copyright holder. A copy of the letter granting permission, identified by table or figure number, should be sent along with the manuscript. A permission request form is provided for the authors use in requesting permission from copyright holders.

Journal Policy on Affiliation with Sanctioned Institutions

At IJBM, we uphold the highest standards of academic integrity and compliance with international laws and regulations. To ensure the ethical and legal standing of all submitted research papers, authors are required to adhere to the following policy regarding affiliation with sanctioned institutions:

1. Declaration of Non-Affiliation: Authors must provide a clear and unambiguous statement confirming their non-affiliation with any institution, organization, or individual subject to sanctions imposed by international sanctions, laws, or regulations. This declaration should be included in the cover letter accompanying their manuscript submission.

2. Sanctioned Entities: Sanctioned entities include those listed on sanctions lists maintained by international authorities, such as the United Nations, the United States Department of the Treasury's Office of Foreign Assets Control (OFAC), the European Union, or any other relevant governing body.

3. Independence and Ethical Research: Authors should affirm that their research is conducted independently and ethically, without receiving any funding, resources, or support from sanctioned sources in connection with the submitted research.

4. Disclosure of Conflicts of Interest: Authors must disclose any potential conflicts of interest that may compromise the ethical and legal standing of their submission. This includes any financial interests or affiliations that could be perceived as influencing the research.

5. Consequences of Non-Compliance: Failure to adhere to this policy, misrepresentation of affiliations, or non-disclosure of conflicts of interest may result in the rejection of the submitted manuscript or further investigation into the matter.

Authors submitting their research papers to IJBM are responsible for ensuring their compliance with this policy. We reserve the right to verify the accuracy of the provided information and take appropriate action in cases of non-compliance.

Page Proofs

Page proofs are sent from the Publisher electronically and must be returned within 72 hours to avoid delay of publication. Generally, peer review is completed within 11-12 weeks, and the editor’s decision is made within 7-14 days of this. A timeline from submission to publication is an average of 14 weeks.

It is important to note that when citing an article from IJBM, the correct citation format is **International Journal of Biomedicine.**